Preliminary studies in imaging neuronal depolarization in the brain with Electrical or Magnetic Detection Impedance Tomography

Ori Gilad

Submitted for the degree of Doctor of Philosophy

Department of Medical Physics & Bioengineering

University College London

2007

ProQuest LLC
789 East Eisenhower Parkway
P.O. Box 1346
Ann Arbor, MI 48106-1346

Declaration:

I, Ori Gilad, confirm that the work presented in this thesis is my own. Where information has been derived from other sources, I confirm that this has been indicated in the thesis.

Signed: Date: 20 Sep 2007

Abstract

Electrical impedance Tomography (EIT) is a novel medical imaging method which has the potential to provide the revolutionary advance of a method to image fast neural activity non-invasively, by imaging electrical impedance changes over milliseconds which occur when neuronal ion channels open during activity. These changes have been estimated to be c.1% locally in cerebral cortex, if measured with applied current below 100Hz. The purpose of this work was to determine if such changes could be reproducibly recorded in humans non-invasively.

First, a novel recessed electrode was designed and tested to determine to enable a maximal current of 1mA to be applied to the scalp without causing painful skin sensation. Modelling indicated that this produced a peak current density of $0.3A/m^2$ in underlying cortex, which was below the threshold for stimulation. Next, the signal-to-noise ratio of impedance changes during evoked visual activity was investigated in healthy volunteers with current injected with scalp electrodes and recording of potential by scalp electrodes (Low Frequency EIT) or magnetic field by magnetoencephalography (Magnetic Detection EIT). Numerical FEM simulations predicted that resistivity changes of 1% in the primary visual cortex translate into scalp voltage changes of 1μV (0.004%) and external magnetic field changes of 30fT (0.2%) and were independently validated in saline filled tanks. In vivo, similar changes with a signal-to-noise ratio of 3 after averaging for 10 minutes were recorded for both methods; the main noise sources were background brain activity and the current source.

These studies with non-invasive scalp recording have, for the first time, demonstrated the existence of such changes when measured non-invasively. These are unfortunately too low to enable reliable imaging within a realistic recording time but support the view that such imaging could be possible in animal or human epileptic studies with electrodes placed on the brain or non-invasively following technological improvements; this further work is currently in progress.

Acknowledgements

This thesis was made possible by the assistance given to me by a number of people. Firstly, my deepest gratitude is given to my supervisor Prof David Holder for his guidance and support throughout this work. In addition I would like to thank Prof Richard Bayford who co-supervised me during the first stages of my studies.

I am particularly grateful to Dr Lior Horesh who developed the key numerical tools for all my modelling studies and assisted with the numerical analysis throughout.

Different parts of the research presented in the thesis would not have materialised without the contribution of the following people:

Dr Andrew Tizzard who provided realistic mesh models of the human head; Prof Richard Bayford and Dr Alistair McEwan who had guided me through the trickery of physiological instrumentation; The EEG Technologists at The Department of Clinical Neurophysiology, UCLH, Mary Boland, Estelle Leigh and Tahlita Mabuza, and the MEG Technologists at the Functional Imaging Laboratory, ION/UCL, Janice Glensman, David Bradbury and Amanda Brennan for helping with human subject preparations and essential technical advice; my colleagues Louise Enfield and Adam Liston who overlapped and guided me through the Crab experiment setup, Lorenzo Fabrizi who assisted during the MEG experiments and Dr Gershon Ahadzi who had literally contributed his brain for countless calibration and pilot studies; my father Ilan Gilad for manufacturing the recessed electrodes; Prof Solange Akselrod who reviewed parts of this thesis; Dr Nachum Ulanovsky for his advice on statistical analysis; my referees Prof Jan De Munck and Prof Louis Lemieux for their comments during the examination and last but not least, the anonymous colleagues, friends, family and members of the public who volunteered to be subjects in my experiments.

This work was supported by the Biotechnology and Biological Sciences Research Council, UK, the Epilepsy Research Foundation, UK, the Ministry of Science & Technology, Israel, and grant 1R01EB006597-01 from The National Institutes of Health, US, to whom I am grateful. I would also like to acknowledge the Department of Medical Physics for their administrative support.

Finally, I am grateful for the continuous support of my wife Yael and kids Shani and Yoav who have kept me going through the harder stages of this work.

Table of Contents

List of figures

List of tables

1. Introduction

1.1 Overview and contributions

Functional neuroimaging has improved greatly in the past two decades but the 'holy grail' would be to image neuronal activity with a time and spatial resolution of about 1 ms and 1 mm respectively; this has not been approached by any method. Electrical impedance Tomography (EIT) is a developing medical imaging method which has the potential to achieve this non-invasively. The principle is that electrical impedance changes over milliseconds when neuronal ion channels open during activity, and this could be imaged by EIT. Using cable theory modelling and animal studies, the size of such changes locally in the cerebral cortex have previously been estimated to be about 1%, provided they are measured with applied current below 100 Hz. The purpose of this thesis was to determine if such changes could be reproducibly recorded in humans with non-invasive recording on or near the scalp.

The following introductory chapter starts with a brief review of functional brain imaging modalities, with an emphasis on those potentially capable of imaging neuronal activity. This is followed by general background on EIT and a review of current knowledge on neuronal activity related impedance changes, previous measurement attempts and a list of important challenges remaining to be addressed. My contribution to this was the extension of cable theory interpretation for the complex case. This is followed by a brief review of dielectric properties of head tissues. This is reduced from an exhaustive literature review which I co-authored but left out of this thesis for brevity. The purpose and design are then stated followed by a list of publications resulting from this thesis.

In Chapter (Ch.) 2, I present a study in which I determined the maximal current and current density which could be used in Low Frequency EIT (LF-EIT) human experiments in terms of safety, skin sensation and minimizing the possibility altering the normal brain function with the applied current. This was achieved using a literature review, novel electrode design, numerical simulations with realistic model of the head and human measurements. This study suggested a maximal injected current of 1 mA and maximal current density of 1 A/m^2 in the brain. The modelling aspects of this chapter were performed with the assistance of Lior Horesh who also developed the numeric tools. All other aspects were the sole contribution of the author.

In Ch. 3 and 5, I present studies in which I performed numerical simulations to estimate the magnitude of the boundary voltages and external magnetic field changes during visual evoked response for LF-EIT and Magnetic Detection EIT (MD-EIT) respectively. This work followed initial work by Gershon Ahadzi, in which I collaborated, and was performed with the assistance of Lior Horesh. Gershon Ahadzi also assisted in the tank validation study in Ch. 3. The author undertook the great majority of the work presented in these chapters.

In Ch. 4 and 6, which were my sole contribution, I undertook a series of non-invasive experimental human studies during visual evoked responses with LF-EIT and MD-EIT respectively. The aim was to measure the boundary voltages and external magnetic field changes associated with neuronal activity so that their SNR could be estimated and implications for image reconstruction could be determined. For these studies, prototype systems were designed and a single current injection electrode pair was used with recordings from multiple electrodes or magnetic field sensors. Changes of a similar magnitude to those estimated by the modelling were recorded synchronously to the Visual Evoked Potentials (VEP) or Visual Evoked Fields (VEF) for both the electric and magnetic cases in approximately 50% of the experiments. However, the SNR was typically too low for allowing imaging at practical recording time and was mainly limited by the background brain activity asynchronous to the visual stimuli.

Ch. 7 is a discussion, where I addressed the questions set in the purpose and design of the introduction (Section 1.7). The implications for designing future imaging system are that these changes are too small for current technology to permit accurate image production with non-invasive recording in humans. Future work is to improve the technique and develop an invasive imaging system for animal brain research and human epilepsy patients with intracranial electrodes.

1.2 Functional brain imaging

1.2.1 The slow component

Several imaging techniques can be used to measure haemodynamic function of the brain with a time resolution limited by the physiological mechanisms which have a time constant of about 1 second. These methods image metabolic changes associated with the brain function such as blood flow, oxygenation, energy consumption and other metabolic processes. The main methods are tracer enhanced CT, Positron Emission Tomography (PET), Single Photon Emission Computerised Tomography (SPECT), functional Magnetic Resonance Imaging (fMRI), optical methods (Near Infra Red Spectroscopy (NIRS) Diffuse Optical Imaging (DOI) and Diffuse Optical Tomography (DOT)) and Electrical Impedance Tomography (EIT) sensitive to impedance changes related to blood volume changes and cell swelling (Table 1-1).

Table 1-1: summary of haemodynamic brain imaging techniques

Method (source)	**Spatial resolution**	**Temporal resolution**	**Limitations**
Tracer CT (Konig, 2003)	1 mm	1 s	X-ray radiation + injection of contrast agent
PET (Robinson, 1999)	4 mm	~30 s	Very expensive, radioactive labelling required
SPECT (Brown, 1999)	7 mm	15 min	Radioactive labelling required
fMRI (Belliveau, 1991; Koretsky, 2004)	0.1–1 mm	1-5 s	Very expensive, not suitable for some patients
NIRS/DOI/DOT (Obrig, 2003; Mehta, 2004)	10-20 mm	0.1–60 s	Research only, cortical surface only
EIT (Tidswell, 2001)	10-20 mm	0.3 s	Research only

1.2.2 The fast component

Another family of imaging methods focus on non-invasive ways to image the neuronal activity itself with the highest possible spatial and time resolutions. At present, a technique producing reliable images with spatial resolution of about 1 mm and time resolution of about 1 ms is not yet available. The theme of this thesis was to estimate possible contribution of EIT methods towards such goal.

Partial achievements have been demonstrated using inverse source modelling of recordings made using electro-encephalography (EEG) and magneto-encephalography (MEG) techniques and the multi-modality fusion of these methods with data from haemodynamic fMRI and anatomical MRI constrains.

Recent experimental methods includes direct mapping of neuronal activity with MRI, Diffuse Optical Imaging (DOI), and the EIT variants presented in this thesis, namely Low Frequency EIT (LF-EIT) and Magnetic Detection EIT (MD-EIT).

Finally, several invasive imaging methods have been developed. These techniques are important for animal models but could be rarely used on humans unless justified by specific clinical conditions such as pre-surgical evaluation. From these I present sub-dural electro-corticography (ECoG), optical imaging with optical dyes and Electron Spin Resonance (ESR).

The potential performance of these methods varies from time resolution of 1 to 100 ms and spatial resolution of 0.05 to 10 mm (Table 1-2). The following elaborate on each method.

Table 1-2: summary of neuronal activity imaging techniques.

Method (source)	**Spatial resolution**	**Temporal resolution**	**Limitations**
Non-invasive methods			
EEG (Baillet, 2001a; Baillet, 2001b; Michel, 2004)	~ 10 mm	~ 1ms	Limited for sources close to the surface
MEG (Hamalainen, 1992; Baillet, 2001a)	~ 10 mm	~ 1ms	Expensive, limited to sulci sources
Multi-modality fusion (Dale, 2001)	<10 mm	~ 1ms	Expensive, research only, haemodynamic and neuronal sources not always correlates
Direct MRI mapping (Xiong, 2003; Lin, 2006)	3 mm	100 ms (20 ms)	Research only, needs to be replicated and refined
DOI (Franceschini, 2004)	10 mm	25 ms	Research only, limited to cortical surface
LF-EIT and MD-EIT (Holder, 1987), this thesis	~ 10 mm	~ 1ms	Research only. Limited SNR. The theme of this thesis
Invasive methods			
ECoG	10 mm	~ 1ms	Slightly enhance EEG accuracy
Optic dyes (Shoham, 1999)	0.05 mm	~ 1ms	Limited 2D area on the surface of the cortex
ESR (Holder, 1987)	?	?	Theoretical application , toxic contrast agents

1.2.2.1 EEG

Electrophysiological methods have long been used to study the function, over milliseconds, of individual neurons. Their depolarisation, or "firing", is well understood, as is the integration of signals on their cell projections, dendrites, from the synapses of neighbouring neurons. Brain function depends on the spatial and temporal synchrony of large populations of neurons.

In EEG, the most widespread monitoring technique, voltage changes on the scalp are measured which provide information about the electrical activity of neurons near the surface of the cortex. Some applications of EEG include recording spontaneous activity during normal and ill conditions such as epilepsy or encephalitis, monitoring sleep stages and characterizing the response stimuli such as visual, auditory or somatosensory.

The magnitude of the signal depends not only on the number and location but also the geometry of the synchronously firing neurons, since it possible for many arrangements to generate currents so that their associated potential distributions cancel. Therefore, EEG is sensitive to the dendritic currents of active pyramidal neurons, oriented parallel to each other so that their potential distributions do not cancel. Temporal resolution is high and data is normally collected at a sampling rate of around 250 Hz, sufficient to describe a 70ms interictal spike, common in epilepsy, with over 17 data points. However, while EEG approximately localises active areas of cortex close to the skull, localisation of deep activity is very unreliable. EEG is non-invasive and safe. It is also inexpensive and widely used as a clinical tool. It is, however, difficult to detect signals from neurons deeper in the brain, and spatial resolution is poor.

EEG can be used as a parametric or an imaging tool in the estimation of EEG sources in the brain (Baillet, 2001a; Baillet, 2001b). In the former, also called inverse dipole modelling, it is assumed that the electrical activity in the cortex can be represented by a few equivalent dipole sources. The number, localization, magnitude and orientation of these are estimated, iteratively, until the calculated potential distribution matches best the measured voltages at the scalp electrodes. For parametric modelling, one assumes / guesses a predefined number of sources. Due to the non-uniqueness of the inverse problem, employing this sole priori assumption may result in non-physical solutions where the sources are found outside the head. For source imaging, the number of unknowns is two orders of magnitude higher than the number of electrodes so the problem is severely underdetermined and difficult to solve without some mathematical trickery. Yet, with sufficient prior information (such as combined fMRI data and individual MRI segmentation of grey matter), special resolution of <10 mm and time resolution of ~1 ms is achieved for most cortical sources, but not for deep sources. See Michel (Michel, 2004) for a recent review of source imaging methods.

1.2.2.2 MEG

MEG also provides information about the electrical activity of pyramidal neurons, similar to EEG, with high temporal resolution (Hamalainen, 1992). Electrodes are replaced by small, inductive coils arranged on the inside of a helmet about 1-3 cm from the subject's scalp. Tiny currents are induced by the changes in magnetic field associated with dendritic currents and these are measured using sensing coils and Superconducting QUantum Interference Devices (SQUIDS) (Baillet, 2001a). The typical magnetic field magnitude outside the head are 10^{-13} and 10^{-12} Tesla for evoked responses and spontaneous brain activity respectively (Cohen, 1968; Hamalainen, 1993). A typical SQUID sensor has a spectral noise density below 5 fT $Hz^{1/2}$ (1 fT = 10^{-15} Tesla) (Brown, 1999), however the main limiting factor for evoked responses studies is the larger signal generated by the spontaneous brain activity. The magnetic field is not attenuated by the skull as the electric potentials so MEG is theoretically more sensitive than EEG (Hamalainen, 1993). The problem of contact impedance is avoided, since the sensors do not come into contact with the scalp, and the positions of the electrodes are well defined. However, MEG apparatus is expensive and immobile. It requires a dedicated, shielded room and also high maintenance costs for the cryogenic system.

In addition, a major difference between EEG and MEG is that EEG is more sensitive to gyal sources as it has limited sensitivity to deep sources while MEG is more sensitive to sulcal sources as the use of sensing coils limit the sensitivity to the radial magnetic field component perpendicular to the coil plane.

Measuring the complete magnetic field vector made of radial and two tangential components as well as their gradients may potentially be beneficial for localizing neuromagnetic sources. In a theoretical and simulation study for a spherical head model and a single di-pole source, including tangential components localized more accurately sources in the centre of the sensor array (Hochwald, 1997). Implementation of a 3D second-order gradiometer array was show beneficial in separating and estimating multiple sources in human measurements during simultaneous application of auditory and median nerve somatosensory stimulation (Kobayashi, 1998). In contrast, an extensive simulation study on various sensor array configurations and a model of physiological correlated noise concluded that a vector magnetometer was superior to radial gradiometer only at the rim of the sensor array. However, the finite dimensions of practical vector magnetometers dictate that they must be positioned farther from the scalp than the radial magnetometers. This small distance increase eliminates their slight advantage at the sensor array rim and for correlated noise (Vrba, 2002). 3D vector magnetic field measurement was also shown beneficial in cardiac (Burghoff, 1999; Di Rienzo, 2005) and spinal cord (Adachi, 2003; Adachi, 2005) application.

1.2.2.3 Multi-modality fusion

Since it does not seem that there is one brain imaging technique that possesses both high temporal and spatial resolution, it has been suggested that different imaging modalities be integrated in order to relate their signals to information processing at the neuronal circuit level (Dale, 2001). There are two main methods to interpret multimodal results, both of which use information about the haemodynamic response to precondition EEG or MEG inverse modelling. The first is the "seeded-dipole" technique, whereby the electrical activity in the brain is represented by a small number of dipoles, as in parametric EEG modelling, described above. The initial guess is informed this time by the activation foci derived from PET or fMRI. The second uses imaging with EEG. Here, dipoles are assigned too many voxels describing the cortical surface and are given orientation perpendicular to this surface. A solution is found for the dipole strength at each of these voxels and data from PET or fMRI is used to bias the solution, spatially, towards areas of the cortex that are haemodynamically active. In addition, anatomical prior information such as individual MRI segmentation of grey matter is commonly used to limit the solution space. Multimodality approaches improve the spatial resolution comparing to EEG or MEG alone and the prior information from anatomical and haemodynamic imaging allow solutions to be obtained in a broader range of cases. However, these methods are still limited to superficial sources and may result in erroneous results as the haemodynamic response is not necessarily correlated in time and space with the neuronal activity.

1.2.2.4 Direct mapping with MRI

The ability to directly detect neuronal magnetic fields by MRI would help to achieve the "holy grail" of neuroimaging, namely both high spatial and temporal resolution without ambiguous localization. Both positive and negative findings have been reported in the literature, with no clear consensus as to the feasibility of direct detection (Hagberg, 2006; Parkes, 2007). In theory, the magnetic fields generated by neurons could affect both the magnitude and phase of the NMR signal (Kamei, 1999; Bodurka, 1999; Bodurka, 2002; Kim, 2002; Kilner, 2004).

The effects of externally applied small (~2 mA) electric current pulses has been shown to be detectable in the human body using MRI (Joy, 1989). The challenge of detecting neuronal currents resulting from brain activity is much more difficult, since these currents are approximately three orders of magnitude smaller, much more transient, and perhaps localized to a smaller region in space, than what has been detected previously using MRI. These ionic currents induce subtle and transient magnetic field changes, depending on their temporal and spatial coherence. The parallel component of these fields to the main B_0 field of the MRI system alters the magnetic phase of surrounding water protons and thus influences the phase and/or magnitude of the MRI signal—depending on the size and geometry of the synchronous current

sources, potentially providing a mechanism for more direct detection of neuronal activity using MRI (Bodurka, 1999; Bodurka, 2002). The phase variations add up to give a resultant transient magnetic field changes as small as 100-200 pT, as theoretically derived and demonstrated in two phantom studies using an electric current dipole (Bodurka, 2002; Konn, 2003).

Much consideration must also be made as to how to separate the fast, neuronal effects changing over tens of milliseconds from slower effects such as the BOLD signal changing over hundreds of milliseconds to seconds.

Konn et al. (Konn, 2004) measured phase changes related to spontaneous α rhythm from visual areas during eyes closed experiment but could not measure changes related to visual evoked activity expected to be an order of magnitude smaller. However, the authors were not certain that the α rhythm activity detected is due to neuronal currents, particularly as unexplained behaviour mimicking α waves occurred in vessels/CSF.

In another study by the same group, Leach et al. (Leach, 2004) reported a significant correlation ($p<.01$, corrected) of the phase image signal to the power of alpha-wave oscillations, as determined from simultaneously acquired electroencephalogram (EEG) data, but found no significant activation by BOLD analysis.

Performing EPI at 1.5 and 3 T, respectively, two other groups reported analysis of both phase and magnitude images. In both, Kilner et al. (Kilner, 2004) found a significant ($p<.05$, corrected) component in the visual cortex that was phase locked to a visual flicker stimulus of 10 Hz, outside the band containing BOLD response. However, a recent study attempting to replicate Kilner's study failed to detect effects of direct neuronal activity (Parkes, 2007). At 3 T, Chu et al. (Chu, 2004) attempted to separate BOLD from neuroelectric signals. However, they were unable to detect fast MR signals associated with a visual stimulus whether they analyzed phase or intensity images.

Chow et al. (Chow, 2006) demonstrated the possibility of detecting changes of 0.15 ± 0.05 % of the equilibrium MR signal acquired at 1.5 T from the optic nerve of dark-adapted adult human subjects which is consistent in amplitude and frequency with the expected magnetic fields from synchronized and extended action potential bursts in axons of the optic nerve due to repetitive strobe light stimulation in the range 0.7–3.3 Hz. The effect may also be consistent with a very fast residual component of the BOLD response; however, this is thought to be less likely at the higher stimulus frequencies used in this study.

Petridou et al. (Petridou, 2006) recently studied rat cell cultures at 7 T in a planar configuration which showed spontaneous electrical activity as detected by a set of surrounding electrodes and which could simultaneously be detected by magnetic modulation in both magnitude and phase spectra (Petridou et al.,2005). The electrical activity was terminated on introduction of a cell toxin (tetrodotoxin) to the preparation and difference spectra formed. The

phase spectra provided a more clear demonstration of the activity than the magnitude spectra in this study.

Xiong et al. (Xiong, 2003) detected a signal decrease of about 1% from baseline in visual, sensorimotor, and pre-motor cortices with appropriate latencies, locations, and lateralities during a visuomotor evoked response paradigm in humans. They produced images with spatial resolution of 3 mm and temporal resolution of 100 ms. These changes were arguably too large to be explained away as the "initial dip" in the BOLD signal and roughly one order of magnitude larger than that predicted by Bodurka et al. (Bodurka, 1999; Bodurka, 2002) for phase images. The measured neuroelectric signal also fell within the range of 0.5–5% predicted by their theoretical modelling based on a quadratic dependence of signal on TE. According to the analysis by Chow et al. (Chow, 2006), no details of Xiong's quadratic model have yet been published. Their study used very long echo times (up to 100 ms) to allow for long phase integration, potentially increasing sensitivity but also creating echo planar images highly prone to distortion and phase accumulation errors due, for example, to residual eddy currents. The images used to calculate their time series data were acquired with long TR (1000 ms) and synthesized retrospectively from six successive runs acquired at approximately 2 min intervals. This makes the time series very vulnerable to motion artefact and slow scanner drifts and, as such, not really suited to measuring waveforms and correlations from real-time processes occurring in the tens of milliseconds range. In addition, recent studies attempting to replicate Xiong's study failed to detect effects of direct neuronal activity (Chu, 2004; Parkes, 2007).

Liston et al. (Liston, 2004b) retrospectively analyzed data acquired as part of an fMRI study to assess the possibility of large spiking currents (finite impulse responses (FIRs)) associated with seizures in epilepsy patients. This study showed possible evidence for detection of generalized spike wave discharge (GSWD) complexes which are thought to be at least twenty times larger than evoked responses, based on EEG voltage measurements. However, according to the analysis by Chow et al. (Chow, 2006) the study was performed with a long TR of 3000 ms, and so the signal time courses were subject to aliasing of the 3 Hz bursts which fell between rebinned slice locations.

Park et al. (Park, 2004; Park, 2006) have studied snail ganglia *in-vitro*, where no BOLD effect occurs, and chemically induced change in extracellular potential. They reported large changes of 3% in the magnitude of the MR signal during neuronal activity which could be ascribed to the reduced partial volume effects in virtue of giant axonal sizes and small imaging voxels.

Overall, the controversy and inconsistency between the different studies measuring both phase and magnitude changes demonstrate that the sensitivity for detecting spontaneous and smaller evoked neuronal currents is too low to be of practical use with existing MRI techniques. Recent advances in development of ultra fast fMRI reconstruction methods have allowed an

improved time resolution of 20 ms which will be essential if direct MRI mapping of neuronal activity can be convincingly shown (Lin, 2006).

1.2.2.5 DOI

According to recent reviews (Mehta, 2004; Steinbrink, 2005), several groups have explored fast changes in optical signals following sensory stimulation (Gratton, 2001; Wolf, 2002; Franceschini, 2004; Boas, 2004; Steinbrink, 2005; Low, 2006; Gratton, 2006). These effects are believed to arise more directly from neuronal depolarization than from metabolism and result from changes in neuronal volume or refractive index and occur within ~1 ms or less of neuronal activation. These faster phenomena alter light scattering by 0.0001-0.01% and remain poorly understood and hard to detect (Cohen, 1973; Stepnoski, 1991).

The fast neuronal signal was detected in the motor cortex with time resolution of 16 ms, spatial resolution of 8 mm, signal to noise of 3.6 and averaging lasting 5 minutes (Wolf, 2002). Gratton's group (Gratton, 2001; Low, 2006; Gratton, 2006) measured the fast optical signal over the visual cortex during visual stimulation. Recent work by Boas's group (Franceschini, 2004; Boas, 2004) report 2D mapping of fast neuronal activity over the surface of the cortex resulting from motor task and somatosensory stimulation with 25 ms time resolution, spatial resolution of ~10 cm and SNR of ~10. However, the encouraging findings of these groups could not be reproduced by other groups employing similar methods (Syre, 2003; Steinbrink, 2005).

Applications of non-invasive optical imaging methods to image the fast neuronal signals are still preliminary and require further validations but are generally seem to be promising way of obtaining information from the surface of the cortex. However, the lack of penetration of near infra-red (NIR) light into the highly scattering white matter limit the fast optical imaging methods form detecting activity in deep structures, providing true 3D imaging.

1.2.2.6 LF-EIT and MD-EIT

EIT has the potential to achieve non-invasive functional imaging of fast neuronal activity in the human brain (Holder, 1987; Boone, 1995b). The principle is that electrical impedance changes over milliseconds when neuronal ion channels open during activity, and this could be imaged by EIT. Imaging neuronal activity using EIT methods is the theme of this thesis and will be described in detail in the following sections and chapters. If successful, this method is expected to achieve a time resolution of about 1 ms, similar to EEG and MEG and spatial resolution of about 1 cm. It is also expected to be more sensitive to deep sources in addition to cortical sources which EEG and MEG methods are mainly sensitive to.

1.2.2.7 Invasive methods

Subdural Electro-corticography (ECoG) and depth electrodes: this is the invasive equivalent of EEG. It is mainly used for pre-surgical localization of epileptic sources and mapping of essential functional regions.

Optic dyes: optical imaging method using voltage sensitive dyes applied to the exposed cortex in vivo (Grinvald, 1992). This method is only used in animal models for brain research but was shown to produce images of neuronal activity with a time resolution of ~1 ms and excellent spatial resolution of 50 μm (Shoham, 1999; Seidemann, 2002). The main limitations of this method are the need for exposure of the brain and that mapping could be achieved only for the outermost layers of the cortex with a depth of less then 1 mm.

Electron Spin Resonance (ESR): this method is based on the electromagnetic field produced by an unpaired electron. Depolarization was previously recorded using potential-sensitive spin label (Cafiso, 1978). This method was suggested by Holder (Holder, 1987) as an alternative method for imaging neuronal activity but has hitherto not been investigated as a result of the possible toxicity of the labelling contrast agent which requires free radicals.

1.3 Electrical Impedance Tomography (EIT)

1.3.1 Introduction to bioimpedance

The body can be considered as a composite volume conductor comprising a number of spatially distributed tissues with differing electrical properties (Geddes, 1967). Electric conduction within biological tissues occurs through movement of mobile ions. Such conduction is related to the ionic content and ionic mobility of each particular tissue type. Functional activity, as well as pathophysiological conditions, results in structural and histological changes in the tissue. These changes accompanied by a characteristic temporal and/or spectral electric behaviour. Knowledge regarding the spatial dielectric properties distribution can provide useful information regarding the functional and pathological condition of the tissues.

Live tissue impedance consist of a resistive (such as the intracellular space, extracellular space and the membrane resistance) and reactive components (such as the bi-lipid layer of the cell membrane); together they manifest a dispersive medium behaviour. Sharp conductivity increase accompanied with a profound decrease of the relative permittivity, occurs in three main steps over frequency, known as the α, β and γ dispersions (Schwan, 1957). (Figure 1-1)

The low frequency α dispersion is associated with three factors: 1) Frequency - dependent conductance of the proteins channels in the cell's membrane. 2) Frequency - dependent counter-ion atmosphere near charged cell surface. 3) Endoplasmic-reticulum effect, which is relevant for muscle tissues only. The β dispersion, typically manifested at hundreds of kilohertz region, is mainly due to the polarisation of cellular plasma membranes, which act as barriers to the flow of ions between the intra and extra cellular media. The plasma membrane capacitance, the cell radius and the fluids conductivities determine the associated relaxation time. Additional contribution to this dispersion is due to polarisation of proteins and other organic macromolecules. The γ dispersion is due to the polarisation of water molecules. Tissue's water displays a broad dispersion spectrum, ranging between 100MHz and few GHz (Schwan, 1983)

Figure 1-1: Distribution of relaxation time of the muscle (Hurt, 1985).

1.3.2 The role of EIT

Electrical Impedance Tomography (EIT) is a developing medical imaging modality that provides information regarding the internal electrical properties inside a body based on non-invasive voltage measurements on its boundary. Data acquisition is performed through an array of electrodes which are attached to the boundary of the imaged object. Sequences of small insensible currents, typically in the order of 1 mA, are injected into the object through these electrodes and the corresponding boundary electric potentials are measured over a predefined set of electrodes. The process is repeated for numerous different configurations of applied current (Figure 1-2). The internal admittivity (or impedivity) distribution can be inferred using this boundary data.

Figure 1-2. EIT data acquisition principle. Single or multi-frequency current waveform are injected through set of electrodes, while boundary voltages are recorded through a predefined set of electrodes (Horesh, 2006a)

EIT was first proposed as a medical imaging method in 1978 by Henderson and Webster (Henderson, 1978), and in 1980 uniqueness was proven for the linearised inverse problem by Calder´on (Calder´on, 1980). The realisation and popularisation of the method can be attributed mainly to Barber and Brown (Brown, 1985; Brown, 1987). The first three-dimensional EIT images were for the chest and were reported in Nature by Metherall and colleagues in 1996 (Metherall, 1996).

The potential medical applications of EIT are vast, including detection and classification of tumours from breast tissue (Mueller, 1999; Mueller, 2001; Soni, 2004), detection of pulmonary emboli and oedema (Newell, 1996; Cheney, 1999), monitoring of pulmonary and cardiac functions (Eyuboglu, 1988; Brown, 1994; Frerichs, 2000; Frerichs, 2002; Isaacson, 2006), gastric imaging (Smallwood, 1994; Soulsby, 2006), imaging the eye (Jurgens, 1996), detection

and monitoring of cerebral ischemia and haemorrhage (McArdle, 1988; Holder, 1992b; Gibson, 2000; McEwan, 2006; Romsauerova, 2006b), localisation of epileptic foci (Bagshaw, 2003; Fabrizi, 2006b), normal haemodynamic brain function (Tidswell, 2001) and neuronal activity (Holder, 1987; Boone, 1995b).

In the 1930's, a similar technique was suggested for geophysics applications, namely Electrical Resistivity Tomography (ERT). This method is used to locate resistivity anomalies using electrodes on the surface of the earth or in bore holes. In the field of industrial process tomography, this method is used to monitor mixtures of conductive fluids in vessels or pipes (Williams, 1995) and for non-destructive testing and evaluation of materials and machine parts (Kaup, 1996; Bryan, 2006).

In the past two decades, there have been major advances in medical imaging, with the development of hard-field imaging methods, such as Magnetic Resonance Imaging (MRI), X-ray Computer Tomography (CT) and Positron Emission Tomography (PET). In spite of their immense benefits, these methods are all immobile, expensive, and image either anatomy or slow metabolic changes over time. Conversely, EIT is non-invasive, portable, inexpensive, and can potentially provide a high temporal resolution of the order of tens of milliseconds.

1.3.3 Imaging haemodynamic brain function with EIT

The main two mechanisms for haemodynamic impedance changes in the brain are:
Impedance decrease due to increased blood volume: during physiological activity, a signal is sent to the blood vessels which increases blood flow and blood volume to that cortical area (Malonek, 1997). As blood has a lower resistivity than the surrounding brain (150 Ωcm and 350 Ωcm, respectively), the increase in the lower resistivity volume of blood will allow more current to flow through that area of tissue and decrease the bulk impedance of that volume of cortex (Figure 1-3 left).

Impedance increase due to cell swelling: during normal function, the size of the conductive extra-cellular space (ECS) is 20% of the brain volume. During epilepsy, moderate cell swelling occurs as water and ions enter the glial cells and the neurones (Lux, 1986), and the volume of the low resistivity ECS is reduced. This will increases the bulk impedance of that area of cortex. Larger changes of cell swelling are seen during ischemia and spreading depression, which cause much larger increases in brain impedance (Holder, 1992a; Boone, 1994) (Figure 1-3 right).

EIT has demonstrated preliminary images for the normal haemodynamic brain function (Tidswell, 2001) (Figure 1-4) and for localisation of epileptic foci (Bagshaw, 2003; Fabrizi, 2006b) (Figure 1-5).

Figure 1-3: Mechanisms of haemodynamic impedance change within the brain. Left: due to blood volume change (neuronal cells in green, blood vessel in the centre of the cells). Right: due to cell swelling (Tidswell, 2006).

Figure 1-4: Examples of EIT images in adults with scalp electrodes during visual evoked responses (Tidswell, 2001).

Figure 1-5: Reconstructions of data collected approximately 6 s prior to the electrographic onset of two right temporal complex partial epileptic seizures (Bagshaw, 2003).

1.3.4 Instrumentation

Three main EIT systems have been recently used in the UCL group for studies on impedance changes in the human brain related to stroke and epilepsy (Fabrizi, 2007)(Figure 1-6):

UCH Mark1b: this utilizes a single four electrode impedance-measuring circuit with an analogue demodulator which is multiplexed to up to 32 electrodes (Yerworth, 2002). It serially addresses software selectable electrode combinations. The current source and cross point switches are included in a small head box separated from the main base box by a ribbon cable of 5 m, which was intended to enable continuous monitoring over days in ambulatory epilepsy subjects. The in-phase component of the impedance is measured with an analogue phase sensitive-demodulation voltage sensing circuit. A programmable gain amplifier is used to minimize the digitization noise for each electrode combination. It operates at a single selectable frequency between 225 Hz and 65.5 kHz and can apply a current of up to 5 mA peak-to-peak at 50 kHz. Leads to the patient are unscreened and so kept as short as possible, typically about 30 cm.

UCH Mark2.5: this utilizes one module of the Sheffield Mark3.5 multifrequency EIT system (Wilson, 2001), which comprises a four electrode impedance measuring circuit, multiplexed up to 32 electrodes (McEwan, 2006). The in-phase voltage is calculated with synchronized digital demodulation and has a single gain which was optimized for the range of the transfer impedance of the head of up to 70 Ω (McEwan, 2006). It can operate at frequencies between 20 Hz and 1.6 MHz. It employs a multifrequency composite waveform and records a

total of 30 frequencies, divided into three sequential packets of ten frequencies (Romsauerova, 2006a). The current is fixed at 0.28 mA peak-to-peak for each frequency. Leads to the patient are unscreened.

KHU Mark1 16 Channel: this comprises a single current source which may address any electrode pair using a multiplexer and 16 parallel voltmeters in a novel radially symmetric architecture (Oh, 2007). It employs a digital phase-sensitive demodulator and current waveform generator. In principle, multiple frequencies may be synthesized and injected from the available range, 39 Hz to 500 kHz. The system employs general impedance converters which are individually calibrated for each electrode recording pair to optimize the output impedance at each frequency and the electrode leads are with an outer shield and inner driven screen.

For the application of measuring impedance changes related to neuronal activity which is the theme of this thesis, these systems were not suitable since they were not designed to operate near DC as would be required for neuronal activity. A dedicated prototype hardware was developed for this application as part of this thesis and is described in Ch. 4 and 6.

Figure 1-6: EIT systems used in this study. Top left—UCH Mk1b; top right—UCH Mk2.5; lower—KHU Mark1 16 channel. The two latter are shown connected to the cylindrical tank (Fabrizi, 2007).

1.3.5 The limitations of EIT

As opposed to hard-field imaging modalities which rely on collimated radiation beams which follow a well-defined straight-line trajectory such as in CT or PET, in EIT the electric current paths are less definite. Electric current propagates in body tissue through ionic interaction, which is intrinsically diffusive. From a mathematical perspective, the problem of recovering inner admittivity distribution from boundary information is a nonlinear *inverse problem*. Moreover, the problem is also severely ill-posed in the sense that even small errors in the measured data may cause arbitrarily large errors in the estimate of the internal admittivity. In the presence of measurement noise, the solution can become unstable. Due to these inherited limitations, the spatial resolution of EIT reconstructed images is generally relatively poor.

1.3.6 Modelling and image reconstruction

EIT images, reconstructed from the boundary impedance measurements, represent a spatially smoothed and low resolution image of the impedance changes within the object, which in this thesis is the human head or head-shaped tank phantoms. In these images, the pixels are inversely related to the conductivity changes, $\Delta\sigma$. These conductivity changes are related to voltage changes measured at the scalp, ΔV, when a current is applied to the head. This relationship is expressed in matrix form by:

$$\Delta V = \mathbf{A}\,\Delta\sigma \qquad (1\text{-}1)$$

Where $\mathbf{A}$ is known as the sensitivity matrix. The problem is to solve the equation to find $\Delta\sigma$, given the changes in the measured boundary voltages, ΔV. There are two steps to this problem:

1. The *forward solution*, which creates a simplified analytical or numerical model of the head (Figure 1-7), in order to calculate the sensitivity matrix, $\mathbf{A}$. Accurate forward models need to be capable of representing reliably the governing partial differential equations (PDE) associated with the problem over complex geometry with an inhomogeneous impedance distribution and non-trivial boundary conditions (Vauhkonen, 1999; Liston, 2004a; Tizzard, 2005).
2. The *inverse solution*, which inverts the sensitivity matrix. Once the inverted sensitivity matrix, $\mathbf{A}^{-1}$ is calculated,

$$\Delta\sigma = \mathbf{A}^{-1}\,\Delta V \qquad (1\text{-}2)$$

From which the image of impedance change in the head can be calculated for any set of measured voltage changes. The conductivity changes, $\Delta\sigma$, at each pixel are inversely related to the resistivity changes in the image. The *inverse solution* procedure uses this information to infer the internal properties from the boundary measurements. Due to the ill-posedness of the problem, conventional image reconstruction methods, such as back projection, cannot be used

reliably. Most reconstruction algorithms for EIT rely on a perturbation approach, in which small variations of the recovered parameters from a known reference state are assumed. Due to the ill-posedness of the problem, a-priori knowledge and assumptions are used in order to regularise and constrain the solution space (Vauhkonen, 1997; Kaipio, 1998). The general approach is to minimise an objective function, which include two main components: one represents the goodness of fit between the forward model and the given data, and the second include additional arguments which represent priors that are used to regularise, and consequently stabilise the solution (Lionheart, 2004).

Figure 1-7:FEM used for forward problem predictions and reconstruction algorithms with realistic geometry. The four layers are brain, CSF, skull and scalp (Bagshaw, 2003).

Image reconstruction can be categorised into two main approaches: *difference imaging* and *static imaging*. In difference imaging, two data sets are measured which correspond to two different target admittivity distributions. Based on the difference between these measurements, the difference in admittivity distributions can be estimated (Barber, 1989; Liston, 2002; Bagshaw, 2003). This approach is relatively robust, since most stationary noise and error sources are cancelled out. In static imaging, the image reconstruction process employs only a single data set of voltage measurements and the aim is to reconstruct the absolute admittivity distribution.

This approach involves highly accurate computation of the forward model in an arbitrary admittivity distribution (simulated reference) (Riu, 1995; Kolehmainen, 1997; Vauhkonen, 2000). Such accurate models are typically of large-scale and therefore, introduce great computational difficulties for forward modelling and inverse problem solution.

Apart from introducing priors into the reconstruction procedure, image fidelity can be improved by the addition of independent information, and, in particular, by harnessing spectral information. This information can be used in order to constrain the inverse solution to physiologically plausible solutions. Moreover, this information is essential for improved forward modelling, which allows accurate predictions of the impact of functional and pathological conditions over the boundary voltage, and therefore assists in acquisition and hardware design. It is, therefore, crucial to get a firm understanding for the spectral tissue characteristics as well as the various mechanisms which characterise functional and pathophysiological behaviour. The addition of spectral information results in the requirement for solving multiple forward and inverse problems of larger scale. This requires development of appropriate forward and inverse problem frameworks which can efficiently treat large-scale problems.

The application of EIT algorithms for the purpose of modelling in this thesis are within the UCL group SuperSolver package (Horesh, 2006c), which incorporates a modified version of the EIDORS 3D package (Polydorides, 2002). The code solved the generalised Laplace equation using Neumann to Dirichlet map to obtain the voltages of each element and used the continuum form of Ohm's law to translate into current densities.

1.3.7 Magnetic methods in EIT

The overall sensitivity of a single EIT measurement to local impedance changes during four terminal measurements (2 drive and 2 measure electrodes) is governed by two physical processes:

1. *Current injection:* only a small proportion of the current injected through the drive electrodes reaches the Region of Interest (ROI) in the brain as a result of a current shunt path over the scalp, the highly resistive skull barrier, an additional shunt path through the CSF and the partial volume of brain ROI in relation to the entire brain volume. In a magnetic equivalent, the current would be induced, for instance by using coils. Due to the transparency of the skull to magnetic field, the induced current could be more focused since there are no shunt paths, the current density at the ROI could be higher and hence the measurement SNR (Freeston, 1995).
2. *Voltage measurement:* in EEG, the electrical potentials measured on the scalp due to endogenous neuronal currents are often strongly influenced by various inhomogeneities in the head, mainly the skull, making accurate determination of the activated area difficult. However, MEG could localize the activity more accurately since the skull is transparent to magnetic field (Hamalainen, 1993). A similar advantage might be beneficial in EIT if magnetic field produced by the injected (or induced) current is measured (Ahlfors, 1992).

Several magnetic variants of EIT have been previously proposed which utilize either MRI, superconducting quantum interface devices (SQUID) used in MEG technology or coils to detect the magnetic field resulting from an injected or induced current. These variants differ by the activation and sensing methods (Table 1-3). In Induced Current EIT (IC-EIT) (Freeston, 1995; Zlochiver, 2004) coils are used to induce currents while electrodes are used to measure voltages. In Magnetic Induction Tomography (MIT) coils are used to induce eddy currents and to measure the external magnetic field (Gencer, 1999; Karbeyaz, 2003; Merwa, 2004; Rosell-Ferrer, 2006). The recently proposed Electromagnetic Impedance Tomography (EMIT) technique (Levy, 2002) uses EIT electrodes for injecting current and measuring voltages, but the boundary voltages are augmented by small number of exterior magnetic field measurements recorded using coils for improving the conditioning of the EIT problem. Another type of magnetic method known as MR-EIT (Ider, 2003), which was derived from Current Density Imaging (CDI) (Joy, 1989), uses magnetic resonance methods to measure the internal magnetic field induced by a current injected from surface electrodes. This method was also combined with conventional surface potential measurements (Voltage Scaled MR-EIT) (Birgul, 2003) or with coils to induce current instead of surface electrodes (Induced Current MR-EIT) (Ozparlak, 2005). The advantages and limitations of the different approaches are discussed elsewhere (Ireland, 2004) and are beyond the scope of this study.

Table 1-3: activation and sensing methods for different magnetic variants of EIT.

Method	Activation	Sensing
EIT	Electrodes	Electrodes
IC-EIT	Coils	Electrodes
MIT	Coils	Coils
EMIT	Electrodes	Electrodes + coils
MR-EIT	Electrodes	MRI
VS-MR-EIT	electrodes	MRI + electrodes
IC-MR-EIT	Coils	MRI
MD-EIT	Electrodes	SQUIDs or coils

1.3.8 Magnetic Detection EIT

Another approach known as Magnetic Detection EIT (MD-EIT) or magnetic impedance tomography was proposed for biomedical applications by Ahlfors and Ilmoniemi (Ahlfors, 1992). This method uses a pair of electrodes to inject current to an object, and an array of SQUIDs to measure the induced magnetic field. They used a single pair of electrodes to inject current at 16 Hz through a saline filled tank containing insulating cylinder, measured the external magnetic field 30-50 mm above the tank by a 24 SQUID system and reconstructed images of current density using minimum-norm estimates (Ahlfors, 1992). The use of MD-EIT for biomedical applications was preceded by geophysics applications with technique termed magnetometeric resistivity (MMR) (Edwards, 1974).

Although SQUIDs have superior sensitivity over coils, they are suitable only for low frequencies below 1 kHz. Therefore, as the typical band of interest for EIT so far was between 1 kHz and 2 MHz (Brown, 2003), most effort was made using the application of sensing coils (Tozer, 1999; Ireland, 2004) to image lung ventilation.

1.4 Impedance changes related to neuronal activity

1.4.1 Mechanism

It is well known that impedance across neurones changes during depolarization due to the action potential. Indeed, recording of impedance across the giant squid peripheral nerve was the way in which the mechanism of the action potential was first discovered by Cole and Curtis in 1939 (Cole , 1939). An 80 times decrease in impedance was found, which was due to increased flow of charged ions through the ion channels which opened in order to conduct the action potential. The basis of the idea for imaging impedance changes with EIT is that such changes will occur in bulk neuronal tissue when neurones in it are discharging. The biophysics of the impedance changes and volume conduction in the head are such that it is unlikely that fields significantly distant from the source will be large if due to action potentials in myelinated white matter. The largest impedance changes will be due, not to action potentials, but to graded neuronal depolarization which occur due to synaptic activity in the dendrites of grey matter (Liston, 2000; Liston, 2004a).

The mechanism is that current flows through the extracellular space in the brain at rest. At the low applied frequencies below 100 Hz envisaged for this application, almost none flows through the intracellular compartment, because the cell membrane at rest has a high resistance. When ion channels open during depolarization, current then flows into the intracellular compartment as well. When the intracellular compartment opens, the overall impedance will fall. This effect is primarily resistive, because the current is passing through saline ions in the intracellular and extracellular compartments, which act as conductance. At high frequencies this application is not expected to work as current can flow through the membrane regardless of the state of ion channels.

Even though the change in membrane resistance is large when ion channels open – about 80x – the net effect on bulk tissue resistance is relatively small – about a 1% decrease, because the extracellular path for the current flow is a very good conductor at rest, and several other factors come into play, such as the tortuosity of the neuronal architecture, proportion of neurones firing, and capacitance of the cell membranes (Liston, 2000; Liston, 2004a).

An important advantage of EIT is that this mechanism effectively rectifies the recording of ionic channel opening – resistance across the membrane can only fall. In this way, impedance falls irrespective of whether the neurotransmitter giving rise to the change is excitatory or inhibitory. One of the drawbacks of inverse source modelling of the EEG or MEG is that positive and negative fields will cancel if excitatory and inhibitory activity occurs in close proximity, so that activity cannot be recorded from a distance. With EIT, only a decrease can occur, so the opportunity to record the changes from a distance are much greater. A similar

rectifying effect occurs with optical methods which rely on changes in mechanical properties of neurones during depolarization, such as birefringence. However, a decreased ability to detect changes due to cancellation occurs with optical recording with voltage sensitive dyes and with MRI of neuronal currents.

1.4.2 Biophysical modelling of the local impedance changes

Biophysical modelling of the mechanisms responsible for such impedance changes were based on cable theory and were developed for the 1D case of compound action potentials (CAP) in a peripheral nerve bundle (Boone, 1995a; Boone, 1995b; Liston, 2000; Liston, 2004a) and for the 3D case of cortical activity during evoked response (Liston, 2000; Liston, 2004a). One important consequence of the modelling was that impedance changes would be maximal below 100 Hz. The models estimated local resistivity changes near DC to be 3.7% for peripheral nerve bundles and 0.06-1.7% for the cortex during ERs (Liston, 2000; Liston, 2004a).

These models depended on several detailed assumptions which are outside the scope of this summary. A critical one was the proportion of neurones which were depolarizing during physiologically evoked activity in cortex; this is not known. The figures above were based on the estimate that this proportion was 10%. If it was higher, then the proportional change would be higher than above. Therefore, the predictions of the cable theory model are limited by the large uncertainties in physiological parameters which make the prediction approximate to about one order of magnitude.

1.4.3 Early animal measurements

Using a four electrode system, and measuring the potential difference produced by current pulses of 0.3-0.7 ms in duration, Freygang and Landau (Freygang, 1955) reported a decrease of 3.1% ± 0.8 (SE) during direct cortical stimulation in the cat which were ascribed to membrane resistance changes of dendrites. Using a two electrode system (which may underestimate the changes) and Wheatstone bridge operating at 35 kHz, a decrease of 0.03 - 0.1% was reported in frog sciatic nerve (Chailakhian , 1957). Their experimental technique was subsequently used by others (Burlakova , 1959; Prudnikova, 1959) to investigate the time relationship between the action potential and the putative impedance change.

During visual and auditory evoked responses in the cat, and with a similar recording system operating at 10 kHz, a decrease of 0.003% in the cortex (Klivington, 1967; Klivington, 1968), and of 0.03% in subcortical nuclei (Galambos, 1968) was observed. The difference in results may partly be because evoked responses (ER), with natural stimulation, activate fewer fibres than the electrical stimuli used by Freygang and Landau (Freygang, 1955).

1.4.4 Validation of the modelling of local impedance changes in crab nerve and rabbit cerebral cortex.

The modelling was validated in direct physiological recording. First, the simpler case of the compound action potential in the unmyelinated walking leg nerve of the crab was addressed. A method was developed to measure the longitudinal impedance change during the depolarisation of the nerve bundle extracted from the walking leg of a crab, Cancer Pagurus (Holder, 1992c; Boone, 1995a; Barbour , 1998; Liston, 2000; Liston, 2004a).

The nerve bundle was suspended by a series of silver electrode hooks (Figure 1-8a) and impedance measurement was performed by injection of a stimulating and recording current, and recording of the resulting voltage (Figure 1-8b). As this contained voltages due to both the action potential and the applied 2 Hz square wave, a sophisticated method for subtraction of the action potential signal was developed (Boone, 1995a). The collective depolarisation of the nerve fibres generated a compound action potential (CAP), which propagated along the nerve (Figure 1-9). Measured resistance changes of 0.5-1.0% were close to those predicted by the cable theory modelling and were taken as evidence that it was valid (Holder, 1992c; Boone, 1995a; Barbour , 1998; Liston, 2000; Liston, 2004a).

(a) *(b)*

Figure 1-8: (a) Photograph and (b) diagram of experimental set-up for measurement of longitudinal resistance changes in unmyelinated crab peripheral nerve axons, suspended on silver electrodes (Liston, 2004a).

Figure 1-9: A typical trace showing the CAP and the percentage resistance change observed when a measurement is made on crab peripheral nerve (Liston, 2004a).

A full study of the amplitude of impedance changes in cerebral cortex has not yet been performed. Some very preliminary measurements have been undertaken in two animals, using electrodes placed on the exposed surface of the cerebral cortex in the anaesthetized rabbit, during a somatosensory median nerve evoked response and using measurement current of 2 Hz square wave, injected between electrodes 1-3 mm apart and measured voltage between electrodes 9 mm apart. Measured changes were 0.01-0.03% (Boone, 1995a). These changes are lower by an order of magnitude from the modelled changes for the cortical case (0.06-1.7%). However, these were collected in an anaesthetized animal in which there was suppression of cortical activity by the anaesthetic, and the response may have been affected by local tissue trauma and bleeding around the electrodes. An earlier attempt on rats using direct electrical stimulation of the cortex and measurement at 50 kHz did not show any changes larger than the sensitivity of the measurement of 0.01% (Holder, 1988).

In view of these results and the earlier animal measurements presented in Section 1.4.3, it is therefore not yet clear what the true changes in cerebral cortex are during evoked activity. Further modelling and non-invasive measurements in humans for quantifying this crucial figure are presented in this thesis whereas further invasive animal models were left for future work.

1.4.5 Previous human measurements

Since EIT was originally proposed for use in imaging neuronal activity (Holder, 1987), very few studies have been presented in which attempts were made to measure impedance changes of neuronal activity on humans. Previous studies suffered from major technical limitations and are described below.

Holder (Holder, 1989) recorded impedance changes at 50 kHz during somatosensory, auditory and visual evoked responses, and was unable to detect any reproducible changes larger than 0.002 or 0.02% (depending on electrode configuration and period of measurement). The negative results could be ascribed to the measurement at 50 kHz instead of low frequencies below 100 Hz, shown in later studies to be essential (Boone, 1995a; Boone, 1995b; Liston, 2000; Liston, 2004a).

Enfield (Enfield, 2005) attempted to measure resistivity changes using 1 Hz square wave on humans during visual evoked responses. The drive electrodes were placed in a polar arrangement on opposite sides of the head above the ears and a pair of recording electrodes where located on the back of the head when the amplitude of the square wave was maximal without saturating the acquisition amplifier. No significant changes which could be regarded as genuine impedance changes were observed. The main limitation in the method which prevented her from obtaining meaningful results was the use of a low dynamic range acquisition system,

insufficient averaging resulting in noise levels in the order of 1% and using sub-optimal electrode placement.

A research group in Process Tomography at Manchester has presented in conference abstracts but not a peer reviewed journal data of images of neuronal activity during visual evoked responses obtained with an industrial 2D EIT system using a frequency of 9.6 kHz in two subjects. They claimed to have recorded boundary voltage changes of about 50% (Murrieta-Lee, 2004; Murrieta-Lee, 2005; McCann, 2005). It is difficult to explain these findings on a physiologically plausible basis as 1) the frequency of 9.6 kHz is too high for neuronal activity related changes to occur as current can flow freely though the capacitive barrier of the cells even during rest. 2) the predicted changes in my modelling study (Ch. 3) were 0.004%; the predicted changes in the order of 0.01% presented in a study by the same group for evoked responses (Towers, 2000) and the magnitude of changes below 1% measured for the haemodynamic changes in the brain during evoked response (Tidswell, 2001) which are expected to be higher than the changes due to neuronal activity. The authors have proposed a mechanism based on changes in the electrochemical state of synaptic connections in response to wide-field sensory stimuli. However, they did not provide any evidence to support the hypothesis that this mechanism could cause macroscopic changes in the volume which would be translated to 50% on the boundary. I therefore submit that the changes measured by this group were probably related to an artefact in their system and not to a physiological effect.

1.4.6 Extension to the complex case

Previously, theoretical and experimental investigations in our group for predicting and measuring fast impedance changes resulting from evoked neuronal activity, were focused on the real part of the impedance (resistivity) and at frequencies below 10 Hz, for which changes are expected to be maximal (Holder, 1992c; Boone, 1995a; Boone, 1995b; Barbour , 1998; Liston, 2000; Liston, 2004a; Enfield, 2005). However, for the cortical case at these frequencies, the physiological noise level originated from spontaneous brain activity is high, for instance about 10 μV in the occipital area when eyes are open. Therefore, measuring impedance changes above 100 Hz which is beyond the typical EEG band could be advantageous in terms of SNR, even though the signal level of the changes is lower. To evaluate this, I used the same equations from the cable theory model developed by Liston (Liston, 2000; Liston, 2004a) to estimate the changes across frequency for the real (resistivity) and imaginary (reactivity) parts of the complex impedance.

Significant changes are estimated to occur also at frequencies above 100 Hz for the reactive part and for the overall complex specific impedance changes (Figure 1-10). For instance, at 150 Hz, these impedance changes are only 2-fold lower than those expected for the resistive part

below 10 Hz. However, spectral analysis of sample EEG signals demonstrated that a 10-fold decrease in the spontaneous brain activity is expected at this frequency. Therefore, a 5-fold overall improvement in SNR would be expected.

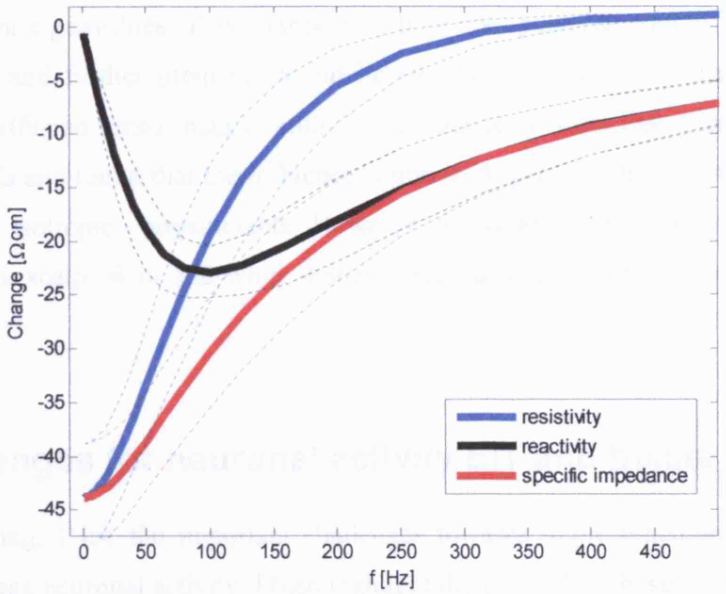

Figure 1-10: the real part (resistivity), the imaginary part (reactivity) and complex specific impedance changes predicted by the cable theory for the cortical model after substituting the frequency range in the equations derived by Liston (Liston, 2000; Liston, 2004a). Dotted lines are the standard deviations resulting from the uncertainties of the model parameter.

1.5 Dielectric properties of the head

The dielectric properties of the head compartments at frequencies below 1 kHz are required when studying the feasibility of developing EIT system for imaging fast impedance changes occurring within this band (see definitions in Appendix A). The dielectric characteristics were incorporated into the head model used in this thesis for estimating the boundary voltage changes (Ch. 3) and magnetic field changes (Ch. 5) resulting from local impedance changes during neuronal depolarization.

There is extensive data published on the dielectric properties of the normal tissues in the head. A recent exhaustive literature review which I co-authored was performed in our research group covering the properties of the skin, scalp, skull, cerebrospinal fluid (CSF), grey and white matter, blood and eyes (Horesh, 2006a; Horesh, 2007b). Representative values from this review were chosen for the simulations in this thesis (Ch. 2, Table 2-1).

Anisotropic conductivity properties are an important feature of the true structure of the head tissue (mainly the white matter, scalp muscle and the skull). This could greatly affect the forward model prediction as well as the inverse problem. Inclusion of anisotropic conductivity

tensors into the head models requires an accurate individual mapping of such properties. Recently, Tuch (Tuch, 2001) suggested to map the conductivity tensor using diffusion tensor MRI. He modelled and measured a strong linear relationship between the conductivity and diffusion tensor eigenvalues. This method may be a very powerful tool to enhance models for EIT purposes and further progress should be closely examined. Haueisen (Haueisen, 2002) adopted the diffusion tensor data to study the influence of brain tissue anisotropy on human EEG and MEG and found that the influence is minor. At present, the EIT methods used in this thesis assume isotropic compartments. However, the conductivity ranges used in this thesis (Table 2-1) for scalp, skull and white matter, cover anisotropic properties available from the literature.

1.6 Challenges for neuronal activity EIT and thesis goals

In the following, I list the important challenges towards implementation of an EIT system capable to image neuronal activity. I then highlight the partial list chosen to be addressed in this thesis.

1. Invasive studies
    a. Quantify local impedance changes in the brain – controlled models for direct measurement of the impedance changes during evoked activity locally in the brain over a range of frequencies. In view of the little volume of data available from previous studies, this is important for validating the cable theory predictions and identifying the optimal frequency. This could be approached using animal models and human epilepsy patients with implanted intracranial electrodes.
    b. Invasive imaging – implementing an imaging EIT system for animal studies and rare clinical cases such as epilepsy patients with implanted intracranial electrodes. The main advantage of this over non-invasive EIT is the absence of the highly resistive skull barrier which could increase the SNR and provide a simpler reconstruction problem.
2. Non-invasive studies
    a. Current level limit – since the SNR in EIT measurements is linear to the applied current level, it is desirable to apply the highest possible current without altering neuronal activity in the brain and causing unpleasant skin sensation due to excitation of skin pain receptors. The goal is to determine the maximal current levels which could practically applied on the scalp following these criteria.
    b. Realistic modelling of expected boundary voltage changes (forward problem). This is important for identifying the optimal electrode placements for real measurements and for evaluating the expected SNR and resulting implications for developing an imaging system.

c. Image reconstruction simulation study (inverse problem). This is important for quantifying the minimal SNR which would still allow reliable image reconstruction and for estimating the feasibility for developing and imaging system.
d. Human measurements – could any changes be measured non-invasively in humans, which what SNR and what are the possible implications for imaging system?
e. Could any of the magnetic variants of EIT be advantageous over conventional EIT for the neuronal activity application? For the evaluation of each magnetic method, forward and inverse modelling as well as actual measurements could be applied.

In this thesis, some of the non-invasive issues were addressed and all invasive aspects were left for future work. These included review of current effects on neuronal activity, skin sensation and the design of a suitable electrode for EIT (item 2a). For conventional EIT with scalp electrodes for applying current and measuring voltages, modelling was conducted for the forward problem (item 2b) but not for the inverse problem (item 2c) and series of human measurements were recorded (item 2d). In addition, similar modelling and human measurements were conducted for one magnetic variant of EIT out of the seven variants that have been previously suggested. This was Magnetic Detection EIT employing scalp electrodes for current injection and a MEG system for recording. More detailed description of the specific aims of this thesis is given in the following purpose and design section (1.7).

1.7 Purpose and design

The purpose of this thesis was to estimate the feasibility of non-invasive imaging of fast neuronal activity using EIT techniques. The long term goal is to develop the technology that will allow production of 3D movies of brain activity with sufficient time and spatial resolution (ideally ~1 ms and ~1 mm).

The specific aims of this thesis and the experimental design to address them are listed below. Modelling, phantom validations and human experiments were performed for both the electric (LF-EIT) and magnetic (MD-EIT) cases (Figure 1-11). To address the different questions, I chose to use visual evoked responses throughout the modelling and experimental studies. Pattern reversal checkerboard stimulation produces a strong response originated from the primary visual cortex V1 area (Di Russo, 2005). Comparing to other ER paradigms such as auditory or somatosensory stimulations, visual stimulation is technically easy to produce and has higher magnitude evoked potentials suggesting a larger population of neurons activated synchronously.

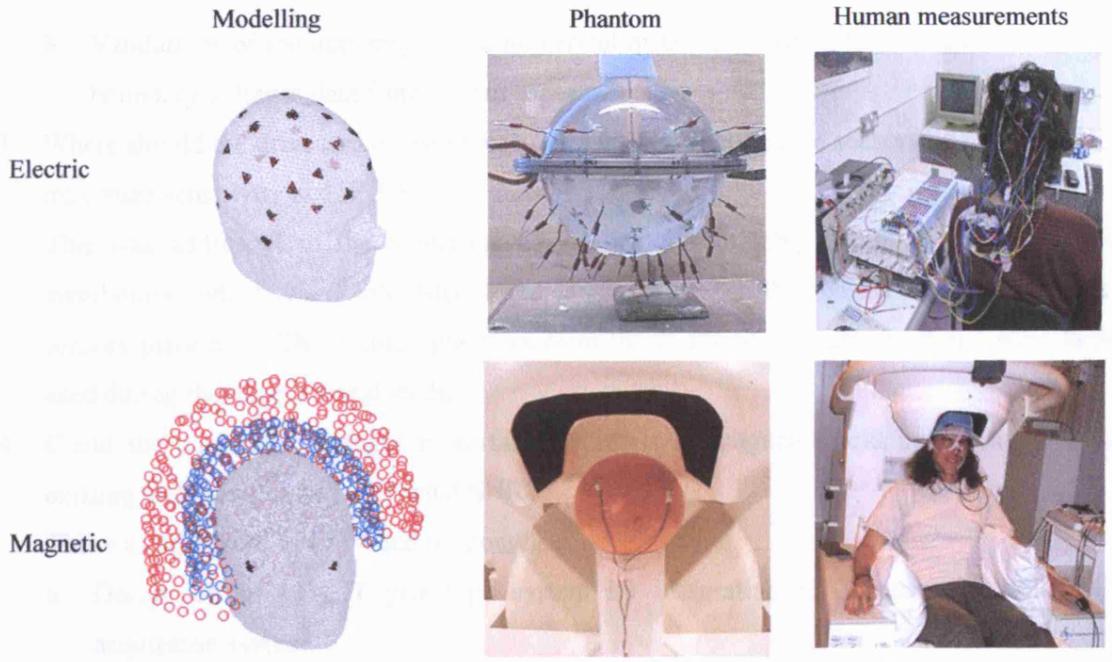

Figure 1-11: Top row – electric case measuring scalp voltages, bottom row – magnetic case measuring magnetic field outside the head. From left to right – numerical modelling, phantom validations and human measurements.

1. What is the highest current level, which could be used to maximize SNR in LF-EIT or MD-EIT experiments in terms of safety, skin sensation and minimizing the possibility altering the normal brain function with the applied current?
   This was addressed in Ch. 2 through:
   a. A literature review to identify and safely limits and current density thresholds for inducing skin sensation and for changing neuronal activity.
   b. Numerical simulations to quantify the current density in the brain and in the visual cortex when different electrode designs are used to inject currents at hundreds of different sites on the surface of a realistic head model.
   c. Novel electrode design for producing uniform current density at the contact area with the skin.
   d. Human experiments for determining skin sensation threshold with EEG electrodes and the novel design.
2. What are the expected changes in scalp voltages and in magnetic field in the vicinity of the scalp during visual evoked responses and LF-EIT or MD-EIT?
   This was addressed in Ch. 3 and 5 through:
   a. Numerical simulations to estimate the magnitude of the boundary voltages and external magnetic field changes during visual evoked response for LF-EIT and MD-EIT respectively.

b. Validations of the accuracy of the numerical methods in saline tank studies and using boundary voltages data from human experiments.

3. Where should the drive and measure electrodes as well as magnetic sensors be positioned to maximize sensitivity and SNR?

   This was addressed in the modelling Ch. 3 and 5 using the results of the numerical simulations, which were calculated for a large set of possible electrodes and magnetic sensors placement. The optimal positions from these sets were highlighted and were later used during the experimental studies.

4. Could the equivalent changes in surface potentials or magnetic field be measured with existing technologies and with what SNR?

   This was addressed in Ch. 4 and 6 through:

   a. Design of an LF-EIT prototype system by integrating EIT apparatus with EEG acquisition system.
   b. Validation of this system's sensitivity to fast resistance changes using resistor network and crab peripheral nerve bundle.
   c. A series of LF-EIT non-invasive human experiments during visual evoked responses with 1 Hz square wave injected current of up to 1 mA.
   d. Design of an MD-EIT prototype system by integrating EIT apparatus with MEG acquisition system.
   e. A series of MD-EIT non-invasive human experiments during visual evoked responses with 1 Hz square wave injected current of up to 1 mA.
   f. In all these experiments, current was injected through a single electrode pair but with recording from multiple electrodes or magnetic sensors.

5. Did the numerical and experimental estimations agree?

   This was addressed in the discussion of the experimental chapters (Ch. 4 and 6) and in the discussion (Ch. 7).

6. What are the main limitations of the modelling and experimental measurements?

   This was addressed throughout the chapters and in the discussion (Ch. 7).

7. Was the electric or magnetic method better and why?

   This was addressed in the discussion (Ch. 7).

8. What are the implications of the present findings for designing non-invasive imaging system?

   This was addressed in the discussion (Ch. 7) in view of the various modelling results and experimental studies.

9. What does the future hold for neural imaging with EIT and other modalities?

   This was addressed in the discussion (Ch. 7) as well as in the introduction (Section 1.2.2) for other modalities.

1.8 Publications resulting from this thesis

Refereed papers

Gilad O, Horesh L, Holder DS (2007) Design of electrodes and current limits for low frequency Electrical Impedance Tomography of the brain. *Medical & Biological Engineering & Computing, 45(7): 621-633*

Conference proceedings

Gilad O, Horesh L, Akselrod S and Holder DS (2007) Statistical analysis of non-invasive Low Frequency EIT human measurements of neuronal activity. *Proc. of XIII International Conf. on Electrical Bio-Impedance and VIII Conference on Electrical Impedance Tomography, IFMBE Vol 17, pp 548-551, Graz, Austria.*

Gilad O, Oh D, Ghosh A, McEvoy A and Holder DS (2007) Towards imaging neuronal activity using intracranial electrodes and low frequency electrical impedance tomography (LFEIT). *Theoretical Neuroscience Network meeting on invasive intracranial electrophysiology of the human brain: "non-clinical" studies in epilepsy patients, KCL, London, UK*

Gilad O, Horesh L, Akselrod S and Holder DS. Electrical impedance tomography – implications for non-invasive imaging of neuronal activity in the human brain. *Bulletin of the Israel Physical Society Vol 52. 2006. 52nd Annual Meeting of the Israel Physical Society, Jerusalem, Israel, December 2006*

Gilad O, Horesh L and Holder DS. Could Synchronized Neuronal Activity be Imaged Using Magnetic Detection Electrical Impedance Tomography (MD-EIT)? *VII International Conference on Biomedical Applications of Electrical Impedance Tomography, Joint Conference of World Congress on Medical Physics and Biomedical Engineering, Seoul, Korea, August 2006*

Gilad O, Horesh L and Holder DS. Use of Magnetoencephalography (MEG) to enhance imaging fast cerebral electrical activity with low frequency Electrical Impedance Tomography (EIT). *British Society for Clinical Neurophysiology, York, UK, 30th June 2006*

Gilad O, Horesh L and Holder DS. Non invasive imaging of synchronized neuronal activity using low frequency electrical impedance tomography. *Jiri Hozman and Peter Kneppo. 11[1], 179-182. 2005. Prague, IFMBE. Proceedings of the 3rd European Medical & Biological Engineering Conference - EMBEC'05. Prague, Czech Republic. 11-20-0005*

Horesh L, **Gilad O**, Romsauerova A, McEwan A., Arridge SR and Holder DS. Stroke type differentiation by multi - frequency electrical impedance tomography - a feasibility study. *Jiri Hozman and Peter Kneppo. 11[1], 1252-1256. 2005. Prague, IFMBE. Proceedings of the 3rd European Medical & Biological Engineering Conference - EMBEC'05. Prague, Czech Republic. 11-20-0005.*

Horesh L, **Gilad O**, Romsauerova A, Tizzard A, Bayford RH and Holder DS. Stroke type detection by Multi-Frequency Electrical Impedance Tomography (MFEIT) - Feasibility study. *VI International Conference on Biomedical Applications of Electrical Impedance Tomography, London, UK, June 2005.*

Gilad O, Horesh L, Ahadzi GM, Bayford RH and Holder DS. Could synchronized neuronal activity be imaged using low frequency electrical impedance tomography (LFEIT)? *VI International Conference on Biomedical Applications of Electrical Impedance Tomography, London, UK, June 2005.*

Gilad O, Ahadzi GM, Bayford RH and Holder DS. Near DC conductivity change measurement of fast neuronal activity during human VEP. *XII International Conference on Electrical Bio-Impedance, p 279-282, Gdansk, Poland, June 2004.*

Ahadzi GM, **Gilad O**, Horesh L, Bayford RH, and Holder DS. An EIT electrode protocol for obtaining optimal current density in the primary visual cortex. *XII International Conference on Electrical Bio-Impedance, p 621-624, Gdansk, Poland, June 2004.*

Holder DS, Bayford RH, Fritschy J, **Gilad O**, Kaube H and Binnie CD. Development of generic software for analysis, archiving & Internet dissemination of brain and systems physiological data *UK E-Science Programme All Hands Meeting, Nottingham, UK, 2004.*

Holder DS, Bayford RH, **Gilad O**, Kaube H and Binnie CD. Development of generic software for analysis, archiving & internet dissemination of brain and systems physiological data. *Bioinformatics workshop, Warwick, UK, October 2003.*

Holder DS, Bayford RH, **Gilad O**, Kaube H and Binnie CD. Development of generic software for analysis, archiving & internet dissemination of brain and systems physiological data. *Grid Outreach Workshop, The Grid in Medicine & Health Applications. Warwick, UK, November 2002.*

Departmental posters and presentation

Gilad O, Horesh L, Ahadzi GM, Bayford RH and Holder DS (2005) Towards imaging synchronized neuronal activity using low frequency electrical impedance tomography (LFEIT). *Poster session, Department of Medical Physics and Bioengineering, University College London, London, UK. 9-3-2005.*

Horesh L, Romsauerova A, **Gilad O**, Bayford RH and Holder DS (2005) Stroke type detection by Multi-Frequency Electrical Impedance Tomography MFEIT - Feasibility study. *Poster session, Department of Medical Physics and Bioengineering, University College London, London, UK. 9-3-2005.*

Gilad O, Ahadzi GM, Bayford RH and Holder DS (2004) Near DC resistivity change measurement of fast neuronal activity during human visual evoked potentials (VEP). *Poster session, Department of Medical Physics and Bioengineering, University College London, London, UK. 24-3-2004.*

Gilad O, Bayford RH and Holder DS (2003) Applying electrical impedance tomography to image neuronal depolarisation in the human brain. *Seminar presentation, Department of Medical Physics and Bioengineering, University College London, London, UK. 24-6-2003.*

Gilad O, Swenne CA, Davrath LR, Akselrod S (2002) An Accurate Characterization of Respiratory Sinus Arrhythmia (RSA) Pattern. *Seminar presentation, The Abramson Centre of Medical Physics, Sackler Faculty of Exact Sciences, Tel-Aviv University, Tel-Aviv, Israel. 11-7-2002*

Gilad O, Swenne CA, Toledo E, and Akselrod S (2002) Synchronization between heart rate, respiration and external sensory stimulation. *Seminar presentation, The Abramson Centre of Medical Physics, Sackler Faculty of Exact Sciences, Tel-Aviv University, Tel-Aviv, Israel. 27-6-2002*

Invited talks

Gilad O, Holder DS (2005) Electrical Impedance Tomography of the Human head. *Part of a lecture series in medical physics methods, The Abramson Centre of Medical Physics, Sackler Faculty of Exact Sciences, Tel-Aviv University, Tel-Aviv, Israel. 3-5-2005*

Holder DS, **Gilad O** (2005) Electrical Impedance Tomography of the Human head. *Queen Square EEG/MEG Club, Institute of Cognitive Neuroscience, University College London, London, UK. 12-5-2005.*

Gilad O, Holder DS (2005) Combined EIT and MEG method for imaging neuronal activity. *Project presentation, Functional Imaging Laboratory, Wellcome Department of Imaging Neuroscience, Institute of Neurology, University College London, London, UK. 20-5-2005.*

Holder DS, **Gilad O** (2005) Electrical Impedance Tomography of Neuronal Firing – Reality or Pipedream. *Department of Physics and Bioengineering, University College London, London, UK. 10-6-2005.*

Provisional plan for refereed papers to be submitted as a result of my work

Gilad O, Horesh L, Holder DS. Sensitivity requirements for non-invasive imaging of synchronized neuronal activity in the human visual cortex using electrical or magnetic detection impedance tomography. (IEEE Trans Biomed Eng)

Gilad O, Holder DS. Towards non-invasive imaging of synchronized neuronal activity in the human visual cortex using electrical electrical impedance tomography. (Neuroimage)

Gilad O, Holder DS. Towards non-invasive imaging of synchronized neuronal activity in the human visual cortex using magnetic detection electrical impedance tomography. (Neuroimage)

Horesh L, Romsauerova A, **Gilad O**, McEwan A, Arridge SR and Holder DS Review of the dielectric properties of the human head for Multi-Frequency Electrical Impedance Tomography (MFEIT). *(Med Biol Eng Comp)*

Horesh L, **Gilad O**, Romsauerova A, McEwan A, Arridge SR and Holder DS. Acute stroke classification by Multi-Frequency Electrical Impedance Tomography (MFEIT): a feasibility study. *(Phys Med.Biol)*

Fabrizi L, McEwan A, Yerworth RJ, **Gilad O**, Bayford RH, Holder DS. EEG signal recovery for clinical trials of simultaneous EEG and electrical impedance tomography (EIT). *(Med Biol Eng Comp)*

Fabrizi L, Horesh L, **Gilad O**, McEwan A, Holder DS. A feasibility study for imaging of epileptic seizures by EIT using a realistic FEM of the head *(Physiol Meas)*.

2. Design of electrodes and calculation of current limits for low frequency Electrical Impedance Tomography of the brain

2.1 Abstract

For the novel application of recording of resistivity changes related to neuronal depolarization in the brain with Electrical Impedance Tomography, optimal recording is with applied currents below 100 Hz, which might cause neural stimulation of skin or underlying brain. The purpose of this work was to develop a method for application of low frequency currents to the scalp, which delivered the maximum current without significant stimulation of skin or underlying brain. I propose a recessed electrode design which enabled current injection with an acceptable skin sensation to be increased from 100 μA using EEG electrodes, to 1 mA in 16 normal volunteers. The effect of current delivered to the brain was assessed with an anatomically realistic finite element model of the adult head. The modelled peak cerebral current density was $0.3A/m^2$, which was 5 to 25-fold less than the threshold for stimulation of the brain estimated from literature review.

2.2 Introduction

Electrical Impedance Tomography (EIT) is a recently developed medical imaging method with which true tomographic images of the internal electrical impedance of the body may be obtained with electrodes placed around the body region of interest. It is safe, portable, inexpensive and rapid. It has particular potential for imaging brain function in the head with scalp electrodes, where it could provide a low-cost portable system for imaging in acute stroke (Horesh, 2005), epilepsy (Fabrizi, 2006b), normal blood volume changes during evoked responses (Tidswell, 2001) or even millisecond scale small impedance changes related to neuronal depolarization during normal activity (Gilad, 2005b). For this purpose, current is injected into the head using surface electrodes on the scalp and images are reconstructed from the resulting scalp potentials. In the past, EIT imaging of brain function has been of differences over time which were principally related to changes in blood volume or cell swelling over tens of seconds, for which an applied current of 50 kHz was suitable (Holder, 1996) or of changes over frequency for cerebral ischemia, for which a set of frequencies between 2 kHz and 1.6 MHz were employed (Yerworth, 2003; Romsauerova, 2006a). However, the biophysics of current flow in the brain is such that applied current starts to pass significantly into the intracellular space above 100 Hz (Boone, 1995a; Liston, 2004a). For applications which require optimal distinction between the extra- and intra-cellular spaces, such as imaging neuronal depolarization (Gilad, 2005b), or distinction between haemorrhage and infarct in stroke (Horesh, 2007a), it is desirable to apply current at frequencies below 1 kHz and ideally below 100 Hz. Unfortunately, the threshold for stimulation of nerves falls rapidly at these frequencies. Whereas 5 mA can be safely injected at

50 kHz, the relevant British Standards (BS5724, 1979) require a current of less than 100 μA below 1 kHz; above these current levels, the risk exists of exciting pain fibres in the skin or neurones in the cerebral cortex. Nevertheless, it is desirable to inject as much current as possible in order to maximise the signal-to-noise ratio. Previous modelling predicted a signal-to-noise of 0.03-0.43 for an applied current of 100 μA while, in human measurements, the signal-to-noise was below 1 for most subjects using a current of 100-200 μA (Gilad, 2005b). A simulation study undertaken in our group, in which expected scalp impedance changes during temporal lobe epilepsy were modelled, showed that a signal-to-noise of 7 was needed to obtain images similar to noise free images (Fabrizi, 2006a); therefore it seemed desirable to increase the applied current by as much as possible.

In principle, EIT may be performed with injection of multiple frequencies at the same time (Yerworth, 2003) or through multiple electrodes simultaneously (Gisser, 1987). In the latter case, the safety considerations relate to the total current transmitted through all electrodes (Lionheart, 2001). The EIT system developed in the authors' group at University College London (UCL) is based on the design of the Sheffield systems (Brown, 1987), and employs the simpler approach of sequential current injection at a single frequency through a pair of electrodes. My immediate goal which led to this work was to determine if small impedance changes related to neuronal depolarization could be recorded with scalp electrodes, using current injection through a pair of electrodes; if successful, I planned to employ an EIT system based on the UCL design which also injected current sequentially through pair of electrodes. In this work, I have therefore just considered the case of current injection through pairs of electrodes.

The purpose of this paper was to develop a method which would allow the maximum permitted current to be delivered safely to the brain for low frequency EIT (below 1 kHz) without altering brain function or causing pain by skin stimulation. In pilot studies, use of conventional EEG cup electrodes caused painful skin sensations when the permitted current of about 200 μA was delivered, so a novel design was assessed, in which the electrode is recessed and filled with conducting gel in order to diffuse the current. In order to assess its effectiveness, it was necessary to determine the peak current density on the cortical surface as well as in a specific region, the primary visual cortex (V1) which was the region of interest in my intended neuronal activity imaging study. This was estimated with the use of a realistic Finite Element (FE) model of the head, as direct measurement was impractical in normal volunteers. The specific issues to be addressed were: a) which electrode design allowed the greatest current to be delivered to the scalp with minimal excitation of skin pain receptors? b) Could this current be delivered without causing significant stimulation of the underlying cerebral cortex or brain?

2.3 Methods

2.3.1 Electrode design for minimizing skin sensation

Eighteen subjects (ten male and eight female, age 23 to 52 years) participated in 25 recording sessions during the experiments described below. All subjects were in good health and had no known neurological conditions. The experiments were approved by the University College Hospitals ethics committee.

2.3.1.1 Experiment 1

Initial experiments were performed with conventional EEG cup electrodes and various arrangements of electrode gel. The recorded variables were the threshold of sensation and the maximal current level that would cause a tingling feeling on the surface of the scalp. A bipolar square wave current (1 Hz rate) was injected using two electrodes placed 5 cm above the inion and 10 cm apart, centred on the midline, in two subjects (one male and one female, age 52 and 31 years respectively). The initial current level was 100 μA and was increased in steps of 100 μA until the subject indicated perception of the current or an unpleasant feeling.

1. Perception was recorded with standard Ag/AgCl EEG cup electrodes of 11 mm diameter applied to abraded skin under the electrodes area using Ten20 conductive EEG paste (D.O. Weaver and Co., Aurora, CO, USA). The conductivity of the Ten20 paste, measured with an HP 4284A impedance analyser, was 0.3718 ± 0.0011 S/m over 20-200 Hz. The thickness of the Ten20 paste buffer layer was approximately 1 mm.
2. The experiment was repeated with the same arrangement and 11 mm diameter electrodes, except that the abraded surface was increased to 30 mm diameter and four times the amount of conductive gel was used to cover the extended area.
3. With the male subject, two additional electrode placements were tested: a) The electrode was placed on top of a 10 mm high cone, 15 mm in diameter at its apex, of conductive paste in the middle of the 30 mm diameter abraded area and b) 4 electrodes linked together using 100 kΩ resistors were placed on one of the 30 mm diameter surfaces.

2.3.1.2 Experiment 2

A conical recessed electrode design was employed (based on (Suesserman, 1991)). It was made from polyoxymethylene (POM), filled with Ten20 conductive EEG paste, and had an Ag/AgCl disc, 14 mm diameter, at the vertex and circular opening to abraded skin of diameter 21 mm (Figure 2-1). The choice of geometrical parameters was based on the conclusions and recommended design in Suesserman's study (Suesserman, 1991): uniform current density was desirable at a) the metallic electrode surface and b) at the electrode aperture where the electrode-skin contact is made.

The former was required to minimize irreversible electrochemical reactions and was achieved by conductive paste filled cylindrical recession of depth r, where r is the metallic electrode radius. This produced uniform current density at the metallic electrode surface but due to charge separation, non-uniformity of 200% was measured at the electrode aperture (Suesserman, 1991).

Uniform current density at the electrode aperture was required to minimize current density at the tissue surface, so preventing tissue damage in their cochlear implant application (Suesserman, 1991) and skin sensation in the EIT application. This was achieved by alteration of the cylindrical recession profile into a conical profile with an r/2 increase in radius along the recessed profile (Figure 2-1). A smaller increase in radius would get closer to the cylindrical case and a larger increase in radius would unnecessarily increase the overall electrode size.

In this EIT application, the choice of r = 7 mm was made after pilot measurements with a larger radius of 9 mm gave similar results.

This design was tested on three subjects (two male, age 27 and 43 years and one female, age 40 years) and compared to a conventional cup EEG electrodes as above, on abraded skin. Current waveform, electrodes positions and measurement protocol were identical to those in Experiment 1. Both the threshold and slightly unpleasant perception levels were recorded.

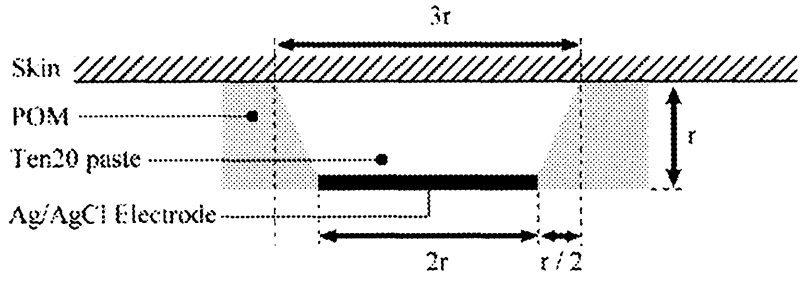

Figure 2-1: cross section of electrode design for conically recessed electrode (r=7mm).

2.3.1.3 Experiment 3

Subjective responses using the conical recessed electrode design as above were recorded in the course of a study intended to detect impedance changes related to neuronal activity (Gilad, 2005b). Eight subjects (two female and six male, age 25 to 43 years) were studied with 1 Hz square wave current and twelve subjects (six female and six male, age 23 to 43 years) studied with 125 Hz sine wave. Only the slightly unpleasant perception level was recorded. As part of the experiment to measure neuronal activity related impedance changes, a fixed current level of 100 μA lower than level perceived as slightly unpleasant was applied 20 times for one minute, with 2 minutes rest intervals.

2.3.2 Finite Element Method (FEM) simulations

A quantitative prediction of the current density in the brain was obtained by using a FE mesh which comprised 53,336 elements and was derived from segmentation of an adult human MRI using a leading industry standard Finite Element Modelling software, I-DEAS software (Tizzard, 2005). Layers were present for the scalp, skull, CSF and ventricles, grey and white matter, eyes, optic canal, olfactory tracts and auditory meatus (Tizzard, 2005; Horesh, 2005). The mesh resolution varied between 0.1 mm^3 over fine structures such as the skull and cerebrospinal fluid, to 500 mm^3 (0.5 cm^3) in the centre of the brain; this permitted accurate representation of fine structures while keeping the overall mesh size to a reasonable size.

The primary visual cortex (V1) was modelled as two intersecting ellipsoids with a total volume of a 9 cm^3 of grey matter only (Figure 2-2a). This volume was chosen to represent a typical volume of V1, taken as a median from volumes of 7.7-14.2 cm^3 measured in 14 brains (Andrews, 1997). Pilot simulations with different volumes of V1 and different geometrical shapes and placement of the ellipsoids around the visual cortex showed that the results could be linearly scaled to the V1 volume and that different geometries within these limits had no significant effect on the overall results.

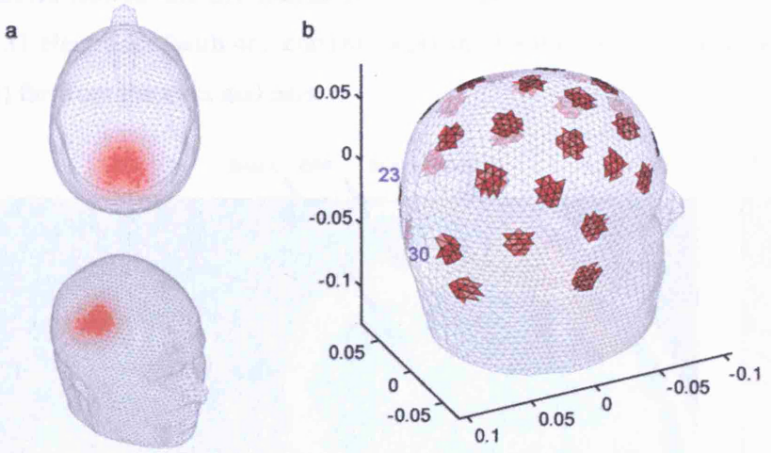

Figure 2-2: a) modelled primary visual cortex area V1. b) Outer scalp surface of the mesh used and the electrode placement for the case of 31 electrodes of 21 mm diameter. Axes are distance in meters.

A set of 31 electrodes, termed the Mark 1b electrode system in our group (Tidswell, 2001) and a single ground electrode, were disposed in a modified 10-20 system (Jasper , 1958) which covered the head (Figure 2-2b). Because of coarse elements on the scalp surface, the electrodes were represented with only 4-12 surface elements of area 0.3-0.6 cm^2 (Figure 2-2b). This limitation of the mesh could, in theory, have caused significant errors in the voltage solution and the derived current densities in the vicinity of the electrodes where the field gradient is higher. However, the objective of these calculations was to estimate current densities in the brain and

not near the electrodes. As the following results show, the calculated current density in the brain was similar for two distinct electrode diameters. Therefore, the coarseness of the mesh at the scalp surface does not appear to degrade the validity of the results.

Current densities were calculated using the UCL group SuperSolver package (Horesh, 2006c), which incorporates a modified version of the EIDORS 3D package (Polydorides, 2002). The code solved the generalised Laplace equation using Neumann to Dirichlet map to obtain the voltages of each element and used the continuum form of Ohm's law to translate into current densities. The numerical solution was performed with a Preconditioned Conjugate Gradient linear solver. The relative residual tolerance was set and monitored to be below 10^{-12}. An incomplete Cholesky factorisation was used as a preconditioner, with a drop tolerance threshold of 10^{-5} (Horesh, 2006c).

A solution was calculated for all $31 \cdot 30/2 = 465$ possible current injection pairs for the real part of the admittivity (conductivity) (Horesh, 2005; Gilad, 2005b; Horesh, 2006b; Horesh, 2006c) (Figure 2-3). When a current pair included at least one of eight electrodes close to the eyes or ears (electrodes 1,2,3,7,12,13,17 or 18), the current density in the brain region increased significantly, probably because the driving electrodes were adjacent to skull foraminae so that additional current flowed into the cranial cavity. Therefore, the following analysis was repeated twice for all 31 electrodes (with 465 current pairs) and for the 23 electrodes (with $23 \cdot 22/2 = 253$ current pairs) far from the eyes and ears.

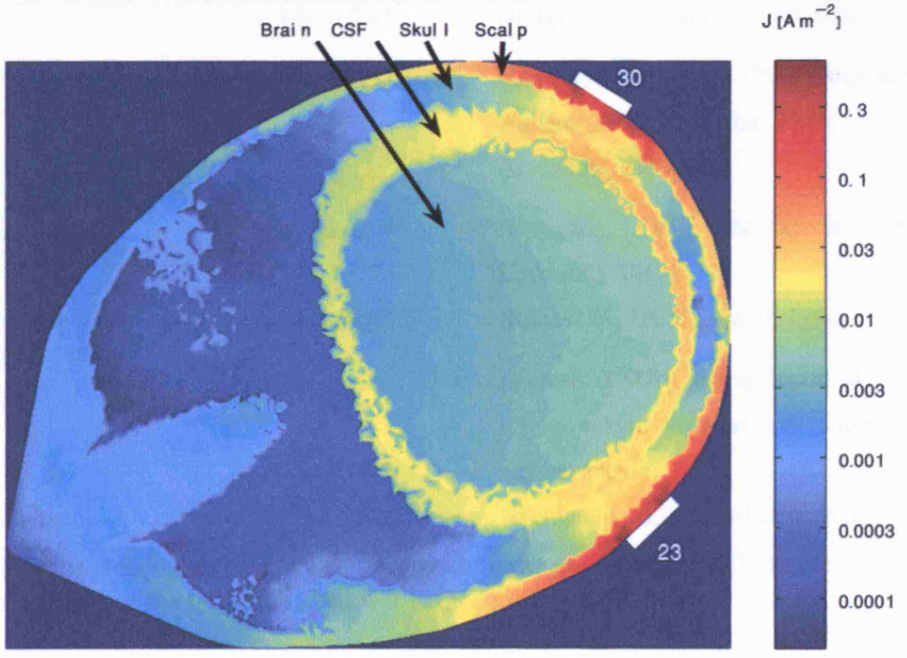

Figure 2-3: example of the current density distribution across a transverse plane through the positions of electrodes 23 and 30 when 100 μA was injected through these electrodes.

The electrode diameter was set to 11 or 21 mm, to represent the EEG and the recessed electrodes respectively, both with a current level of 100 μA. In each case, the current density was calculated for the entire head and the maximal value was calculated for grey and white matter in the brain and the primary visual cortex. The conductivity values of the different compartments of the model were obtained from published literature (Horesh, 2007b) and solutions were calculated for the minimum, median and maximum values for each of scalp, skull, grey and white matter (Table 2-1). The solutions regarded all conductivities as isotropic. However, the ranges given in Table 2-1 for scalp, skull and white matter, cover anisotropic properties available from the literature. The calculation of maximal current density across the 465 and the reduced 253 current pairs was therefore repeated 3^4=81 times for all conductivity permutations (3 values to each of 4 variable compartments). Final current density values were then taken only from the calculation with the median conductivities (0.30, 0.015, 0.30 and 0.25 S/m for scalp, skull, grey and white matter respectively). In addition, for evaluating the variability in this final current density which resulted from the uncertainty in conductivities taken from the literature, the minimal and maximal values across all 81 conductivity permutations were calculated.

Table 2-1: Conductivities used for the head model

Tissue	σ [S/m] [a]	Reference and remarks
Scalp	0.1,0.30,0.45	(Burger, 1943; Burger, 1960; Gabriel, 1996)
Skull	0.005,0.015,0.030	(Law, 1993; Gabriel, 1996; Oostendorp, 2000; Akhtari, 2002; Hoekema, 2003)
CSF	1.79	(Baumann, 1997)
Grey matter	0.20,0.30,0.45	(Freygang, 1955; Ranck, Jr., 1963; Van Harreveld, 1963)
White matter, optic canal & auditory meatus	0.18,0.25,0.30	(Ranck, Jr., 1965; Gabriel, 1996)
Eye	1.15	(Horesh, 2007b) superposition of cornea, lens, retina, sclera, vitreous and aqueous humours compartments
Olfactory tract		Average of skull and white matter

[a] The minimum, median, and maximum for each tissue are presented. These were obtained from a literature review for properties below 1 kHz.

2.4 Results

2.4.1 Electrode design for minimizing skin sensation (Table 2-2)

2.4.1.1 Experiment 1

With abrasion just under a conventional cup electrode (session 1), the threshold of sensation was 100-200 μA and became slightly unpleasant at 400 μA. With 9-fold extension of the abraded area to a circular area, diameter 30 mm, (session 2), the threshold of sensation approximately doubled. Use of a cone of paste or 4 linked electrodes gave similar results. In all studies, after about 30 sec of current application, accommodation occurred; the sensation decreased and in most cases was absent if the current was reapplied at the initial threshold of sensation.

2.4.1.2 Experiment 2

For comparison of thresholds for the recessed electrode compared to a conventional cup electrode, thresholds of sensation were 600-1000 and 200-300 μA respectively. The slightly unpleasant threshold could not be obtained for the recessed electrode even with the highest current level tested of 1100 μA, but was 400-600 μA for conventional cup electrodes.

2.4.1.3 Experiment 3

With use of the recessed cup electrode in eight subjects, the level for slightly unpleasant sensation was 950 ± 180 (600-1100) μA for a 1 Hz square wave current and in twelve subjects, this level was 960 ± 190 (600-1200) μA for a 125 Hz sine wave current (Mean ± SD (range)). The slightly unpleasant level was not reached in Experiment 2. This was probably due to variability in threshold in different subjects. There was no significant difference between the data collected for the two frequencies and between female and male subjects.

Table 2-2: Current level thresholds measured in the three experiments [μA].

			Abrasion diameter and electrode design		
	f [Hz]	N	1cm EEG	3cm EEG	2.1cm recessed
Experiment 1 (raw data)			F,M	F,M	
Threshold of sensation	1	2	100,200	200,400	
Slightly unpleasant level	1	2	400,400	700,1000	
Experiment 2 (raw data)			F,M,M		F,M,M
Threshold of sensation	1	3	300,200,200		1000,700,600
Slightly unpleasant level	1	3	600,400,500		>1100
Experiment 3 (mean ± SD)					
Slightly unpleasant level	1	8			950 ± 180
Slightly unpleasant level	125	12			960 ± 190

f – Current frequency, N – number of subjects, F – Female, M – Male.

2.4.2 FEM simulations

Maximal current densities calculated with the FEM were approximately 0.3 (0.143-0.970) A/m^2 (for the median conductivity (range)) in the brain with 31 electrodes, 11 mm in diameter. This maximal current density was located just beneath the nearest orifice (eye or ear). The current density in V1 was one thirtieth of this. With larger electrodes, 21 mm in diameter, maximal current through the brain decreased to about two thirds while that through V1 remained unchanged. With 23 electrodes, after excluding those close to the eyes and ears, maximal current through the brain decreased by 7 to 10-fold and was located just beneath the current injection electrodes. The current density through V1 was again unchanged (Table 2-3). The two electrode diameters gave similar results for all cases.

Table 2-3: Maximal current density across electrode pairs and conductivity sets[a].

Site	Diameter [mm]	J [Am^{-2}] 31 electrodes	J [Am^{-2}] 23 electrodes
Brain	11	0.296[b] (0.143-0.970)[c]	0.033 (0.026-0.097)
V1	11	0.010 (0.003-0.035)	0.010 (0.003-0.035)
Brain	21	0.191 (0.089-0.664)	0.034 (0.024-0.099)
V1	21	0.010 (0.003-0.032)	0.010 (0.003-0.032)

[a] All results are for a current level of 100 μA. Values for the 21 mm diameter electrodes can be scaled by a factor of 10 to predict values for current level of 1 mA.
[b] Outside brackets: maximal current density across current pairs for the median conductivities
[c] Inside brackets: min-max range across the 81 conductivity permutations.

2.5 Discussion

2.5.1 Current safety limits for applied low frequency currents to the human head and skin.

Safety limits for applied low frequency currents have been proposed mainly in relation to transcranial Direct Current Stimulation (tDCS) (Priori, 2003; Nitsche, 2003a; Nitsche, 2003b) and are based on animal studies which demonstrated that a sensible current density below 250 A/m^2 at 50 Hz does not induce brain tissue damage even when applied over 7 hours (McCreery, 1990). The mechanisms which may cause tissue damage are interaction between the field and permanent large dipoles (such as DNA molecules) at fields above 10 kV/m, generation of dipoles by fields above 1 kV/m and electrical breakdown of cell membranes (electroporation) at fields above 100 kV/m (Foster, 2003).

EIT applications usually comply with the International Electrotechnical Commission (IEC) standard (IEC60601-1{ed3.0}, 2005), and the equivalent standard of the British Standard Institute (BSI) (BS5724, 1979) which specify a 'patient auxiliary current' limit of 100 μA from 0.1 Hz to 1 kHz ; then $100f$ μA from 1 kHz to 100 kHz where f is the frequency in kHz ; then 10 mA above 100 kHz. This standard is based on limitation of the current to 10% of the average threshold of sensation when current is applied to the skin using surface electrodes. This corresponds to a widely cited study in which a mean perception current of 1.1 mA was observed between DC and 200 Hz, for hand holding of a copper wire of d = 3.3 mm in diameter. The subjects' subjective sensation was slight warmth at DC, tingling for 100-200 kHz, and above this, heat (Dalziel, 1972). However, this standard applies to current inadvertently injected through leakage; current deliberately injected for therapeutic purposes, such as for TMS, nerve conduction studies or electroshock for severe depression, may clearly exceed this and is permitted.

This standard defines the limits by setting a total current value, rather than current density across the electrode-skin interface, which first principles suggest are more likely to be the critical parameter, presumably because this quantity can easily be measured. The true parameter of interest is the peak current density at any point in the subject. Because current is not emitted uniformly across an electrode (Gisser, 1987; Cheng, 1989; Suesserman, 1991; Paulsen, 1992; Hua, 1993) and its spread through the immediate tissue may not be uniform, accurate spatial current density can only be inferred by numerical modelling, and this would not have been available at the time.

For estimating the current density of perception as determined by Dalziel, let us consider a copper wire with length L between 10 to 50 mm, which gives rise to a current density of $1.1mA/(\pi dL)$ = 2-11 A/m^2. The IEEE standard (IEEE Std C95.6-2002, 2002) requires the

current limit below 3 kHz to be 1.5 mA for a skin contact area of 1 cm^2, typically for a finger pulp area, and 3 mA for a hand grasp area of 15 cm^2. Assuming uniform current density over the contact area, these values define the current density range to be 2-15 A/m^2, which is similar to the range calculated from Dalziel's data.

2.5.2 Modification of electrode design in order to increase uniformity of current injection across the skin.

In a transmitting electrode, most current passes though the edge, according to the principle of charge separation (Gisser, 1987; Cheng, 1989; Suesserman, 1991; Paulsen, 1992; Hua, 1993). There have been several different approaches in which electrode geometry has been altered in order to attempt to distribute the current more evenly. The term "non-uniformity" used below refers to the ratio of peak current density recorded near the edge of the electrode to that in its centre.

In principle, current might be applied more evenly if the electrode surface is recessed from the skin and current is diffused through a conductive gel to the skin, possibly with a surrounding resistive barrier to constrain the current. The simplest approach is to employ a buffer layer of conductive gel between the electrode and skin. For electrodes 10 cm in diameter, non uniformity was reduced from 260% to 120% by using 1.5 mm of a buffer layer with 60 Ωm resistivity. The non-uniformity decreased monotonically as the buffer layer thickness and resistivity increased. A reduction from 200% to 160% was also obtained by adding a ring of higher resistivity of 100 Ωm around the perimeter (Krasteva, 2002a). For a planar copper electrode, 9 mm in diameter, a radially varying conical recession appeared to be the best design. This achieved almost uniform current density at the skin, in contrast to the original, cylindrical or exponentially recessed designs, for which non-uniformity was about +150, +200 or -80% respectively (Suesserman, 1991). A similar improvement was noted for a larger defibrillation electrode, 9 cm in diameter, with stepwise conical recession by 4 mm (Papazov, 2002). As might be expected from charge separation, alteration of the boundary shape alone led to no significant improvement. There was still substantial non-uniformity of current injection at the boundary of clover, daisy, and spiral-shaped electrodes (Papazov, 2002) or with inclusion of openings in defibrillation electrodes (Krasteva, 2002a). A recessed electrode design was also used in a Magnetic Resonance EIT application to avoid artefacts in MR images near the electrodes due to the RF shielding effect of copper electrode (Lee, 2003). However, this application did not address the issue of current density uniformity on the surface of the imaged object.

An alternative approach is to use a conductive gel with gradually increasing resistivity towards the edge. The non-uniformity of a circular electrode, 50 mm in diameter, decreased from 140% to 80% when a homogeneous layer of 40 Ωm was interposed. Further non-

uniformity reduction to 20% was obtained by a 7-step concentric resistivity layer, with varying resistivity from 30 Ωm to 140 Ωm (Papazov, 2002). The use of saline-soaked pads under the defibrillation electrodes with more than 150 subjects did not show even a single case of skin reddening, which suggested a more uniform distribution of the current (Papazov, 2002). In a clinical study in which biopsy histology was evaluated during transthoracic cardioversion, a 15% reduction in damage was observed with use of electrodes which had a stepwise increased resistivity of 200 times towards the edge (Garcia, 1998).

Overall, it appears that the best design is a conically recessed electrode, which is capable of producing a uniform current distribution at the skin; the drawback is that the electrode has a higher geometric profile.

In this study, a recessed electrode design has been developed which has enabled application of an average of 860 ± 190 (500-1100) μA to the scalp (values from second part of Experiment 3 minus 100 μA) with minimal painful skin sensation; this is about 8 times greater than the limit of 100 μA which would otherwise have applied from safety limits for auxiliary current. The threshold of sensation was 3-fold higher and the slightly unpleasant threshold was doubled compared to thresholds obtained with a conventional cup electrode.

2.5.3 Thresholds at which low frequency currents stimulate neuronal tissue

The principal mechanism by which nerve fibres and cerebral cortex are stimulated from 1 Hz to 3 kHz is membrane polarization. Magnetohydrodynamic effects, which apply to forces on moving charges in fluids, dominate biological reactions below 1 Hz. (IEEE Std C95.6-2002, 2002; Foster, 2003).

Three thresholds for excitation may be distinguished for the interaction of DC to 300 Hz with neuronal tissue (Radiat Prot Dosimetry, 2003). The first, highest, threshold relates to frank nerve excitation. This occurs at an electric field strength higher then 5-25 V/m (Reilly, 1998). Assuming a cerebral conductivity of 0.3 S/m for grey matter at low frequencies (Ranck, Jr., 1963), this corresponds to a current density threshold of $J = \sigma E = 1.5\text{-}7.5$ A/m^2. This value is in broad agreement with theoretical modelling by Rattay (Rattay, 1998; Rattay, 1999) for the various neuron types in the Central Nervous System (CNS), using a compartment model and equivalent electrical network. The theory predicts the influence of electrical and geometrical parameters on the excitation threshold. A 0.1 ms stimulating pulse is given from a point source in a homogenous sphere from a distance of 1 to 9 mm from various positions around the neuron and at positive (cathodic) and negative (anodic) polarities. The threshold current densities were from 9 to 338 A/m^2 for anodic stimulation and 3 to 707 A/m^2 for cathodic stimulation. The large range indicates the importance of the geometrical placement of the source relative to the axis of the axon.

The second threshold is related to changes in neuronal excitability which occur below the excitation level through the effects of electric field polarization on the membrane potential and field induced changes in the rhythmic behaviour of networks of interacting neurons. It is approximately five times lower than the threshold for full excitation. Such changes have been reported with an applied electric field as low as 2-4 V/m (0.6-1.2 A/m^2 for a brain conductivity of 0.3 S/m) (Bawin, 1984; Bawin, 1986; Saunders, 2002; Jefferys, 2003). In conditions where membrane sensitivity is enhanced, such as epilepsy, this threshold could be lower (Durand, 2003). In conditions simulating epilepsy, factors such as the presence of GABA blockers (Kayyali, 1991), elevated potassium concentration (Traynelis, 1988), low calcium concentrations (Haas, 1984) or increased extracellular resistance due to cell swelling (Ghai, 2000), render the neuronal tissue hyperexcitable as the membrane potential of many neurons is close to threshold for firing. In addition, specialized neuronal structures with a high degree of synaptic convergence, such as purkinje cells in the cerebellum which receive about 200,000 synaptic inputs, may have a lower threshold. For instance, the electric field threshold in the extracellular fluid in the retina for phosphene induction was 10-60 mV/m at 20-25 Hz (0.003-0.018 A/m^2 for retina conductivity of 0.3 S/m) (Saunders, 2002; Taki, 2003; Attwell, 2003). In contrast, Lindenblatt and Silny (Lindenblatt, 2002) suggested a threshold similar to other excitable tissues. They used a detailed 3D model of the eye with sub-millimetre resolution and current threshold measured by Carstensen (Carstensen, 1985) for phosphene thresholds to show that currents are enhanced in small localized regions close to the optic nerve due to current being preferentially carried by blood vessels. They found threshold values for the retina of 1.8 A/m^2 at 60 Hz and 0.3 A/m^2 at 25 Hz.

Two separate standards follow data on changes in retinal function and accordingly set much lower exposure limits, which are about 100-fold lower than the threshold required for full nerve excitation. These standards are largely based on the work of Reilly (Reilly, 1998; Reilly, 2002a; Reilly, 2002b; Reilly, 2003). The IEEE standard (IEEE Std C95.6-2002, 2002) sets standard exposure values for electric and magnetic fields for specified tissue types. The peak in-situ electric field limit for stimulation of synaptic brain tissue is 0.025 V/m for frequencies below 20 Hz and $0.025/f$ V/m for frequencies above 20 Hz where f is the frequency in Hz. This limit was chosen to be 0.333 of the median threshold of 0.075 V/m, for alteration of synaptic activity in the brain by a 25 ms pulse or 20 Hz sine wave. The factor of one third was introduced so that the threshold was set to include 99% of the population. Assuming a conductivity of $\sigma = 0.3$ S/m, the electric field threshold E = 0.075 V/m translates into a current density threshold of 0.0225 A/m^2. According to the ICNIRP standard (ICNIRP, 1998), induced current density of 0.01-0.1 A/m^2 (RMS) or 0.014-0.14 A/m^2 (peak) will cause functional changes in the nervous system. The restriction is set to 0.057 A/m^2 up to 1 Hz, $0.057/f$ A/m^2 for frequencies between 1-4 Hz and 0.014 A/m^2 from 4 Hz to 1 kHz, all peak values.

The third threshold marks the lowest theoretical limit at which induced electric fields might be capable of inducing biological effects in a single neuron and is about three orders of magnitude lower again. Weaver et al (Weaver, 1998) calculated a minimum threshold of around 10 mV/m for an elongated cell and Adair et al (Adair, 1998) suggested a minimum theoretical sensitivity of 1 mV/m (0.0003 A/m^2 for a brain conductivity of 0.3 S/m) for systems in which integration of an induced electrical signal takes place over a large number of cells. Nevertheless, highly specialized sensory structures in some animals such as sharks and rays, can be sensitive to about 0.5 μV/m (Adair, 1998; Saunders, 2002; Saunders, 2003). The "bulk" endogenous tissue current density level in the human brain is 0.001-0.01 A/m^2 (Bernhardt, 1979; Saunders, 2002). Application of tDCS, which produced a current density of about 0.01 A/m^2 on the cortical surface for several minutes, resulted in long lasting effects on neuronal excitability as well as on cognitive function (Priori, 2003; Nitsche, 2003a; Nitsche, 2003b). This low threshold is less relevant for my EIT purpose as I do not intend to deliver any DC component at all by transmitting at two balanced polarities.

These studies are summarised in Table 2-4. For the purpose of defining a limit for EIT applications at low frequency, the current density level of concern is that which will not significantly alter brain function while EIT current is injected. For this, the threshold for changing nerve excitability or synaptic activity appears most relevant. The most pertinent appears to be 0.6-1.2 A/m^2 (Bawin, 1984; Bawin, 1986; Saunders, 2002; Jefferys, 2003) (italic line in Table 2-4). I am not utilising the lower values derived for retinal stimulation (Saunders, 2002; Taki, 2003; Attwell, 2003) because Lindenblatt and Silny (Lindenblatt, 2002) have shown that retinal threshold is as high as the threshold for altering nerve excitability in the brain. therefore, I discount the values set by both standards (ICNIRP, 1998; IEEE Std C95.6-2002, 2002) which rely on the lower retinal threshold values and accordingly utilise a safety factor of about 100x below the threshold for full nerve excitation. Hence, the threshold I believe to be appropriate is about five times lower than the value for full nerve excitation in the brain.

Table 2-4: Summary of safety limits and physiological thresholds.

Effect	Site	E [Vm^{-1}]	J [Am^{-2}]	f [Hz]	Reference
Brain tissue damage	Brain	830	250	50	(McCreery, 1990)
Skin sensation	Hand	9-50	2-11	0-200	(Dalziel, 1972)
Skin sensation	Hand	9-68	2-15	0-3000	(IEEE Std C95.6-2002, 2002)
Nerve excitation	Brain	5-25	1.5-7.5	0-300	(Reilly, 1998)
Nerve excitability[a]	*Brain*	*2-4*	*0.6-1.2*	*0-300*	*(Bawin, 1984; Bawin, 1986; Saunders, 2002; Jefferys, 2003)*
Nerve excitability	Retina	0.01-0.06	0.003-0.018	20-25	(Saunders, 2002; Taki, 2003; Attwell, 2003)
Nerve excitability	Retina	1,6	0.3,1.8	25,60	(Lindenblatt, 2002)
Nerve excitability	Retina	0.075 0.075f/20	0.0225 0.0225f/20	0-20 20-1000	(IEEE Std C95.6-2002, 2002)
Nerve excitability	Retina	0.19 0.19/f 0.047	0.057 0.057/f 0.014	0-1 1-4 4-1000	(ICNIRP, 1998)
Low theoretical limit	Brain	0.001	0.0003	0-300	(Saunders, 2002)
Endogenous currents	Brain	0.003-0.03	0.001-0.01	0-300	(Bernhardt, 1979; Saunders, 2002)

[a] Study from which threshold is taken for this work.
E – Electric field, J – current density, f – frequency

2.5.4 Effect of skull and extra cerebral layers on current applied to scalp

Current applied to the scalp will be attenuated by the scalp, skull and cerebrospinal fluid (CSF) before reaching the cerebral cortex. For the purposes of this work, it was important to estimate peak current density in the brain, in order to avoid any stimulation of cerebral activity by the injected current. To my knowledge, these effects have not been accurately quantified previously – the use of a Finite Element Model for this was one of the purposes of this paper. The following is a brief review of previous work in the literature and an attempt to estimate the order of magnitude of any likely effect.

Using current density MR imaging in the rabbit, 15% of the current penetrated the skull and the remaining 85% flowed through the scalp (Joy, 1999). In contrast, in a celebrated study using saline soaked human skull and validated using a three sphere analytic model, intracranial current was estimated to be 45% (Rush, 1968). It was also observed that when electrodes were placed directly over a suture, the current density in the cortex immediately underneath increased

three times from that predicted for normal skull. Lowered skull resistivity in the presence of suture lines was also measured by Law (Law, 1993). For the following estimation, I chose the average penetration current from the above figures to be 30%.

The transition of the current though the various layers before it reaches the cortex and the shunting effects across the scalp and CSF may roughly be estimated to decrease the effective current density just beneath 11 mm diameter electrode by an order of magnitude. Taking the 30% current penetration and the 10-fold factor due to current spreading, the current density on the surface of the cortex may be roughly estimated to be perhaps 3% of that on the surface of the scalp. For a current of 100 μA, with a 1 Hz square wave injected through a pair of 11 mm diameter surface electrodes, the current density on the scalp may be estimated to be about 1 A/m^2. Therefore, the estimated current density on the surface of the cortex may be expected to be of the order of 0.03 A/m^2. This rough estimate suggests that the limit on injectable current is therefore likely to be the current that can safely be injected on the scalp without causing painful cutaneous, rather than cortical stimulation.

2.5.5 FEM simulations

According to the more precise estimation in this study using FEM, the maximal current density in the entire brain when injecting 1 mA of current through the recessed electrodes far from eyes and ears was 0.34 (0.24-0.99) A/m^2 (for the median conductivities (range)). This is 2 to 4-fold lower than the guide threshold I chose for changing the excitability of neuronal tissue (0.6-1.2 A/m^2) (Bawin, 1984; Bawin, 1986; Saunders, 2002; Jefferys, 2003) and 5 to 25-fold lower than the threshold for nerve stimulation (1.5-7.5 A/m^2) (Reilly, 1998). The V1 region of interest, which was well away from any possible shunt paths through the orbital or auditory meati, received a 3-fold lower current density of 0.10 (0.03-0.32) A/m^2 (for the median conductivities (range)). However, for most applications, it is desirable to avoid stimulation of any part of the brain and placement of electrode near large foramina should be done with caution.

I believe that this use of a FEM to estimate current densities in the head for EIT is the first application of its kind and was also published in a peer review journal (Gilad, 2007b). Similar approaches have been employed for other applications such as calculating current density in the eye (Lindenblatt, 2002), beneath external defibrillation electrodes (Krasteva, 2002a) and beneath transcranial magnetic stimulator (Kowalski, 2002; Krasteva, 2002b; Miranda, 2003).

A recent study by a research group at Manchester reproduced the modelling results with a larger mesh and slightly different conductivities and concluded that for a current of 1 mA applied on the scalp, the maximal current density n the brain was 0.5 A/m^2 (Davidson, 2007) which confirms my results.

The accuracy of the FEM simulations for predicting current density in the brain was limited by a) using isotropic tissues in the head model, b) uncertainty of conductivities in the literature, c) a single generic mesh without variation for different geometries in different subjects and d) limited resolution for fine structures in the brain and for electrode geometry. However, I believe that the results are of acceptable accuracy because a) I have validated this method for tank measurements and boundary voltage measurements in humans (Gilad, 2005b) (see also Ch. 3), b) for the case of 100 μA current passing through 11 mm diameter electrodes and excluding the electrodes close to the eyes and ears, the predicted grand maximum current density of 0.033 (0.026-0.097) A/m^2 (for the median conductivities (range)) in the brain agrees with the qualitative estimation described in the introduction (0.03 A/m^2) and finally c) current flowing though a more realistic anisotropic scalp with tangential muscle fibres and layered skull structure will have greater shunting than the modelling suggests; this would further reduce the current density in the brain compared to the estimated values. The values presented are therefore, of course approximate, but I believe they still give a reasonable guide to an order of magnitude.

2.5.6 Implications for EIT

A subjective method was used to assess sensation. More formal pain scales are available such as the Visual Analogue Scale, the Verbal Rating Scale and the Numerical Rating Scale (Williamson, 2005) and these might be preferable in the future for objective assessment in designing high current level EIT instruments for clinical practice and for support of any regulatory approval procedures. However, from many years experience with EIT, I have observed that two critical thresholds are relevant for any sensation induced by current – that of any perceptible sensation at all – viz. tingling – and that at which the tingling became sufficiently strong to make the subject request cessation of the test. These are the thresholds which will, in practice, limit the clinical and experimental usability of EIT in the long run and so were chosen for this study.

There is controversy in the literature over the magnitude of the current density threshold which changes excitability of neuronal tissue. Most data are based on measurements and simplified models of retinal stimulation and suggest a low threshold of 0.003-0.018 A/m^2. The standards based on these data set limits of 0.01-0.1 A/m^2 (ICNIRP, 1998; IEEE Std C95.6-2002, 2002). In contrast, the study of Lindenblatt and Silny (Lindenblatt, 2002) suggested a higher retinal threshold two orders of magnitude greater, which was similar to other excitable tissues using a detailed 3D model of the eye with sub-millimetre resolution. I have adopted this greater threshold for cortical tissue in this study but this is open to question. Future applications of the proposed current injection values should include testing of cognitive function and evoked

responses in order to validate these conclusions empirically. I have since conducted a human study with these settings (Gilad, 2006), described in this study as Experiment 3; although cognitive function was not formally assessed, the subjects reported no ill effects or any evidence of cortical stimulation such as phosphenes or fortification spectra.

In most clinical EIT studies, the applied current has been set at that permitted for auxiliary leakage current. The findings here are that a greater current can be safely applied and tolerated but the position with respect to safety guidelines is unclear. Greater currents may certainly be applied for therapeutic purposes, but the position with respect to that specifically for diagnostic purpose appears not to be defined. A current density of 2.2 ± 0.6 A/m^2 on the surface of the scalp may be calculated from the data of Experiment 2, which is at the lower limit of the range of 2-11 A/m^2 calculated from Dalziel (Dalziel, 1972) and the range 2-15 A/m^2 set by the IEEE standard (IEEE Std C95.6-2002, 2002). The IEC (IEC60601-1{ed3.0}, 2005), and BSI (BS5724, 1979) standards specify 10% of these values as the 'patient auxiliary current' limit in medical instruments. I submit that the higher level could safely be used for EIT; perhaps this issue could be included in any future revisions of the safety standards.

2.5.7 Future work

Further work would be to define current limits for higher frequencies up to 2 MHz, account for cases of simultaneous transmission through multiple electrodes and of multiple frequencies through individual electrodes. A reduction in frequencies below 100 Hz has been found to be needed for multifrequency recording with EIT with current injection from 20 Hz – 1.6 MHz in packets of 10 simultaneous frequencies, each frequency with applied current of 0.28 mA (Romsauerova, 2006a). When transmitting through multiple electrodes, current level from each electrode will have to be lower than 1 mA as this will already reach the limit for changing neuronal activity when transmitted from one pair. Mechanical improvements to the electrode design are also desirable to minimize size and burden for application of multiple electrode arrays. This could be achieved by implementing the technique of interfacing with layers of varying and high resistivity as proposed by Papazov (Papazov, 2002).

3. Low frequency EIT of evoked physiological activity in the brain with scalp electrodes: simulation of expected changes with a Finite Element Model of the head

3.1 Abstract

EIT has the potential to achieve non-invasive functional imaging of fast neuronal activity in the human brain. During evoked responses, fast (~1ms) local impedance changes of ~1% at frequencies below 100 Hz, may be estimated to occur using cable theory modelling and animal studies. The purpose of the work in this chapter was to estimate the expected EIT voltage changes recorded on the scalp during visual stimulation and to suggest the optimal electrode placements for real human measurements out of a pre-defined set of electrode positions. This was achieved by utilizing an anatomically realistic Finite Element Model of the adult head, conductivity values estimated from the literature and solution of the forward problem. Only the real part of the impedance change was considered since pilot simulations on the imaginary part revealed that it would provide negligible changes at low frequencies.

The validity of this method was assessed by comparing the model predictions with boundary voltages from human experiments and with both boundary voltages and boundary voltage changes caused by a sponge perturbation in a saline filled spherical tank. In these studies there was a correlation between measured and predicted boundary voltages and changes of R = 0.87-0.98, suggesting that the modelling methods were valid.

The model estimated that resistivity changes of 1% in a 9 cm^3 primary visual cortex during evoked responses translated into an average scalp voltage changes of 0.54 ± 0.36 μV or 0.0018 ± 0.0014% (Mean ± SD) for a current level of 1 mA and were expected to be measured with an SNR below 2, which was limited by the averaged background EEG noise. The maximal change in the most sensitive electrode combination was double. These findings suggest that imaging system is not practical at this stage as about 6 hours were estimated to be required for recording with sufficient SNR and multiple current pairs. The optimal electrode placements were with current injected from adjacent (5 cm apart) or semi-adjacent (10 cm apart) electrodes on the back of the head and recording from electrodes near to these.

The results of this study were used in the following Ch. 4 in which I present my attempts to measure on humans the changes predicted in this study. Future work include estimating the minimal SNR needed for imaging, investigating the effect of anisotropy, the possible contribution of multiple current patterns and refinements to the head model.

3.2 Introduction

3.2.1 Bioimpedance changes during functional brain activity

EIT is a new non-invasive functional imaging technique potentially capable of measuring fast (~1 ms) neuronal activity in the human brain, which is yet to be reliably achieved by any other method (Holder, 1987). EIT is also able to measure slow (~1 sec) impedance changes related to haemodynamic processes (Tidswell, 2001). Arrays of EEG type surface electrodes are applied on the scalp, a low level of current is applied through pairs of electrodes and voltages are measured through other pairs. Recordings from multiple current pairs allow reconstruction of the internal impedance properties.

My aim was to develop a non-invasive method for measuring resistivity changes related to neuronal activity. Studies into imaging of brain function require active and synchronised neuronal activity at a known brain region. This can be achieved by visual stimulation, such as a bright flash or pattern reversal checkerboard screen, which causes activity in the visual cortex. The brain activity generates potentials on the scalp at the back of the head known as Visual Evoked Potentials (VEP).

There are two main mechanisms for bioimpedance changes during normal functional brain activity:

Slow changes: More blood flows into active brain tissue as a result of increased metabolic activity. The increase in blood volume causes local impedance changes of about 2% over tens of seconds; impedance changes of about 1% have been recorded with scalp electrodes during the human VEP (Tidswell, 2001).

Fast changes: The change of resistive properties in individual neurones underlies all neural activity. When an action potential propagates along a nerve, ion channels in the cell membrane open to allow ions to flow. The electrical resistivity of the cell membrane decreases during neuronal depolarisation, thus allowing external current to flow more freely through the cell (Cole , 1939). These changes last tens of milliseconds. Biophysical modelling has suggested that they are maximal at frequencies below 100 Hz, (Boone, 1995a; Liston, 2000; Liston, 2004a). This is because membrane capacitance limits the current from flowing into the cell at low frequencies whereas at high frequencies the current can flow through the membrane regardless of the state of ion channels. When the activity of a population of neurones displays spatial and temporal coherence such as in visual evoked response, it will be accompanied with resistivity change of the active tissue as a whole.

The magnitude of such fast changes has been assessed by other investigators in our research group in the past, by modelling and in animal studies (Table 3-1). Mathematical modelling, based on cable theory, estimated local resistivity changes near DC to be 3.7% for peripheral

nerve bundles and 0.06-1.7% for the cortex during Evoked Potentials (EP) (Boone, 1995a; Liston, 2000; Liston, 2004a). These predictions agreed with decreases in resistance of 0.5-1.0% measured during the compound action potential in crab peripheral nerve (Holder, 1992c; Boone, 1995a; Boone, 1996) and decreases of 0.01-0.03% in some pilot studies on the surface of the cerebral cortex of the anaesthetised rabbit during median nerve evoked responses (Boone, 1995a; Boone, 1995b).

Such local changes in the cerebral cortex may be expected to be diminished substantially when recorded on the scalp, because of partial volume effects and the resistance of the skull to applied current. Liston estimated the boundary voltage changes to drop by a factor of 10 to 0.006-0.17% (Liston, 2004a). This was relying on a crude estimate made of the relation between the local change and the change in a 4-terminal measurement on the scalp (Boone, 1995a). A ratio of 10:1 was suggested since cortical resistivity changes of 5%, related to blood volume changes, caused 0.5% mean, positive voltage changes on the scalp (Tidswell, 2001).

Ahadzi (Ahadzi, 2004a) then solved the EIT forward problem, for an anatomically realistic model of the head using Finite Element Method (FEM), in order to model the expected boundary voltage changes on the scalp, when a 1% local resistivity changes occurred at the visual cortex during the VEP. Boundary voltage changes were estimated to be 0.02-0.04% for optimal four terminal resistivity measurements. These numeric predictions of Ahadzi (Ahadzi, 2004a) and approximate estimations of Liston (Liston, 2004a) are further refined in the present study. According to results of these studies, the required sensitivity for measuring the small resistivity changes on the scalp is in the range of 0.01-0.001%.

Table 3-1: Summary of predicted and measured fast resistivity changes [%].

	Cable Theory	FEM	Experimental
Crab peripheral nerve	~ 3.7 (Boone, 1995a; Liston, 2000; Liston, 2004a)	-	0.5-1.0 (Holder, 1992c; Boone, 1995a; Boone, 1996)
Rabbit cortex, EP	0.06-1.7 (Boone, 1995a; Liston, 2000; Liston, 2004a)	-	0.01-0.03 (Boone, 1995a; Boone, 1995b)
Human scalp, EP	0.006-0.17 (Liston, 2004a)	0.02-0.04 (Ahadzi, 2004a)	-

3.2.2 SNR requirements for human head EIT

A key issue for determining the feasibility of imaging neuronal activity with EIT is to estimate the minimal SNR for the measured changes, which would still allow reliable image reconstruction. This may be addressed by reviewing past studies on EIT of the human head from our research group at UCL.

Tidswell et al. (Tidswell, 2001) reconstructed images of impedance changes mostly related to regional cerebral blood volume (rCBV) changes from humans during visual (n=13), motor (n=20) or somatosensory (n=18) tasks. They used a modified HP 4284A impedance analyzer and measured at 50 kHz. Significant impedance changes were defined as those more than 2 standard errors of the mean (SEM) from the baseline impedance in two or more consecutive stimulus frames. Such significant impedance changes were seen in 25, 26 and 12% of the electrode combinations in each subject for visual, motor, and somatosensory paradigms, respectively. Reproducible boundary voltage changes of about 0.5% and 0.2% (peak and mean respectively) were measured in 51/52 recordings. However, only 19 recordings produced images with significant changes in the correct cortical area. The remaining recordings either produced significant changes elsewhere (n=18) or did not produce any changes in the image (n=14). The mean SNR of the boundary voltage changes in the first two groups producing significant changes in the image was 1.3±0.6 (range 0.5-3.4). A later study (Bagshaw, 2003) has demonstrated on 2 visual and 2 motor task recordings from Tidswell's data that using a realistic head model produces better quality images as opposed to the homogeneous sphere model used in Tidswell's study. This was followed by re-analysis of the full data with the realistic head model resulting in 38/52 images with significant changes in the correct cortical area instead of 19 (Tidswell, 2006).

To evaluate the effect of noise on image reconstruction, Tidswell (Tidswell, 2006)(Section 2.3.2.4 in his thesis) simulated an image with a single superficial impedance change which produced an average boundary voltage change of 0.4 % from an unreported percentage of significant channels. The size of the impedance change was not reported but was assumed to be 12% from the context of this study simulating the changes obtained in humans. Random noise, normally distributed with a mean of 0 and standard deviation of 0.1 % to 1.0 % in 0.1 % steps was then added to the boundary voltages. This decreased the SNR between the averaged significant boundary voltage changes and the added noise from 4 to 0.4, a similar range to that measured in the human raw data (Tidswell, 2001; Tidswell, 2006). The effect of decreased SNR below 1.0 produced distortions in the images and this was taken as the minimal SNR required for reliable imaging. At SNR levels less than 0.5, the images appear to have 2 impedance increases in opposite sides of the images, whereas there was only one impedance change in the artificial data.

In another tank study (Tidswell, 2006), the HP system was calibrated with a head shaped tank which contained a skull and a test object of a Perspex rod (infinite contrast) or sponge of 12% contrast similar to the impedance change found in rabbits during brain activity (Holder, 1996). It was possible to obtain reliable images of the Perspex or sponge which were located superficially on the inner side of the skull in 4/5 positions and deep in one position. The SNR for the average of the absolute changes from all 258 channels was 0.9±0.2 and 3.2±1.3 and the mean localization error in the image was 2.5 and 1.3 cm for the sponge and Perspex rod respectively.

In another study, intended to compare electrode systems from different manufacturers, Tidswell et al. (Tidswell, 2003) measured the SNR of the voltage changes when a Perspex rod was inserted into a realistic, saline-filled head-shaped tank with real human skull and vegetable skin to simulate human skin. They used the UCLH Mk 1b system (Yerworth, 2002) measuring at 38.4 kHz. For calculating the SNR for each electrode combination, the signal was the mean of 10 s of stable changes during insertion of the Perspex rod and the noise was the rms value for the entire baseline of 40 s prior to the insertion. The overall SNR was taken to be the mean SNR for 10% of electrode combinations with the largest signals. Electrode combinations which exceeded the noise limit of 1% of the baseline impedance were excluded before this calculation. Satisfactory images of the test object, although somewhat blurred, were produced. The mean SNR was 2.3±0.2 and varied with relation to different electrode systems used. Image reconstruction gave a minimal localization error of 2 cm which could be related to inaccuracies in the forward model and inverse solutions rather than just to noise. In the same study, impedance changes mostly related to rCBV changes were produced in healthy volunteers (n=16 recordings from 6 subjects) during voluntary sequential finger–thumb apposition of the right hand (Tidswell, 2003). The mean SNR in these measurements was 2.9±0.4 but image reconstruction of this data was not evaluated by the authors. This mean SNR was higher than that for the tank studies since more electrode combinations were excluded as they exceeded the noise limit of 1%.

The same UCLH Mk 1b system was then used on 9 neonates during 8Hz flash visual stimulus, and a passive-motor stimulus in which either wrist was flexed and extended at 1.5Hz for up to 25s (Tidswell, 2006). The average SNR, calculated by averaging the 10% of electrode combinations with the highest absolute impedance change, was 2.0±1.0 (0.6-3.4) and 1.7±0.9 (0.6-3.8) and changes over the expected brain area were observed in 3/4 and 6/8 visual and motor stimulus recordings respectively. A recent study has demonstrated on 2 recordings from this data set that the SNR and subsequent image quality could be significantly improved using Principal Component Analysis (PCA) (Abascal, 2007b).

A recent simulation study on temporal lobe epilepsy examined the effect of added noise on the reconstructed image (Fabrizi, 2006a). Forward solution simulations using a realistic 3D model of the human head showed that about 15% impedance changes in lateral temporal lobe

region of volume 18 cm^3 during focal epilepsy seizure, mostly related to cell swelling, translated into about 1% maximal changes in the mean of electrode combinations with the greatest 1% of changes for the real part of the boundary voltages at 50 kHz. For the image reconstruction study, Fabrizi et al. used a subset protocol which consisted of 258 electrode combinations which had maximal changes of only 0.2% and an average of 0.14% for the 10% highest changes. This was less than the maximal change of 1% originally modelled since 1) this subset of 258 combinations did not include the most sensitive channels and 2) the average of the top 10% of the changes was used rather than the maximum. White noise of RMS 0.3-0.4% whose magnitude was obtained from tank measurements with the UCLH Mk 2.5 system (Fabrizi, 2007; Romsauerova, 2007) was added to the boundary voltage changes. The possibility of reducing the noise with time averaging was considered for a system with (i) serial current injections and voltage measurements (10x noise reduction for a theoretical 100 data sets per second); (ii) serial current injections, but parallel voltage measurements (30x noise reduction); (iii) parallel current injections and voltage measurements (160x noise reduction). For superficial changes in the temporal lobe, images with added noise became similar to noise free images in the case of 10-fold reduced noise. The SNR for the 10% highest changes in this case was therefore 0.14% / (0.35%/10) ~ 4 for the least severe case of noise reduction by 10x. It could well be that the minimal SNR to allow reliable image reconstruction was below 4 but as only SNR values of 4, 12 and 64 were tested, this could not be derived from this study. However, more realistic considerations, not taken into account in their study, could limit reliable reconstruction at the SNR they have determined. These include accounting for additional errors due to inaccurate electrode positions, differences between the realistic head geometry and the standard head mesh and inaccurate registration of conductivities.

Overall, an SNR between 1 and 4 in the boundary voltage changes has allowed meaningful human head EIT image reconstruction under different conditions of human, tank and simulation studies (Table 3-2). The SNR values from the in-vivo studies on adults (Tidswell, 2001; Tidswell, 2003; Tidswell, 2006) or neonates (Tidswell, 2006) were treated with caution since the true distribution of the changes in the brain was unknown, the determination of the correct cortical area for the expected changes was qualitative and the minimal SNR required in the boundary voltage changes for reliable imaging could be higher than quoted for these study.

The results from tank or simulation studies were regarded as more reliable since the true conductivities and geometry of the head model and test objects as well as the position of the test objects were known. However, the minimal SNR in these studies was probably underestimated since additional factors limiting the image reconstruction in-vivo were not taken into account and their effects on the minimal SNR requirements are difficult to quantify. A partial list of these factors include uncertainties in the conductivities, geometry and electrode positions as well as various sources of physiological noise and not accounting for anisotropic properties.

Furthermore, none of the previous studies simulated the conditions expected in neuronal activity EIT. In particular, the main differing factor is the nature of the noise. In the previous studies, where the recorded changes were related mainly to rCBV changes, the noise present at 40-50 kHz originated from various instrumentation sources and physiological noise dependent on autonomic activity of muscle and blood vessels, variations in skin properties, and oscillations of the body temperature. The band of interest for the changes was below 1 Hz since this was the expected bandwidth of the blood volume changes and the overall noise at this band was estimated to be normally distributed (Tidswell, 2006; Fabrizi, 2007). The EIT image reconstruction spatially integrates information from typically 258 electrode combinations recorded from up to 31 electrodes at slightly different times. Assuming that the noise from the different combinations was to some extent independent, this spatial integration has an averaging effect on the noise which effectively increased the SNR in the resulting image.

However, in neuronal activity EIT, the main source of noise is expected to be the spontaneous brain activity since the recording is made below 100 Hz. The expected impedance changes due to neuronal activity are more rapid than blood volume changes and cover a similar band of 100 Hz as the spontaneous brain activity. In addition, the EEG band includes oscillations at specific frequencies such as the alpha waves at 8-13 Hz from the occipital region and the beta waves at 13-30 Hz from the parietal and frontal lobes (Malmivuo, 1995). The various sources of spontaneous brain activity may be highly correlated between different recording electrodes and the averaging effect in reducing the noise during EIT image reconstruction is therefore expected to be less compared to the case of imaging blood volume changes. Thus, the SNR requirement for the boundary voltage changes is expected to be higher. This limiting factor could be minimized if the impedance changes could be separated from the EEG sources with methods such as PCA (Abascal, 2007b) or if recording would be performed just above the EEG band between 100 Hz and 1 kHz where the EEG noise is significantly reduced (Section 1.4.6). It is difficult to predict the propagation of noise through image reconstruction without performing tank or simulation studies with added noise of spontaneous brain activity and these are left for future work.

Under these limitations, the upper limit of 4 for the required SNR from Fabrizi's study (Fabrizi, 2006a) was chosen as a guide for the minimal SNR required for neuronal activity EIT. For evaluating the feasibility of implementing such method, this SNR value was compared to the results of the numerical simulations (Ch. 3 and 5) or human measurements (Ch. 4 and 6).

Table 3-2: Summary evidence for minimal SNR required for EIT of the human head.

Study	EIT system	SNR Mean±SE (range)	Image reconstruction
Humans during visual, motor or somatosensory tasks	HP 4284A	1.3±0.6 (0.5-3.4)	Correct cortical region in 38/52 recordings
Simulated data with added noise (Tidswell, 2001; Tidswell, 2006)		1 (tested 0.4-4)	Significant artefact appeared below this level
Head shaped tank + sponge	HP 4284A	0.9±0.2	Localization error ~ 2.5cm
+ Perspex rod (Tidswell, 2006)		3.2±1.3	Localization error ~ 1.3cm
Head shaped tank + Perspex rod (Tidswell, 2003)	UCLH Mk1b	2.3±0.2	Minimal localization error of 2cm
Humans during motor task (Tidswell, 2003)	UCLH Mk1b	2.9±0.4	-
Neonates during visual stimulus	UCLH Mk1b	2.0±1.0 (0.6-3.4)	Correct cortical region in 3/4 and 6/8 recordings
motor stimulus (Tidswell, 2006)		1.7±0.9 (0.6-3.8)	
Simulation of temporal lobe epilepsy (Fabrizi, 2006a)	UCLH Mk2.5	~4 (tested 4,12,64)	Images with added noise were similar to noise free images

3.2.3 Purpose

The purpose of this study was to estimate the expected voltage changes recorded on the scalp, resulting from assumed changes of 1% in local conductivity during visual stimulation causing Visual Evoked Responses (VER) and recorded by LF-EIT measurement, using simulations with a detailed Finite Element (FE) model of the adult head. The anticipated utility of this was to set a specification for further human measurements and provide a guide for assessing if any human changes appeared to be physiologically reasonable and so not due to artefact. Secondary purposes were:

1. To estimate the effect of electrode size on the resulting changes.
2. To estimate the effect of current injection electrodes proximity to the orifices (eyes and ears) on the resulting changes. The current level there is limited to 100 μA instead of 1 mA to avoid possible alteration of the underlying neuronal tissue by the injected current (Ch. 2).
3. To estimate the electrode placement most likely to yield optimal signal changes.

3.2.4 Design

3.2.4.1 Estimated changes

Previous FEM simulations done by Ahadzi and this author (Ahadzi, 2004a), have estimated the boundary voltage changes due to local conductivity change in the visual cortex. In this study, these were refined, using a realistic head model and a solver of the forward electromagnetic problem developed in our group (Horesh, 2006c). Exhaustive calculations were performed over a space of physiologically sensible conductivity values and all possible 4 terminal current injection and measurement placements. The quantitative procedure was similar to the current density calculations described in Section 2.3.2 and yielded a range of expected boundary voltage changes for different electrode combinations. Inspection of the electrode combinations which gave the largest changes permitted selection of those likely to yield the greatest sensitivity in future experimental work (Ch. 4).

3.2.4.2 Validation

The predictions obtained using FEM simulations with a forward solver were independently validated in three cases:

1. Comparison of boundary voltages on the human head with modelling predictions.
2. Comparison of boundary voltages in a spherical tank filled with saline to predictions from a homogenous spherical FE model.
3. For the same spherical tank, comparison of the changes in boundary voltages to the predicted changes when a local conductivity change was produced by insertion of a sponge.

3.3 Methods

3.3.1 Head model

The head was modelled using the Finite Element Method. The model incorporated a realistic head mesh of 53,336 elements, which comprised the following domains: scalp, skull, CSF and ventricles, grey and white matter, eyes, optic canal, olfactory tracts and auditory meatus. This mesh was produced using the I-DEAS software (Tizzard, 2005). Boundary voltages were calculated using the SuperSolver software package developed in our group (Horesh, 2006c), which incorporates a modified version of the EIDORS 3D package (Polydorides, 2002). This solver was used to numerically calculate the real part of the admittivity (conductivity) (Horesh, 2005; Gilad, 2005b). See Ch. 2 for further details on the model.

3.3.2 Electrodes and current level

A set of 31 electrodes and 1 ground, termed as the Mark 1b electrode system in our laboratory (Tidswell, 2001), were placed in a modified 10-20 electrode system (Jasper , 1958) on the surface of the scalp; this covered the entire scalp (Figure 2-2b). This was repeated for 2 different electrode diameters of 11 and 21 mm which are the diameters of the two electrode designs used in the experimental parts of this thesis.

A current level of 1 mA was used for both electrode diameters. The calculated voltages could then be linearly scaled for different current levels.

3.3.3 Perturbation

The volume of the primary visual cortex (V1) has an inter-individual variation in the range 7.7-14.2 cm^3 measured in 14 brains (Andrews, 1997). For this study, V1 was modelled as two intersecting ellipsoids with a total volume of a 9 cm^3 of grey matter (Figure 2-2b), which is the mean volume in Andrews's study.

Pilot simulations with different volumes of V1 and different geometrical placement of the ellipsoids showed that 1) the results can be linearly scaled to the V1 volume and 2) that different geometries within the bounds of Andrews et al have no significant importance on determining the overall results. Therefore, the choice of V1 volume and geometrical placement of the ellipsoids was considered to be satisfactory for the purpose of predicting the order of magnitude of boundary voltage changes.

3.3.4 Conductivities

Conductivity values of the different compartments of the model were obtained from the detailed review of the dielectric properties of the human head (Horesh, 2007b). In order to allow for uncertainties in the true conductivity values for each tissue, three values – minimum, maximum and typical median, were chosen from the literature for scalp, skull, grey and white matter (Ch. 2, Table 2-1). In order to allow for all permutations of these, the calculations were repeated 3^4=81 times using different combinations of conductivities. The CSF and eyes conductivities were maintained fixed, the optic canal and auditory meatus were set as white matter and the olfactory tracts was the set as the average between the skull and white matter (Ch. 2, Table 2-1).

3.3.5 Protocol

Forward solution and boundary voltages were calculated for all 31·30/2 = 465 possible current injection pairs with and without the perturbation of 1% increase in conductivity of the visual cortex. For each current injection pair, the boundary voltages across all possible 29·28/2 = 406 pairs of the remaining 29 electrodes were calculated. One of each pair of reciprocal electrode combination was discarded as they produce the same results (for example: [I 1,2 ; V 3,4] and [I 3,4 ; V 1,2] are equivalent current and voltage pairs). The magnitude of the voltage changes was the difference δV between the boundary voltages V_1 without the perturbation and V_2 with the perturbation. δV was therefore calculated for all the electrode combinations (465 current pairs · 406 voltage pairs / 2 reciprocal electrode combinations = 94,395). This entire protocol was repeated for the 81 different conductivity combinations σ_i (i = 1, 2,..., 81) and then for the two different electrode diameters.

3.3.6 Data analysis

The difference δV was mostly negative since the decreased resistance in the brain lowered the overall voltage. However, some small positive changes were possible since the total voltage depend on the resistivities of the difference compartments and perturbation but also on the current density distribution. This could, in some electrode combinations, be combined into a small voltage increase. Therefore, the following analysis was applied on the absolute value of these changes.

Let $\left|\delta V^{\sigma_i}\right|$ be the set of 94,395 absolute voltage differences for a conductivity set σ_i and one of the electrode diameters. Most of the 94,395 electrode combinations were linearly dependent in a sense that they could be reproduced by a linear combination of other electrode combinations. For example, [I 1,2 ; V 3,4] could be reproduced by subtracting the voltages

from [I 1,2 ; V 3,5] and [I 1,2 ; V 5,4]. Therefore, a subset of independent electrode combinations with the highest voltage changes was selected. This reduced the number of electrode combinations to 840 (30 independent current pairs · 28 independent voltage pairs = 840). From each such subset (for different σ_i and electrode diameter), the mean and standard deviation of the absolute voltage changes was calculated and defined as d_i. This voltage value was also converted to percentage units by normalizing to the mean boundary voltages V_1. A final representative value for the changes was then calculated as the mean D of the 81 d_i values and their standard deviation reflecting the effect of conductivities variability in the literature. To estimate the best case scenario, the same calculations were repeated when defining d_i as the maximal absolute changes rather than the mean.

Effect of orifices: for evaluating the influence of a possible shunting of applied current through the orifices, the above calculations were repeated after excluding from the current injection protocol 8 electrodes which were close to the eye or ear (electrodes 1,2,3,7,12,13,17 or 18) resulting in 23·22/2=253 current pairs out of the original 465 pairs. In this case, the total number of electrode combinations was 253 · 406 / 2 = 51,359 and after selecting the independent combination with the highest changes this reduced to 22 · 28 = 616 combinations.

Effect of conductivities: for evaluating the influence of each of the four adjustable conductivities (grey matter, white matter, skull and scalp) on the resulting changes, the 81 d_i values for all the conductivity combinations was expressed as a four dimensional function $d_i = f\left(\sigma_{grey}, \sigma_{white}, \sigma_{skull}, \sigma_{scalp}\right)$ where each of the four variables had three possible values. For each possible value of a certain compartment, there were 27 d_i values which were averaged and presented against the conductivity of the chosen compartment. This was applied only for the case of excluding electrodes closest to the orifices with 21 mm electrode diameter.

Optimal electrode combinations: for the given set of electrode positions, the ten electrode combinations which gave the largest absolute changes for the median conductivities were selected. This was repeated for the two electrode diameters and with and without the electrodes closest to the orifices.

3.3.7 Validations

Predicted voltages and changes: the boundary voltages and boundary voltage changes were predicted using the same method as described in Section 3.3.1. For the human case, the median of the variable conductivities were initially used (0.30, 0.015, 0.30 and 0.25 S/m for scalp, skull, grey and white matter respectively). However, the average ratio (or slope of linear regression) between the predicted and measured voltages had a bias of 30% from unity so this was compensated by repeating the calculations with scalp conductivity of 0.1 S/m. The reported results are only from the second set of calculations.

For the homogeneous spherical tank, a mesh of 225,000 elements was used and conductivity of 0.39 S/m was allocated to represent the measured conductivity of the 0.2% saline used in the experiment. The electrode positions of the model were placed at the experimental positions in either human or tank experiments.

Human measurements: a detailed description of the experimental setup is presented in Ch. 4. Briefly, 21 standard Ag/AgCl EEG electrodes (11 mm diameter) were placed on the back of the head centred above the visual cortex (5 cm above the inion of the occipital bone). In contrast to the modified 10-20 electrode system used in the modelling study to cover the entire head, the choice of clustering the electrodes on the back of the head in the human measurements was made following the conclusion presented later in this chapter, that the most sensitive electrode combinations for measuring impedance changes in the visual cortex are located on the occipital area. The reference and ground electrodes for all channels were the standard EEG positions Fz (forehead) and Cz (vertex) respectively. Two electrodes were used to inject current and the rest were used to record voltages. In 50% of the experiments, two 21 mm diameter recessed design electrodes (see Ch. 2) were used to inject the current.

Recordings were made during 10 experiments from 7 subjects (2 male, 5 females, age 25-42 years). One subject was repeated twice and another subject three times, allowing estimation of the reproducibility of the results. Each experiment included two recordings with the same electrode positions. In each recording, 2 electrodes were used to inject a 1 Hz bipolar square wave current within the range of 100-1000 μA and the remaining 19 electrodes were used to record the voltages. The differences between the two recordings were in the current pair used or in the technical variation of the setup (see Ch. 4). In each recording, data was recorded for 10 minutes allowing averaging of 600 square wave periods. Recordings were made during rest and during a presentation of full field checkerboard visual stimulation. However, for the purpose of this validation, only the control data during rest was used to measure the boundary voltages developing on the scalp as a result of the square wave current.

The voltages were recorded using an extended dynamic range EEG system (SD128 or SD32, Micromed, Italy with dynamic range of ±12.8 and ±102.4 mV respectively). The boundary voltages were in the order of 1-100 mV and were measured with standard error (SE) below 1 μV limited by the background brain activity producing EEG signal. After excluding 2 current injecting electrodes out of the 21 electrodes, 18 independent measurement pairs with the highest boundary voltages were selected out of the remaining 19 electrodes. The two recordings in each of the 10 experiments yielded a total of $10 \cdot 2 \cdot 18 = 360$ data points.

Tank experiment: the tank experiment was done with the same recording setup on a spherical tank (19 cm diameter) filled with 0.2% saline (conductivity 0.39 S/m) and 31 Ag/AgCl 2 mm diameter ball electrodes placed over one hemisphere. The local resistivity perturbation in the visual cortex area was simulated using a sponge ellipsoid of height 5 cm and diameter 2.66

cm with volume 18.5 cm^3 made of 5% weight/volume polyurethane which produced a 19% increase in resistivity when measured directly with a Hewlett Packard HP 4284A Impedance Analyzer at 20 Hz (Figure 3-1); it was placed on a porous wooden support 3 mm in diameter and 19 cm long. Data was acquired and averaged for one minute.

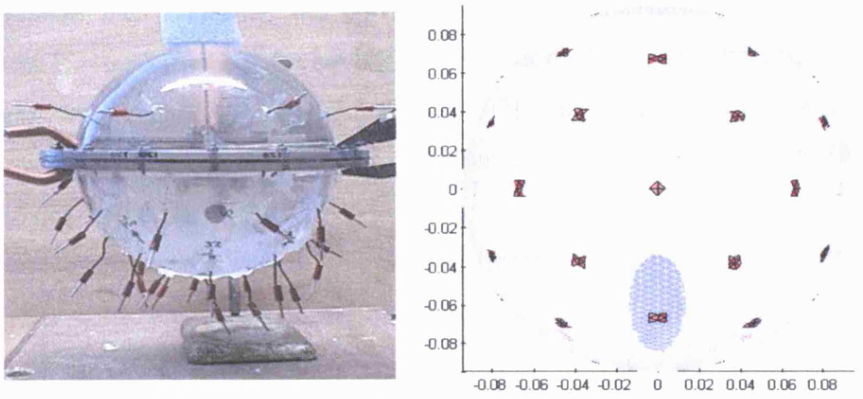

Figure 3-1: Left – side view of the spherical tank. Right – bottom view of the spherical mesh. Red - electrodes; blue - ellipsoid perturbation. Axes are in meters.

Data analysis: first order linear regression was used to compare the measured and predicted boundary voltages and boundary voltage changes for both tank and human measurements. All data from the human and tank experiments as well as the modelling predictions, were normalized as if the current level used was 100 μA. For the human experiments, the data from the two recordings of each experiment were grouped and the linear regression parameters, the correlation coefficient R, and the p value for having no correlation were calculated for the 10 experiments. The mean R, p value and slope were then calculated together with the standard deviation (SD) of the 10 slopes. For the tank experiment, R, p value, the slope and the standard errors E_a and E_b of the regression coefficients were calculated for the two cases of boundary voltages and boundary voltage changes. For evaluating the reproducibility of the slope when recordings were repeated from the same subjects, the slope values for the 10 experiments were displayed.

3.3.8 Statistics

The values for the slope of the linear regression were given as mean±SD for the human measurements so the SD reflected inter and intra subject slope variability. The slopes for the tank study were given as mean±SE so the SE reflected the accuracy of the model in predicting the experimental tank measurements. The final values for the estimated voltage changes in the human model were given as mean±SD. The SD provided bounds for the possible estimated changes and was originated from the uncertainty in the conductivity values taken from the literature.

3.4 Results

3.4.1 Validations

For the human measurements, the correlation between measured and predicted boundary voltages was R = 0.93 ($p < 10^{-9}$ for having no correlation; N = 10 experiments, each with n = 36 data points), with a slope of 1.0 ± 0.3 (Figure 3-2). The intra subject slope variability from repeated recordings was visually similar to the inter subject slope variability (Figure 3-3, too few data to quantify this).

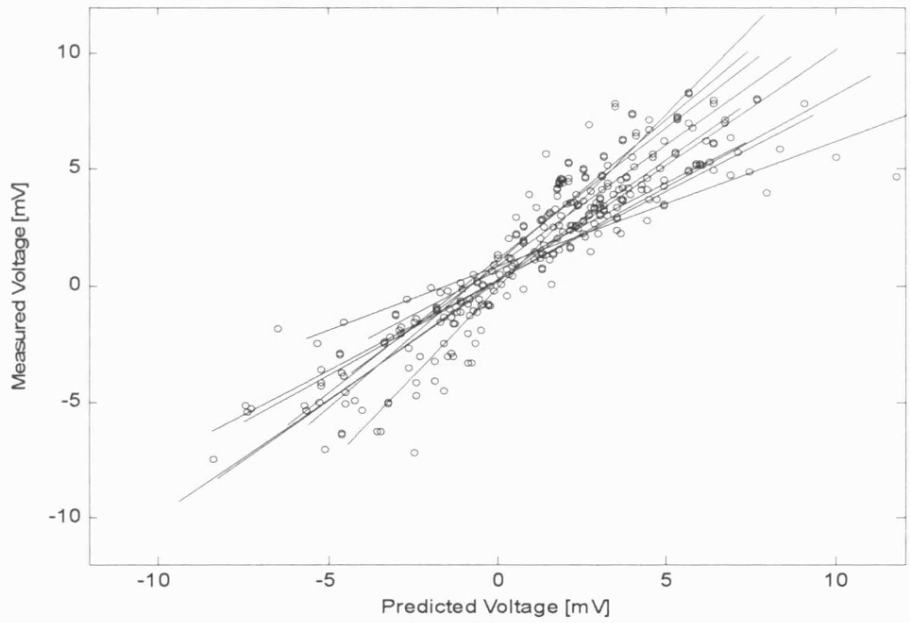

Figure 3-2: Measured vs. predicted boundary voltages for the 10 human experiments.

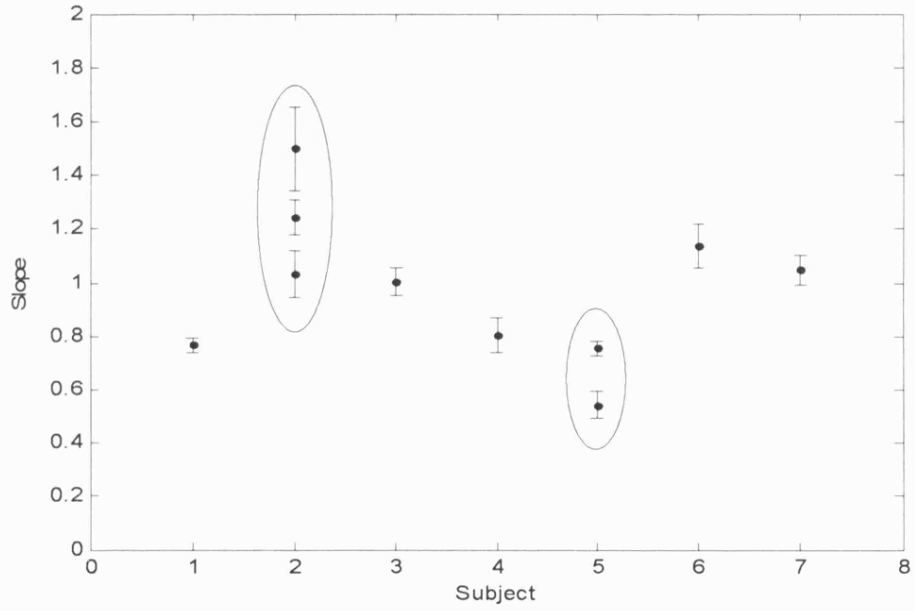

Figure 3-3: slope values for the different subjects. Repeated recordings of subject 2 and 5 are marked with ellipsoids.

For the tank measurements, the correlation between measured and predicted boundary voltages was R = 0.98 ($p < 10^{-67}$; N = 95), with a slope of 1.02 ± 0.02 (Figure 3-4). For the changes due to sponge perturbation, the correlation was R = 0.87 ($p < 10^{-28}$; N = 95), with a slope of 1.04 ± 0.06 (Figure 3-5).

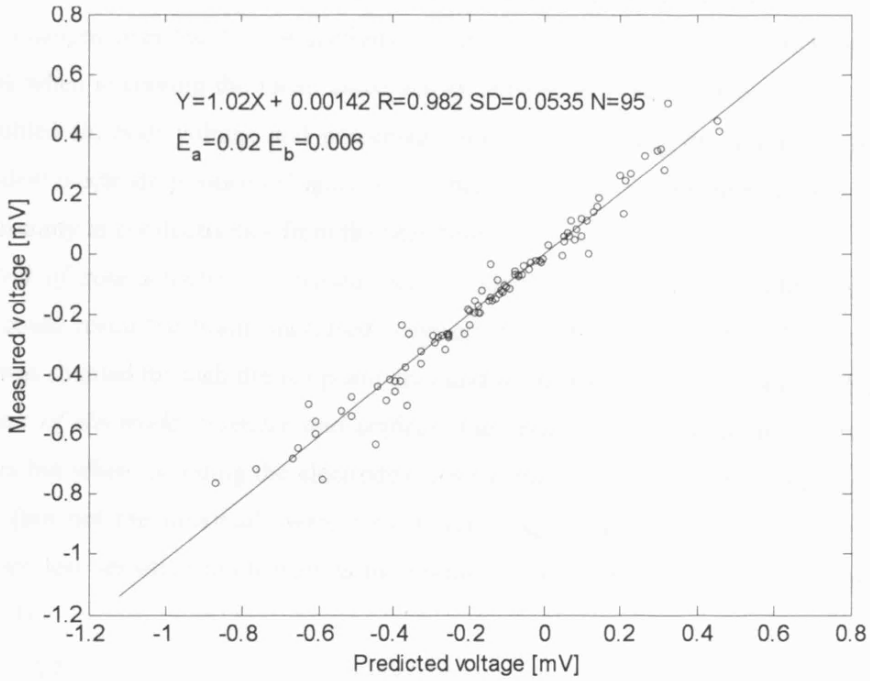

Figure 3-4: Measured vs. predicted boundary voltages for the spherical tank.

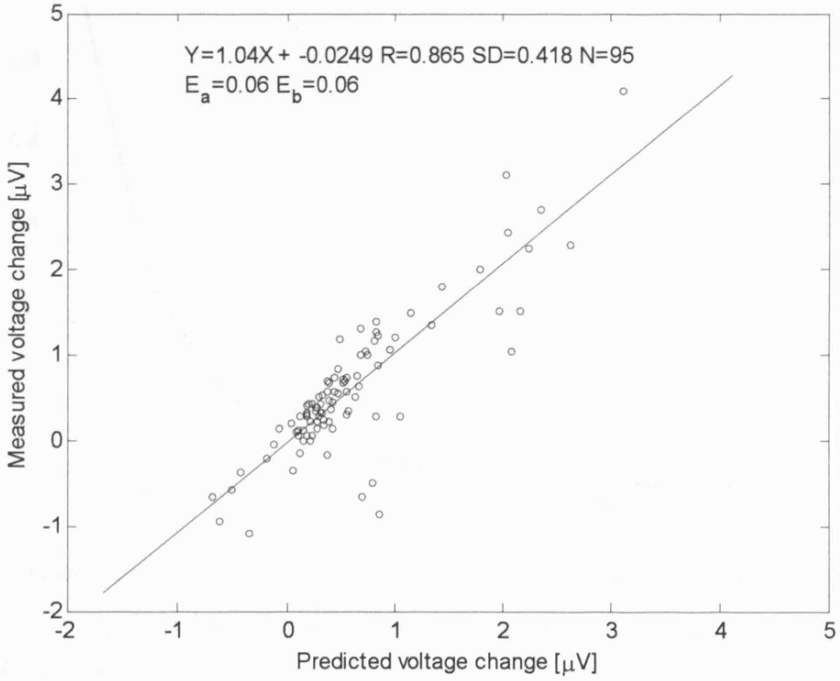

Figure 3-5: Measured vs. predicted boundary voltage change for the spherical tank.

3.4.2 Estimated changes

The magnitude of the changes: the distribution of the voltage changes in the independent electrode combinations most sensitive to the visual cortex was bell shaped. When considering all possible current injection electrode combinations, most of the changes are very small (Figure 3-6). For the 21 mm diameter electrodes, after excluding the electrodes close to the orifices, the average changes over the 81 conductivity combinations were D = 0.54 ± 0.36 μV; 0.0018 ± 0.0014% when averaging the mean value across independent electrode positions. This average was doubled (in both voltage and percentage units) when taking the maximal change across independent electrode positions (Figure 3-7, Table 3-3). In the values given above, SD reflected the uncertainty in conductivities from the literature.

Effect of conductivities: increased skull conductivity increased the changes since more current could reach the brain, increased scalp conductivity decreased the changes since more current was shunted through the scalp and grey and white matter had minor effect (Figure 3-8).

Effect of electrode diameter and orifices: the results were similar for the two electrode diameters but when including the electrodes close to the orifices for current injection, the mean changes (but not the maximal) were 10% lower, suggesting that the electrodes close to the orifices are less sensitive to changes in the visual cortex compared to the remaining electrodes (Table 3-3).

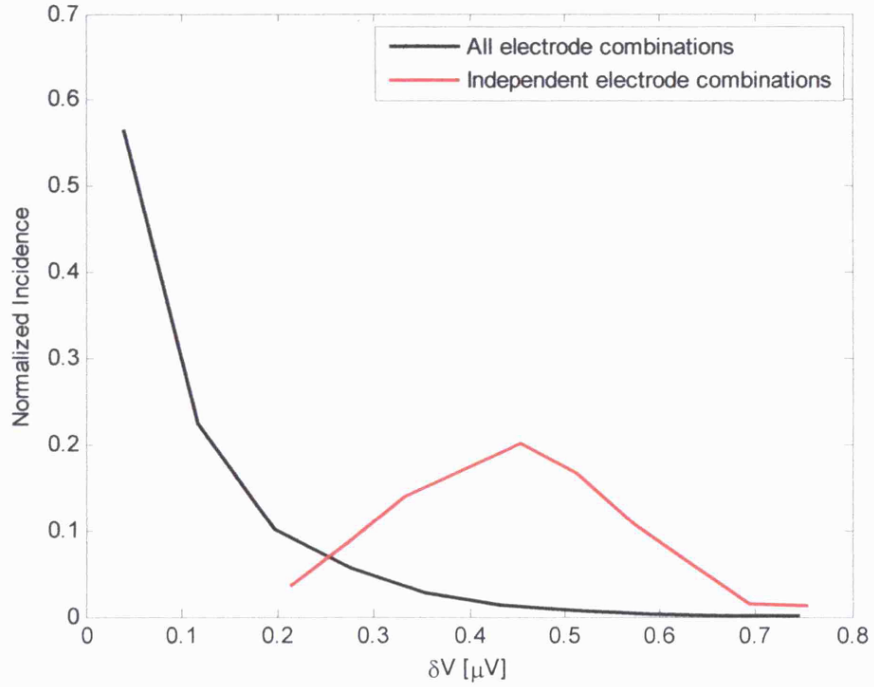

Figure 3-6: normalized incidence of the voltage changes from all electrode combinations (n=51,359) and from the subset of independent combinations most sensitive to the visual cortex (n=616). This is for the case of 21 mm diameter, median conductivity values and excluding current injection close to the orifices.

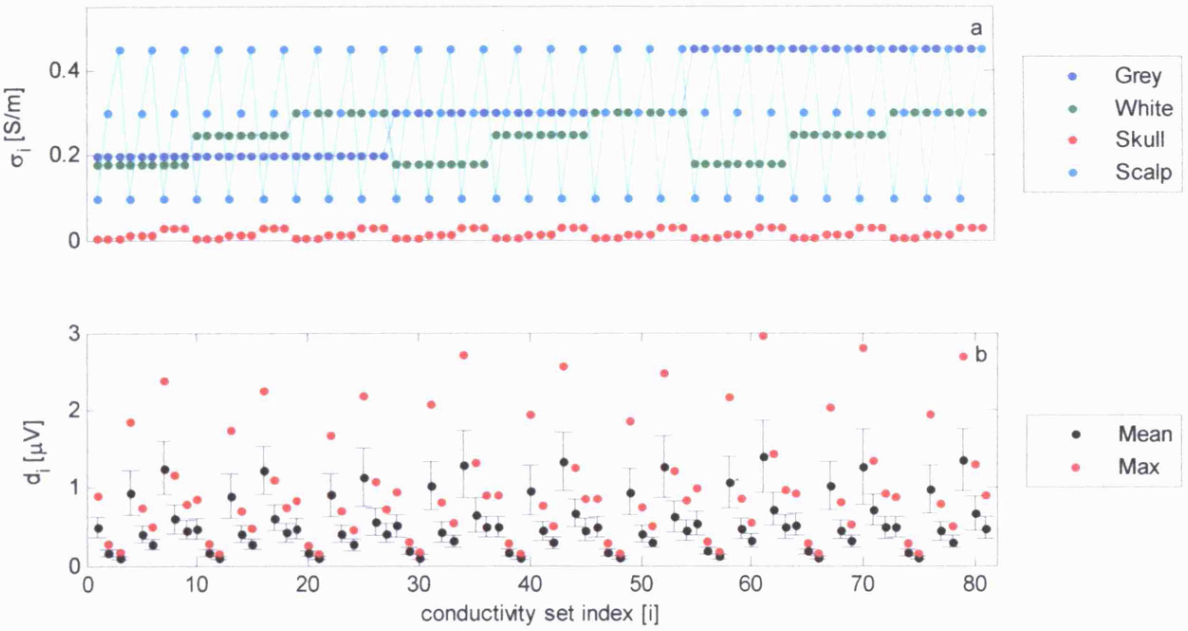

Figure 3-7: a) the 81 conductivity sets σ_i (points were connected for clarity). b) The mean of the changes from independent electrode combinations (error bars are the SD) and the maximal changes (red dots) This is for the case of 21 mm diameter and excluding current injection close to the orifices

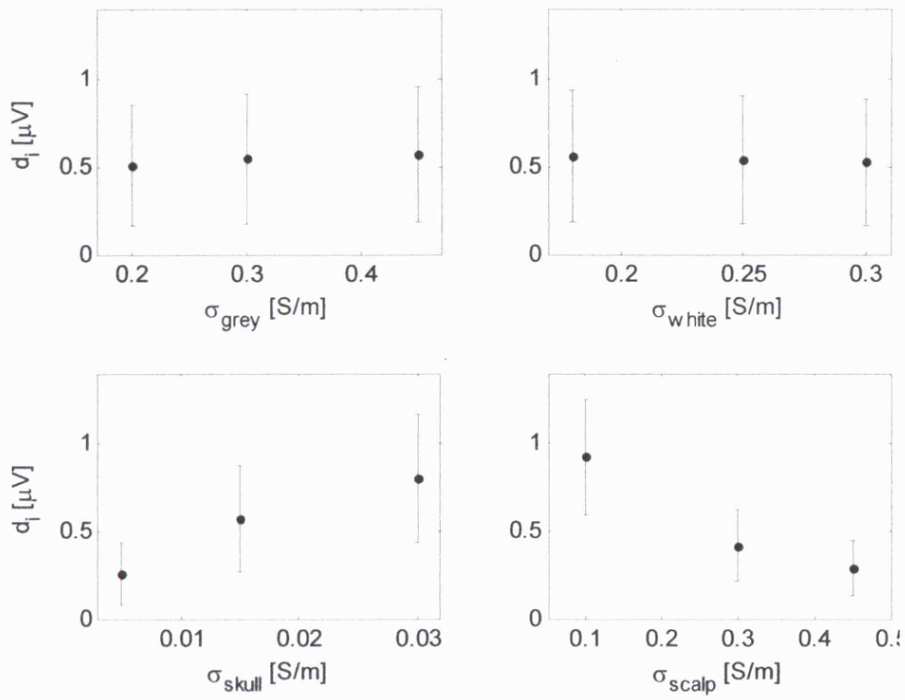

Figure 3-8: effect of the four conductivities on the average changes. Each point in a graph is the average of 27 d_i values with the same conductivity as the compartment on the x axis. The error bars are the SD.

Table 3-3: mean (maximum in brackets) voltage changes for all independent electrode combinations and all conductivity sets.

Electrode diameter [mm]	Exclude electrodes near the orifices?	D [μV]	D [%]
11	Yes	0.56 ± 0.38 (1.08 ± 0.80)	0.0020 ± 0.0016 (0.0043 ± 0.0035)
	No	0.50 ± 0.34 (1.08 ± 0.80)	0.0020 ± 0.0016 (0.0043 ± 0.0035)
21	Yes	0.54 ± 0.36 (1.03 ± 0.75)	0.0018 ± 0.0014 (0.0039 ± 0.0034)
	No	0.49 ± 0.34 (1.03 ± 0.75)	0.0018 ± 0.0014 (0.0039 ± 0.0034)

3.4.3 Optimal electrode placement

For the 21 mm diameter electrodes, the electrode combination which gave the largest peak change for the median conductivities was with current injection over the occipital region with an adjacent (5 cm apart) pair of electrodes (29 and 30) and recording immediately lateral to these (23 and 27) (Figure 3-9). The electrode combinations for the ten uppermost changes were all around the occipital area (Table 3-4). These combinations included current injection from semi-adjacent (10 cm apart) electrodes on the back of the head and recording from electrodes near to these. The current electrodes could be replaced with the measurements according to the reciprocity principle.

For the 11 mm electrodes, the uppermost two combinations were identical to the case with the 21 mm and out of the remaining eight, six were identical but at different list order.

Effect of the orifices: for both electrode diameters, identical optimal electrode combinations were obtained when including or excluding the electrodes closest to the orifices.

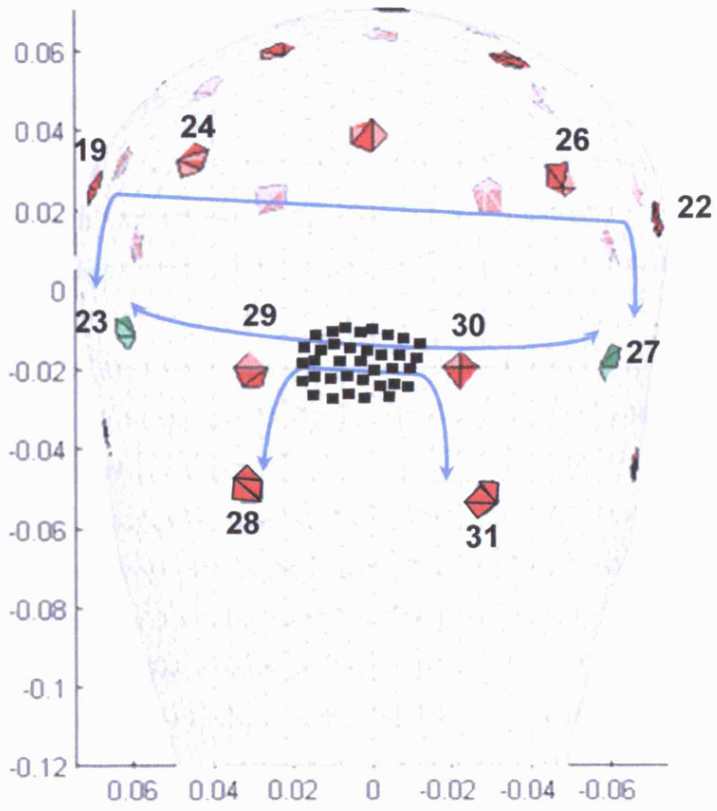

Figure 3-9: the electrode combination which gave the largest peak change for the median conductivities (blue arrow).The black dots mark the surface projection of the modelled visual cortex. The view is on the back of the head and the axes are in metres.

Table 3-4: ten uppermost sensitive electrode combinations for 21mm diameter and median conductivities. Electrode numbers are as marked in Figure 3-9.

δV [μV]	δV [%]	Current pair	Measure pair
0.78	0.0034	29 30	23 27
0.77	0.0014	23 30	19 27
0.76	0.0014	24 30	23 31
0.75	0.0011	23 31	19 30
0.74	0.0011	24 30	19 31
0.74	0.0015	27 28	26 29
0.73	0.0020	23 30	24 27
0.73	0.0014	19 30	23 27
0.72	0.0010	23 30	19 31
0.72	0.0012	22 28	26 29

3.5 Discussion

3.5.1 Summary of results

For the studies intended to validate the modelling method, there was a high correlation between measured and predicted boundary voltages (human measurements: R = 0.93; slope 1.0 ± 0.3, phantom: R = 0.98; slope 1.02 ± 0.02) as well as for the sponge perturbation (R = 0.87; slope 1.04 ± 0.06).

The magnitude of the averaged boundary voltage changes due to 1% conductivity increase of 9 cm^3 volume of visual cortex for the 21 mm diameter electrodes and after excluding the electrodes close to the orifices was 0.54 μV (0.0018%) when using 1mA of EIT current. With respect to variable conductivities due to uncertainty in the literature, this varied by 0.36 μV (0.0014%). When averaging the maximal changes for each conductivity set the changes were 2 times higher than those for the mean changes. Values were most sensitive to the choice of skull and scalp conductivities. The results were similar for the two electrode diameters but when including the electrodes close to the orifices for current injection, the mean changes (but not the maximal) were 10% lower, suggesting that the electrodes close to the orifices are less sensitive to changes in the visual cortex compared to the remaining electrodes.

The combinations which gave the largest peak changes were with current injection over the occipital region with an adjacent (5 cm apart) or semi-adjacent (10 cm apart) pair of electrodes and recording immediately lateral to these.

3.5.2 Technical issues

The changes presented in this study are given in both voltage and percentage units. The use of voltage units is essential when comparing the EIT changes with physiological and other sources of noise to estimate the SNR that could be achieved in realistic human measurements. However, these changes were calculated for a specific current level, 1 mA in this study, and need to be linearly scaled when other current levels are considered. The use of percentage units relative to the magnitude of the EIT boundary voltage has been used as a convention in EIT studies and is easy to interpret. However, such figures should be treated with caution as the magnitude of the changes, in voltage units, is not linearly related to the magnitude of the standing voltages and erroneous results could be obtained. An example of this is the values given in Table 3-4 for the top 10 highest changes. The variation in the voltage changes is only 10% (0.72-0.78 μV) whereas the variation in the percentage changes is almost 300% (0.0012-0.0034%). Therefore, I decided to use voltage units when interpreting the results but included translation to percentage values in order to be consistent with the convention.

3.5.3 Validations

Overall, the three different validations done with human and tank measurements suggest that the estimation methods are valid and that the estimated changes resulting from neuronal activity are within the correct order of magnitude.

For the human measurements, the average slope was 1.0 ± 0.3 (R = 0.93). The dispersion around a unity slope was related to the following limitations of the model: 1) inaccurate registration of conductivities in the different compartments of the mesh, 2) usage of single standard head geometry in the mesh which did not take into account individual differences in anatomy, 3) projection of the electrode positions from the individual head geometry onto the standard mesh and 4) no allowance for tissue anisotropy.

In two subjects with repeated recordings, the intra subject variance of the slope, was of the same order of magnitude as the inter subject variance (Figure 3-3). The intra subject variance was ascribed to the different electrode positions in repeated experiments in the order of 2 cm, which were projected differently on the standard mesh.

For the tank measurements, the slope was 1.02 ± 0.02 (R = 0.98) for the boundary voltages and 1.04 ± 0.06 (R = 0.87) for the sponge perturbation. Apart from validating the modelling methods, the latter result was encouraging, since the changes related to the sponge were three orders of magnitude smaller than the boundary voltages and close to the effective sensitivity of the recording system of the order of 1 μV.

A separate validation study done on a realistic human shaped tank with skull and saline using a different experimental setup than the one used in this study, gave a slope of 0.89 (R = 0.89) when comparing measured and predicted boundary voltages (Horesh, 2006a). In the same study, the measured and predicted changes in boundary voltage resulted from a sponge perturbation, were on the same order of magnitude but were not correlated. This was ascribed by the author to limitations in the sensitivity of the experimental setup and lack of mechanical stability of the skull within the tank (Horesh, 2006a).

3.5.4 Estimated changes and SNR

The magnitude of the averaged estimated changes was 0.54 μV (0.0018%) per 1% conductivity perturbation in 9 cm^3 of visual cortex. This was doubled for the maximal change over electrode combinations. These results can be linearly scaled if the assumption of conductivity perturbation and volume are modified within the same order of magnitude. The physiological noise level obtained from background brain activity in the occipital area when eyes are open is about 10 μV

and after averaging 1000 stimuli for 10 minutes, this noise reduces to 10 μV / √1000 = 0.3 μV. This predicts an SNR of only 1.7 for the averaged changes and 3.5 for the maximal values.

The implications for implementing an imaging system based on the present method are limited as the estimated average SNR for allowing image reconstruction was about 4. This was obtained from reviewing previous applications of human brain EIT and specific considerations for the neuronal activity case (Section 3.2.2). This required SNR of 4 was for the average of 10% the changes in a protocol of 258 electrode combinations. For the purpose of comparing this value to the estimated SNR from my model, I chose to take the average SNR obtained for the mean and maximal changes in my independent electrode protocol (1.7+3.5)/2 = 2.6. Longer averaging over about 30 minutes (10 minutes x $(4/2.6)^2$) could improve the SNR to the desired level but just for one current pair. A possible way to reduce this averaging time is to record at higher frequency above the EEG band which was estimated to enhance the SNR by a factor of 5 (Section 1.4.6) and hence reduce the averaging time by a factor of 25. Exploring this possibility was left for future experimental work.

In addition, for image reconstruction, data is needed from multiple current injection pairs. For obtaining previous EIT images of haemodynamic changes in the brain, an electrode protocol consisting of 21 current pairs, each with 12 voltage measurement pairs was used (Tidswell, 2001; Tidswell, 2006). Due to reciprocity, similar results could be obtained with 12 current pairs, each with 21 voltage measurements. Since multiple voltage measurements could be done in parallel, the limiting factor is the number of current pairs. For 12 current pairs and 30 minutes that might be needed for sufficient SNR, the overall recording time would be 6 hours which is impractical for human subjects to tolerate. This could be partly overcome by employing multiple current injection schemes but these will have to inject lower current levels to adhere safety standards which will decrease the SNR.

I therefore conclude that non-invasive imaging with LF-EIT method is not feasible with present technology. Future effort should be focused on achieving substantial improvement in SNR without averaging for a long time.

The effect of different conductivity estimates: the standard deviation of the averaged predicted changes D resulted from the different conductivity values used in the 81 sets. The analysis of the effect of each compartment on the resulting changes d_i (Figure 3-8) reveal that the choice of grey and white matter conductivities has minor influence on the model estimations. However, increased skull conductivity *increased* the changes as more current could penetrate the skull and reach the brain. On the other hand, increased scalp conductivity *decreased* the changes because more current was shunted through the scalp and did not flow through the skull into the brain. Therefore, the choice of skull and scalp conductivities was an important factor in this model determining the magnitude of the changes.

Effect of electrode diameter and orifices: the same maximal changes and up to 10% differences for the average changes were obtained when electrodes close the orifices were included or excluded from the protocol and for the two electrode diameters (Table 3-3). These finding suggests that the sensitivity for internal impedance changes under the model conditions is weakly dependent on the area of the surface electrodes. This allows the use of large and small electrodes for current injection and voltage measurements interchangeably. These results agree with a previous 2D simulation study on errors of static EIT, showing that for changes of -33 and +166% in the electrode diameter, there were no significant changes in the reconstructed image (Kolehmainen, 1997). Therefore, as discussed in Ch. 2, the use of large electrodes for current injection reduces the current density on the surface and allows an increase in the current level of up to one order of magnitude, without causing inconvenient skin sensation or altering brain function.

In addition, the highest changes were originated from electrodes far from the orifices which can carry the maximal current of 1 mA without the possibility of altering the underlying neuronal activity limiting the current level in these to 100 μA (Ch. 2). The implications of this for imaging neuronal activity in the visual cortex area is that excluding these electrodes from the protocol will not reduce the estimated changes.

3.5.5 Optimal electrode placement

Estimating the optimal electrode placement was important for designing actual human measurements to attempt measuring neuronal activity related changes in single channel measurements. This is a preliminary requirement for allowing estimation of the actual SNR of such changes before approaching the more demanding imaging problem.

The combinations which gave the largest peak changes were with current injection over the occipital region with an adjacent (5 cm apart) or semi-adjacent (10 cm apart) pair of electrodes and recording immediately lateral to these (Table 3-4 and Figure 3-9). All these optimal combinations were intuitively justified as the close current injection pair was sensible for obtaining high current density in the occipital cortex just below the electrodes and the recording pair was located where high boundary voltage is expected near the two injection electrodes.

The reciprocity principle allows each resulted optimal electrode placement to be interchangeably considered as reciprocal current injection and measurement pairs. The optimality obtained from this study is limited to the pre-defined set of electrode positions and is not generalized to any electrode position.

3.5.6 Future work

Several studies are suggested for future work:

1. Reconstruction study: the main limitation of the minimal SNR estimation required for image reconstruction (Section 3.2.2) was the uncertainty about how the image reconstruction would be effected by noise originated from spontaneous brain activity which is not normally distributed and could be highly correlated between recording channels. An initial design of such a study could be to calculate the boundary voltage changes using the forward solution, introduce increasing levels of additive and/or multiplicative noise originated from real LF-EIT human recordings and using various inverse solution methods to reconstruct the images and estimate their quality. A similar study has already been done in our research group for the case of imaging cell swelling effects during epilepsy (Fabrizi, 2006a). Additional considerations will need to be taken to introduce biases related to inaccurate mesh, electrode positions and conductivities as well as minimizing the effect of the 'inverse crime', a term related to solving the inverse problem for changes generated from the same mesh and not from real data.
2. Multiple current injection patterns: trigonometric multiple current patterns have been developed for optimizing the distinguishability of conductivities (Isaacson, 1986; Demidenko, 2005). For imaging neuronal activity, the use of multiple current patterns could allow minimizing the acquisition time comparing to single current pairs. However, the safely limits for total current and current density in the brain may require using lower current levels which will reduce the SNR and increase the averaging time. The different theoretical trade-offs need to be evaluated and supported by simulation studies.
3. The effect of anisotropy: scalp, skull and white matter has anisotropic conductivity properties which are not taken into account in our isotropic forward solver. Recent improvements to the solvers used in our group (SuperSolver) have incorporated the framework for anisotropic solutions (Horesh, 2006a; Abascal, 2007a; Abascal, 2007b). However, the present limitation for using it in modelling studies is the insufficiently accurate head model registering the anisotropic properties for each element and exact physiological knowledge about these properties. Recent advances in diffusion MRI may be valuable for mapping anisotropic properties which were found to be linearly related to diffusion properties (Tuch, 2001).
4. Refinements to the model: incorporating more accurate head model with finer structures and update the conductivity values used when new measurements of the dielectric properties of the head tissues will become available in the literature.

4. Low frequency EIT of evoked physiological activity in the brain with scalp electrodes: measuring changes non-invasively in humans

4.1 Abstract

According to the modelling in Ch. 3, the maximal boundary voltage changes due to 1% conductivity increase of 9 cm^3 volume of visual cortex during visual evoked responses (VER) was 1.03 ± 0.75 μV (0.0039 ± 0.0034 %) when using 1mA of EIT current. The purpose of this chapter is to measure these changes non-invasively in humans in order to compare to the modelling prediction, estimate the actual SNR that could be achieved and evaluate the implications for designing an EIT based non-invasive functional imaging system for imaging fast neuronal activity in the human brain.

A prototype low frequency EIT (LF-EIT) system was developed for measuring the real part of the impedance change and novel signal processing techniques were applied to separate the EIT and VEP components recorded within the same band, optimize SNR and detect the underlying changes. In this study, 20 recordings were obtained from 7 healthy subjects. A 1 Hz square wave current of up to 1 mA was applied through a pair of occipital electrodes synchronously to 2 Stimuli/sec pattern reversal chequerboard VER. Voltages were recorded from 19 electrodes over the occipital area and averaged over 10 minutes.

In this study, for the first time, non-invasive measurement of fast resistivity changes related to neuronal activity were measured. Significant changes were observed in 35% of individual recordings with SNR between 2 and 5. When applying a group average over 80% of the recording without a strong α rhythm component, the magnitude of the underlying signal was 0.25 ± 0.07 μV (0.0008 ± 0.0002 %) for an average current level of 295 μA and SNR of 3.4 and was peaking at 130 ms after the visual stimulus. when normalized to current injection of 1mA, this became 0.85 ± 0.07 μV (0.00080 ± 0.00006 %) with SNR of 12.1.

Overall, these changes agreed with the modelling predictions. At present, the implications for imaging system are limited at this stage since about 7 hours were estimated to be required for recording data from multiple current injection pairs with sufficient SNR, which is not practical when recording on humans. The SNR was mainly limited by background brain activity. Several improvements to the hardware and protocol are suggested which could potentially reduce the total recording time to several minutes and could make this methods practically tolerable to human subjects.

4.2 Introduction

The ultimate goal of the work in this thesis was to develop a non-invasive imaging method capable of imaging the impedance changes over milliseconds, occurring when neuronal ion channels open during activity, with scalp electrodes. In order to achieve this, it was first necessary to demonstrate that reliable impedance changes could be recorded during physiologically evoked activity with scalp electrodes in human subjects. In this chapter, I present an experimental study using a prototype system in which such changes were recorded, for the first time. No imaging was undertaken; the goal of this study was to determine if such changes could reliably be recorded in several channels positioned over active cerebral cortex.

4.2.1 Expectations based on modelling and physiological considerations.

The exact magnitude of the impedance change in cerebral cortex is not exactly known but modelling work in our group and previous experimental studies in the literature have been reviewed in Sections 1.4 and 3.2.1. In summary, these local changes are probably about 1%, if recorded below 100 Hz. In order to be useful for non-invasive imaging, it is necessary to record these changes with scalp electrodes. The signal recorded on the scalp may be expected to be much smaller, because of partial volume effects and diversion of applied current by the resistive skull. This has been estimated in Ch. 3, using a Finite Element Model and the resulting maximal changes in boundary voltages during LF-EIT measurement due to 1% conductivity increase of 9 cm^3 volume of visual cortex during visual stimulation are expected to be 1.03 ± 0.75 μV (Mean ± SD) or 0.0039 ± 0.0034 % for an applied current of 1 mA (mean changes were half of this).

The critical issue is whether it is likely to be possible to detect such small changes against the endogenous scalp EEG and other sources of noise. The physiological noise level obtained from background brain activity in the occipital area when eyes are open is about 10 μV. This would clearly drown out individual impedance changes, but could be reduced by averaging. On the assumption that a subject could tolerate 10 minutes of repeated stimulation, and stimulation rate of 2 Stimuli/sec, 1200 averages could be expected in one recording, which in theory could reduce the background noise to about 0.3 μV, and so a SNR of about 3. It might be expected that inter-subject averaging could improve the SNR further.

Since EIT was originally proposed for use in imaging neuronal activity (Holder, 1987), very few studies have been presented in which attempts were made to measure impedance changes of neuronal activity on humans and these suffered from major technical limitations. In these studies changes were not observed at all (Holder, 1989; Enfield, 2005) or measured but were probably related to an artefact in their system and not to a physiological effect (Murrieta-Lee, 2004; Murrieta-Lee, 2005; McCann, 2005) (see Section 1.4.5 for details).

4.2.2 Purpose

The purpose of this study was to determine if reproducible changes in boundary voltages due to impedance changes in the brain could be recorded with scalp electrodes and LF-EIT during visual evoked responses.

4.2.3 Experimental design

Experiments were undertaken in adult human subjects during full field pattern reversal visual evoked response paradigm. Total of 20 LF-EIT recordings were recorded from 7 subjects. A prototype LF-EIT system was developed consisting of a current source applying 1 Hz square wave of up to 1 mA through standard EEG or recessed design electrodes for reducing skin current density at high current levels (Ch. 2), a modified EEG system for data acquisition and standard equipment for applying visual stimulation. Following the optimal electrode positions modelled in Ch. 3 likely to record the largest impedance change during visual evoked responses, 21 electrodes were placed over the occipital part of the scalp and were used for recording of both the visual evoked potential and low frequency resistance change (Figure 4-1). The low frequency resistance changes were recorded by a method originally proposed by Boone (Boone, 1995a) for separating the resistance changes from the EP signals when they are recorded within the same frequency band. The data from all the recordings was pooled for enhancing the SNR. The sensitivity of the prototype system to fast resistivity changes was validated on a resistor network and crab peripheral nerve using the same instrumentation, protocol and data analysis as for the human recordings.

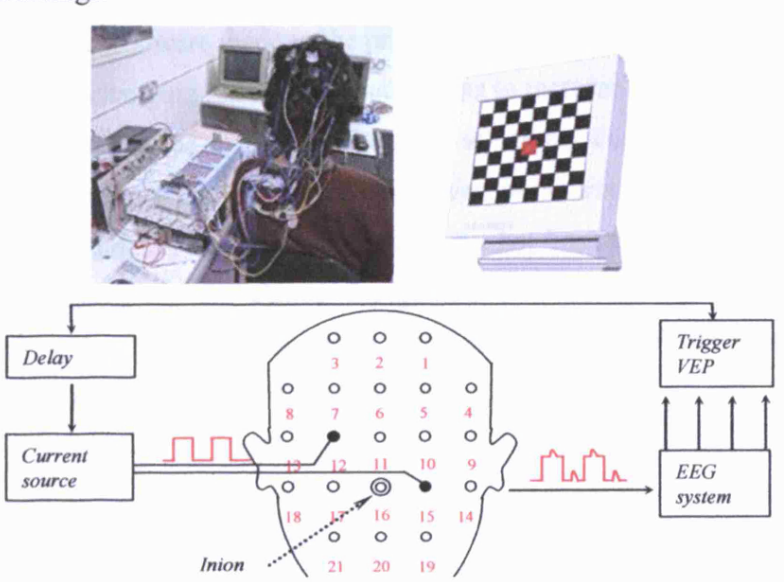

Figure 4-1: The experimental setup - pattern reversal checkerboard induced VEP, current was injected through a pair of electrodes and 19 remaining electrodes were used for recording.

4.3 Methods

4.3.1 Subjects and recordings

Total of 20 LF-EIT recordings were made from 7 normal subjects with age range of 25 to 42 (5 female and 2 male). Female subjects were preferred as they show an average of 50% higher VEP magnitude which might be related to thinner skull or smaller head but is not well understood (Stockard , 1979; Binnie, 1995; Shibata, 2000). Higher VEP magnitude is estimated to be proportional to synchrony of neuronal activity and therefore is expected to increase the SNR of the resistivity change measurements. Three out of the seven subjects used their own spectacles in the experiment to correct for minor vision defects of magnitude up to +1.25D.

Each subject was recorded twice during a recording session and subject 2 and 5 were repeated 3 and 2 times respectively on different days. The LF-EIT recordings were numbered between 1 and 10 followed by A or B to mark the two recordings made in each session (Table 4-1). Any one recording (A or B) comprised 10 minutes of stimulation with the chequerboard and 10 minutes of control with impedance recording but no visual stimulation. The control series was needed in order to estimate the settling square wave response without the superadded impedance change, as this was needed for subtraction in calculation of the impedance response. Each 10 minute session was split into one minute periods with a break of one or two minutes in order to maximise attention.

The second recording (B) was with current injection from a different electrode pair or with the same current pair as in (A) but with a minor change to the procedure. In the course of this study, some minor changes were made to the procedure, in the hope that they might increase the SNR – these included changing the current source so as to increase applied current and use with this of recessed electrodes, as well as introducing additional cognitive task to maintain the subject alertness and minimise alpha rhythm. However, in the event, these did not significantly alter the findings, so all data with these minor variations has been pooled.

To avoid confusion, the impedance change and VEP derived from one data set of 10 minutes stimulus and 10 minutes control is referred to as an "LF-EIT recording" and the component one minute recording as "1 minute recording".

Table 4-1: Summary of subjects, recordings and experimental setup.

Recording	Subject	Male/ Female	Age	Current [μA][a]	Display	EEG system	Current source[b]	N'[c]
Recordings with two current pairs								
1A,1B	1	F	29	200,200	CRT	DS128	CM	10,10
2A,2B	2	F	25	150,150	CRT	DS128	CM	10,6
3A,3B	3	F	31	150,150	CRT	DS128	CM	10,10
4A,4B	4	F	25	170,170	CRT	DS128	CM	10,10
5A,5B	2	F	25	150,130	CRT	DS128	CM	10,10
Recordings with one current pair and two current sources								
6A,6B	5	M	42	100,100	CRT	DS128	DS5,CM	10,10
7A,7B	6	F	27	100,100	CRT	DS128	DS5,CM	8,10
Recordings with one current pair and without/with cognitive task								
8A,8B	7	M	31	500,500	LCD	DS32	DS5	10,5
9A,9B	5	M	42	1000,1000	LCD	DS32	DS5	10,10
Recordings with one current pair, without cognitive task and two display devices								
10A,10B	2	F	25	1000,1000	LCD,CRT	DS32	DS5	10,10

[a] Current level for recording 1 (left) and 2 (right). [b] CM – custom made.
[c] N' - number of valid 1 minute recordings (Section 4.3.6.4).

4.3.2 VERs

A full field pattern reversal black/white checkerboard was generated with a Pattern 10 device (Micromed s.r.l, Treviso, Italy) while the subject was seated in a dark room, 70 cm from a 14" computer cathodic ray tube (CRT) screen in 15/20 LF-EIT recordings or 150 from an LCD projector (Hitachi, model CP-X275) with projected area of 59 x 44 cm in 5/20 LF-EIT recordings. The greater distance of the LCD projector screen brought the object closer to optical infinity and was intended to reduce de-focusing of the eye due to tiredness of the eye muscles. The subjects were requested to focus on a centred fixation yellow square on the screen (size of one check). Check size was 41.7' (60' = 1°), field size 22°x17° (32x24 checks) and 100% contrast for both CRT and projector displays. The 10 separated 1 minute recordings were made to minimize accommodation as well as de-focusing due to tiredness of the eye muscles. The stimuli rate was 2 reversals/sec in all subjects apart from a rate of 4 reversals/sec used in LF-EIT recordings 7A and 7B.

During the control 1 minute recordings, the screen was turned off and the subject was instructed to focus on a fixation point made from a constant green light emitting diode. To reduce the effect of alpha rhythm as a result of drowsiness, an ambience light was turned on which comprised a 40W bulb directed away from the subject.

4.3.3 Electrodes and placement

A dedicated electrode system termed V21 (Figure 4-2a) was defined for this study and included 21 standard Ag/AgCl EEG electrodes of 11 mm diameter placed on the back of the head centred above the visual cortex (5 cm above the inion of the occipital bone). Horizontal and vertical spacing between electrodes was 5 cm. The reference electrode for all channels was Fz (frontal bone) and the ground was Cz (vertex); both belong to the standard 10-20 electrode system (Jasper , 1958) (Figure 4-2b). A subset of 11 electrodes (Figure 4-2a) was common to the Mark 1b electrode system used for the modelling (Figure 2-2b). Two additional EEG electrodes were placed on the left and right side of the front of the chest to record the electrocardiogram (ECG) signal for possible removal of artefact caused by the cardiac signal. In the last 6/20 LF-EIT recordings (8A,B – 10A,B) recordings, the two current injection electrodes were replaced by the 21 mm diameter recessed design presented in Ch. 2 for reducing the current density at the skin contact and allow the use of higher current levels.

Figure 4-2: a) V21 electrode system on the back of the head (red). A subset of 11 electrodes is common to the Mark 1b electrode system (black numbers, solid circles). Electrodes 29 and 30 (Mark 1b) are 5 cm from the centre instead of 3 cm in the original Mark 1b system. b) top view of standard 10-20 electrode system (Jasper , 1958) (source http://faculty.washington.edu/chundler).

4.3.4 Equipment

4.3.4.1 Data acquisition

In the first 14/20 LF-EIT recordings, signals were recorded using a SD128 EEG acquisition system (Micromed s.r.l., Treviso, Italy) with ±12.8 mV extended dynamic range (MRI mode), 16bit resolution (391 nV), 1024 Hz sampling rate, 268 Hz anti-aliasing filter, high pass input filter of 0.15 Hz (40 dB/decade), common mode rejection ratio > 105 dB @ 50 Hz and input impedance > 1000 GΩ. The high dynamic range was needed to allow recording of both high level boundary voltages generated by the applied current in the order of 10 mV and the low level EEG signal and resistivity change signals of 0.1 to 10 μV. The 21 electrodes were recorded on channels 1-21, left and right ECG were recorded on channels 30 and 31 respectively and 2 Hz trigger pulses generated internally were recorded on channel 32. These pulses were used to trigger the visual stimulation and the square wave current source.

In the last 6/20 LF-EIT recordings, higher current levels required a higher dynamic range. The acquisition system was replaced with a modified version of SD32R EEG system (Micromed s.r.l., Treviso, Italy) with ±102.4 mV extended dynamic range (MRI mode) and 22 bit resolution (49 nV). The 6 bit difference from the 16 bit SD128 system improved the dynamic range by 3 bits (±102.4 mV instead of ±12.8 mV) and the voltage sensitivity by 3 bits (49 nV instead of 391 nV).

4.3.4.2 Current source

In 12/20 LF-EIT recordings, a bipolar square wave current of level 100-200 μA was applied to the head using an isolated custom made constant current source initially introduced in Appendix B of Boone's thesis (Boone, 1995a). The linear response range of loads for which the deviations from constant current are negligible was for loads of up to 70 kΩ (Appendix B of this thesis) while the contact impedance which was the main load in these human experiments was about 1 kΩ. When the external load is within the linear range, the impedance changes of the load due to neuronal activity will alter the current and produce a negligible bias of 10^{-5} in the impedance measurement. The current source was calibrated so that the DC offset was <10 μA as required by safety regulations (BS5724, 1979; IEC60601-1{ed3.0}, 2005). The current level was set to the highest level which did not saturate the SD128 acquisition system, up to the 200 μA limit of the current. Two out of the four subjects felt a slight tingling sensation during the first few seconds after the current was applied in the first few 1 minute recordings. According to the review presented in Ch. 2, the lower limit for the threshold for skin sensation is 2 A/m^2, which is indeed the current density estimated beneath 11 mm diameter electrodes when 100-200 μA are applied.

In 8/20 LF-EIT recordings, a commercial DS-5 unit was used (Digitimer, Welwyn Garden City, UK) to deliver up to 1 mA and was used as a current amplifier driven by the waveforms generated by the custom made current source. The 5-fold increase in current level was compensated by the increased surface area of the 21 mm diameter electrodes resulting in a similar current density and sensation effects felt by the subjects (see Ch. 2). The linear response range was for loads of up to 300 kΩ with negligible bias of 10^{-4} (Appendix B). A 1 μF capacitor was connected in parallel to the input stage to reduce the bandwidth of the square wave transients which produced ripples after being amplified by the DS-5 unit.

4.3.4.3 Triggering

The master triggers for the system were 2 Hz rate pulses generated by the EEG acquisition system, which directly triggered the Pattern 10 visual stimulator and were also delayed by 350 ms by a DDU-315 counter timer unit (Digitimer, Welwyn Garden City, UK; the five counters were set to 490, 350, 350, 0 and 0 ms and the output was TTL port A) before triggering the 1 Hz current source square wave. This produced a 150 ms delay between the beginning of each square wave polarity (500 ms long) and the visual stimulation triggers. This delay was chosen to position the P100 peak of the VEP at the centre of each current polarity phase (150 + 100 = 250 ms). When the DS-5 unit was used to apply a higher current, the custom-made constant current source was set to deliver a fixed current of 50 μA into a variable resistor (Muirhead and Co. model A-25-L) of 0-10 kΩ, producing a voltage of 0-0.5 V. this was connected to the input of the DS-5 unit and was mapped to produce current of 0-1 mA (Figure 4-3).

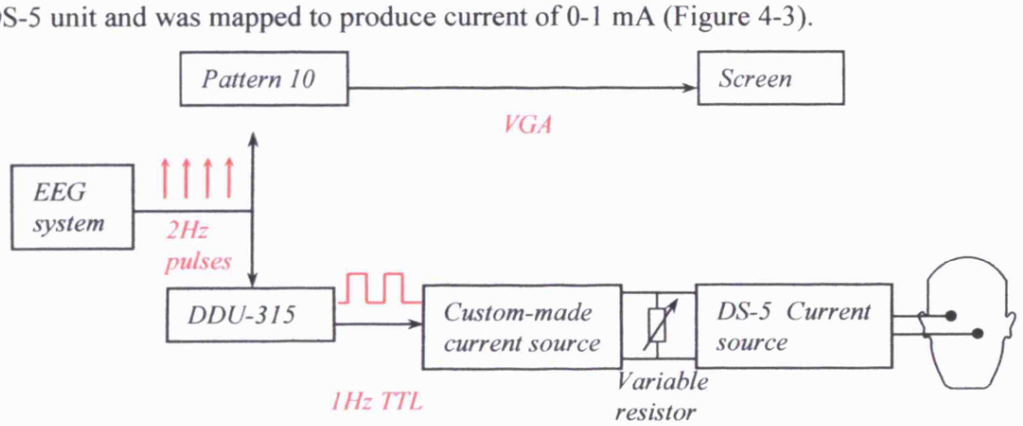

Figure 4-3: block diagram of the trigger path.

4.3.5 Protocol

20 LF-EIT recordings were obtained from the 7 subjects (Table 4-1). Each LF-EIT recording included N = 10 *active* 1 minute recordings with EIT current and visual stimuli interleaved with N = 10 *control* 1 minute recordings with EIT current but without visual stimuli. This gave 10 minutes each of active and control data available for averaging. Electrodes [10 13] were used to

apply the current in LF-EIT recordings 1A-5A and electrodes [9 12] were used in all other 15/20 LF-EIT recordings. These pairs were a subset of the recommended set of pairs obtained by the modelling (Ch. 3) and were chosen to be symmetrically placed on both sides of the visual cortex. In LF-EIT recordings 8B and 9B, a cognitive task was introduced for reducing α rhythm but was not shown to be effective. This was to press a button several times during the 1 minute recordings as a response to a sound tone of 1 kHz and 0.5 sec duration (Table 4-1).

For each subject, seven 1 minute recordings were made in addition to the two LF-EIT 10 minutes recording sets (Table 4-2). One minute recording number 1 and 4 were a background EEG for estimating the background noise and number 2 and 3 were with visual stimuli and were used to train the subject to relax and focus on the fixation point. Two sets of 20 one minute recordings comprised the two LF-EIT recordings. Each LF-EIT recording was made of 10 alternations between a control and an active one minute recording. The total number of stimuli in the active recordings for grand averaging was thus 2 reversals/sec x 60 sec x 10 repeated 1 minute recordings = 1200 stimuli. One minute recordings number 45-47 were additional background EEG and VEP controls to allow validation of possible effects of the EIT current on the normal brain function (Table 4-2).

The entire experiment lasted an average of 4 hours for each subject. The first hour was devoted to placing the electrodes on the head and attaching the electrodes (contact impedance <5 kΩ for the recording electrodes and <1 kΩ for the current injection electrodes, measured at 11.7 Hz). The subject was trained to relax and hence avoid muscular activity of the face, neck and chin during the recordings. The recording time lasted 1.2 to 2.5 hours depending on technical problems and resting breaks of variable duration required to keep the subject alert. The 3D electrode positions were measured using MicroScribe 3D digitiser (Immersion Corporate, CA, USA) at the end of the experiment.

Table 4-2: recording protocol of two LF-EIT recordings in one subject.

Number	Type	
1	Background EEG	
2,3	Visual stimuli (VEP)	
4	Background EEG	
5-23 odd	Control (EIT Current)	} LF-EIT Recording A
6-24 even	Active (Visual stimuli + EIT Current)	
25-43 odd	Control (EIT Current)	} LF-EIT Recording B
26-44 even	Active (Visual stimuli + EIT Current)	
45	Background EEG	
46,47	Visual stimuli (VEP)	

4.3.6 Data analysis

The data analysis section is organized according to the processing stages. First, the original methods proposed by Boone et al. (Boone, 1995a) for separating the resistance changes δ from the EP signals was described this method is based on summation and subtraction off the two polarities of the recorded square wave. Second, two separate algorithms has been developed for rejecting individual 1 second segments with outliers or with low VEP amplitude in order to increase the SNR in the averaged waveforms. This was also applied for rejecting entire 1 minute recordings which with attenuated VEP, presumably due to poor attention by the subject. Third, a linear model has been formulated for estimating the VEP and δ waveforms from individual LF-EIT recordings using a Maximum Likelihood estimator. Forth, data form different channels was combined for constructing a set of linearly independent measurement pairs. Fifth, statistical analysis was applied to the raw data for identifying significant changes in the δ waveform. Finally, data from all LF-EIT recordings has been grouped and the estimation and statistical analysis have been repeated.

4.3.6.1 Explanation of method for simultaneous recording of evoked potential and resistance change

The visual stimuli were delayed by 150 ms from the beginning of each of the square wave polarities and were therefore expected to produce the main component of the VEP, the P100, about half way into the 500 ms square wave (Figure 4-4). The resulting signal V recorded from the scalp was a composite signal made of three components: 1) the bi-polar voltage resulting from the square wave current flowing through the volume conductor and producing a boundary voltage on the scalp. This was supposed to be constant due to the constant current at each polarity but consisted of baseline settling time artefact due to the AC coupling of the acquisition system and the fast switching between polarities. This component was termed *b*. 2) the VEP signal which was termed *v* and 3) local decreases δ in the voltage of the square wave resulting from resistivity decreases occurring during neuronal activity, mostly expected at the same time of the P100 peak (Figure 4-4). In addition, instrumentation noise, non-synchronous brain activity signals originating from other parts of the brain, and other physiological noise such as cardiac, muscular, eyes and respiratory signals were all present in the total signal V.

The VEP and the voltage change δ related to resistivity decreases were separated by the method proposed by Boone (Boone, 1995a). In principle, the impedance change could be recorded by a single square with visual stimulation followed by a second square wave without visual stimulation and another with visual stimulation without a square wave. The impedance change could then be obtained by subtraction of the latter two waves from the first wave, but this would require three square waves per recording and also may cause electrode polarization if

a monopolar square was were always used. Boone's method employs visual stimulation on both cycles of a square wave and so reduces the number of recordings needed and provides charge balance at the electrodes. Addition of the two opposing polarities of the square wave causes cancellation of the square wave and impedance change, and so yields the VEP; subtraction cancels the VEP and leaves a square wave of double amplitude with superimposed impedance change. In principle, this could have been avoided by subtraction of a modelled square wave. This was not possible in practice, as the injected square wave was distorted into a falling exponential curve which resulted from a high pass filter coupling at the input stage of the acquisition amplifier, plus non-idealities due to electrode charging. This waveform therefore varied from experiment to experiment and I elected to subtract it empirically by making a paired control recording without visual stimulation.

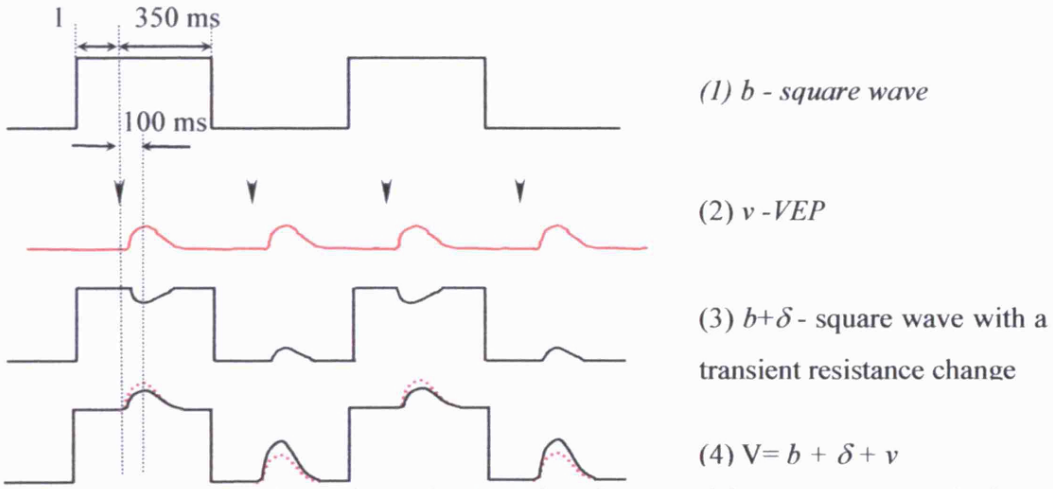

Figure 4-4: The recorded signal may be viewed as the sum of three components: 1) the injected square wave in the absence of stimuli, 2) the VEP triggered by the visual stimuli (black arrows) and 3) decreases δ in the square wave due to the resistance decrease accompanying neuronal activity. These are summated to a composite wave (4). Red dotted line is the VEP. In practice, the square wave was 3-4 orders of magnitude larger than the VEP and δ.

Terms used below are : Sum_a and $Diff_a$ are the sum and difference of the two polarities of the square wave, and δ is the potential due to an impedance change produced from Sum_a after subtraction of the control summed wave, Sum_c, divided by 2. (Figure 4-5)

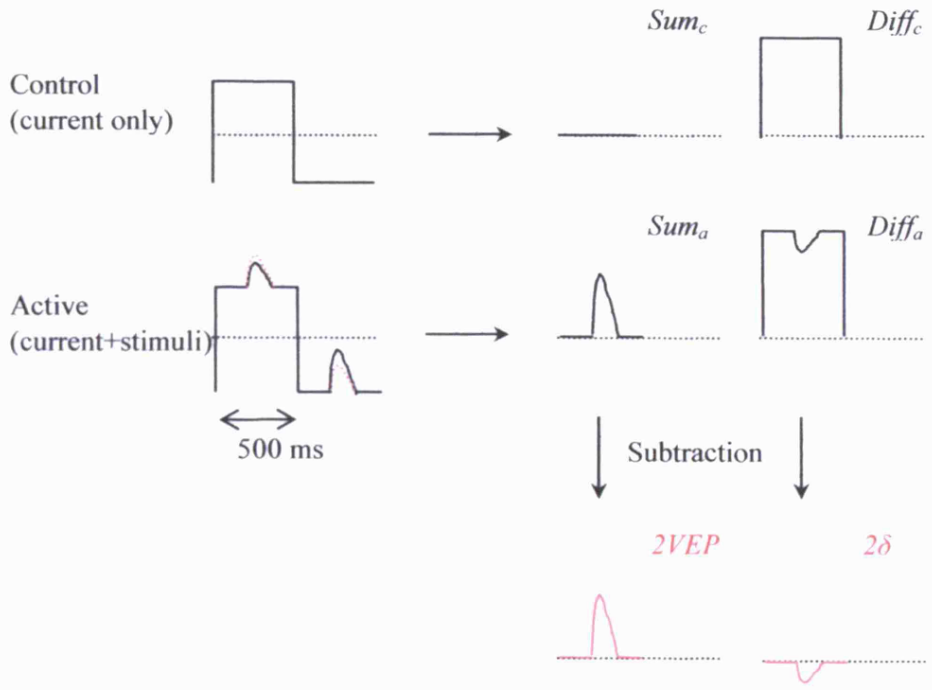

Figure 4-5: Derivation of the final VEP and δ waveforms (red) from the average of the control and active 10 minutes LF-EIT recordings using summation and subtraction of the two polarities followed by a second subtraction between the control and active recordings. For the purpose of explanation, the square wave is shown as square; in practice it was a falling exponential of variable shape.

4.3.6.2 Filtering and segmentation

Filtering: 50 Hz mains noise and its first harmonic at 100 Hz were filtered by applying a 4th order Butterworth filter with stop band of 1 Hz bandwidth centred at 50 and 100 Hz. The 4th order was used as it was found to have the most stable gain and phase across the pass band when evaluating 3rd to 8th order filters.

Segmentation: each 1 minute recording was segmented into n = 60 square wave periods of m = 1024 samples consisting of 2 VEPs in the active 1 minute recordings and inserted into a data matrix $D^{m \times n}$ (the m x n notation means m by n matrix).

4.3.6.3 Selection of segments with optimum SNR

In the following section, a method for removal of noisy outliers and low amplitude VEPs within each 1 minute recording is described following by a more detailed formulation.

Step 1 - removal of noisy outliers. Visual inspection of the raw data indicated a spread of noise in the component 1 second epochs, usually due to movement or muscle artefact. Typically, the square wave was about 1 mV high, on which were superimposed variable movement and muscle artefact and eye blink potentials, of about 100 μV. Each 1 minute recording consisting of n segments was treated separately and noisy outliers were removed by

an iterative method in which the rms error was estimated with respect to a running mean. The proportion removed was set to a fixed proportion of each 1 minute recording, as this appeared empirically to produce the best results by visual inspection. The remaining traces, on inspection, then contained negligible muscle, movement or eye blink artefacts. This exclusion was set at 15% for the stimulus recordings (Active). This yielded an inclusion factor of 85% or $p_1 = 0.85$ and the number of segments remaining after exclusion was defined as $n' \quad p_1 n$.

Step 2 - exclusion of low amplitude VEPs. Some variability in the VEP waveforms was noted, reflecting different levels of synchrony (Brazier, 1964), especially in relation to drowsiness. These were further removed from the n' segments remaining after *Step 1* by the following method. The VEP for each 1 second square wave was calculated by addition of the two opposite polarity square wave components; this comprised the average of the two VEPs from each half cycle. The idealized VEP for all of these in one 1 minute recording was estimated as the 1st principal component. The n' component VEPs in this set were ranked according to their similarity to this 1st PC. The number for inclusion in the data set was estimated by a function which calculated the optimum SNR in the data set according to the number included. In the event, this omitted about another 15% of segments in the active 1 minute recordings with an inclusion factor p_2 which yielded $n'' \quad p_2 n' \quad p_1 p_2 n$ remaining segments.

These methods differ from that customarily employed in neurophysiological response analysis, in which a simple threshold is used to exclude noisy data. This method appeared to be superior on visual inspection of traces and has been implemented.

Number of traces omitted. For active recordings with visual stimulation, this removed about 30% of recordings within each 1 minute recording (this varied slightly according to the proportion of VEPs excluded). It was not possible to match numbers for the controls, as these did not contain a VEP, so numbers were closely matched by exclusion of the noisiest 30% for controls ($p_1 = 0.70$).

Channels omitted. For the active recordings with visual stimulation, the above two procedures were carried out on channel 11, located 5 cm above the inion bone above the visual cortex, as this channel generally contained the largest VEP (Figure 4-2). Each 1 second square wave omitted was then translated to the other 18 channels. For control recordings, there was no VEP, so the outlier omission procedure was performed individually for all 1 second recordings on all 19 channels.

Step 1: discarding outlier segments.

An iterative process was used to identify a cluster of segments with maximized similarity and to discard a fixed proportion of the outlier segments. This was applied to unprocessed 1 second

square wave segments. The similarity was defined as the mean of the least squares of the difference from the mean of the cluster (Gilad, 2005c).

For the control 1 minute recordings, the algorithm was applied on the data matrix $D^{m \times n}$ where m = 1024 is the number of data points and n =60 is the number of segments. For the active 1 minute recordings, the two polarities of the square wave were averaged to discard the square wave prior to the processing. Thus, the data matrix $D^{m \times n}$ was replaced by $M^{m/2 \times n}$ where the elements of M relate to the elements of D by:

$$M_{ij} = \frac{1}{2}\left(D_{ij} + D_{(i+512)j}\right) \qquad (4\text{-}1)$$

Where i = 1,2,...,m/2 and j = 1,2,...,n (m = 1024, n = 60). In addition, a 4th order Butterworth low pass filter with cut off of 40 Hz and removal of any linear baseline trend was applied to all n segments of the resulting $M^{m/2 \times n}$.

The algorithm used k iterations where the iteration number is superscripted. The algorithm started by calculating the initial average vector waveform $\overline{M^0}$ with elements:

$$\overline{M^0}_i = \frac{1}{n}\sum_{j=1}^{n} M_{ij} \qquad i = 1,2,\ldots,m/2 \qquad (4\text{-}2)$$

A distance function Var_j was defined as the sum of the squared differences from the mean $\overline{M^0}$ and was calculated for each of the n segments:

$$Var_j = \sum_{i=1}^{m/2}\left(\overline{M^0}_i - M_{ij}\right)^2 \qquad j = 1,2,\ldots,n \qquad (4\text{-}3)$$

From the n values of Var_j, a subset $\{s^1\}$ was selected to include the $n' = p_1 n$ smallest values for Var_j. This subset marked the n' segments which were most similar to the average waveform under the definition of the distance function. A new average waveform $\overline{M^1}$ was then calculated using the subset $\{s^1\}$ where,

$$\overline{M^1}_i = \frac{1}{p_1 n}\sum_{j \in \{s^1\}} M_{ij} \qquad (4\text{-}4)$$

The algorithm performs k iterations for convergence into a fixed subset of segments $\{s^k\}$, which defines the final averaged waveform $\overline{M^k}$:

$$\overline{M^k}_i = \frac{1}{p_1 n}\sum_{j \in \{s^k\}} M_{ij} \qquad (4\text{-}5)$$

In each iteration after the first one, the mean waveform was evaluated by averaging the remaining n' segments from the previous iteration and the outliers were evaluated again from the total of n segments. Up to k = 6 (typically 3 or 4) iterations were required before convergence was reached.

This algorithm is a heuristic approach to discard outliers which are significantly different from a set of similar waveform. This method was validated empirically by visual inspection of the final outcome to make sure that no apparent outlier was included in the final average (Figure 4-6a).

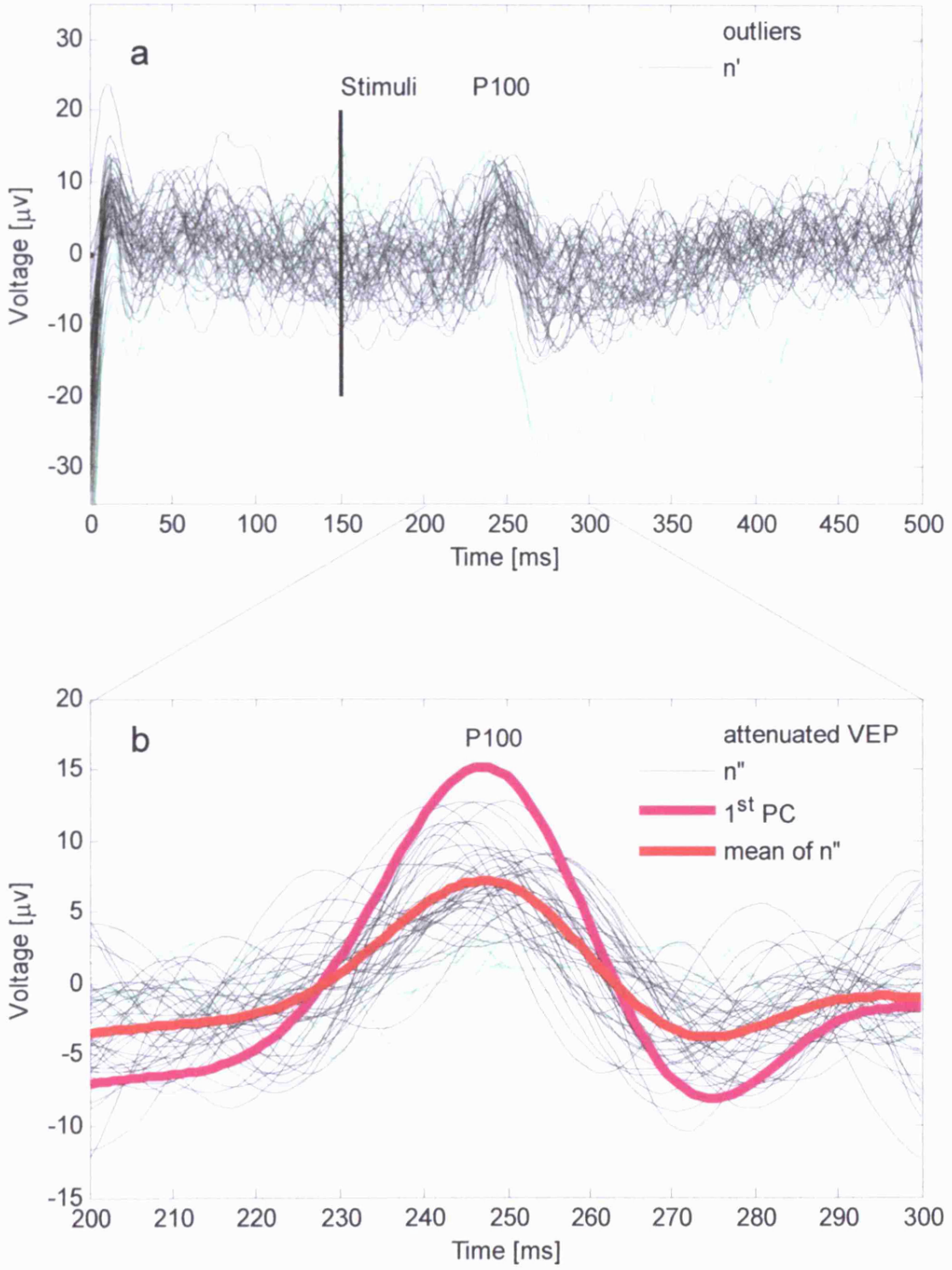

Figure 4-6: (a) outlier removal (Step 1) and (b) magnification of the 100 ms central region containing the P100 showing the attenuated VEP removal (Step 2). The 1st principal component is shown normalized to its eigenvalue (channel 11, LF-EIT recording 2B).

For a control 1 minute recording without visual stimuli, only Step 1 was applied with discarding of 30% (inclusion factor $p_1 = 0.70$) of the segments with remaining $n' \quad p_1 n = 0.7 \cdot 60 = 42$ segments. This was applied separately for all 19 channels of the V21 electrode placements and on the data matrix $D^{m \times n}$. The value of p_1 was chosen as the maximal value which eliminates most outliers by means of visual inspection and was set to be constant throughout the analysis. For the active 1 minute recordings, Step 1 was applied with discarding of 15% (inclusion factor $p_1 \quad 0.85$) to allow for the further reduction in Step 2.

Step 2 discarding segments with attenuated VEPs

For the active 1 minute recordings with visual stimulation, the remaining n' segments after the outlier removal in Step 1, were further reduced to remove attenuated VEP segments using the following procedure:

1 The data matrix $M^{m \times n}$ was further reduced to $\tilde{M}^{m' \times n'}$ where n' is the remaining segments after the outlier removal in Step 1, *and* $m' = 102$ focuses on a 100 ms time window around the expected location of the P100 peak, centred around 250 ms from the beginning of each segment (Figure 4-6b).

2 The first principal component vector P^1 (of length m') of $\tilde{M}^{m' \times n'}$ was calculated. The first principal component is the eigenvector that corresponded to the largest eigenvalue of the covariance matrix of $\tilde{M}^{m' \times n'}$. This eigenvalue was typically 60% of the sum of all eigenvalues.

3 The gain of the projection of the n' segments on P^1 was calculated using the dot product:

$$g_j = \sum_{i=1}^{m'} P_i^1 \tilde{M}_{ij} \qquad j = 1, 2, \ldots, n' \tag{4-6}$$

4 The n' gains g_j were sorted in a descending order to generate the set $\tilde{g}_j$

5 A threshold of uppermost gains was chosen adaptively by maximizing a cost function proportionate to the SNR after averaging n'' segments ($1<n''<n'$):

$$\hat{SNR}(n'') \sim \frac{mean \quad gain}{random \quad noise} \sim \frac{\frac{1}{n''}\sum_{j=1}^{n'} \tilde{g}_j}{\frac{1}{\sqrt{n''}}} = \frac{1}{\sqrt{n''}} \sum_{j=1}^{n'} \tilde{g}_j \tag{4-7}$$

The random noise decreases with averaging but the mean gain also decreases. Therefore, the n'' value maximizing this expression was numerically identified.

6 The value of n'' which maximized $\hat{SNR}(n'')$ gave an inclusion factor $p_2 = n''/n' = 0.67 \pm 0.11$ (mean ± SD) across the 10 different 1 minute recordings and 20 LF-EIT recordings. Thus, $n'' = p_1 p_2 n = 0.85 \cdot (0.67 \pm 0.11) \cdot 60 = 34 \pm 6$ (Figure 4-6b).

4.3.6.4 Further VEP exclusion for 1 minute recordings with poor responses

For estimating the VEP and voltage changes δ related to neuronal activity as well as applying statistical analysis, the *n'* and *n''* segments from the control and active 1 minute recordings were pooled over the N=10 repeated 1 minute recording in each of the LF-EIT recording. However, visual inspection of these, in some cases, indicated that the averaged *n''* VEPs over 1 minute was small, presumably due to poor attention by the subject (Figure 4-7). In the event, these 1 minute recordings were excluded using the same procedure described in Step 2 above. In 3/20 LF-EIT recordings, 4, 2 and 5 one minute average VEPs were excluded so that N' was 6, 8 and 5 in LF-EIT recordings 2B, 7A and 8B respectively (Table 4-1).

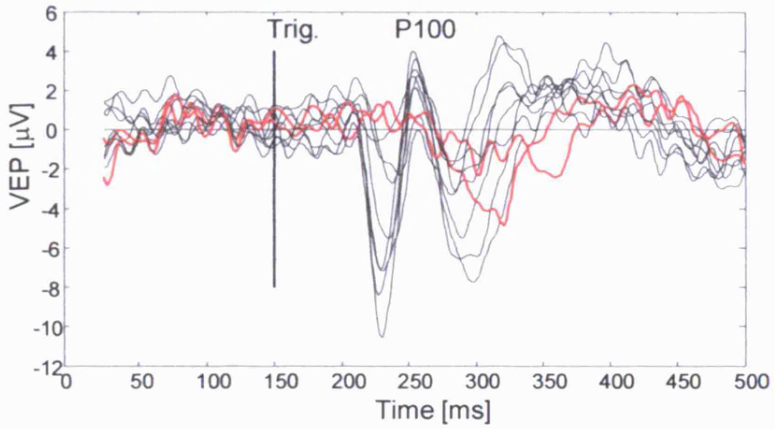

Figure 4-7: an example of 2 attenuated VEP waveforms (red) out of the 10 one minute recordings (7A LF-EIT recording).

4.3.6.5 Estimation of VEP and resistivity change components

Following the exclusion of outlier segments, segments with low amplitude of VEP and whole 1 minute recordings with poor response, the *n'* and *n''* segments from the control and active 1 minute recordings were pooled over the N' repeated 1 minute recording in each of the LF-EIT recording. A 4th order Butterworth low pass filter with cut off frequency of 40 Hz was applied on individual segments to improve the SNR. In order to remove ringing artefacts caused by the polarity transitions of the square wave, the segments had sections from 0 to 100 ms and 400 to 500 ms removed so that the final trace was 300 ms long.

In the following, a linear was applied to formalize the original method developed by Boone (Boone, 1995a) for estimating the VEP (*v*) and boundary voltage changes δ (Figure 4-4). This was done separately for each of the 20 LF-EIT recording and also after pooling the data from all LF-EIT recordings.

The measured voltage from a single channel $V_i^{(j)}$ was defined for the ith time point (i = 1,2,...,m/2 ; m = 1024) and jth segment. For the active recordings, j = 1,2,…,n''N' (typically n''N'

= 340) are the segments during applied stimulation and positive (C_1) or negative (C_2) current injection. For the control recordings, j = 1,2,....n'N' (typically n'N' = 420) are the segments during positive (C_3) or negative (C_4) current injection but no stimulation. $V_i^{(j)}$ was then modelled as:

$$V_i^{(j)} = \begin{cases} v_i + \delta_i + b_i + \varepsilon_{ij} & \text{if } j \in C_1 \text{ (stim - positive current)} \\ v_i - \delta_i - b_i + \varepsilon_{ij} & \text{if } j \in C_2 \text{ (stim - negative current)} \\ +Gb_i + \varepsilon_{ij} & \text{if } j \in C_3 \text{ (rest - positive current)} \\ -Gb_i + \varepsilon_{ij} & \text{if } j \in C_4 \text{ (rest - negative current)} \end{cases} \quad (4\text{-}8)$$

where v is the VEP component, δ is the boundary voltage change due to local resistivity change in the brain, b is the baseline boundary voltage due to the square wave current, ε is a Gaussian noise mainly due to background brain activity and G is a gain factor due to the decay of the current source batteries along the recording resulting in small difference in square wave amplitude between the control and active recordings. Although the baseline boundary voltage is supposed to be constant along time due to the application of a constant current, it is distorted by the IIR filter at the input stage of the acquisition amplifier and possibly by variations in contact impedance at the current injection sites. Since the baseline boundary voltage b was about 4-5 orders of magnitude larger than the change δ, these variations were significant and had to be calibrated by the control recordings to allow estimation of b_i. This model was abbreviated by:

$$V_i^{(j)} = \alpha_j v_i + \alpha_j \beta_j \delta_i + \gamma_j b_i \quad (4\text{-}9)$$

Where α, β, and γ are design indicators:

$$\alpha_j = \begin{cases} 1 & \text{if } j \in C_{1,2} \\ 0 & \text{if } j \in C_{3,4} \end{cases} \quad \beta_j = \begin{cases} +1 & \text{if } j \in C_{1,3} \\ -1 & \text{if } j \in C_{2,4} \end{cases} \quad \gamma_j = \begin{cases} \beta_j & \text{if } j \in C_{1,2} \\ \beta_j G & \text{if } j \in C_{3,4} \end{cases} \quad (4\text{-}10)$$

The Maximal Likelihood (ML) estimators of the model parameters v, δ, b and G are given by minimizing the cost function:

$$Cost(v,\delta,b,G) = \sum_{i,j} \left[V_i^{(j)} - \left(\alpha_j v_i + \alpha_j \beta_j \delta_i + \gamma_j b_i \right) \right]^2 \quad (4\text{-}11)$$

This cost function was minimized separately for each time point i:

$$\begin{cases} \dfrac{\partial Cost}{\partial v_i} = -2 \sum_{j \in C_{1,2}} \left[V_i^{(j)} - \left(v_i + \beta_j (\delta_i + b_i) \right) \right] = 0 \\ \dfrac{\partial Cost}{\partial \delta_i} = -2 \sum_{j \in C_{1,2}} \beta_j \left[V_i^{(k)} - \left(v_i + \beta_j (\delta_i + b_i) \right) \right] = 0 \\ \dfrac{\partial Cost}{\partial b_i} = -2G \sum_{j \in C_{3,4}} \beta_j \left[V_i^{(j)} - \beta_j G b_i \right] = 0 \end{cases} \quad (4\text{-}12)$$

The partial derivative with respect to G yielded the same equation as obtained for b_i. Since there was an equal number of positive and negative current injection, $\sum_J \beta_J = 0$ and $\beta_J^2 = 1$ which yields

$$\begin{cases} v_i = \dfrac{1}{N_{1,2}} \sum_{J \in C_{1,2}} V_i^J \\ \delta_i + b_i = \dfrac{1}{N_{1,2}} \sum_{J \in C_{1,2}} \beta_J V_i^J \\ b_i = \dfrac{1}{GN_{3,4}} \sum_{J \in C_{3,4}} \beta_J V_i^J \end{cases} \tag{4-13}$$

Where $N_{1,2}$ is the total number of segments in C_1 and C_2 (typically 680) and $N_{3,4}$ is the total number of segments in C_3 and C_4 (typically 840). For estimating v and δ these become:

$$\begin{cases} v_i = \dfrac{1}{N_{1,2}} \sum_{J \in C_{1,2}} V_i^J \\ \delta_i = \dfrac{1}{N_{1,2}} \sum_{J \in C_{1,2}} \beta_J V_i^J - \dfrac{1}{GN_{3,4}} \sum_{J \in C_{3,4}} \beta_J V_i^J \end{cases} \tag{4-14}$$

Since the derivatives of the cost function wih respect for G yielded the same equation as obtained for b_i and additional criteria was sought for estimating G. The baseline boundary voltage b was about 4-5 orders of magnitude larger than the change δ. Therefore, a tiny mis-registration of G will produce a large bias in δ due to unbalanced baseline between the active and control recordings. Therefore, the gain G was determined by the additional criteria which would zero any DC (or bias) component:

$$\sum_i \delta_i = 0 \tag{4-15}$$

Or

$$\sum_i \left[\frac{1}{N_{1,2}} \sum_{J \in C_{1,2}} \beta_J V_i^J - \frac{1}{GN_{3,4}} \sum_{J \in C_{3,4}} \beta_J V_i^J \right] = 0 \tag{4-16}$$

And finally

$$G = \frac{N_{1,2}}{N_{3,4}} \frac{\sum_i \sum_{J \in C_{3,4}} \beta_J V_i^J}{\sum_i \sum_{J \in C_{1,2}} \beta_J V_i^J} \tag{4-17}$$

Eq. 4.14 provided the estimation the VEP and the voltage changes resulting from impedance changes. In fact, this formulation is similar to the previously described intuitive calculation (Section 4.3.6.1) based on the mehod proposed by Boone (Boone, 1995a). The first part of Eq. 4.14 estimates the VEP by adding the two polarities of the square wave and second part estimates the voltage changes by subtracting them and also accounting for the baseline which

was estimated separately from the control recordings (third part of Eq. 4.13). The calculation of the gain between the active and control recordings due to the decay of the battery driven current source (Eq. 4.17) is different from the previous method applying a detrending algorithm but in practive gives an identical results.

4.3.6.6 Differential measurement

According to the modelling in Ch 3, the electrode combinations which gave the largest boundary voltage changes were with current injection over the occipital region with an adjacent (5 cm apart) or semi-adjacent (10 cm apart) pair of electrodes and recording immediately lateral to these. In this study, there was one current injection pair in each of the 20 recordings and 19 recording electrodes over the occipital region with respect to Fz. Therefore, channels from pairs of electrodes were subtracted to form differential measurement over the occipital region. However, most of the 19·18/2=171 possible pairs are linearly dependent (for example [1,3] can be derived from [1,2] and [2,3]). How to select 18 independent pairs out of the 171 possible?

Estimating the magnitude of the changes using the same technique as in Ch. 3 but with real electrode positions measured on the head during this experiment, revealed that the predicted changes are proportionate to the measured boundary voltage (square wave amplitude) calculated as the median of the b_i values estimated in Eq. 4-13 (Figure 4-8). Therefore, 18 pairs with the uppermost boundary voltage which are linearly independent were selected for further analysis (e.g. Figure 4-8). For estimating δ and b in Eq. 4-13, the measured voltages $V_i^{r(j)}$ from a single channel were replaced by the voltage difference from 18 combinations. However, for estimated v (the VEP) the original $V_i^{r(j)}$ for a signal channel were used since the convention for presenting VEPs is with the reference electrode at the frontal area (Fz).

The resulting v_i and δ_i waveforms were gated between 100 and 400 ms (-50 to 250 ms relative to the stimuli) to ignore ripples from the square wave rise and fall times. In addition, δ_i was also translated to percentage units by normalizing to the median of the b_i.

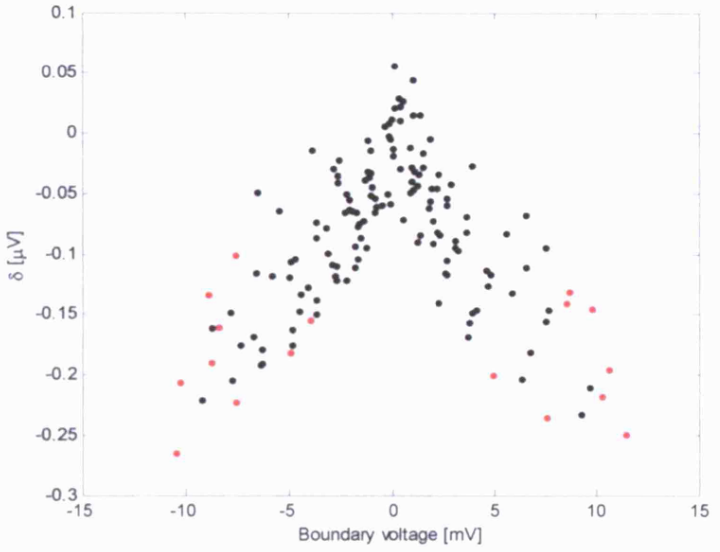

Figure 4-8: predicted voltage change δ versus measured boundary voltages b for 171 electrode combinations. Electrode positions were from recording 3A projected on the realistic head mesh. The 18 uppermost boundary voltages from independent electrode pairs are in red.

4.3.6.7 Statistical analysis for identifying significant changes

During membrane depolarization in the brain, the resistivity decreases and the changes in the boundary voltage δ_i are expected to be negative at some of the time points following the visual stimulation. Therefore, for detecting significant decreases, a separate series of typical length $N_{1,2}$=680 were constructed for each time point i following the definition for δ_i in Eq. 4-13:

$$\Delta_i = \left\{ \beta_j V_i^j - b_i \right\} \;\; ; \;\; j \in C_{1,2} \qquad (4\text{-}18)$$

The baseline b_i was estimated using the expression in Eq. 4-13 and a *t-test* was applied to determine if the mean of the series Δ_i (which is δ_i) is negative. Changes were regarded negative for $p<0.05$. Estimation of the mean (δ_i), standard error (SE_i) and significance test was applied separately to each time point in each of the 18 differential channels and for the 20 LF-EIT recordings. The channel with the uppermost boundary voltage (square wave amplitude) was taken as a representative channel. In each of the 20 recordings, it was noted if there was a significant decrease in a region longer than 25 ms within the expected region between 50 and 250 ms after the visual stimulation. Minimal significant duration of 25 ms was chosen due to the 40 Hz low pass filter applied to the signal. No correction has been made to the statistical test. However, similar regions of significant changes longer than 25 ms were detected for lower threshold of $p<0.002$ which comply with the Bonferroni correction for 25 time points.

4.3.6.8 Changes grouped from all LF-EIT recordings

In the course of this study, some minor changes were made to the procedure, in the hope that they might increase the SNR – these included using two symmetrically placed pairs of current

injection electrodes in 5/20 LF-EIT recordings, changing the current source so as to increase applied current and use with this of recessed electrodes, as well as introducing additional cognitive task to maintain the subject alertness and minimise alpha rhythm. However, in the event, these did not significantly alter the findings, so all data with these minor variations has been pooled for increasing the SNR.

Prior to the group average, 4/20 recordings with α rhythm amplitude above 20 μV in the raw data were excluded since they were expected to obscure the changes δ when the remaining 16 recordings are averaged.

The amplitudes of the boundary voltage (square wave) for the 18 linearly independent measurement pairs were sorted in a descending order for each of the remaining 16 LF-EIT recordings. Then, the raw data for the channel with uppermost boundary voltage was grouped from all 16 recordings. The same calculations for estimating v, δ, b, G, SE and the p value were repeated as for individual recordings. This was repeated for each of the channels along the list of sorted boundary voltages. This was performed for 14 out of the 18 channels since up to 4/19 electrodes in each recording were technically faulty due to poor contact to the skin. Since the lowest boundary voltages did not produce significant changes, only 10/14 channels with uppermost boundary voltages were presented.

The local resistivity decreases in the brain decrease the boundary voltages. Therefore, it was possible to group the data from different channels in different recordings even though the current injection level and exact electrode positions as well as the current injection pair were different.

The representative amplitude of the observed significant changes was taken as the peak of the change for the channel with uppermost boundary voltage together with its SE and p value. The range for the 10 channels was also calculated and the results were translated to percentage units.

4.3.7 Experimental validation

For validating the sensitivity of the prototype system to fast resistivity changes, measurements were made on a resistor network and crab peripheral nerve

4.3.7.1 Resistor network

A rapid resistance change of 0.00087% (approximately 0.001%) of a load R_{load} was simulated with a parallel resistor R_{cal} which was coupled to the circuit for 50 ms at the middle of the 500 ms period of each square wave polarity using a solid state relay. Electrode contact resistance and static parts of the brain which do not change were simulated with fixed resistors R_e (Figure 4-9). The current level was 1 mA.

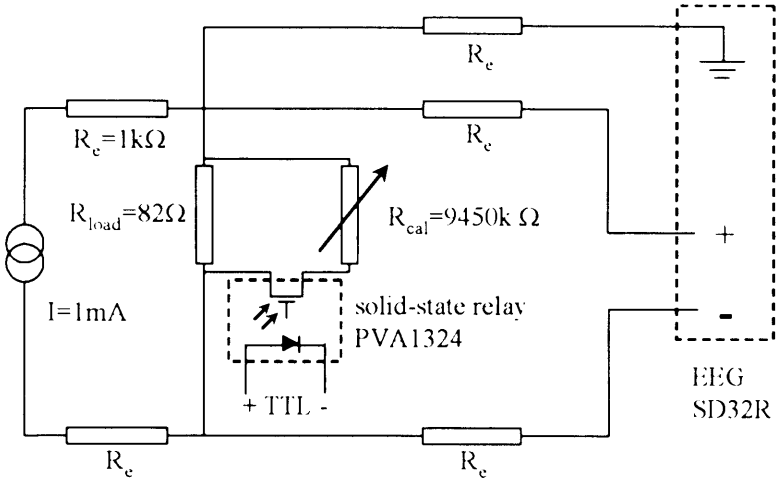

Figure 4-9: circuit diagram of the experimental setup.

4.3.7.2 Crab peripheral nerve

Resistance changes were measured during Compound Action Potentials (CAP) of crab peripheral nerve using the hardware setup, recording protocol and data analysis designed for the human experiments. This allowed comparison to previous crab studies (Liston, 2004a) and validation of the methods on a simpler one dimensional case before approaching 3D measurements on humans. One 10 minutes LF-EIT recording was made from one crab nerve.
The nerve bundle preparation and electrode arrangement were similar to previous studies discussed earlier (Section 1.4.4)(Liston, 2004a).

Briefly, a nerve bundle about 10 cm long was extracted from the walking leg of a crab, *Cancer Pagurus*, suspended by a series of silver electrode hooks at various distances from each other and lowered into an ice-cooled bath of Ringer's solution (an electrolyte) between measurements for preservation purposes (Figure 1-8a). When raised out of the electrolyte, the nerve bundle was stimulated at one end with about 5 V, 0.1 ms pulses while a single channel 4 terminal LF-EIT recordings were made with subthreshold applied current of 5 μA between 1mm spaced electrodes (Figure 1-8b). One measurement electrode was placed 3 millimetres more

proximal to the site of nerve stimulation than the current driving electrodes and the other placed several centimetres more distal.

The shape of the CAP near the stimulator resembled that of an action potential (AP) that may be seen on an individual fibre. However, the magnitude of the CAP decreased and its spread increased due to dispersion as it passes along the nerve. The placing of one measurement electrode close to the stimulating electrodes and another at a large distance ensured that the measured CAP was monophasic and the placing of the former several length constants upstream of the proximal drive electrode ensured that the current injection did not have an effect on the shape of the measured CAP. This enabled separation of that part of the recorded signal that was the CAP and that which was the associated resistance change.

4.4 Results

4.4.1 Experimental validation

Resistor network: the mean resistance change was 0.0007 ± 0.0003 % (n=50) with SNR of 2 limited by instrumentation noise (Figure 4-10).

Crab peripheral nerve: a peak change of 20 μV was observed at the same time as the peak of the CAP. This corresponded resistivity decrease of 0.2 ± 0.04% (n = 2) (Figure 4-11).

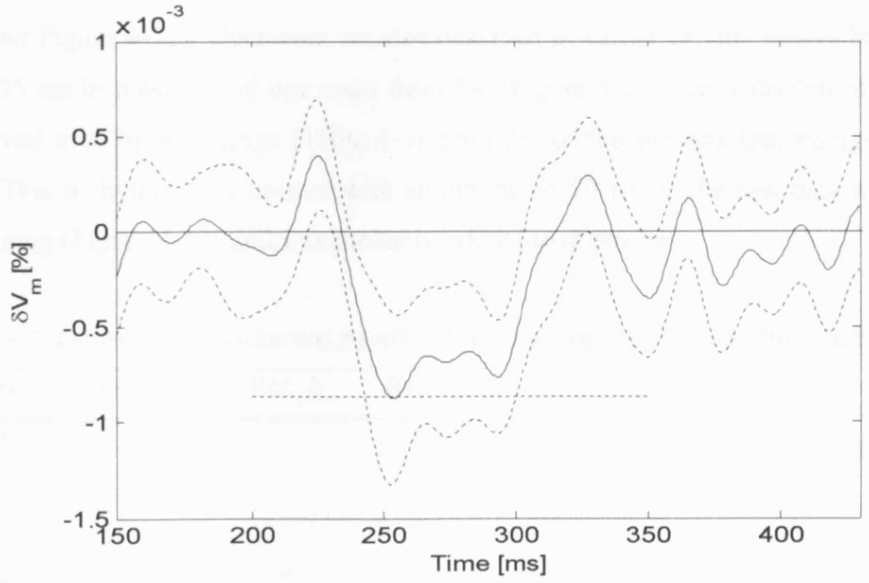

Figure 4-10: resistor network validation: voltage changes with SE during 0.00087% resistance changes between 250 and 300 ms. The horizontal dotted line is the calculated change.

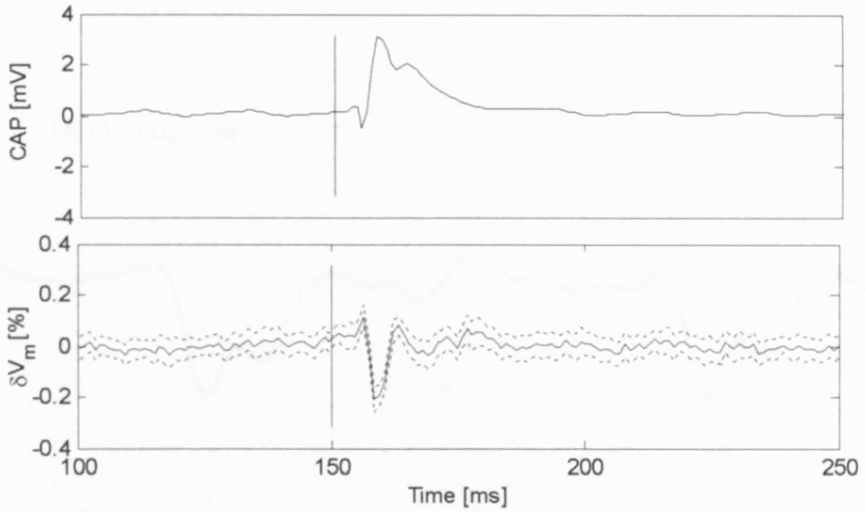

Figure 4-11: Crab peripheral nerve validation on a single nerve after averaging for 10 minutes: the upper panel is the CAP after stimulating at 150 ms peaking after about 10 ms. Lower panel is the measured voltage changes showing resistance decrease of about 0.2% occurring at the same time as the CAP peak.

4.4.2 Human measurements

4.4.2.1 Individual recordings

Significant voltage decreases lasting more than 25 ms at the most expected delay between 50 and 250 ms were observed in 35% (7/20) of the recordings with SNR between 2 and 5 (Table 4-3 and Figure 4-12). Decreases we also observed in earlier or later delays but they lasted less than 25 ms in most recordings apart from 5A (Figure 4-12). An α rhythm of 10 to 12 Hz was observed in 4/20 recordings (Table 4-3) from 2/7 of the subjects (recordings 3A, 3B, 9A and 9B). This α rhythm was present with amplitude of 50 μV is the raw data and 2 μV after the averaging (Figure 4-12) and was probably related to drowsiness.

Table 4-3: presence of α rhythm and significant decreases between 50 and 250ms lasting more than 25ms.

Rec.	α -rhythm	Rec. A	Rec. B
1			+
2			+
3	+		
4		+	
5			
6		+	
7			
8			+
9	+		
10		+	+

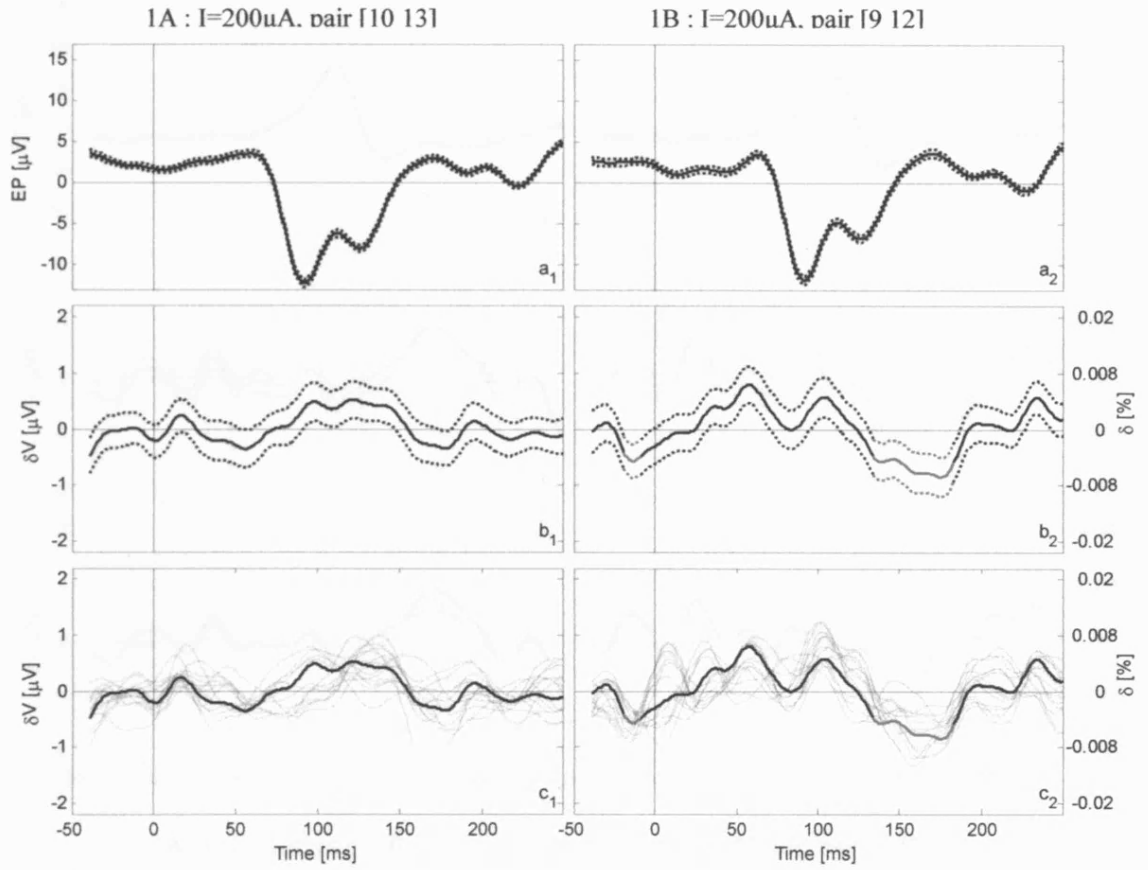

Figure 4-12: results from two LF-EIT recordings 1A (a_1-c_1) and 1B (a_2-c_2) taken from the same subject. .a) averaged (solid) ±SE (dotted) VEP from channel 11 (Oz-Fz) located 5 cm above the inion. A vertical line marks the visual stimulation at 0 ms. b) Average (solid) ±SE (dotted) voltage changes in the channel with uppermost boundary voltage. Significant decreases are marked in red ($p < 0.05$). Volts and percentage units apply for both left and right panels. c) Same as (b) for the 10 channels with uppermost boundary voltage but without SE (for brevity). Significant decreases are marked in orange and the channel in black and red is the same as in (b). All 20 LF-EIT recordings are presented in the following pages. Recordings 8A and 8B with the different stimulation rate and delay (4 Hz at 50 ms instead of 2 Hz at 150ms) was shifted 100 ms to the right to fit to the other recordings.

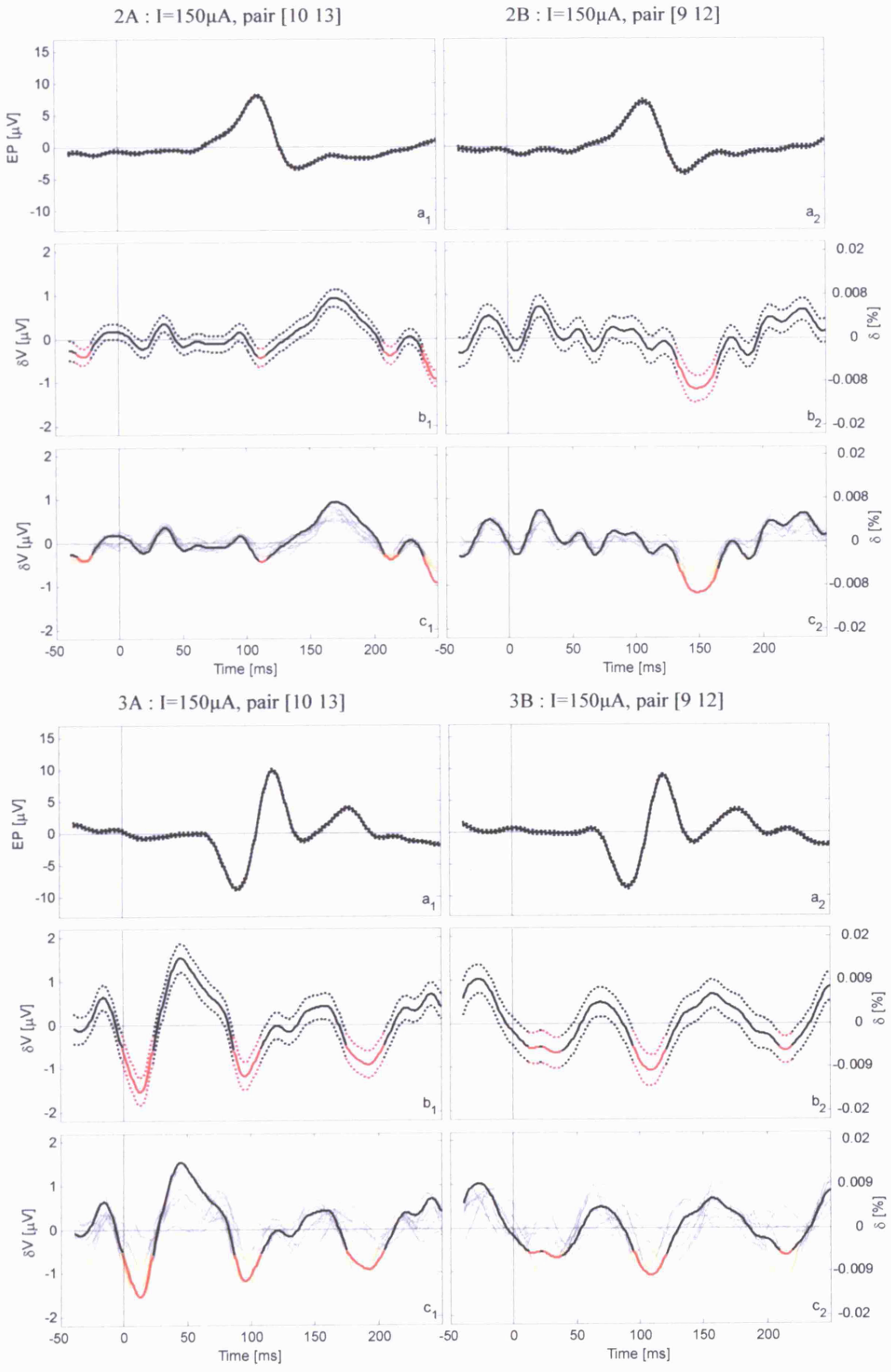

Figure 4-12: continued.

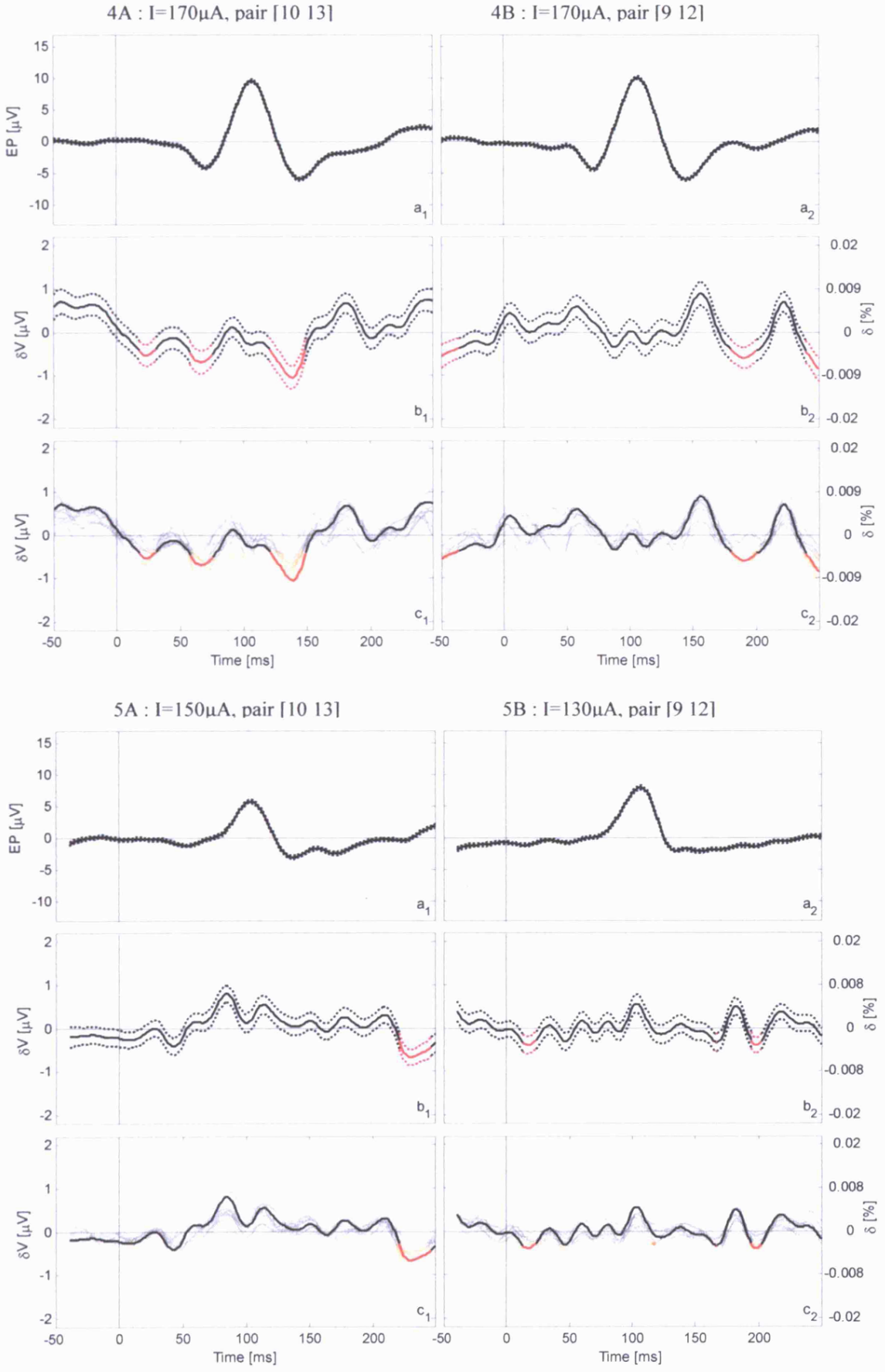

Figure 4-12: continued.

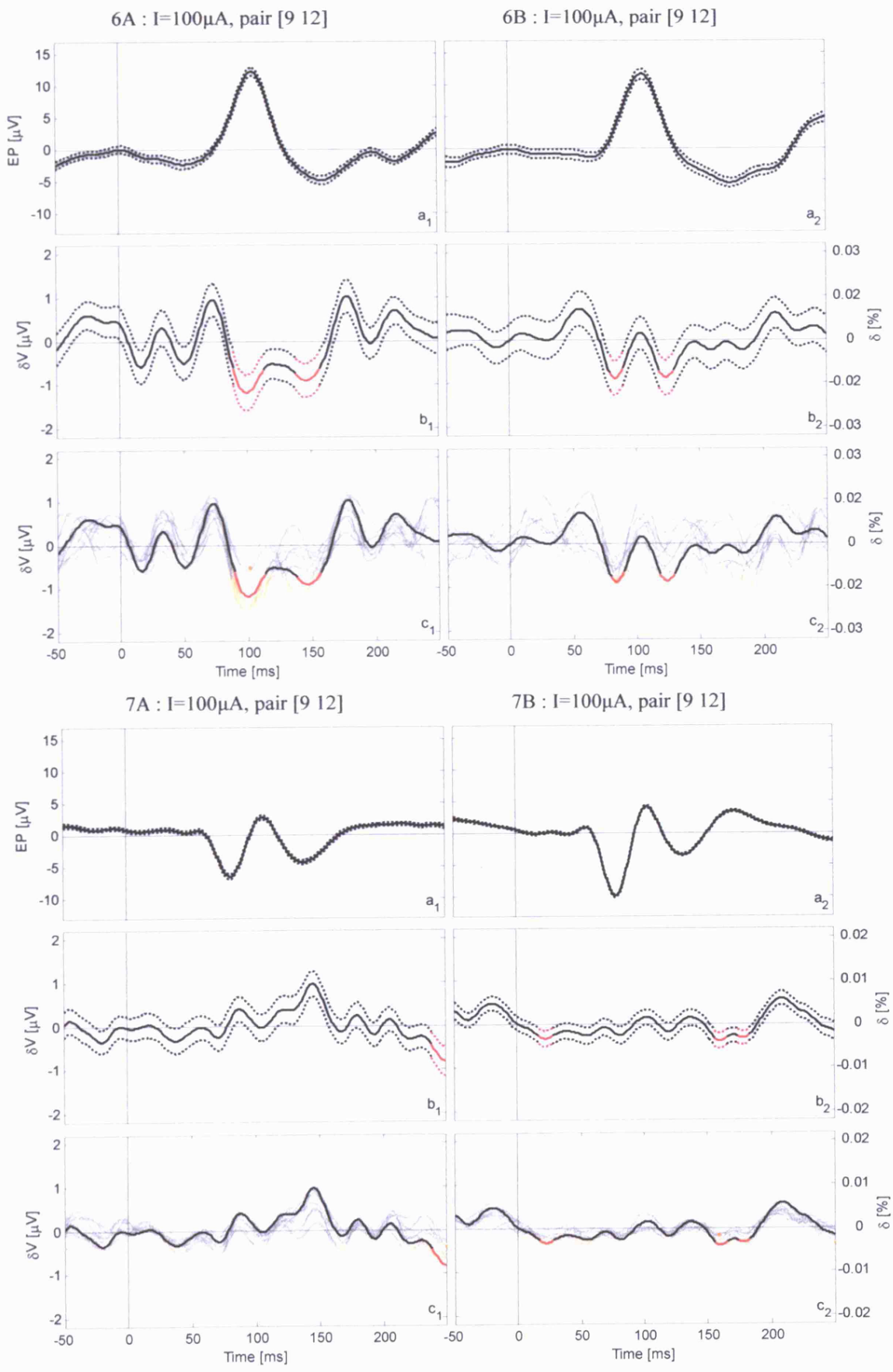

Figure 4-12: continued.

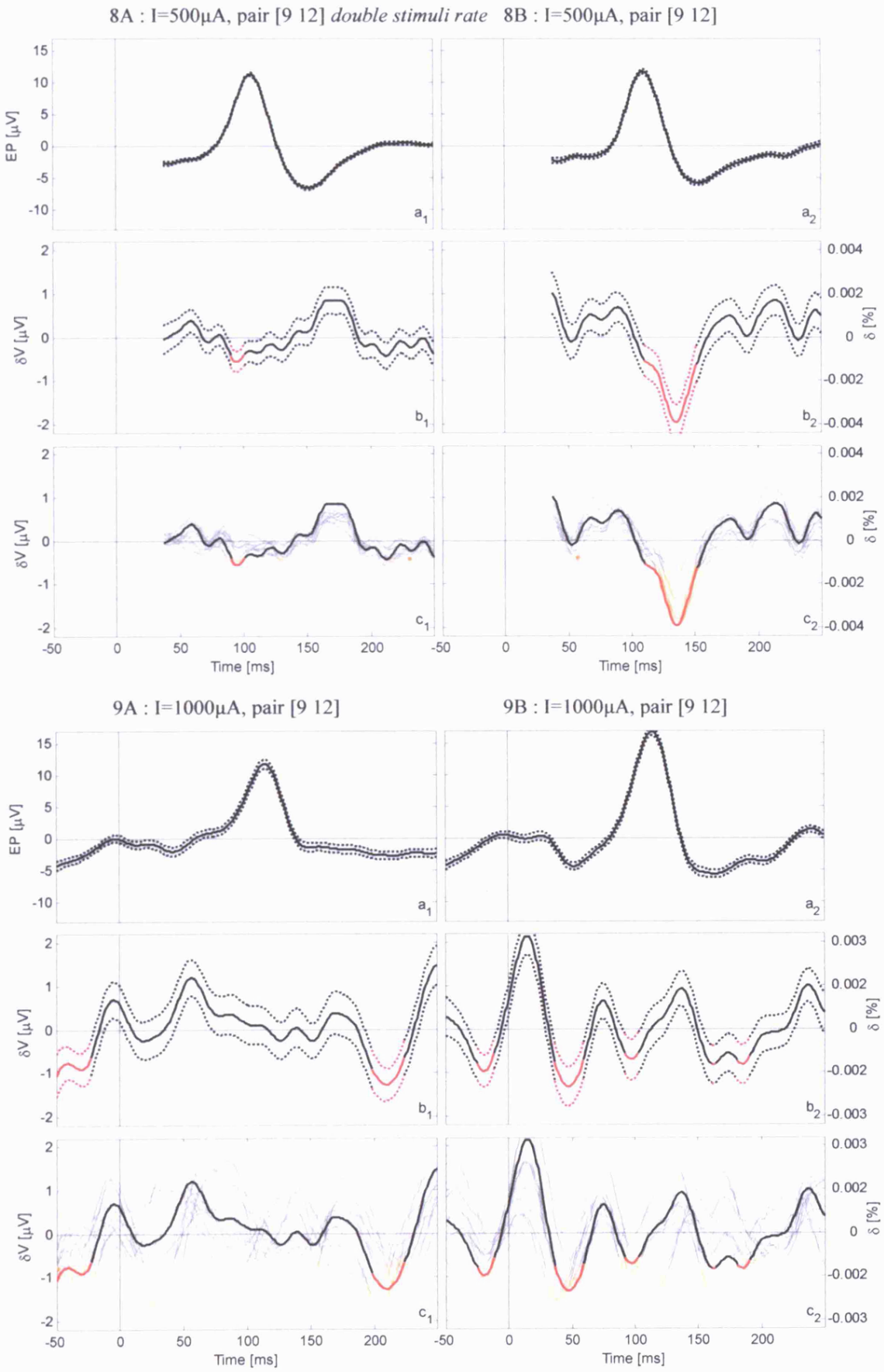

Figure 4-12: continued.

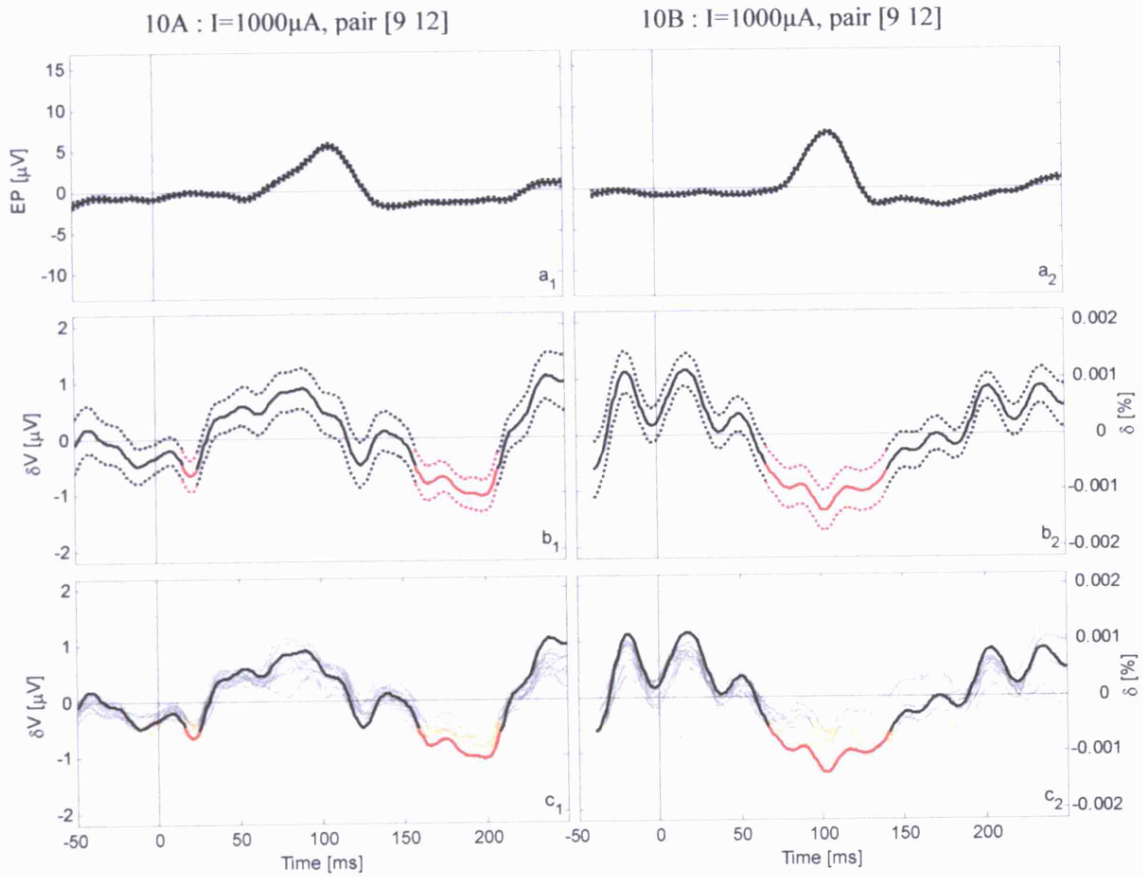

Figure 4-12: continued.

4.4.2.2 Changes grouped from all LF-EIT recordings

The group average of 16/20 LF-EIT recordings after excluding those with a strong α rhythm, had a significant change between 100 and 150 ms (Figure 4-13). This voltage decrease for the channel with maximal boundary voltage was peaking at 130 ms and was 0.25 ± 0.07 μV (mean ± SE; p = 0.0002; $N_{1,2}$ = 9822) or 0.0008 ± 0.0002 %. The SNR in this case was 0.25 / 0.07 = 3.6. The average current injected was 295 μA producing maximal boundary voltage of 38 mV (transfer impedance of about 130 Ω).

For the 10 channels (out of up to 18 channels) with the highest boundary voltage the group average gave change in the range of 0.13–0.31 μV (0.0004–0.0010 %) (Figure 4-13c). The boundary voltages were in the range 26–38 mV.

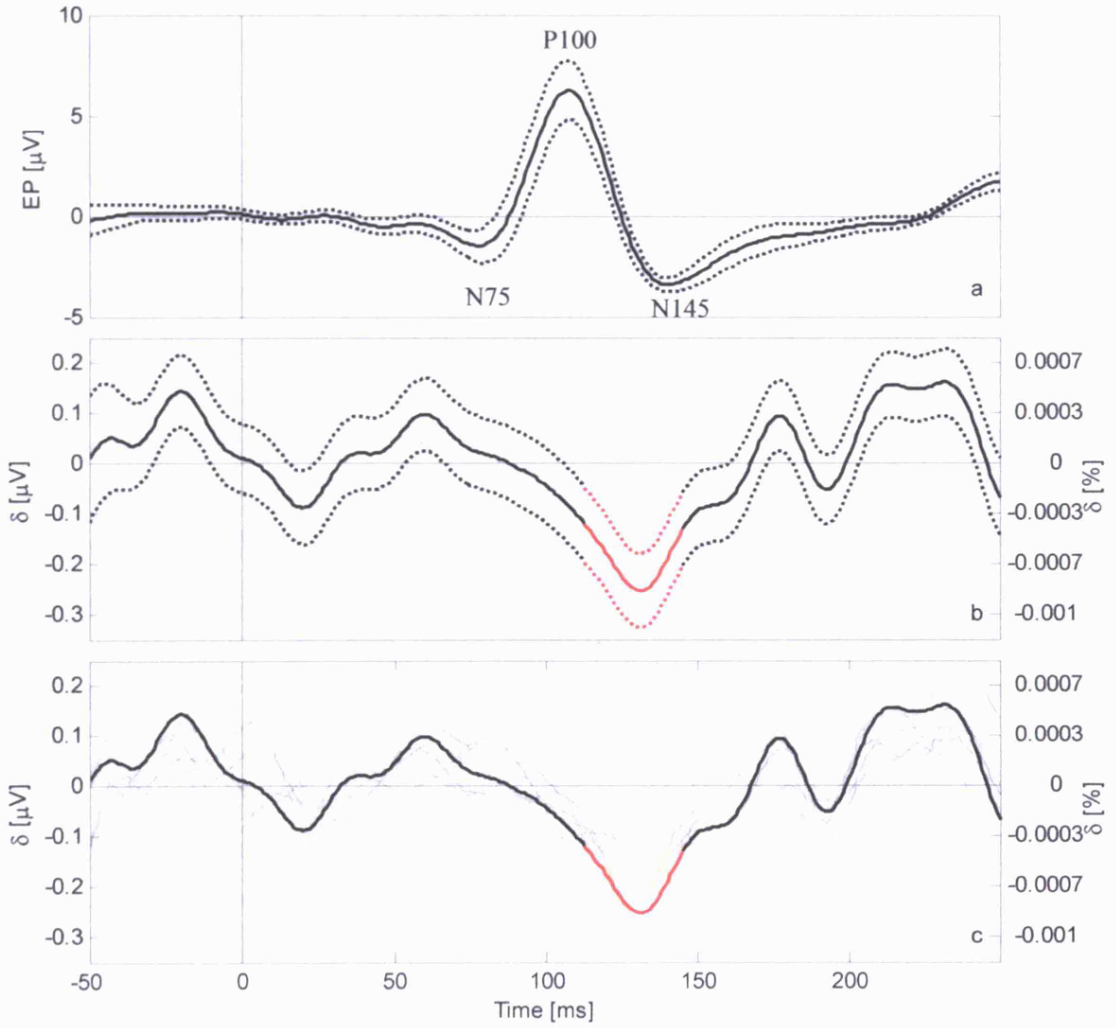

Figure 4-13: same as Figure 4-12 but for the group average of 16 recordings. a) Averaged (solid) ±SE (dotted) VEP from channel 11 (Oz-Fz) with the maim components marked. b) Average (solid) ±SE (dotted) voltage changes in the channel with uppermost boundary voltage. Significant decreases are marked in red (p < 0.05). c) Same as (b) for the 10 channels with uppermost boundary voltage but without SE (for brevity). Significant decreases are marked in orange and the channel in black and red is the same as in (b).

4.5 Discussion

4.5.1 Summary of results

Significant voltage decreases lasting more than 25 ms at the most expected delay between 50 and 250 ms were observed in 35% (7/20) of the LF-EIT recordings with SNR between 2 and 5. After excluding 4 LF-EIT with strong α rhythm, 80% (16/20) of remaining LF-EIT recordings were group averaged. For the channel with maximal boundary voltage, a significant negative peak of 0.25 ± 0.07 μV (mean ± SE; p = 0.0002; $N_{1,2}$ = 9822) or 0.0008 ± 0.0002 % was peaking 130 ms after the stimulus with an SNR of 3.6 (Figure 4-13). For the 10 channels with the highest boundary voltage this negative peak was in the range of 0.13–0.31 μV (0.0004–0.0010 %).

4.5.2 Technical issues

Bandwidth limiting: in this study, low pass filter of 40 Hz was applied to reduce the noise with the hope to increase the SNR. In the event, the VEP signal contains higher frequency components which were suppressed by the smoothing. The impedance changes are expected to have similar bandwidth to the VEP since they reflect the neuronal activity directly. However, since the impedance changes are rectified and are sensitive to the overall depolarization, their bandwidths might be lower. Introducing low pass filter of 40 Hz limit the effective time resolution to about 25 ms. This could be reduced in future studies by increasing the bandwidth if improvements to the method would provide higher SNR.

Current level: since the development of the recessed electrode design for applying higher current levels (Ch. 2) was done in parallel to this study, the average current level of the group average was 295 μV. this was below the maximum of 1 mA which according to Ch. 2 could be applied without producing significant skin sensation and altering the underlying brain function. A higher current could linearly increase the signal level and hence the SNR of the measured changes and such study was left for future work.

Square wave non-idealities: ringing artefact due to switching of the current polarity limited the usable time to 300 ms out of each 500 ms half cycle. Furthermore, the AC coupling in the acquisition system distorted the baseline of each square wave polarity leading us to double the recording time by adding the control recordings without visual stimuli to calibrate this effect. Improving these hardware issues in future designs could substantially decrease to acquisition time by a factor of 4 for achieving similar SNR.

4.5.3 Validations

The measurements on a resistor network showed that the instrumentation, protocol and data analysis methods are sufficiently sensitive for measuring changes of 0.001% (0.7 μV for this case), which is the magnitude of the changes expected from the modelling (Ch. 3). Therefore, additional sources of physiological noise, not present in the resistor network measurements, appear to be the bottleneck for the sensitivity in human measurements.

The measurements on crab peripheral nerve bundle showed that the methods designed for the human measurements could reproduce the changes measured in previous studies with a similar waveform (Section 1.4.4)(Liston, 2004a).

4.5.4 Comparison between modelling and measurements

The source of noise: the physiological noise level obtained from background brain activity in the occipital area when eyes are open is about 10 μV originated from background brain activity. After averaging over 16 recordings of ten minutes long and 2 Stimuli/sec, this noise is expected to decrease to 10 μV / √(16 rec · 10 min · 60 sec · 2 Stimuli/sec) = 0.07 μV. This estimation agrees with the actual SE value of 0.07 μV obtained from the group average of the channel with uppermost boundary voltage. This suggests that most of the noise is of physiological origin and not due to instrumentation noise.

Estimated changes: according to the modelling in Ch. 3, the magnitude of the maximal boundary voltage changes due to 1% conductivity increase of 9 cm^3 volume of visual cortex was 1.03 ± 0.75 μV (0.0039 ± 0.0034 %) when using 1mA of EIT current.

Measured changes: in this study, the measured change for the channel with maximal boundary voltage was 0.25 ± 0.07 μV (0.0008 ± 0.0002 %) for an average current level of 295 μA. The physiological origin of the noise suggests that as long as the instrumentation noise is low, the overall noise will not increase if the current would be increased to 1 mA (factor of 1 mA / 295 μA = 3.4). This will directly increase the magnitude of the voltage changes while keeping the noise or SE at the same level. In percentage units, normalized by the boundary voltage, the change will remain the same but the SE will decrease by the above factor. Therefore, if these experiments would be repeated with a current level of 1 mA and averaged over the same amount of time, the measured changes are estimated to increase to 0.85 ± 0.07 μV (0.00080 ± 0.00006 %) with an anticipated SNR increasing to 0.85 / 0.07 = 12.1. This anticipated change for current of 1 mA agrees with the model prediction (0.85 vs. 1.03 μV). However, when normalizing to percentage units, the model prediction is 5-fold higher (0.0039 vs. 0.0008 %). This is due to a technical reason; the normalization in the model is done using more electrodes (31 vs. 10 for the measurements) so the average boundary voltage when including those further from the current injection site was lower.

4.5.5 Could these changes be due to an artefact?

The evidence from this study that support the possibility that the measured changes were genuine were: 1) the magnitude and SNR of the measured changes agreed with the estimations obtained from the modelling and 2) the significant changes were observed at a delay of 100-150 ms which is the P100-N145 components region.

However, the main possible source of artefact is the potential alteration of the VEP waveform by the applied current, which could change its symmetry in the presence of positive or negative current polarity. The result of this would be that the VEP waveform would not entirely vanish through the subtraction procedure producing a residual VEP component additional to the resistivity changes. Although current level of up to 1 mA was shown to be sufficiently low to avoid such effect (Ch. 2), this still remains a possibility as only small margins were taken to maximize the SNR in the measurements.

There are several validations which could be applied to exclude such a possibility for artefact. However, the low SNR limit their practical application. For a higher SNR of about 10 which might be achieved in the future, the following validations could be employed:

1. *Constant percentage changes with different current levels*: repeated recordings with different current level should result in the same changes in percentage units. This will not be the case if the changes are due to an artefact since different current levels will alter the VEP waveform to a different extent.
2. *Intra recording reproducibility*: showing similar changes when analysing two halves of the same recorded dataset.
3. *Intra subject reproducibility*: showing similar changes in recordings from the same subject under identical conditions recorded days or weeks apart.
4. *Inter subject consistency*: changes in different subjects should show reasonable agreement in terms of delay, magnitude and waveform. This is limited by differences of gender, age, geometry and electrical properties of the different head compartments, size and shape of the visual cortex V1 area and difference in the response to visual stimuli.

Another possible source of artefact is the impedance changes related to rCBV effects appearing as neuronal activity related changes. However, the expected changes due to neuronal activity are expected to be rapid and to occur over a time course of tens or hundreds of milliseconds. Changes due to rCBV effects would occur over several seconds. These would vanish during the analysis procedure applied in this study and would be included in the estimation of the boundary voltage baseline waveform b_i.

4.5.6 Implications for designing future imaging systems

This study provided the first evidence for the feasibility of non-invasive measurement of fast resistivity changes related to neuronal activity in the human brain while our ongoing work has been partly published (Gilad, 2004; Gilad, 2005a; Gilad, 2005b; Gilad, 2007a).

With the existing method, the anticipated SNR when using a single current injection pair and current of 1 mA is 12.1 after averaging over 320 minutes (16 LF-EIT recordings of 10 minutes of control and active recordings). The minimal SNR requirement for reliable image reconstruction was estimated to be 4 (Section 3.2.2). Hence, the recording time could be reduced from 320 minutes to $320 / (12.1 / 4)^2 = 34$ minutes.

In addition, for image reconstruction, data is needed from multiple current injection pairs. For obtaining previous EIT images of haemodynamic changes in the brain, an electrode protocol consisting of 21 current pairs, each with 12 voltage measurement pairs was used (Tidswell, 2001; Tidswell, 2006). Due to reciprocity, similar results could be obtained with 12 current pairs, each with 21 voltage measurements. Since multiple voltage measurements could be done in parallel, the limiting factor is the number of current pairs. For 12 current pairs and 34 minutes that might be needed for sufficient SNR, the overall recording time would be about 7 hours which is impractical for human subjects to tolerate.

However, several improvements could dramatically reduce the total recording time. Overcoming the square wave non-idealities of ringing artefact and distortions due to AC coupling could allow stimulating at a double rate and avoiding the control recording respectively. This will reduce the recording time by a factor of 4 while achieving the same SNR. Another possible improvement is to record the impedance changes above the EEG band which could enhance the SNR by a factor of 5 (Section 1.4.6). This could potentially allow decreasing the recording time further by a factor of 25. Furthermore, recording at higher frequency would discard the problems related to the square wave and may provide a total reduction in recording time of up to 100 fold down to about 5 minutes if all are successfully implemented. These improvements could allow a tolerable recording time in the order of several minutes and are left to be evaluated in future work.

I therefore conclude that non-invasive imaging with LF-EIT method is not feasible with present technology. Future efforts should be focused on achieving a substantial improvement in SNR while decreasing the total recording time.

4.5.7 Future work

The following future work is suggested in descending importance:

1. Animal models and recordings on humans with intracranial electrodes to allow quantification of the changes with better SNR conditions, validations that they are genuine and refinement of the technology for recording the changes over shorter acquisition time. This could lead to the development of an invasive imaging system which could be used in brain research. This is part of ongoing work in our laboratory as part of an NIH funded project.
2. Measurements above the EEG band for possible improved SNR. Measurement of changes in the complex admittivity rather than the real resistivity presented in this study could significantly reduce the main source of physiological noise. However, the magnitude of the changes above 100 Hz is expected to be lower (Section 1.4.6).
3. Applying other types of EPs from areas in the brain where background brain activity is lower such as the somatosensory and auditory evoked responses. However, the magnitude of these EPs is lower comparing to VEP and the overall SNR might be similar.

5. Magnetic detection EIT of evoked physiological activity in the brain with scalp electrodes and MEG: simulation of expected changes with a Finite Element Model of the head

5.1 Abstract

In Magnetic Detection EIT (MD-EIT) current is injected through surface electrodes and the magnetic field produced by the distribution of that current in the volume conductor is measured using MEG or room temperature. This might be advantageous over conventional EIT since the transparency of skull to magnetic field might allow more focused image reconstruction. In addition, MD-EIT allows about 10 times more sensors than practically available in EIT studies which could potential improve the performance of image reconstruction or reduce the number of current injection pairs and hence total acquisition time.

The purpose of this study was to estimate the expected magnetic field changes during MD-EIT measurement with a realistic MEG system during visual stimulation and to suggest the optimal magnetic field sensors and current injection electrode placements for real human measurements out of a pre-defined set of electrode positions. This was achieved by utilizing an anatomically realistic model of the adult head, conductivity values estimated from the literature, solution of the forward problem for calculating current densities and Biot-Savart law with parameters from a specific MEG machine available for experiments for calculating the magnetic fields. Only the real part of the impedance change was considered since pilot simulations on the imaginary part revealed that it would provide negligible changes at low frequencies.

The validity of this method was assessed by comparing the model predictions with magnetic fields changes caused by a sponge perturbation in a saline filled spherical tank, showing a correlation of R = 0.81 between measured and predicted magnetic field changes. The model estimated that resistivity changes of 1% in a 9 cm^3 primary visual cortex during evoked responses translated into an average magnetic field changes of 4.7 ± 1.9 fT; 0.007 ± 0.003% (Mean ± SD) in the radial component of the magnetic field for a current level of 1 mA and were expected to be measured with an SNR below 2, which was limited by the averaged spontaneous brain activity. The maximal change in the most sensitive sensors and current injection electrodes was 6-fold higher (27 fT).These findings suggest that production of images with MD-EIT is not practical at this stage as about 6 hours were estimated to be required for recording with sufficient SNR and multiple current pairs. The optimal electrode placements were with current injected from pairs 5 or 10 cm apart over the occipital area and recording from magnetic sensors near the midline at the border between the parietal and occipital sensor groups. The estimated SNR of the MD-EIT method was similar to that estimated for the LF-EIT method in Ch. 3.

The results of this study were used in the following Ch. 6 in which I present my attempts to measure on humans the changes predicted in this study. Future work include estimating the minimal SNR needed for imaging, investigating the effect of anisotropy, refinements to the head model and design of a phantom with rapid impedance change.

5.2 Introduction

The previous modelling Ch. 3 and the experimental Ch. 4 described LF-EIT measurements using scalp electrodes to inject current and to measure voltage changes. These were shown to provide insufficient SNR for EIT image reconstruction when applying a practically feasible acquisition time. Several magnetic variants of EIT have been described in Section 1.3.7 and 1.3.8. In this study, the possible use of Magnetic Detection EIT (MD-EIT) (Ahlfors, 1992; Tozer, 1999; Ireland, 2004) for imaging neuronal activity was evaluated.

The use of MD-EIT with MEG as the sensing device to detect and image impedance changes related to neuronal activity was initially proposed in our group by Ahadzi et al (Ahadzi, 2004b). The proposed method was to inject EIT current into the head through a pair of surface electrodes and to measure the magnetic field induced by the distributed current. The local impedance change will perturb the current flow inside the head and hence alter the magnetic field outside the head. Ahadzi et al (Ahadzi, 2004b) performed an initial numerical simulation study to determine whether such a task was theoretically plausible. The head was modelled as concentric spheres to mimic the scalp, skull, cerebrospinal fluid and brain using the finite element method and the magnetic field 1 cm away from the scalp was estimated. An impedance change of 1% in a 2 cm radius (volume 33.5 cm^3) in the brain was modelled as the region of depolarization and a constant current of 100 μA was injected into the head from diametrically opposite electrodes. The model predicted that the static magnetic field is about 10 pT and changed by about 3 fT (0.03%) on depolarization. As the noise in a typical MEG system in the frequency band 1–100 Hz is about 7 fT, the authors concluded that these predicted changes are at the limit of detectability, similar to the situation in conventional EIT measurements. However, they also noted that there may be advantages to MEG since the magnetic field directly traverses the skull, and instrumentation errors from the electrode–skin interface will be obviated.

5.2.1 SNR requirements for human head MD-EIT

An important factor for estimating the feasibility of imaging neuronal activity with MD-EIT is the minimal SNR of the changes in magnetic fields outside the head, required for reliable image reconstruction. In previous studies on EIT of haemodynamic changes in the human brain, the SNR of the boundary voltage changes was between 1 and 4 (Section 3.2.2). For the specific application of imaging neuronal activity with LF-EIT, the upper value of 4 was chosen since there was uncertainty about how the image reconstruction would be effected by noise originated from spontaneous brain activity which is not normally distributed and could be highly correlated between recording channels (Section 3.2.2).

However, for MD-EIT, the little volume of published data did not include relevant information on the minimal SNR requirements. An SNR of 60-90dB with the noise originated from the instrumentation, was sufficient for practical 2D reconstruction in saline tank (Ahlfors, 1992) and human thorax (Tozer, 1999; Ireland, 2004) with large contrast of Perspex rod and air respectively. However, the effective SNR in their raw data was not reported. For the neuronal activity application, the impedance contrast is about 1% and the physiological noise, mainly related to spontaneous brain activity is expected to dominate the noise level and hence the effective SNR.

For the purpose of discussion, an un-established cautious assumption was made that the minimal SNR required for MD-EIT would be similar to that for LF-EIT. This requires further research which was left for future work.

5.2.2 Purpose

The purpose of this study was to estimate the expected magnetic field changes recorded outside the head during MD-EIT. The specific situation modelled was during Visual Evoked Responses (VER). Modelling was undertaken with a detailed FE model of the adult head and realistic properties of a specific MEG machine available for experimental use. The anticipated utility of this was to set a specification for further human measurements and provide a guide for assessing if any human changes appeared to be physiologically reasonable and so not due to artefact. Secondary purposes were:

1. To estimate the effect of current injection electrodes proximity to the orifices on the resulting changes since the current level there is limited to 100 μA instead of 1 mA to avoid possible alteration of the underlying neuronal tissue by the injected current (Ch. 2).
2. To estimate the current injection electrode and the position of magnetic sensors most likely to yield optimal signal changes in human measurements.

5.2.3 Design

5.2.3.1 Estimated changes

For predicting the changes in magnetic fields which result from local conductivity change in the visual cortex, the FEM simulations done by Ahadzi (Ahadzi, 2004b) were refined, using a realistic head model and a solver of the forward electromagnetic problem developed in our research group. The magnetic field induced by the distributed current densities was calculated using the Biot-Savart law at realistic gradiometer positions parameters, taken from the specifications of the MEG machine which was available for experimental use. Exhaustive calculations were performed over all possible current injection electrodes and magnetic sensors

placements as well as over a space of physiologically sensible conductivity values to provide bounds for the estimated changes. Inspection of the combinations which gave the largest changes permitted selection of those likely to yield the greatest sensitivity and suggest the optimal current injection electrodes and magnetic sensors placement.

5.2.3.2 Validation

The predictions obtained using FEM simulations with a forward solver were validated in spherical tank filled with saline by comparing the model predictions with magnetic fields changes caused by insertion of a sponge perturbation.

As described for a forward solver for MR-EIT (Lee, 2003), the magnetic field produced by passage of current through a volume conductor can be divided into three components: 1) the magnetic field produced by the high current density passing through the non-twisted part of the leads, when they split to deliver current to the two distant electrodes, 2) the magnetic field produced by the high current density on the electrode plates and 3) the magnetic field produced by the distribution of current within the entire volume conductor.

For my MD-EIT method, a head or a tank are positioned in a MEG system with leads delivering current to a pair of electrodes attached to the scalp or to the surface of a tank. As the leads and electrode plates are closer to the magnetic sensors comparing to the current distribution in the volume conductor (head or phantom), they produce the major part of the magnetic field at the sensors.

Thus, for comparing measured and predicted static fields, the exact geometry of the leads and electrodes has to be measured and the resulting magnetic field components have to be calculated. However, my aim was to measure magnetic field *changes* resulting from neuronal activity using a differential measurement, where measured fields from perturbed and non-perturbed states were subtracted. For an identical head or tank position inside the scanner during perturbed and non-perturbed recordings, the contribution of the leads and electrodes will vanish through the subtraction and the resulting field changes will be the result of local impedance perturbation, which affected the distribution of currents within the volume conductor.

For measurements in humans, the impedance perturbation is a transient, along a time course similar to that of evoked response and changes from baseline are expected over several hundreds of milliseconds. It is therefore assumed that for such a short time course, the position of the head in the MEG system remains fixed and the contribution of the leads and electrodes will vanish when subtracting perturbed and non-perturbed measurements. Longer term movements of the head along seconds or minutes will produce a bias field additional to the differential measurements. Such movements were practically minimized to about 1 mm and vanished by applying the baseline calibration as described in the experimental Ch. 4.

For a phantom measurement, I chose a saline filled spherical tank as the volume conductor and a sponge as a resistivity perturbation. The sponge perturbation is static and does not appear as a transient along hundreds of milliseconds as in the human case. Therefore, it was vital to maintain the position of the tank in the scanner as well as the leads geometry when manipulating the sponge, so that the differential measurement will reflect the changes in magnetic field produced only by the perturbation. This would make a method of placing the sponge inside the tank between the two recordings impractical. An alternative method for manipulating the perturbation within the volume of the tank using pulling strings was devised. This allowed recording when the perturbation was located at two different places inside the volume conductor and a differential measurement between these two cases. This was compared to modelling calculations reflecting these two cases, which were subtracted. The model did not include the leads and electrodes geometry as they were assumed to vanish through the differential measurement.

5.3 Methods

5.3.1 Estimated changes

5.3.1.1 Head model and forward solution

The current density vector **J** at each element was calculated using the UCL group SuperSolver package (Horesh, 2006c) using the same technique and realistic head model described in Ch. 2 and 3.

5.3.1.2 Electrodes and current level

The same set of 31 electrodes and 1 ground were disposed on the surface of the scalp covering the entire head (Sections 2.3.2 and 3.3.2 ; Figure 2-2b). The electrode diameter was 21 mm and a current of 1 mA was injected through pairs of electrodes. These diameter and current level were chosen according to the results of Ch. 2, which suggested a recessed electrode design allowing current of 1 mA without causing unpleasant skin sensation and altering the neuronal activity in the brain and were later used for the magnetic experimental work presented in Ch. 6. The calculated magnetic fields could then be linearly scaled for different current levels.

5.3.1.3 Perturbation

The region defined as confining the primary visual cortex (V1) was modelled as described in Section 3.3.3.

5.3.1.4 Conductivities

As described in Section 3.3.4, Table 2-1 specifies the conductivity values registered to the different compartments of the model and 81 conductivity combinations were used in the simulations to reflect the uncertainty in the literature.

5.3.1.5 Magnetic sensors

The MEG system available for the experimental study (Ch. 6) was a CTF MEG 275 (VSM MedTech Ltd., Coquitlam, BC Canada (Vrba, 2001)) located at the Functional Imaging Laboratory, UCL, UK. I therefore used the specifications of this system for this simulation study in order to obtain realistic results comparable to the experimental measurements. This system is equipped with 275 sensors (Figure 5-1), made of SQUIDs and a gradiometers made of two parallel coils of radii R = 0.9 cm sensing the difference in magnetic field between the first coil close to the head and the second coil located D = 5 cm away from the first coil (Figure 5-2a,b).

In my model, the position of the mesh within the coils array was the average position of real human subjects in the MEG scanner obtained from the dataset described in Ch. 6. For this position, the distance between the lower coils and the scalp was 2.5-4.5 cm. For the occipital and parietal sensors most relevant for these simulations (Figure 5-1), this distance was 2.5-3.7 cm. Out of these distances, 1.7 cm is the distance between the coil and the inner surface of the MEG helmet.

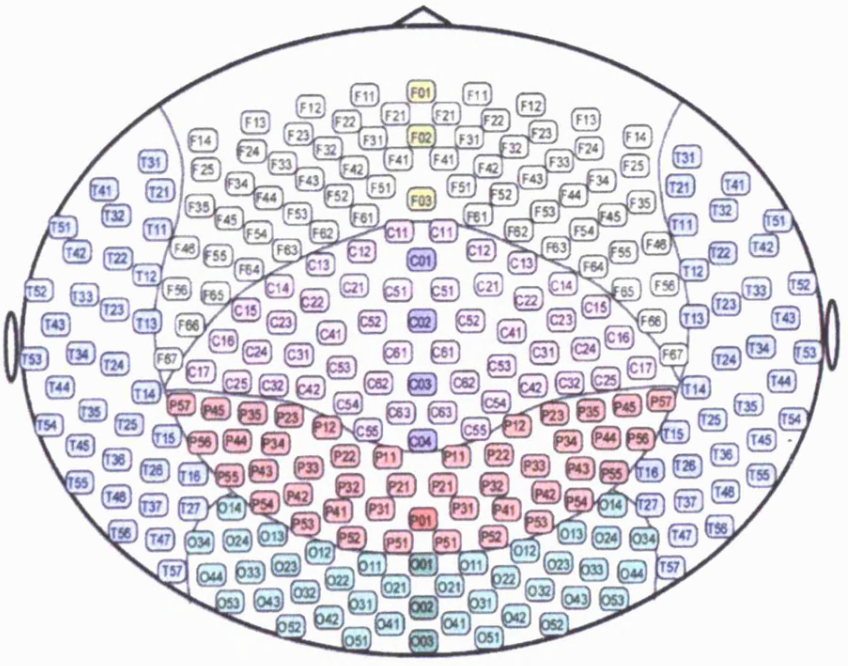

Figure 5-1: flatten layout of the 275 sensors segmented according to the brain lobes (Frontal, Central, Parietal, Occipital and Temporal).

Let $\mathbf{B}_k$ (k = 1, 2) be the magnetic field vectors at the centre of the two coils. $\hat{\mathbf{n}}$ is a unit vector perpendicular to the plan of the two parallel coils and pointing outward from the underlying surface of the scalp. Note that $\hat{\mathbf{n}}$ is not essentially perpendicular to the scalp surface as the head geometry is not identical to the placement of the sensors within the scanner. As a coil is only sensitive to the magnetic field perpendicular to its plane, $\mathbf{B}_k$ was divided into a radial component to the $\hat{\mathbf{n}}$ direction ($\mathbf{B}_k^{rad}$) and a tangential component perpendicular to $\hat{\mathbf{n}}$ and on the coil plane ($\mathbf{B}_k^{tan}$) (Figure 5-2b). I was therefore only interested in the radial component of the magnetic field reflecting the sensitivity of existing MEG systems. However, I have also examined the tangential component because of the possible contribution it may offer on conventional MEG applications (See section 1.2.2.2).

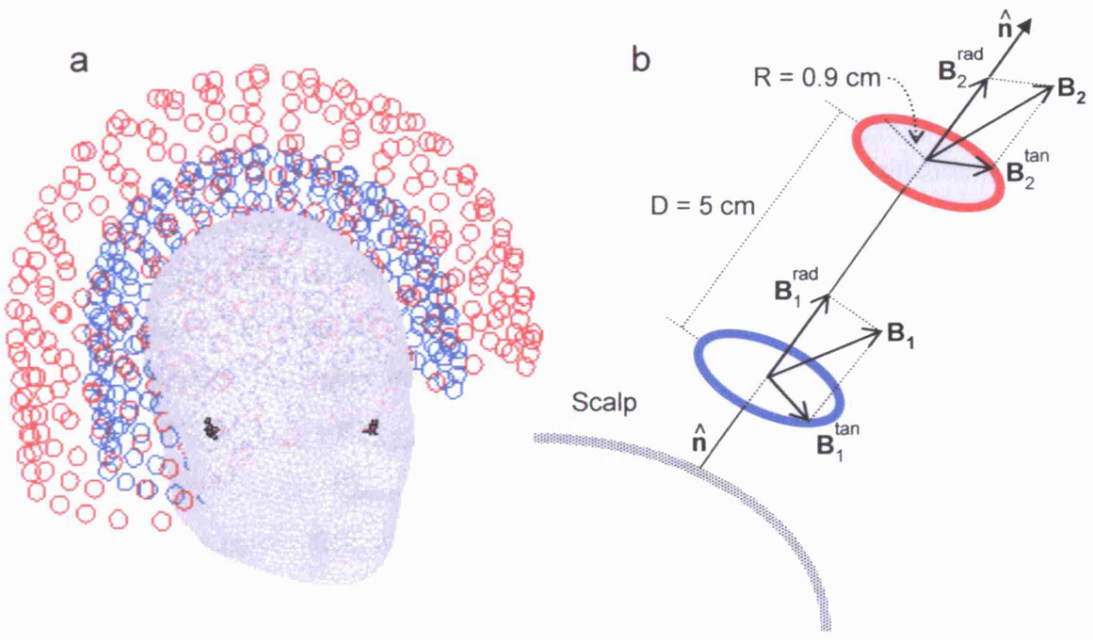

Figure 5-2: a) two layers of 275 coils (blue and red circles) were placed around the realistic head mesh. b) Radial and tangential components of the magnetic field at the centres of the two gradiometer coils.

5.3.1.6 Magnetic field calculation

The Biot–Savart law describes the magnetic field generated by electrical current flow:

$$\mathbf{B}(\mathbf{r}) = \frac{\mu_0}{4\pi}\int_{\Omega}\mathbf{J}(\mathbf{r}')\times\frac{\mathbf{r}-\mathbf{r}'}{|\mathbf{r}-\mathbf{r}'|^3}dv' \qquad (5\text{-}1)$$

Where $\mathbf{r}$ is the centre of the coil, $\mathbf{r}$-$\mathbf{r}'$ represents the distance between the source $\mathbf{J}(\mathbf{r}')$ and the measured $\mathbf{B}(\mathbf{r})$. The integral is performed over the entire volume conductor Ω carrying the current, and $\mu_0 = 4\pi\cdot10^{-7}$ TmA^{-1} [Tesla meter $Ampere^{-1}$] is the permeability of free space. Body tissue has such a weak magnetic susceptibility, that the permeability of tissue can be taken to be

the same as for free space. Therefore, it can be assumed that the human body is 'transparent' to low-frequency magnetic fields (Williamson, 1981) (page 152). The discrete form of the Biot–Savart law of the k^{th} coil (k = 1, 2) is given by:

$$\mathbf{B}_k(\mathbf{r}) = \frac{\mu_0}{4\pi} \sum_{i=1}^{NE} \mathbf{J}(\mathbf{r}_i) \times \frac{\mathbf{r} - \mathbf{r}_i}{|\mathbf{r} - \mathbf{r}_i|^3} \Delta v_i \qquad (5\text{-}2)$$

Where $\mathbf{J}(\mathbf{r}_i)$ is the current density at the i^{th} element (i = 1, 2... NE = 53,336) of the 3D head mesh and Δv_i is the volume of this element. The radial and tangential projections were then calculated using the dot product with the unit vector $\hat{\mathbf{n}}$ perpendicular to the coil plane:

$$\begin{aligned} \mathbf{B}_k^{rad} &= (\mathbf{B}_k \cdot \hat{\mathbf{n}})\hat{\mathbf{n}} \\ \mathbf{B}_k^{tan} &= \mathbf{B}_k - \mathbf{B}_k^{rad} \end{aligned} \qquad (5\text{-}3)$$

and the radial and tangential components from the two coils were subtracted to reflect a differential gradiometer measurement:

$$\begin{aligned} \mathbf{B}^{rad} &= \mathbf{B}_2^{rad} - \mathbf{B}_1^{rad} \\ \mathbf{B}^{tan} &= \mathbf{B}_2^{tan} - \mathbf{B}_1^{tan} \end{aligned} \qquad (5\text{-}4)$$

For a specific current injection electrode pair and magnetic sensor, the calculation was repeated for the rest and perturbed states of the primary visual cortex. The change in V1 conductivity, produced changes in the current density distribution $\mathbf{J}$, hence changing the induced magnetic field components $\mathbf{B}^{rad}$ and $\mathbf{B}^{tan}$. The final quantity of interest in this study was the difference between the perturbed and non-perturbed states:

$$\begin{aligned} \delta\mathbf{B}^{rad} &= \mathbf{B}^{rad}_{perturbed} - \mathbf{B}^{rad}_{non\ perturbed} \\ \delta\mathbf{B}^{tan} &= \mathbf{B}^{tan}_{perturbed} - \mathbf{B}^{tan}_{non\ perturbed} \end{aligned} \qquad (5\text{-}5)$$

Calculating the magnetic field at the centre of the coils is only a first approximation since the field is not necessarily homogenous across the coil plane. However, this was show to be negligible using a numerical study with a planner mesh model of the coils (Appendix C).

5.3.1.7 Protocol

For each magnetic sensors, the changes $\delta\mathbf{B}^{rad}$ and $\delta\mathbf{B}^{tan}$ were derived from the magnetic field calculations for the two coils, perturbed and non-perturbed states. These were then repeated for all 31·30/2 = 465 possible current injection pairs generated from the 31 electrodes, all 275 sensors and the 81 different conductivity combinations.

5.3.1.8 Data analysis

The analysis of the magnetic field changes was similar to the one performed for the voltage changes in Section 3.3.6 and is described again for clarity with the relevant changes in notation and sensor numbers.

Magnitude of changes: unlike the voltage differences in the LF-EIT case which was mostly negative, the difference $\delta \mathbf{B}^{rad}$ could be bi-polar. This was because the magnetic field is only depending on the current distribution in the volume and the relative projection of that current on the sensor. Local conductivity increases in the brain is changing the volume distribution of the constant current which could produce either positive of negative change in a given magnetic field sensor. Therefore, the following analysis has been applied on the absolute value of these changes.

Let $\left|\delta \mathbf{B}^{rad}\right|^{\sigma_c}$ be the absolute values of a set of 465·275 = 127,875 magnetic field changes $\delta \mathbf{B}^{rad}$ for all current pairs and magnetic sensors and a specific conductivity set σ_c (c = 1, 2...81). Most of the 465 current injection electrode combinations were linearly dependent in a sense that they could be reproduced by a linear combination of other electrode combinations. For example, [I 1,2] could be reproduced by subtracting the results from [I 1,3] and [I 3,2]. Therefore, a subset of independent current injection electrode combinations with the highest magnetic field changes was selected. This reduced the number of independent current pairs to 30 and the size of the total subset of $\left|\delta \mathbf{B}^{rad}\right|^{\sigma_c}$ values to 30·275 = 8250. From each such subset (for different conductivity combination), the mean and standard deviation of the absolute changes was calculated and defined as d_c. This value was also converted to percentage units by normalizing to the mean magnetic field $\mathbf{B}^{\text{rad}}_{non\ perturbed}$. A final representative value for the changes was then calculated as the mean D of the 81 d_c values and their standard deviation reflecting the effect of conductivities variability in the literature. To estimate the best case scenario, the same calculations were repeated when defining d_c as the maximal absolute changes rather than the mean.

Effect of orifices: for evaluating the influence of a possible shunting of applied current through the orifices, the above calculations were repeated after excluding from the current injection protocol 8 electrodes which were close to the eye or ear (electrodes 1,2,3,7,12,13,17 or 18) resulting in 23·22/2=253 current pairs out of the original 465 pairs. In this case, the total number of electrode combinations was 253 · 275 = 69,575 and after selecting the independent current injection combination with the highest changes this reduced to 22 · 275 = 6050 combinations.

Effect of conductivities: for evaluating the influence of each of the four adjustable conductivities (grey matter, white matter, skull and scalp) on the resulting changes, the 81 d_c values for all the conductivity combinations was expressed as a four dimensional function $d_c = f\left(\sigma_{grey}, \sigma_{white}, \sigma_{skull}, \sigma_{scalp}\right)$ where each of the four variables had three possible values. For each possible value of a certain compartment, there were 27 d_c values which were averaged

and presented against the conductivity of the chosen compartment. This was applied only for the case of excluding electrodes closest to the orifices.

Optimal current injection electrodes and magnetic sensors: for the given set of electrode positions, the electrode combinations and magnetic sensors which gave the largest absolute changes for the median conductivities were identified. This was repeated with and without the electrodes closest to the orifices.

The same analysis was applied to the values of the tangential component.

5.3.2 Validation

5.3.2.1 Phantom construction and perturbation

A spherical tank of 14.86 cm diameter was filled with 0.2% saline (conductivity 0.39 S/m). Two Ag/AgCl, 10 mm diameter, surface electrodes were glued on the inner surface of the tank. Two leads were coming out of the tank through 1 mm diameter holes, running to the centre point between the two electrodes and from there twisted all the way out of the scanner until it reached the current injection apparatus (Figure 5-3).

The local resistivity perturbation was simulated using a sponge sphere of volume 9.85 cm^3 and 19% increase in resistivity which was suspended on a plastic fishing line tied along the diameter of the z axis of the tank. The line ran through a loop at the bottom of the tank and two 1 mm diameter holes at the top of the tank. This allowed positioning of the sponge along the z axis with a precision of up to 5 mm.

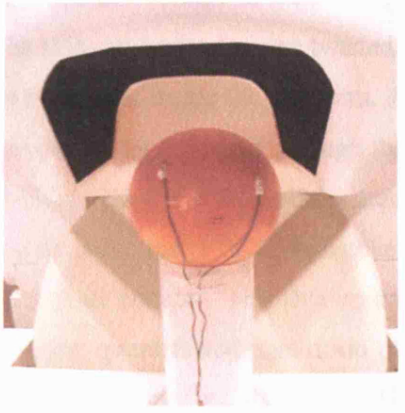

Figure 5-3: the spherical tank with the two electrodes placed in the MEG scanner before being raised to its final position. Note: although not shown in this picture, the leads were twisted all the way up to the middle point between the two electrodes.

5.3.2.2 Numerical modelling

The numerical calculations for the magnetic fields were done as described in Section 5.3.1. A spherical mesh of 225,000 elements was used and conductivity of 0.39 S/m was allocated to the entire volume. The actual current electrode positions, sponge perturbation geometry and

positions were allocated as well as the position of the tank within the scanner and the resulting magnetic sensors positions. The tank position was taken as the average tank position throughout the repeated actual measurements (see below). Calculations were repeated for the two sponge positions (top and middle of the z axis) and subtracted to obtain predictions for the differential measurements.

In addition, for estimating the effect of tank position variance on the magnetic field changes, the calculations were repeated for the 12 positions of the tank during the repeated measurements. For evaluating the effect of the limited precision of the sponge positioning along the z axis, the initial calculation was repeated after lowering the top sponge position by 5 mm.

5.3.2.3 Instrumentation

A current of 1 mA was delivered at 23.53 Hz through the two electrodes into the tank (Figure 5-4). The CTF MEG 275 (VSM MedTech Ltd., Coquitlam, BC Canada) system was used to generate the trigger signal for the current source by setting the Digital to Analog Converter (DAC1) channel to deliver 23.53 Hz. This rate was chosen to obtain an integer 51 samples per sine wave cycle when sampled with the 1200 Samples/Sec rate during the final acquisition stage of the magnetic field sensors. To maximize the SNR of the trigger signal, the maximal DAC amplitude of ±10V P-P was used and then attenuated to ±1V P-P using a voltage divider made of two resistors of 987 and 99.6 kΩ. The signal was then attached to the arbitrary waveform constant current source DS-5 unit (Digitimer, Welwyn Garden City, UK). Coupling attenuation of 3 dB across the DS-5 input reduced the voltage to ±0.5V P-P which was then translated to current of 1 mA at the output. The two output leads were twisted and passed into the Magnetic Shielded Room (MSR) and to the electrodes inside the phantom. Apart from being twisted, each lead was also coated with a shield which was grounded through the ground of the DS-5 unit.

The data acquisition of the MEG system was a parallel sampling of the 275 channels set to a rate of 1200 Samples/Sec with a dynamic range of 32 bits obtained by combining 20 bits per magnetic flux quantum and 12 bits reset counter. This dynamic range covers a total magnetic field range of 1360nT with a resulting quantization resolution of $1360nT/2^{32} = 0.317$ fT. The specified and actual noise levels of this system were 10 fT rms/√Hz.

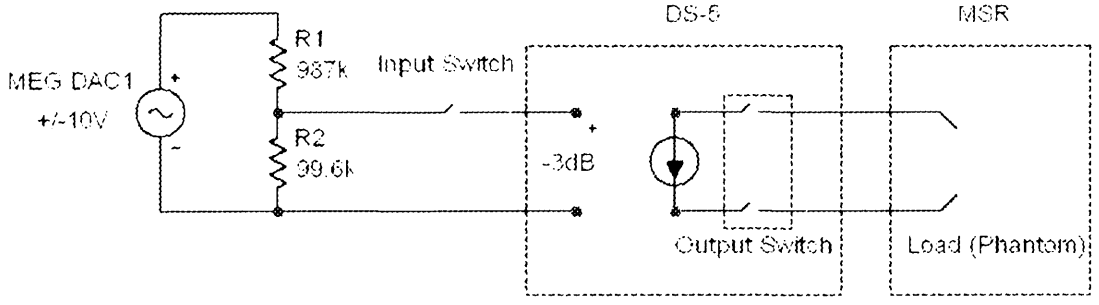

Figure 5-4: schematic diagram of the current source in the MEG setup.

5.3.2.4 Protocol

A total of 12 recordings of 80 seconds were recorded. These were alternating between the middle (odd recordings) and top (even recordings) position of the sponge along the z axis.

The tank position in the scanner was measured at the beginning and the end of each recording using the built in localization procedure of the MEG scanner which applied current through three localization coils attached to the phantom at three fiduciary points. The positions of the localization coils, electrodes and z axis on the phantom were measured with a 3-D Polhemus digitization system (3SPACE ISOTRAK II, Polhemus Inc., Colchester, VT, USA) with specified accuracy of 2.5 mm.

5.3.2.5 Data analysis

The data analysis included the following steps:

1. For reducing the measurement noise, each of the 275 recorded channels was filtered by a 4th order Butterworth filter with pass band of 5 Hz bandwidth centred on the carrier frequency of 23.53 Hz.
2. Non-synchronous amplitude demodulation:

   Given a cosine waveform *s(t)* of amplitude *a(t)* along the 80 sec recording,

   $$s(t) = a(t)\cos\omega t \qquad (5\text{-}6)$$

   Where $\omega = 2\pi f$ and $f = 23.53$ Hz is the carrier frequency,

   The Hilbert transform[1] (Oppenheim, 1999) is defined as

   $$\hat{s}(t) = \frac{1}{\pi}\int_{-\infty}^{\infty}\frac{s(t)}{t-\tau}d\tau \qquad (5\text{-}7)$$

   and if *a(t)* is band limited as applicable after applying the band pass filter in step 1, the Hilbert transform of *s(t)* is:

   $$\hat{s}(t) = a(t)\sin(\omega t) \qquad (5\text{-}8)$$

   The analytic representation of *s(t)* is defined in terms of the Hilbert transform:

   $$s_a(t) = s(t) + i\hat{s}(t) \qquad (5\text{-}9)$$

   Where $i = \sqrt{-1}$ and

   $$s_a(t) = a(t)[\cos\omega t + i\sin\omega t] = a(t)e^{i\omega t} \qquad (5\text{-}10)$$

   The discrete form and practical considerations related to the finite nature of *s(t)* are described elsewhere (Oppenheim, 1999; Wikipedia contributors, 2006) and are implemented in the Matlab *'hilbert'* function which I used. The amplitude demodulation was realized by taking the absolute of the analytic representation:

   $$a(t) = |s_a(t)| \qquad (5\text{-}11)$$

---

[1] See also Wikipedia for a simple description of the Hilbert transform (Wikipedia contributors, 2006).

3. Calculating the median amplitude along the 80 sec.
4. Subtracting the data from each pair of recordings taken when the sponge was at the top and middle of the z axis to obtain the differential measurement.
5. Averaging the data from the 6 recording pairs and calculating the standard deviation SD_1 reflecting the variation across experimental repetitions.
6. Selecting the less noisy channels with $SD_1 < 200$ fT.
7. First order linear regression was used to compare the measured and predicted absolute magnetic field changes for the selected channels with lower SD_1. The regression parameters, correlation coefficient and standard deviation SD_2 of the data points around the regression line were calculated.

An additional analysis was performed to estimate the effect of geometrical tank movements (SD_3) across the experimental repetitions on the resulting standard deviation SD_4 of the magnetic field measurements across the 6 repetitions using modelling predictions for all different tank positions. Finally, modelling results from the shifted top sponge position were used to evaluate the standard deviation SD_5, resulting from the limited precision of the sponge positioning along the z axis in repeated recordings.

5.3.3 Statistics

For the validation study, the values for the slope of the linear regression were given as mean ± SE. The SE was used to demonstrate how accurate the model predicted the experimental tank measurements. The final values for the estimated changes in the human model were given as mean ± SD. The SD provided bounds for the possible estimated changes and was originated from the uncertainty in the conductivity values taken from the literature.

5.4 Results

5.4.1 Validation

For the changes due to sponge perturbation, the correlation between measured and predicted absolute magnetic field changes for channels with $SD_1 < 200$ fT was $R = 0.81$ ($p < 10^{-42}$; $N = 189$), with a slope of 1.06 ± 0.06 and offset 75 ± 5 fT (Figure 5-5). The standard deviation around the regression line was $SD_2 = 65$ fT.

For evaluating the effect of the tank motion along the 12 recordings, the following measurements has been made: 1) SD_3 of the tank position across the 12 recordings was 0.05 mm and 2) SD_4 of the predicted magnetic field changes for the 6 repeated pairs using different tank

positions was <5 fT for all 275 channels. The limited precision of the sponge positioning along the z axis was resulting in a standard deviation of SD_5 = 40 fT.

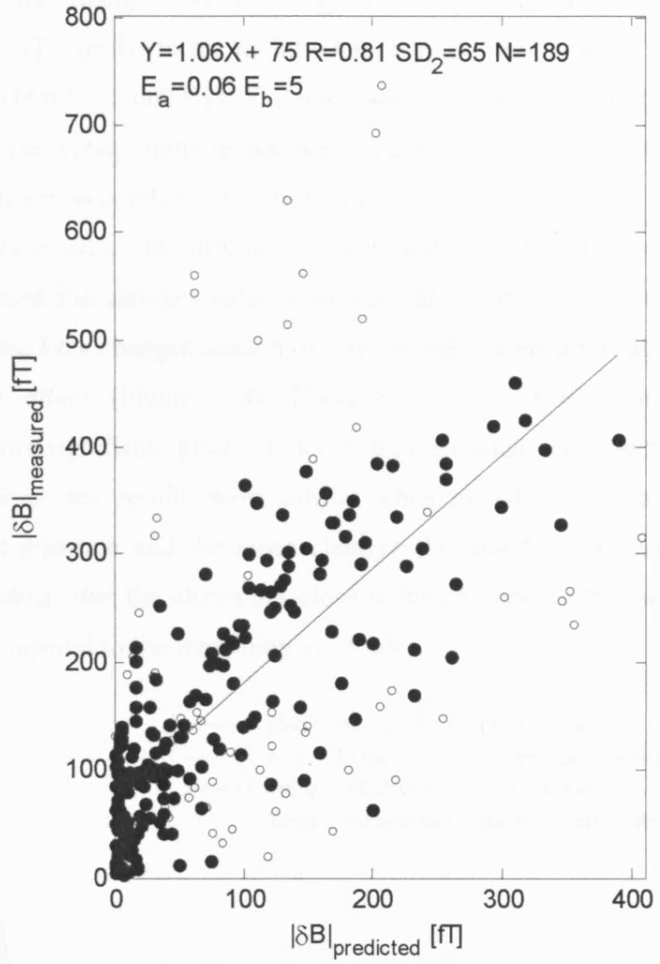

Figure 5-5: measured vs. predicted absolute magnetic field changes for the spherical tank (radial component). Solid dots are channels with SD_1 < 200 fT.

5.4.2 Estimated changes

The magnitude of the changes: When considering all possible current injection electrode combinations, most of the magnetic field changes are very small since most of the magnetic sensors are located far from the visual cortex and many current pairs does not deliver much current to the visual cortex (Figure 5-6). When selecting the independent current injection combinations most sensitive to the visual cortex, a higher proportion of measurements carry significant information (Figure 5-6). For the radial component, after excluding the electrodes close to the orifices, the average changes over the 81 conductivity combinations were D = 4.7 ± 1.9 fT; 0.007 ± 0.003% when averaging the mean value across independent current electrode positions and magnetic sensors. This average was 6-fold higher (27 fT) when taking the maximal change across independent electrode positions (שגיאה! מקור ההפניה לא נמצא., Table 5-1).

However, the percentage change for averaging that maximal value was 0.2%, 30-fold higher than that for the mean, since the percentage scale is not linear and the static magnetic field was low for these maximal changes. For the tangential component, the changes in physical units were D = 3.3 ± 1.4 fT, similar to the radial component but one order of magnitude smaller in percentage units (0.0007 ± 0.0003%), The maximal changes were 7 and 3-fold higher for the magnetic field and percentage units respectively (Table 5-1). In all the values given above, SD reflected the uncertainty in conductivities from the literature.

Effect of conductivities: similarly to the LF-EIT case (Ch. 3, Figure 3-8) increased skull conductivity increased the changes since more current could reach the brain, increased scalp conductivity decreased the changes since more current was shunted through the scalp and white matter had minor effect (Figure 5-8). However, unlike LF-EIT, increased grey matter conductivity has more significant effect of increasing the changes (Figure 5-8).

Effect of orifices: the results were similar when including the electrodes close to the orifices for current injection and the mean changes (but not the maximal) were 3-4% lower (Table 5-1), suggesting that the electrodes close to the orifices are less sensitive to changes in the visual cortex compared to the remaining electrodes.

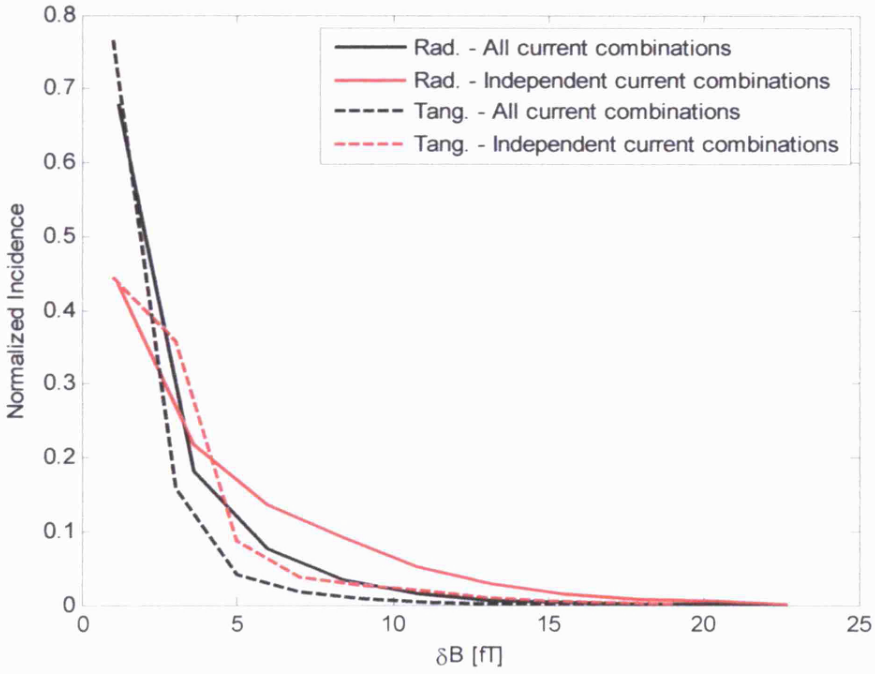

Figure 5-6: normalized incidence of the magnetic field changes from all current injection combinations (n=69,575) and from the subset of independent combinations most sensitive to the visual cortex (n=6050). This is for both radial and tangential components for the case of median conductivity values and excluding current injection close to the orifices.

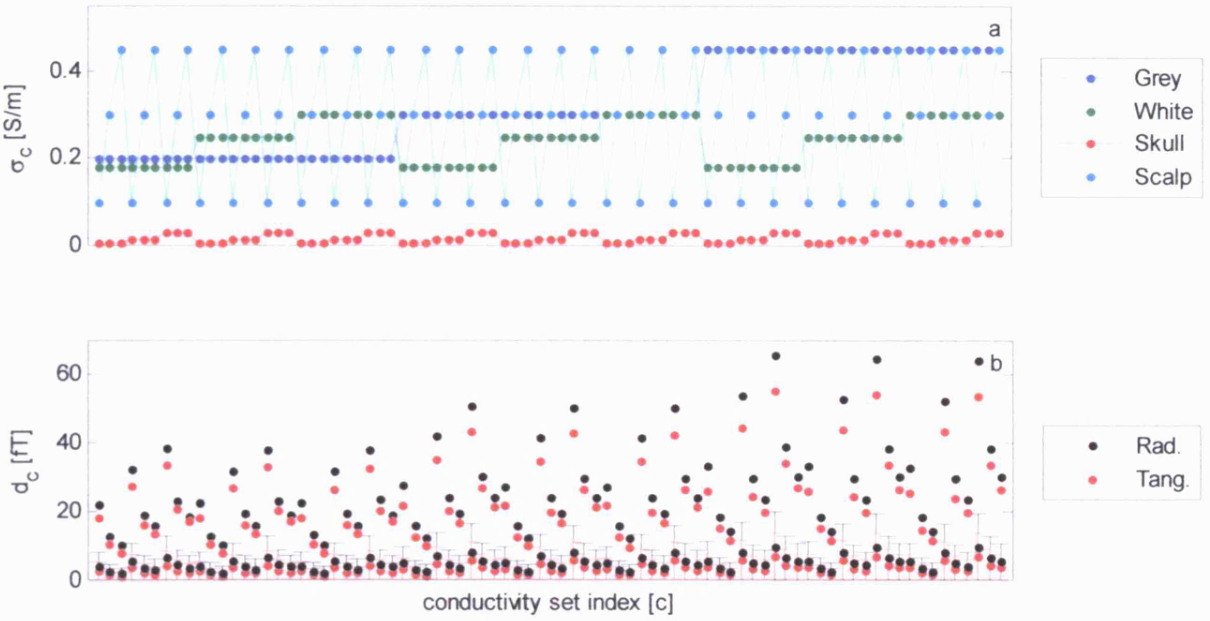

Figure 5-7: a) the 81 conductivity sets σ_c (points were connected for clarity). b) The mean of the changes in the radial (back) and tangential (red) components from independent current electrode combinations with SD as error bars. The maximal changes are also marked with no error bars. This is for the case of excluding current injection close to the orifices.

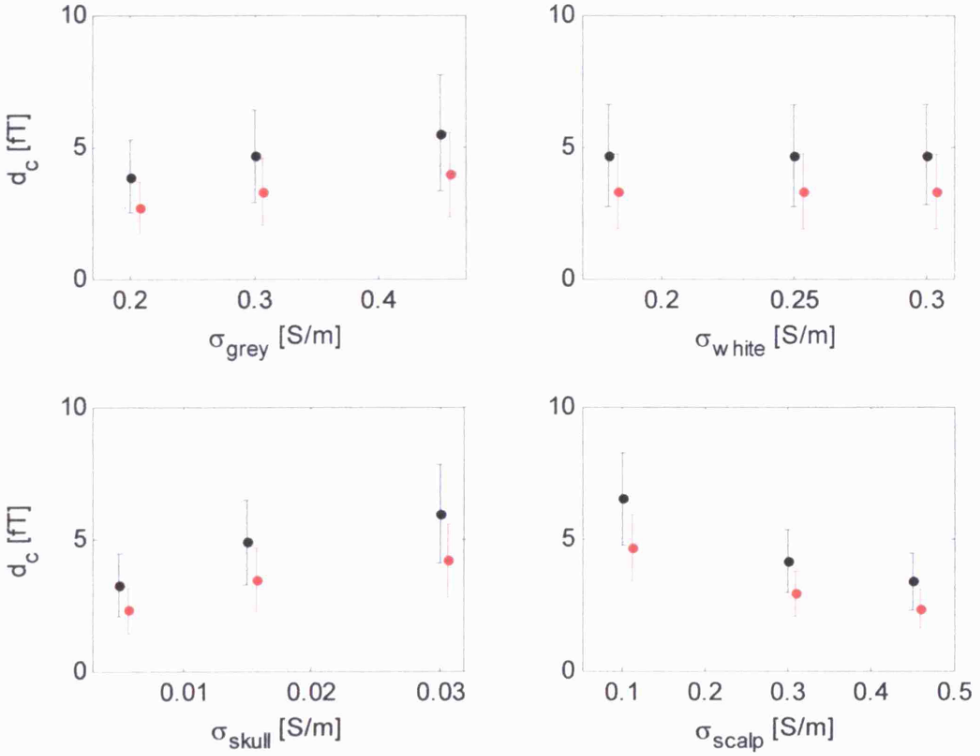

Figure 5-8: effect of the four conductivities on the average changes. Each point in a graph is the average of 27 d_c values with the same conductivity as the compartment on the x axis. The error bars are the SD. The radial component is in black and the tangential component in red was lightly shifted to the right for clarity.

Table 5-1: mean (maximum in brackets) magnetic field changes for all independent current combinations and all conductivity sets.

Magnetic field component	Exclude electrodes near the orifices?	D [fT]	D [%]
Radial	Yes	4.7 ± 1.9 (27 ± 13)	0.007 ± 0.003 (0.2 ± 0.5)
	No	4.5 ± 1.9 (27 ± 13)	0.007 ± 0.003 (0.2 ± 0.5)
Tangential	Yes	3.3 ± 1.4 (23 ± 11)	0.0007 ± 0.0003 (0.002 ± 0.001)
	No	3.2 ± 1.4 (23 ± 11)	0.0007 ± 0.0003 (0.002 ± 0.001)

5.4.3 Optimal electrode and magnetic sensors placement

For the radial case, the current injection electrode pairs which gave the four uppermost changes for the median conductivities were semi-adjacent (5-10 cm apart) over the occipital region: pairs [23 26], [23 27], [23 30] and [29 30] as marked in Figure 3-9, Ch. 3). In all these cases, the most sensitive magnetic sensors were over the midline at the border between the parietal and occipital sensor groups (e.g. sensors LP52, LP52, RP51 in Figure 5-1; Figure 5-9 left). This area was just above the modelled visual cortex.

For the tangential component, the same current injection electrodes gave the largest changes but the most sensitive magnetic sensors were lower on the occipital sensor group (Figure 5-9 right).

Effect of the orifices: similar optimal current injection electrodes and magnetic sensors were obtained when including or excluding the electrodes closest to the orifices

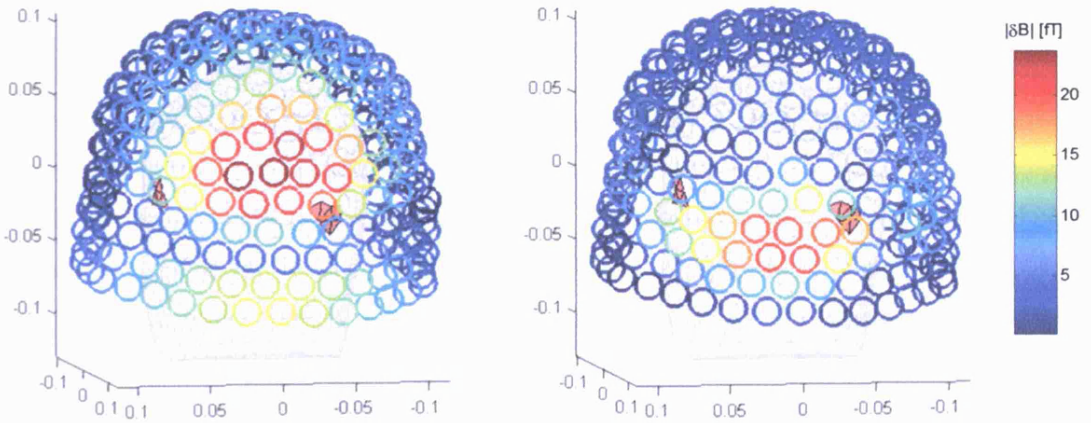

Figure 5-9: example for the distribution of the absolute changes across the magnetic sensors in the radial (left) and tangential (right) components (for σ_{median} and current injection pair [23 30] marked in solid red).

5.5 Discussion

5.5.1 Summary of results

For the sponge perturbation study intended to validate the modelling method, there was a high correlation between measured and predicted magnetic field changes (R = 0.81; slope 1.06 ± 0.06).

The magnitude of the simulated changes in magnetic field due to conductivity changes related to neuronal activity in the visual cortex after excluding the electrodes close to the orifices was 4.7 fT (0.007%) for the radial and 3.3 fT (0.0007%) for the tangential component. With respect to variable conductivities due to uncertainty in the literature, this varied by 1.9 fT (0.003%) and 1.4 fT (0.0003%) respectively. When averaging the maximal changes for each conductivity set the changes were 6 and 7-fold higher for the radial and tangential components respectively but when translating to percentage units this was changed to 30 and 3-fold due to the non-linearity when converting to percentage. Values were most sensitive to the choice of skull and scalp conductivities. the results were similar when including the electrodes close to the orifices for current injection and the mean changes (but not the maximal) were 3-4% lower (Table 5-1), suggesting that the electrodes close to the orifices are less sensitive to changes in the visual cortex compared to the remaining electrodes.

The combinations which gave the largest peak changes were with current injection over the occipital region with an adjacent (5 cm apart) or semi-adjacent (10 cm apart) pair of electrodes and recording with magnetic sensors above the visual cortex.

5.5.2 Technical issues

The changes presented in this study are given in both magnetic field and percentage units. The use of magnetic field units is essential when comparing the MD-EIT changes with physiological and other sources of noise to estimate the SNR that could be achieved in realistic human measurements. However, these changes were calculated for a specific current level, 1 mA in this study, and need to be linearly scaled when other current levels are considered. The use of percentage units relative to the magnitude of the MD-EIT static field has been used as a convention in EIT studies and is easy to interpret. However, such figures should be treated with caution as the magnitude of the changes, in magnetic field units, is not linearly related to the magnitude of the static field and erroneous results could be obtained. An example of this is that a similar estimated magnetic field changes for the radial and tangential components (4.7 and 3.3 fT) had an order of magnitude difference when translated into percentage units (0.007 and 0.0007%). This difference was obtained since unlike the tangential component, the radial

component at the sensors near the current injection sites is less sensitive to the current density flowing down from the electrodes into the head. Therefore, I decided to use magnetic field units when interpreting the results but included translation to percentage values in order to be consistent with the convention.

5.5.3 Validation

The measured changes agreed with modelling for the sponge perturbation in a tank, suggesting that the estimations made for the neuronal activity in humans are within the correct order of magnitude. The variability between repeated measures produced SD_2 = 65 fT around the regression line containing data between 0 to 500 fT (Figure 5-5). This could be due to the following factors:

1. Miss-registration of sponge position in repeated measures caused by the flexibility of the pulling string estimated to produce SD_5 = 40 fT which could partly explain SD_2.
2. Movement of the tank position across the repeated measures due to the string pulling. These movements were of SD_3 = 0.05 mm which could introduce maximal changes of 5 fT which could not fully explain SD_2.

These could be overcome by designing a phantom with transient impedance changes at a define location. This would simulate more realistically neuronal activity related changes without simulating a differential measurement with two static measurements. Construction of such phantom was left for future work

The linear regression also had an offset of 75 fT (Figure 5-5), which could be related to a bias from miss-registration of the entire phantom position within the MEG scanner. This could be due to the specified accuracy of 2.5 mm of the Phloem's digitizer used to measure the positions of the electrodes and localization coils and 1-2 mm errors in placing the localization coils on the tank. Each of these two factors was estimated to produce offset of about 20 fT. The offset could be minimized by searching the 3D space of several mm around the original measured position but this was left it beyond the scope of this validation study.

5.5.4 Estimated changes and SNR

For the radial component which is the most relevant for measurement in a MEG system, the magnitude of the estimated changes was 4.7 fT for the mean and 27 fT for the maximal changes. These changes were per 1% conductivity perturbation in 9 cm^3 of visual cortex and can be linearly scaled if the assumption of conductivity perturbation and volume are modified within the same order of magnitude. The physiological noise level obtained from background brain activity in the occipital area when eyes are open is about 200 fT (Cohen, 1968; Hamalainen,

1993) and after averaging 1000 stimuli for 10 minutes, this noise reduces to 200 fT / $\sqrt{1000}$ = 6.3 fT. This predicts an SNR of only 0.74 for the mean changes and 4.3 for the maximal values.

The implications for implementing an imaging system based on the present method are limited as the average SNR for allowing MD-EIT image reconstruction is not known but was cautiously estimated to be about 4 (Section 5.2.1). This required SNR of 4 was for the average of 10% the changes in a protocol of 258 electrode combinations. For the purpose of comparing this value to the estimated SNR from my model, I chose to take the average SNR obtained for the mean and maximal changes in my independent electrode protocol (0.74+4.3)/2 = 2.5. Longer averaging over about 30 minutes (10 minutes x $(4/2.5)^2$) could improve the SNR to the desired level but just for one current pair. A possible way to reduce this averaging time is to record at higher frequency above the EEG band which was estimated to enhance the SNR by a factor of 5 (Section 1.4.6) and hence reduce the averaging time by a factor of 25. Exploring this possibility was left for future experimental work.

In addition, for image reconstruction, data is needed from multiple current injection pairs. For obtaining previous EIT images of haemodynamic changes in the brain, an electrode protocol consisting of 21 current pairs, each with 12 voltage measurement pairs was used (Tidswell, 2001; Tidswell, 2006). Due to reciprocity, similar results could be obtained with 12 current pairs, each with 21 voltage measurements. In the MD-EIT presented in this model, the magnetic recording is done in parallel from 275 sensors so the limiting factor is the number of current pairs. For 12 current pairs and 30 minutes that might be needed for sufficient SNR, the overall recording time would be 6 hours which is impractical for human subjects to tolerate. This could be partly overcome by employing multiple current injection schemes but these will have to inject lower current levels to adhere safety standards which will decrease the SNR. In addition, the amount of magnetic sensors (275) is an order of magnitude greater than the 21 measurement pairs for the previous EIT application. This could allow some reduction in the number of current pairs for achieving similar results. However, a quantitative estimation of such possible improvement requires further investigation which was left for future work.

I therefore conclude that non-invasive imaging with LF-EIT method is not feasible with present technology. Future effort should be focused on achieving substantial improvement in SNR without averaging for a long time.

Effect of the orifices: the same maximal changes were obtained when electrodes close the orifices were included or excluded from the protocol. This means that the highest changes were originated from electrodes far from the orifices which can carry the maximal current of 1 mA without the possibility of altering the underlying neuronal activity limiting the current level in these to 100 μA (Ch. 2). The implications of this for imaging neuronal activity in the visual cortex area is that excluding these electrodes from the protocol will not compromise the estimated changes.

5.5.5 Optimal electrode and magnetic sensors placement

Estimating the optimal electrode and magnetic sensor placement was important for designing actual human measurements to attempt measuring neuronal activity related changes in single channel measurements. This is a preliminary requirement for allowing estimation of the actual SNR of such changes before approaching the more demanding imaging problem.

The combinations which gave the largest peak changes were with current injection over the occipital region with an adjacent (5 cm apart) or semi-adjacent (10 cm apart) pair of electrodes and recording with magnetic sensors above the visual cortex (Figure 5-9). These optimal combinations were intuitively justified as the close current injection pair was sensible for obtaining high current density in the occipital cortex just below the electrodes and the optimal recording magnetic field sensors were located above the ROI. The optimality obtained from this study is limited to the pre-defined set of electrode positions and magnetic sensors and is not generalized to any electrode position.

5.5.6 Comparison to previous studies

The use of MD-EIT with MEG as the sensing device to detect and image impedance changes related to neuronal activity was initially proposed in our group by Ahadzi et al (Ahadzi, 2004b).

Modelled changes: Ahadzi's numerical simulations predicted maximal changes of 3 fT (0.03%) for current of 100 μA, which can be factored to 30 fT (still 0.03%) for a current of 1 mA. To compare Ahadzi's results with this study, the maximal estimated changes were taken as a reference. These were obtained for the radial component while excluding electrodes close to the orifices (Table 5-2). In spite of several key differences between Ahadzi's study and my more detailed study (Table 5-2), this maximal changes in physical units were strikingly similar. However, the percentage changes were an order of magnitude higher for the radial and lower for the tangential components. This could be possibly explained by the absolute measurement of the magnetic field by Ahadzi while I estimated the radial and tangential components separately. When these are averaged, the 0.2 and 0.002% become 0.02%, which is similar to the 0.03% given by Ahadzi.

Table 5-2: comparison between Ahadzi's (Ahadzi, 2004b) and this study.

	Ahadzi	Gilad (this study)
Predicted changes	30 fT (3fT for 100μA)	Radial 27 ± 13 fT ; Tangential 23 ± 11 fT
(change 1%, I = 1mA)	0.03%	0.2 ± 0.5% ; 0.002 ± 0.001%
Component	Absolute B	Radial projection
Magnetic sensor model	Single coil	Realistic - difference between 2 coils
Coil-scalp distance	1 cm	Lower coil 2.5-3.7 cm for occipital and parietal sensors
Mesh	Concentric spheres	Realistic
Perturbation volume	33.5 cm^3	9 cm^3
Conductivities	1 set:	81 sets covering literature uncertainty
	Brain, CSF, skull and scalp.	Ahadzi's values are within ranges used here
	0.25, 1.79, 0.018 and 0.44 S/m	
Protocol	1 diametric current pair	465 current pairs
	3 magnetic sensors	275 sensors
	15 perturbation positions	1 perturbation position

SNR estimation: in Ahadzi's study, they compared the predicted changes of 3 fT for current of 100 μA to the typical sensor noise of 7 fT in MEG systems to conclude that this is at the border of detectability with SNR of the order of 1. For 1 mA, the changes would rise to 30 fT and the SNR to 4.3. In my study, the changes were calculated for a current level of 1mA, the noise was taken as the background brain activity of about 200 fT (Cohen, 1968; Hamalainen, 1993) with an averaging protocol of 1000 stimuli. According the calculations in Section 5.5.4, this would also give an SNR of about 4.3 for the maximal changes.

5.5.7 Future work

Several studies are suggested for future work:

1. Reconstruction study: since no data is available on the minimal SNR required for reliable image reconstruction with MD-EIT a reconstruction study is proposed. This would include implementing an inverse solver for the MD-EIT problem as suggested by other workers (Ahlfors, 1992; Tozer, 1999; Ireland, 2004), simulating changes with the forward solver used in this chapter and introducing realistic noise from the human measurements presented in Ch. 6. The application of an inverse solver for MD-EIT could be also used for image reconstruction of future data sets with enhanced SNR.
2. The effect of anisotropy: scalp, skull and white matter has anisotropic conductivity properties which are not taken into account in out isotropic forward solver. Recent improvements to the solvers used in our research group (SuperSolver) have incorporated the

framework for anisotropic solutions. However, the present limitation for using it in modelling studies is the insufficiently accurate head model registering the anisotropic properties for each element and exact physiological knowledge about these properties. Recent advances in diffusion MRI may be valuable for mapping anisotropic properties which were found to be linearly related to diffusion properties (Tuch, 2001).

3. Refinements to the model: incorporating more accurate head model with finer structures and update the conductivity values used when new measurements of the dielectric properties of the head tissues will become available in the literature.
4. Design of a 3D phantom with rapidly changing impedance in an ROI, suitable for both LF-EIT and MD-EIT recordings. This would be a more realistic simulation of neuronal activity related changes and will bypass the additional technical problems related to differential measurements with *static* changes such as insertion of sponge perturbation.

6. Magnetic detection EIT of evoked physiological activity in the brain with scalp electrodes and MEG: measuring changes non-invasively in humans

6.1 Abstract

According to the modelling in Ch. 5, the maximal magnetic field changes due to 1% conductivity increase of 9 cm^3 volume of visual cortex during visual evoked responses (VER) was 27 ± 13 fT when using 1mA of EIT current. The purpose of this chapter is to measure these changes non-invasively in humans in order to compare to the modelling prediction, estimate the actual SNR that could be achieved and evaluate the implications for designing an MD-EIT based non-invasive functional imaging system for imaging fast neuronal activity in the human brain.

A prototype MD-EIT system was developed for measuring the real part of the impedance change and novel signal processing techniques were applied to separate the EIT and visual evoked fields (VEF) components recorded within the same band, optimize SNR and detect the underlying changes. In this study, 9 recordings were obtained from 5 healthy subjects. A 1 Hz square wave current of up to 1 mA was applied through a pair of occipital electrodes synchronously to 2 Stimuli/sec pattern reversal chequerboard VER. Magnetic fields were recorded from 275 sensors using MEG and averaged over 10 minutes.

In this study, for the first time, non-invasive measurement of fast resistivity changes related to neuronal activity were measured using MD-EIT. Significant changes of 60 ± 30 (range 30-130) fT and SNR of 3.2±0.7 with an average current level of 875 μA were observed mostly from the occipital and parietal sensor regions in all subjects. Visualization of the spatial distribution of the magnetic field changes in the recording with the largest change, revealed main negative components at 70 and 110 ms located in the left and right occipital sensor regions which coincide in time but not in space with the VEF components. Group average did not improve the SNR due to uncontrolled alignment of the head position between recordings.

Overall, these changes agreed with the modelling predictions. At present, the implications for imaging system are limited at this stage since about 3 hours were estimated to be required for recording data from multiple current injection pairs with sufficient SNR, which is not practical when recording on humans. The SNR was mainly limited by background brain activity and additional noise from the current source located outside the MSR. Several improvements to the hardware and protocol were suggested which could potentially reduce this total recording time to several minutes and could make this methods practically tolerable to human subjects.

6.2 Introduction

The ultimate goal of the work in the thesis was to develop a non-invasive imaging method capable of imaging the impedance changes over milliseconds, occurring when neuronal ion channels open during activity. This was previously addressed in Ch. 4 with scalp electrodes to inject current and record voltages, where impedance changes were recorded during physiologically evoked activity for the first time. In this chapter, magnetic detection method was evaluated in the same way but with current injected with scalp electrodes and magnetic field changes were recorded in a MEG system, adopted as a magnetic detection EIT system. No imaging was undertaken; the goal of this study was to determine if such changes could reliably be recorded in some of the magnetic sensors positioned around the head. To my knowledge, this is the first experimental application of MD-EIT for the human head.

6.2.1 Expectations based on previous studies and modelling

Ahlfors and Ilmoniemi (Ahlfors, 1992) originally proposed to use MD-EIT for static impedance imaging of the head and demonstrated the method with a single pair of electrodes which inject current at 16 Hz through a saline filled tank containing insulating cylinder. An array of 24 SQUIDs was used to measure the induced magnetic field 30-50 mm above the tank and to image current density. The Sheffield group developed MD-EIT using coils and presented measurements on phantom and thorax from 2 human subjects (Tozer, 1999; Ireland, 2004).

The use of MD-EIT with MEG as the sensing device to detect and image impedance changes related to neuronal activity was initially proposed in our group in a simulation study (Ahadzi, 2004b), which was extended in Ch. 5 of this thesis. The model estimated that resistivity changes of 1% in a 9 cm^3 primary visual cortex during evoked responses translated into an average magnetic field changes of about 5 fT and maximal changes of 27 fT at the most sensitive sensors, when applying 1 mA of MD-EIT current.

6.2.2 Purpose

The purpose of this study was to determine if reproducible changes in magnetic field due to impedance changes in the brain could be recorded with scalp electrodes and MD-EIT during visual evoked responses.

6.2.3 Experimental design

Experiments were undertaken in adult human subjects during full field pattern reversal visual evoked response paradigm. Total of 9 MD-EIT recordings were recorded from 5 subjects. A prototype MD-EIT system was developed consisting of a current source applying 1 Hz square wave of up to 1 mA through recessed design electrodes for reducing skin current density at high current levels (Ch. 2), which was integrated into an MEG system available at the Functional Imaging Laboratory, UCL. Following the optimal electrode positions modelled in Ch. 5 likely to record the largest impedance change during visual evoked responses, 2 electrodes were placed over the occipital part of the scalp for current injection and the MEG sensors were used for recording of both the visual evoked field (VEF) and low frequency resistance change (Figure 6-1). The low frequency resistance changes were recorded by a method originally proposed by Boone et al. (Boone, 1995a) for separating the resistance changes from the EP signals when they are recorded within the same frequency band. The data from all the recordings was pooled for enhancing the SNR.

Figure 6-1: left - the current injection electrodes placed over the back of the head. Right – the subject was sited in the MEG scanner with current electrodes, localization coils and finger oxymeter attached.

6.3 Methods

6.3.1 Subjects and recordings

Total of 9 MD-EIT recordings were made from 5 normal subjects with age range of 28 to 43 (1 female and 4 male). One active recording was made in subjects 1 and 2 with simultaneous application of visual stimulus and EIT current. In the remaining subjects, a control recording was made with visual stimulus and no EIT current followed by another active recording. In the last subject another active recording has been made. Each of the 9 MD-EIT recordings consisted of 9 to 20 repeated 1 minute recordings. The MD-EIT recordings were numbered between 1 and 5 followed by A and B to mark the control and active recordings made in each session and C for a third active recording in subject 5 (Table 6-1).

Subjects 2 and 4 had minor imperfections in visual acuity requiring corrective lens of strength up to up to ±1D which were not worn during the experiment due to mechanical limitation of the MEG helmet.

Table 6-1: Summary of subjects, recordings and experimental setup.

Recording	Subject	Gender [M/F]	Age	Current [μA]	N_A'/N_A ($N_{1,2}$)[a]	N_B'/N_B ($N_{1,2}$)	N_C'/N_C ($N_{1,2}$)
1B	1	M	31	700		10/10 (306)	
2B	2	M	43	900		8/10 (272)	
3A,3B	3	M	33	900	9/10 (306)	20/20 (680)	
4A,4B	4	M	28	1000	9/9 (306)	15/15 (510)	
5A,5B,5C	5	F	29	800	9/10 (340)	9/10 (340)	10/10 (340)

[a] N_A' is the number of valid 1 minute recordings out of N_A used for averaging after excluding 1 minute recordings with large head movements, corrupted data file or attenuated EPs (Section 4.3.6.4). $N_{1,2}$ is the number of half square wave cycles used for averaging (Section 4.3.6.5)

6.3.2 VERs

A full field pattern reversal black/white checkerboard of rate 2 reversals/sec was generated with Cogent 2000[2] software (installed on a separate computer termed Trig PC) while the subject was seated in the MEG scanner, 52-56 cm from a semi-transparent screen, while a projector positioned outside the magnetically shielded room (MSR) illuminated the screen from the back through a set of two mirrors.

The check size was 30' (60' = 1°), the projected area was 32 x 24 cm, the field size was 40°x30° (64x48 checks) and the contrast was 100%. The subjects were requested to focus on a centred fixation yellow square on the screen (size of one check). In each 1 minute recording, the visual stimulation lasted 30 sec. The separated 1 minute recordings were made to minimize accommodation as well as de-focusing due to tiredness of the eye muscles.

During head localization or recording without visual stimuli, the entire screen was grey at the median level between black and white and the fixation point was a green square. When the subject was allowed to relax between 1 minute recordings, the entire screen was black with a

[2] Cogent 2000 developed by the Cogent 2000 team at the FIL and the ICN and Cogent Graphics developed by John Romaya at the LON at the Wellcome Department of Imaging Neuroscience (available at http://www.vislab.ucl.ac.uk/Cogent/).

blue fixation point. To reduce the effect of alpha rhythm as a result of drowsiness, an ambience light was turned at normal room illumination.

6.3.3 Electrodes and placement

According to the modelling study (Ch. 5), semi-adjacent placement of current injection electrode above the visual cortex would produce the maximal change in the external magnetic field during VER. Therefore, a pair of electrodes was placed 5 cm to the right and left of the estimated position of the visual cortex, taken as 5 cm above the inion of the occipital bone (Figure 6-1, left). The electrodes were the 21 mm diameter recessed design (Ch. 2) for reducing skin current density at high current levels. The electrode position in the magnetic sensor space was different in each active recording due to the different position of the head and the differences in head geometry between subjects (Figure 6-2).

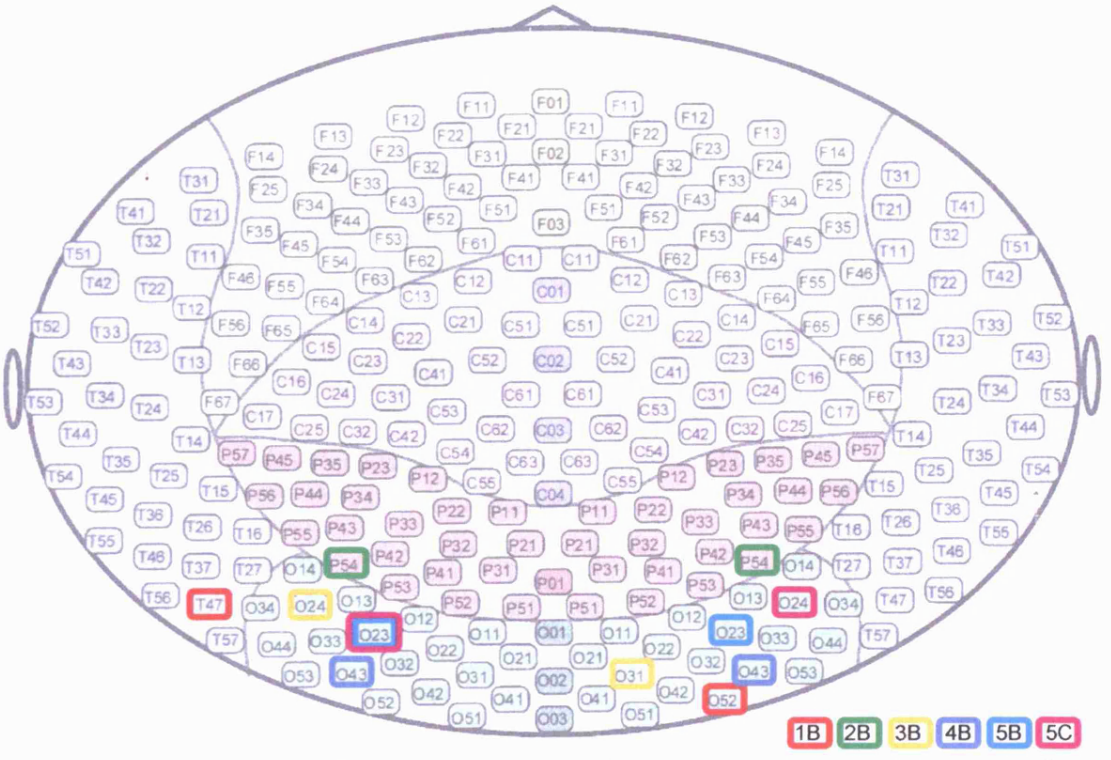

Figure 6-2: magnetic sensors nearest to the current injection electrodes in 6 active recordings.

6.3.4 Equipment

6.3.4.1 Data acquisition

The data acquisition of the MEG system (CTF MEG 275, VSM MedTech Ltd., Coquitlam, BC Canada) was made of a parallel DC coupled sampling of the 275 channels which was set to a rate of 1200 samples/sec. The dynamic range was 32 bit obtained by combining 20 bits per magnetic flux quantum and 12 bits reset counter. This dynamic range covers a total magnetic

field range of 1360 nT with a resulting quantization resolution of $1360nT/2^{32}$ = 0.317 fT. The specified noise level of this system was 10 fT rms/√Hz. The static magnetic field produced by the EIT current reached an order of 10 nT for the magnetic sensors close the electrodes and leads. The modelling (Ch. 5) predicted neuronal activity related changes of about 30 fT, which are 6 orders of magnitude smaller than the maximal static field. The dynamic range and quantization resolution were therefore sufficient to record these changes. Further technical details about the sensors geometry were given in the modelling study (Ch. 5). The signal from a finger pulse oxymeter was recorded on an auxiliary channel for possible removal of artefact caused by the heart electrical signals. A technical limitation prevented recording the ECG signal. A digital signal producing the triggers for the square wave and visual stimuli was recorded on another auxiliary channel.

6.3.4.2 Current source

A 1 Hz bi-polar square wave current of level 700 to 1000 μA was applied to the head, which was 100 μA less than the slightly unpleasant level reported by the subject during the preparation procedure. A TTL trigger signal was obtained from Trig PC and controlled an isolated custom made constant current source (Section 4.3.4.2) which produced a current of I_1 = 100 μA. An arbitrary waveform constant current source DS-5 unit (Digitimer, Welwyn Garden City, UK) was used to amplify I_1 and produce I_2 = 100-1200 μA according to the value of a variable resistor R_1 = 1-12 kΩ connected between the output and input of the custom made and DS-5 units. The current I_2 at the DS-5 output was then applied to the head (Figure 6-3).

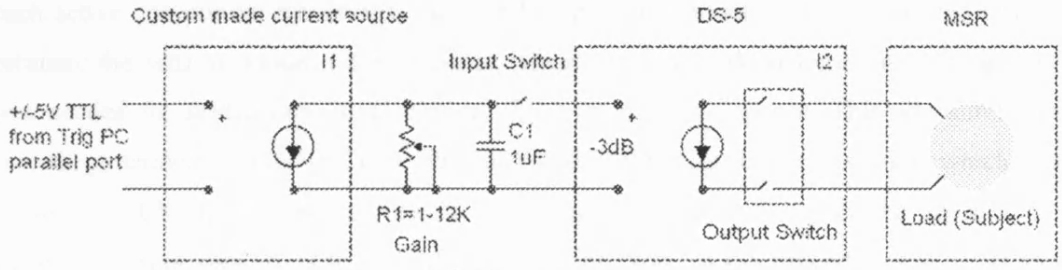

Figure 6-3: the current source setup.

A capacitor C_1 = 1 μF was connected on the input of the DS-5 unit to limit the bandwidth of the square wave and hence reduced the slew rate over the rise time and fall time. In the absence of such a capacitor, the rise time or fall time was about 1 μs which produced a slew rate which was one order of magnitude above the permitted slew rate of the MEG machine, which caused reset problems in the magnetic field feedback loop and producing erroneous results[3].

---

[3] According to the MEG specification, the maximal slew rate is $100{,}000\Phi_0$/sec @ 60 Hz, where Φ_0 = 0.3571 nT is the magnetic field equivalent of the magnetic flux quantum for this specific machine. This translates into a maximal slew rate of 35.71 nT/ms. When the resistor R_1 was set to 1 kΩ, the current was

The output of the DS-5 unit was calibrated for a baseline offset of <1% prior to each experiment to minimize the pure DC component to be below 10 μA as required by safety regulations (BS5724, 1979; IEC60601-1{ed3.0}, 2005). The two output leads were twisted and passed into the MSR and connected to the electrodes. The leads were also coated with a shield which was grounded via the DS-5 unit.

6.3.4.3 Triggering

Trig PC generated the triggers for the visual stimuli, and a delayed trigger of 350 ms for the two 500 ms phases of the 1 Hz square wave current (Figure 4-4). This resulted in a 150 ms delay between the beginning of each 500 ms square wave polarity phase and the visual stimuli triggers. This was designed to position the P100 peak of the VEP or the M100 peak of the VEF at the centre of each current polarity phase (150 + 100 = 250 ms).

6.3.5 Protocol

A total of 3 control and 6 active MD-EIT recordings were made (Table 6-1). A *control* MD-EIT recording consisted of N_A 1 minute recordings of visual stimuli but no EIT current. An *active* MD-EIT recording consisted of N_B 1 minute recordings with visual stimuli and EIT current. The visual stimuli were off for 30 sec and then on for 30 sec of each control or active 1 minute recording. This way, each control one minute recording consisted of 30 sec of only background brain activity and 30 sec of additional VEF and each active one minute recording consisted of 30 sec of EIT current without VEF and 30 sec of EIT current with VEF. The first 30 seconds of each active one minute recordings, made of EIT current without VEF were needed in order to estimate the settling square wave response without the superadded impedance change, as this was needed for subtraction in calculation of the impedance response. This was similar to the recordings termed 'control' in Ch. 4. The control MD-EIT recording in this study, which was not obtained in Ch. 4, was used to imitate the active MD-EIT recording in the absence of EIT current and was used to 1) to quantify the baseline noise in the procedure for extracting the impedance changes and 2) to validate that the normal VEF waveform obtained during the control MD-EIT recording was not distorted by the presence of the current during the active MD-EIT recording although I have previously shown that 1 mA could be safely applied on the head without altering the underlying brain function (Ch. 2).

---

100 μA and the maximal magnetic field over the 275 sensors was 0.5 nT. For a capacitor C_1 = 1 μF the time constant is $\tau = R_1C_1$ = 1 ms and the resulting slew rate was 0.5 nT/ms which is 2 orders of magnitude below the maximal allowed slew rate. For different current levels controlled by the value of R_1, both the maximal magnetic field and the time constant increased linearly so the slew rate remained constant.

For most of the recordings, N_A and N_B were 10 and the total number of stimuli in the active 1 minute recordings available for averaging was thus 2 reversals/sec x 30 sec x 10 one minute recordings = 600 stimuli.

The entire experiment lasted an average of 3 hours for each subject. The first hour was devoted to placing the electrodes on the head and attaching the electrodes (contact impedance <1 kΩ measured at 11.7 Hz). The subject was trained to relax and hence avoid muscular activity of the face, neck and chin during the recordings. The recording time lasted 1 to 2 hours depending on the number of 1 minute recordings, technical problems and resting breaks of variable duration required to keep the subject alert.

The head position in the scanner was measured before and after each 1 minute recording using the built in localization procedure of the MEG scanner applying current through three localization coils attached to the head at three fiduciary points. This localization lasted approximately 30 sec and was used to quantify the head movements during and between 1 minute recordings which were minimized to about 1 mm using sponges to fix the head position in the helmet. The subject was instructed to stay still during the 2 minutes of the localization, 1 minute recording and second localization. The positions of the localization coils and electrodes on the head.were measured with a 3-D Polhemus digitization system (3SPACE ISOTRAK II, Polhemus Inc., Colchester, VT, USA) with a specified accuracy of 2.5 mm. The absolute position of the head in the MEG helmet was not controlled over the 9 MD-EIT recordings and thus varied by about 1-2 cm.

6.3.6 Data analysis

The data analysis was similar to the electrical case (Section 4.3.6) and is briefly described below with details on minor differences.

1. *Filtering and segmentation.* 50 Hz notch filter was applied to remove mains noise and the 1 minute recordings were segmented into 1 second periods.
2. *Selection of segments with optimum SNR:* in each 1 minute recording, outliers and segments with low amplitude VEF were discarded using the same method as in Section 4.3.6.3. Low amplitude VEF was identified using the channel with the highest M100 peak and the exclusions were translated to the other 274 channels.
3. *Further VEF exclusion for 1 minute recordings with poor responses.* This was done as in Section 4.3.6.4. 1 or 2 one minute recordings were excluded in 4/9 MD-EIT recordings (Table 6-1).
4. *Estimation of VEP and resistivity change components:* the same linear model was applied to estimate the VEF and magnetic field changes δ using Maximal Likelihood minimization (Section 4.3.6.5). This was applied separately for each channel and each MD-EIT recording

after applying a low pass filter with cut off frequency of 40 Hz on individual segments to improve the SNR.

5. *Segmenting the 275 channels into subgroups:* different regions of the head were analyzed separately by segmenting the data from the 275 sensors into 10 sub groups according to the channel definitions of the MEG system: left and right occipital (19·2 on left and right +3 on midline = 41 channels), parietal (22·2+1=45), frontal (33·2+3=69), central (24·2+4=52) and temporal (34·2=68). This step replaced the calculation of linearly independent differential channels applied for LF-EIT (Section 4.3.6.6).
6. *Statistical analysis for identifying significant changes:* this was similar to the analysis in Section 4.3.6.7. However, the changes in magnetic field are not rectified as the changes in boundary voltages (Ch. 5). Therefore, significant changes were identified as 'mean is different from zero' and not as 'mean is negative' as used for the electric case. In the electric case, the channel with the uppermost boundary voltage was selected as a representative channel with expected high boundary voltage changes. In the magnetic case this was not possible sue to the uncontrolled large static field of the current electrodes and leads. Therefore, in each subgroup of sensors, the channel of uppermost absolute change within the expected time window of 50 to 250 ms was selected.
7. *Spatial distribution of the VEF and δ waveforms.* The active MD-EIT recording (5C) with the highest changes was graphically displayed at several time points to illustrate the spatial distribution of the changes over the 275 sensors.
8. *Changes grouped from all MD-EIT recordings:* data was grouped separately for the 3 control MD-EIT recordings and for 4/6 active MD-EIT recordings after excluding 2 active recordings (1B and 2B) with head position in the MEG helmet different by more than 2 cm from the remaining 4 recordings. This criterion was applied since the average distance between magnetic sensors is about 2 cm and the data from the 4 grouped recordings could be regarded as originating from the same sensor. The estimation of the VEF and δ components and the statistical analysis were then repeated.

All the results are given in physical units of fT. Translating into percentage units was not possible due to the uncontrolled strong static magnetic field originated from the current flowing through the leads and the electrodes which was about 6 orders of magnitude larger than the measured magnetic field changes.

6.4 Results

6.4.1 Individual recordings

The VEF from both active and control recordings included three main components similar to the N74-P100-N145 sequence of the VEP and additional later components (Figure 6-4). The magnitude and delay of these components agreed with a study of similar stimulating parameters (Hashimoto, 1999).

Significant magnetic field changes in the δ waveform lasting more than 25 ms at the most expected delay between 50 and 250 ms, were observed in 2/30 sensor groups in the 3 control MD-EIT recordings (3 recordings times 10 sensor groups = 30) and 16/60 sensor groups in the 6 active recordings (6 recordings times 10 sensor groups = 60). These were mostly in the occipital and parietal regions (Table 6-2 and presentation of right occipital channels in Figure 6-4). Changes were also observed in earlier or later delays but were lasting less than 25 ms in most cases and were not included in Table 6-2. In one of the two cases of significant changes in the control recording (4A), an α rhythm of 9 Hz probably related to drowsiness was observed in the left occipital sensor region which produced artefactual significant changes (Figure 6-4)

The SNR of the maximal significant changes in the 16/60 active sensor groups was 3.2±0.7 (mean±SD, range 2.3-5). The amplitude of these changes was 60±30 fT (range 30-130 fT) and the noise level (SE) was 20±9 fT (range 10-39 fT). The largest change of 130±34 fT (mean±SE, SNR=3.7, p=0.003) was observed in the left occipital sensor region of recording 5C.

The average noise level (SE) in each control recording after averaging for 9 minutes was 9.8±2.8 fT (mean±SD) while for the active recordings after averaging for 8-20 minutes it was 16±8 fT. This was due to mean background noise in the raw data of 160 and 310 fT in control and active recordings respectively, suggesting that the current source introduced additional noise to the endogenous physiological noise from the brain.

Table 6-2: sensor regions with significant changes between 50 and 200ms lasting more than 25ms[a].

Subject	Recording A	Recording B	Recording C
1		O_R P_L F_R	
2		F_L C_L T_L	
3	-	O_{LR} P_L T_{LR}	
4	O_L(α rhythm)	O_L	
5	P_L	P_L	O_{LR} P_R

[a] O, P, F, C, T - Occipital, Parietal; Frontal, Central and Temporal. Subscript L - left, R - right.

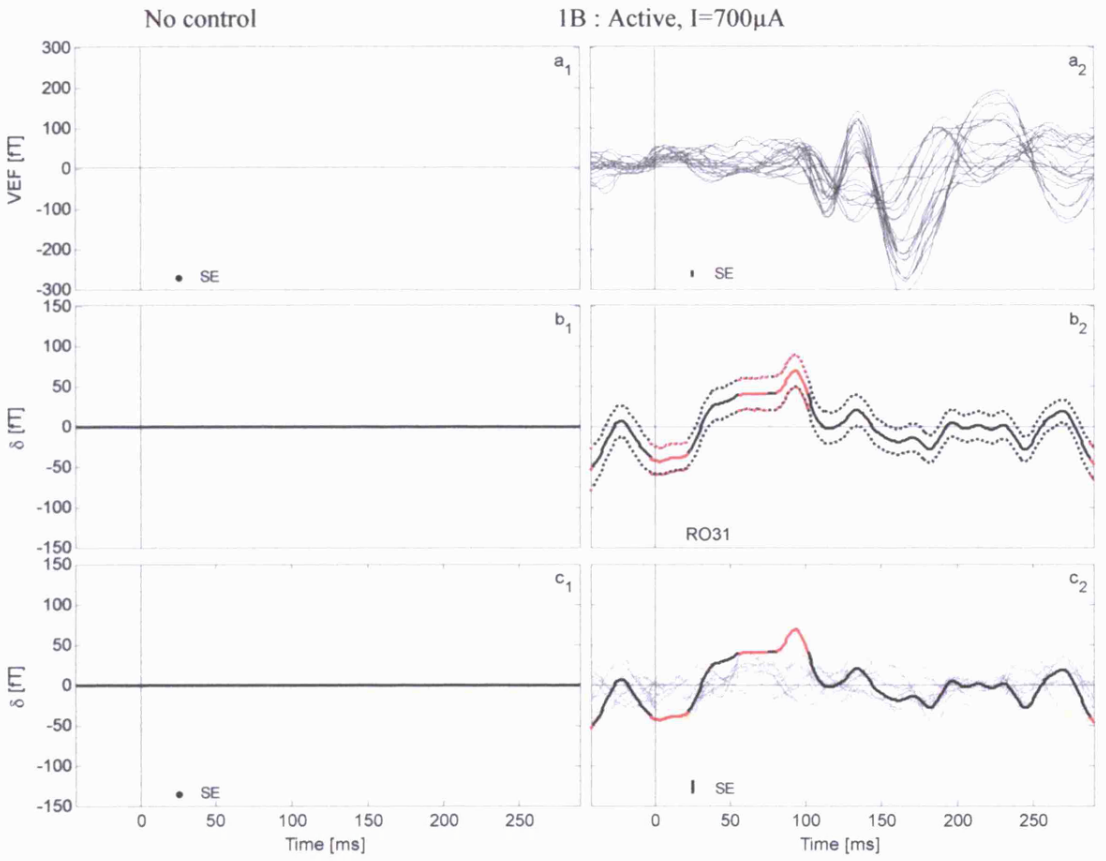

Figure 6-4: results from 19 right occipital channels from all MD-EIT recordings: left – control recordings without current 3A, 4A and 5A (a_1-d_1, see following pages) and right – active recordings with current 1B, 2B, 3B, 4B, 5B and 5C (a_2-d_2). a) VEF for all channels (median SE is marked at the bottom-left corner). A vertical line marks the visual stimulation at 0 ms. b) Average (solid) ±SE (dotted) magnetic field changes in the channel with uppermost and significant change between 50 and 250 ms. Significant changes are marked in red ($p < 0.05$). The channel name marked according to the map in Figure 6-2 c) Same as (b) for all channels but without SE (for brevity, median SE is marked at the bottom-left corner).Significant changes are marked in orange and the channel in black and red is the same as in (b).

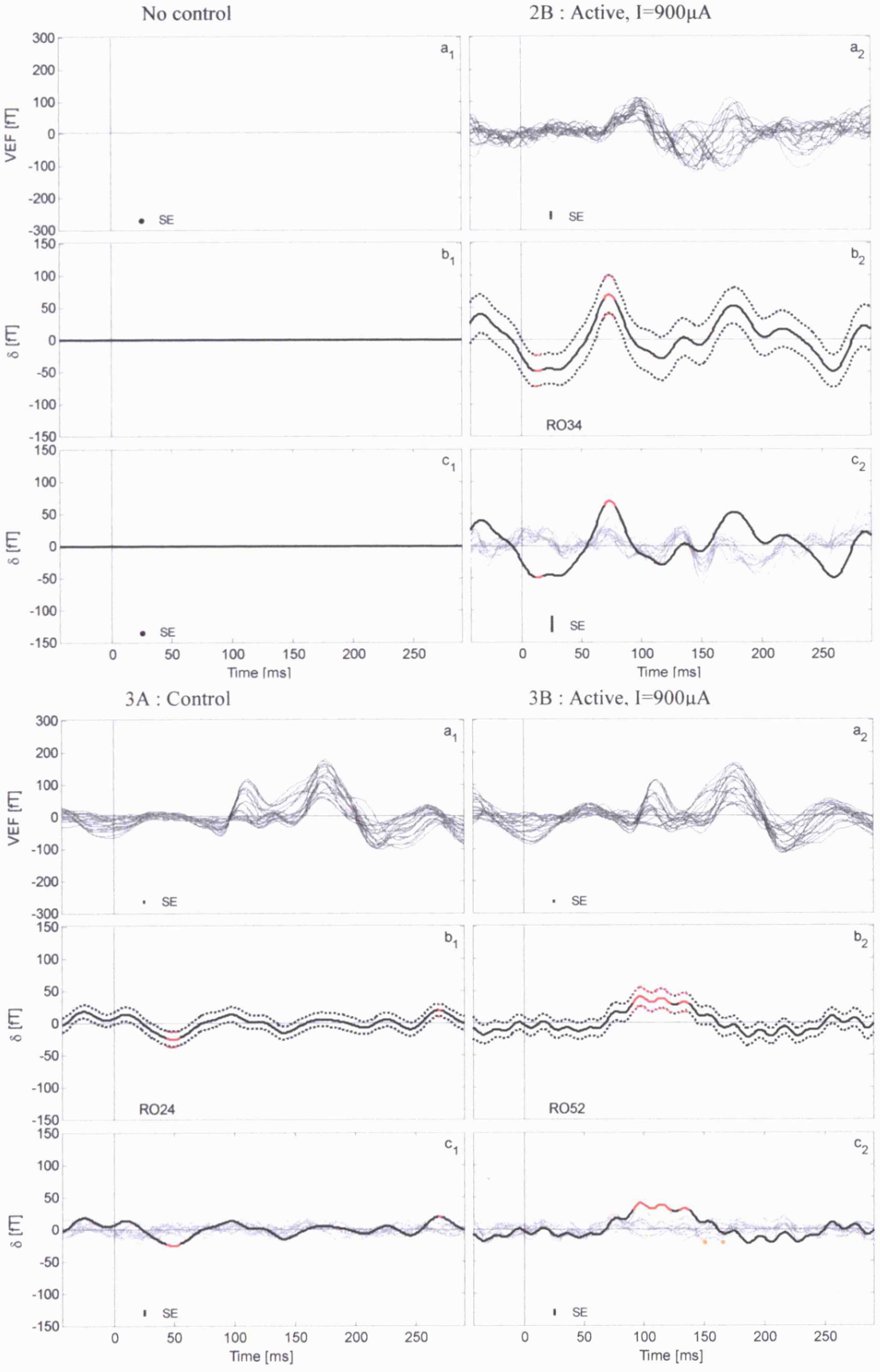

Figure 6-4: continued.

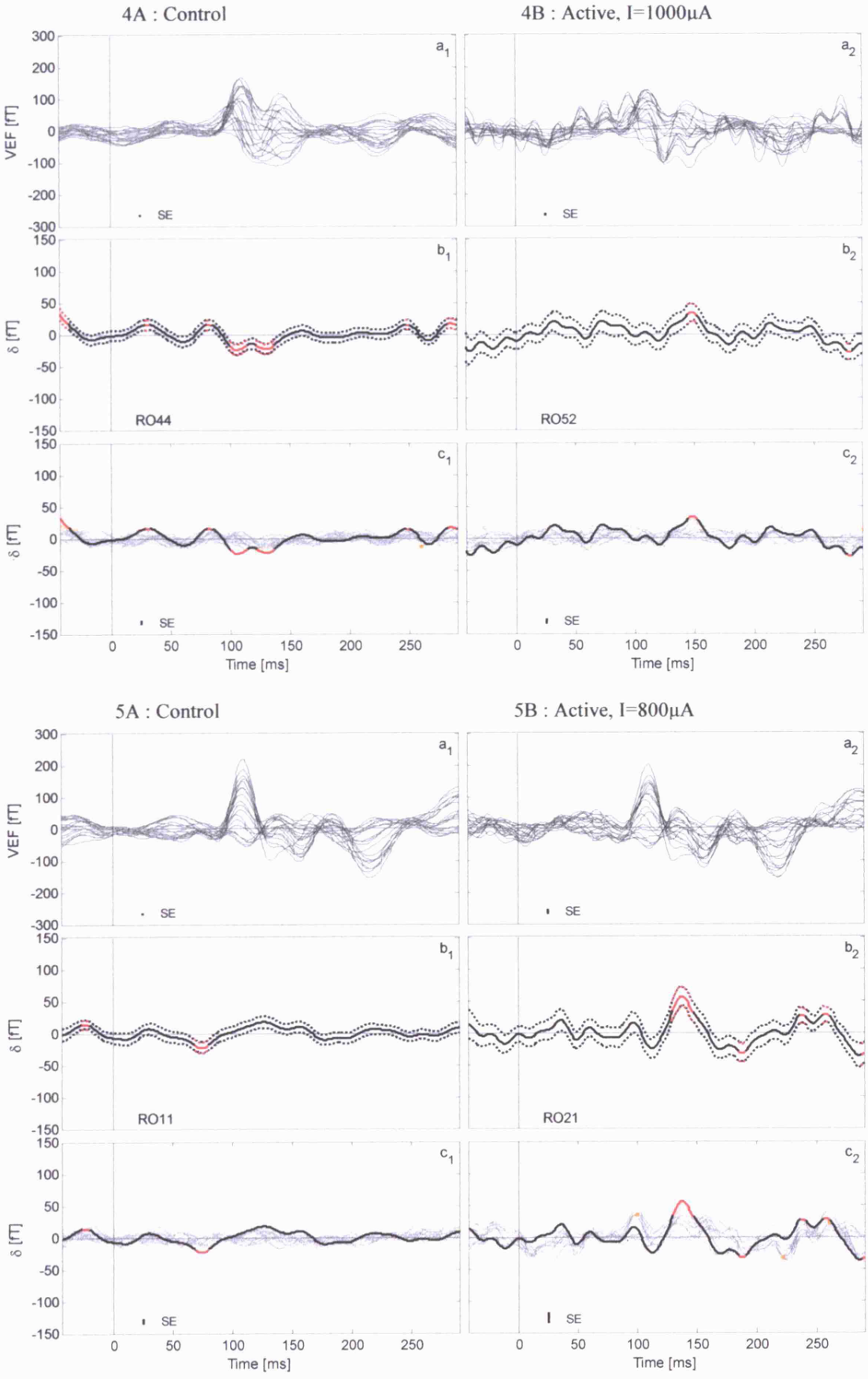

Figure 6-4: continued.

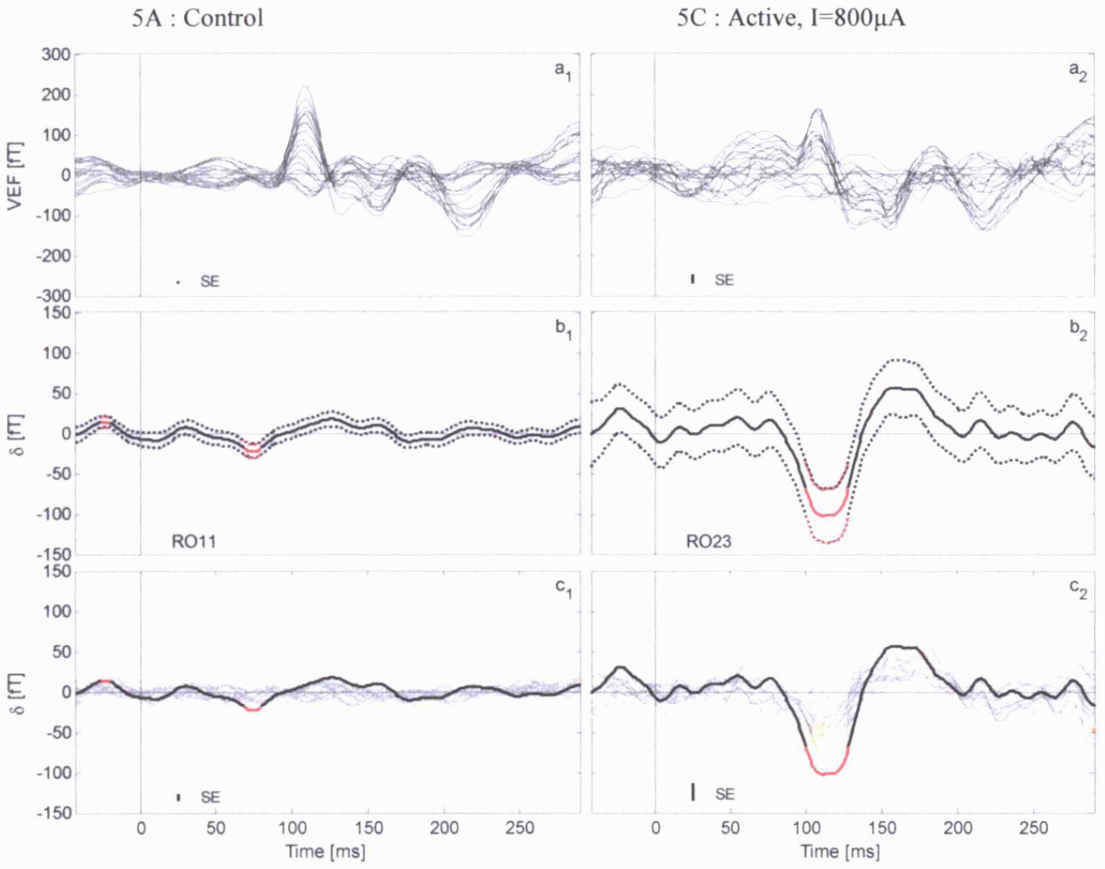

Figure 6-4: continued.

Since the highest magnetic field changes were observed in recording 5C, this recording was used to visualize the spatial distribution of the VEF and magnetic field changes signals. The VEF had the main components at 70, 110, 140 and 220 ms (Figure 6-5, lower left panels) showing magnetic field distribution typical to a rotating di-pole (Figure 6-5, upper left panels). No source fitting has been applied in this study; only the magnetic field distribution over the MEG sensors has been presented. The magnetic field changes δ due to possible resistance change in the visual cortex had negative components at 70 and 110 ms located mainly in the left and right occipital sensor regions respectively. These were followed by more shallow positive components at 140 and 175 ms located over the entire occipital sensors. The latter component at 175 ms does not exist in the VEF and at the time of the last VEF component at 220 ms there was no visible δ component (Figure 6-5, right panels).

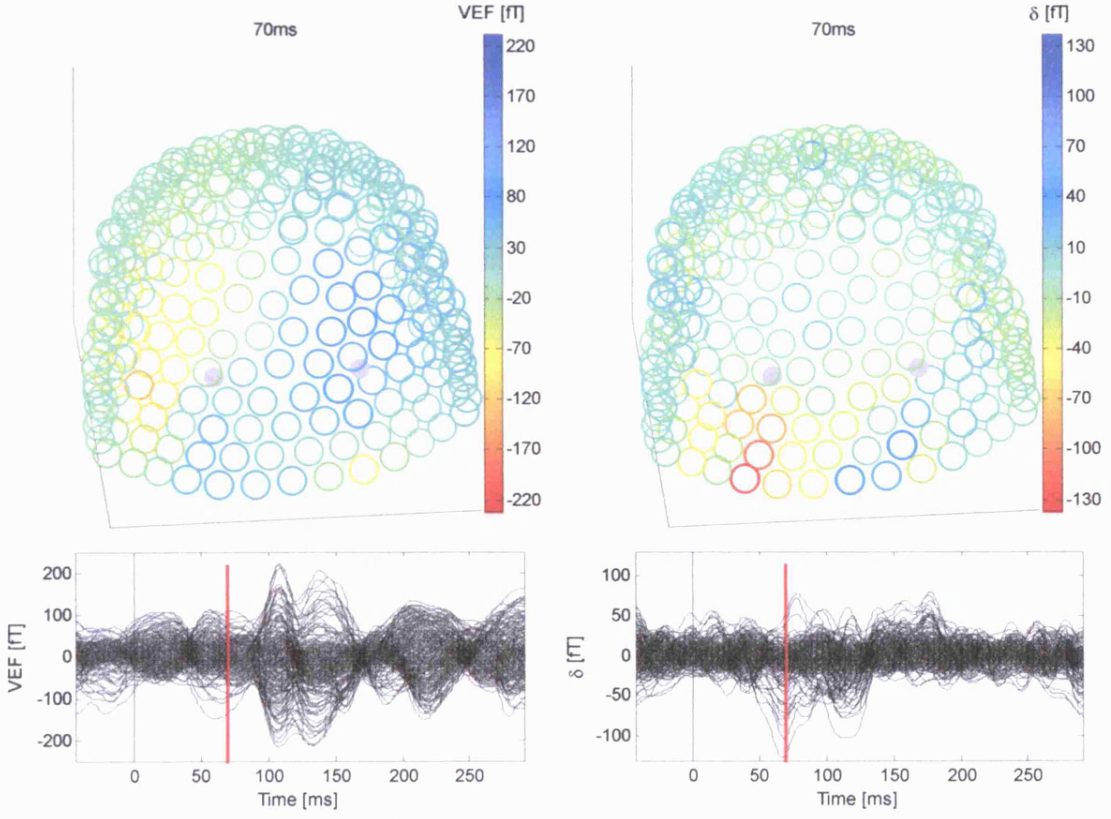

Figure 6-5: upper panel - spatial distribution of the VEF (left) and δ (right) waveforms for active MD-EIT recording 5C at 70 ms after the stimulus. View is from the back of the sensor array where the two current injection electrodes (grey circles) were attached to the head. Lower panels: waveforms for all 275 MEG sensors with a red line at the time of spatial presentation. The following pages present the distribution for 110, 140, 175 and 220 ms after the stimulus.

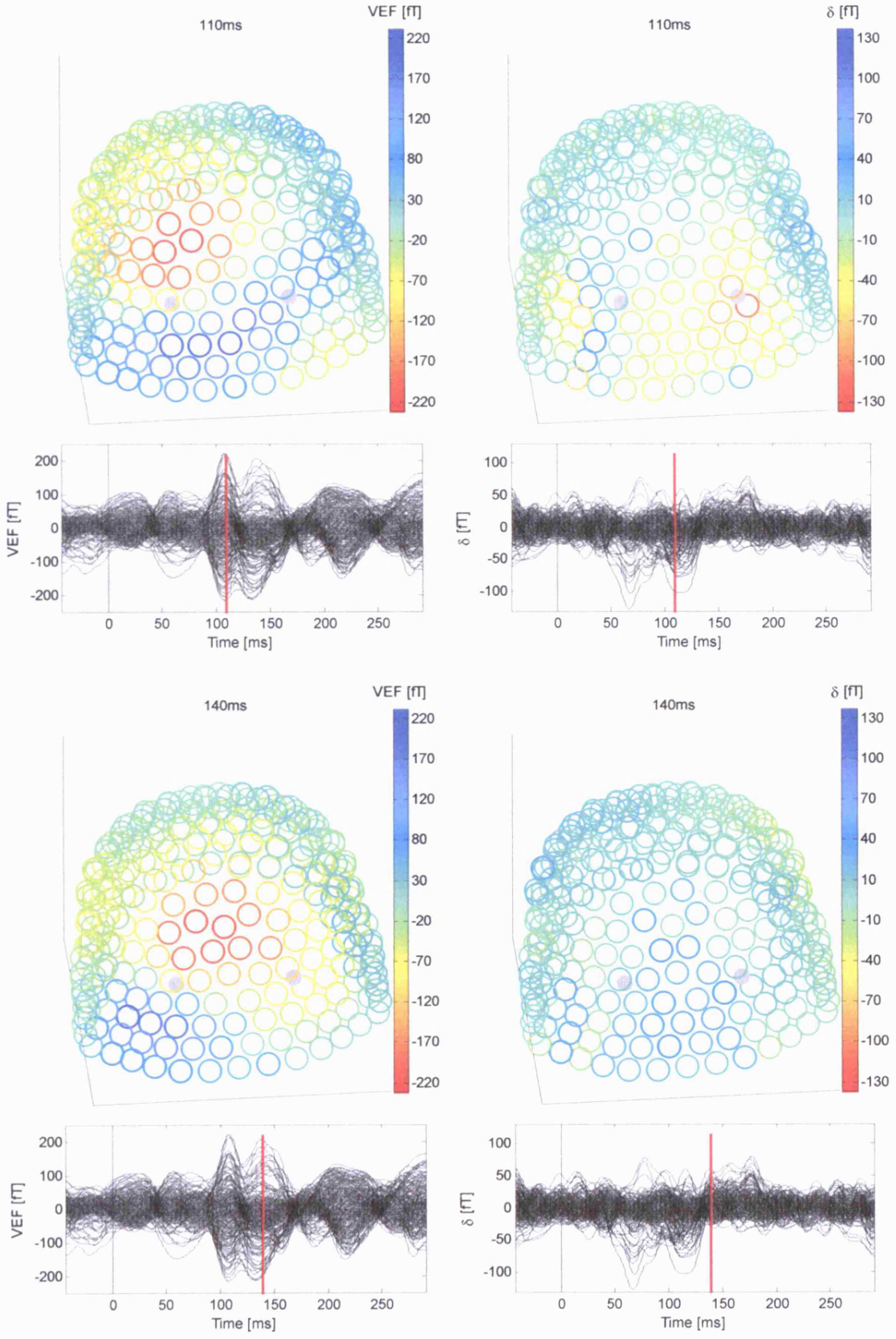

Figure 6-5: continued.

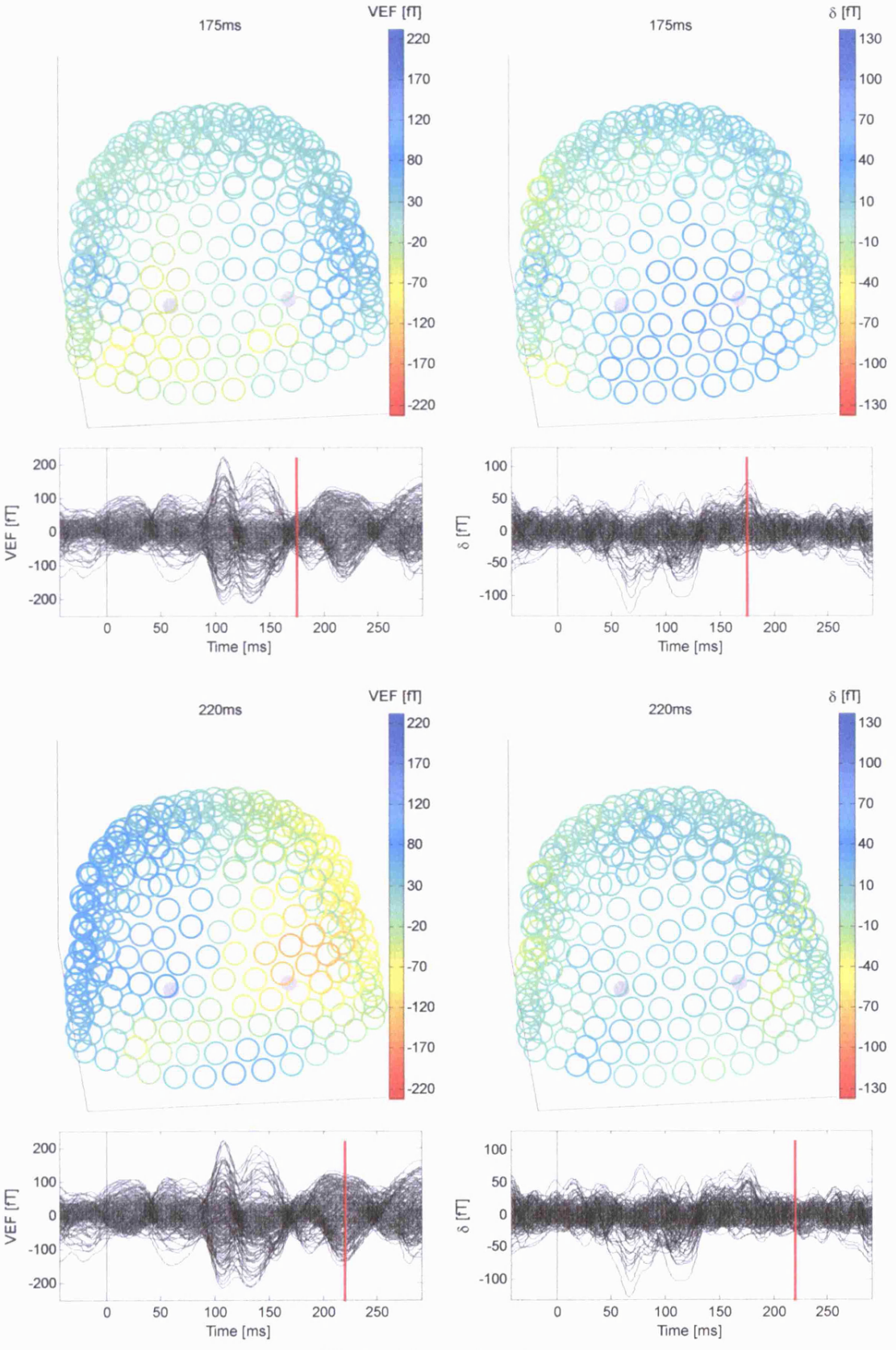

Figure 6-5: continued

6.4.2 Changes grouped from all MD-EIT recordings

Group average was applied with 3 control and 4 active MD-EIT recordings after excluding 2 active recordings with head position shifted by more than 2 cm from the remaining 4. Averaging over a dataset with head positions not perfectly aligned in the MEG helmet over recordings has reduced the amplitude of the VEF from about 200 fT in individual recordings (Figure 6-4) to about 100 fT in the group average (Figure 6-6). Since the magnetic field changes due to impedance changes are bi-polar, they were also attenuated over averaging instead of being integrated. Significant changes lasting more than 25 ms were observed only in the right occipital sensor group of the active recordings (Figure 6-6). The maximal change in this sensor group was 27 ± 9 fT (mean ± SE; p = 0.002; $N_{1,2}$ = 1870) with SNR of 3. The average current injected for the active group average was 875 μA.

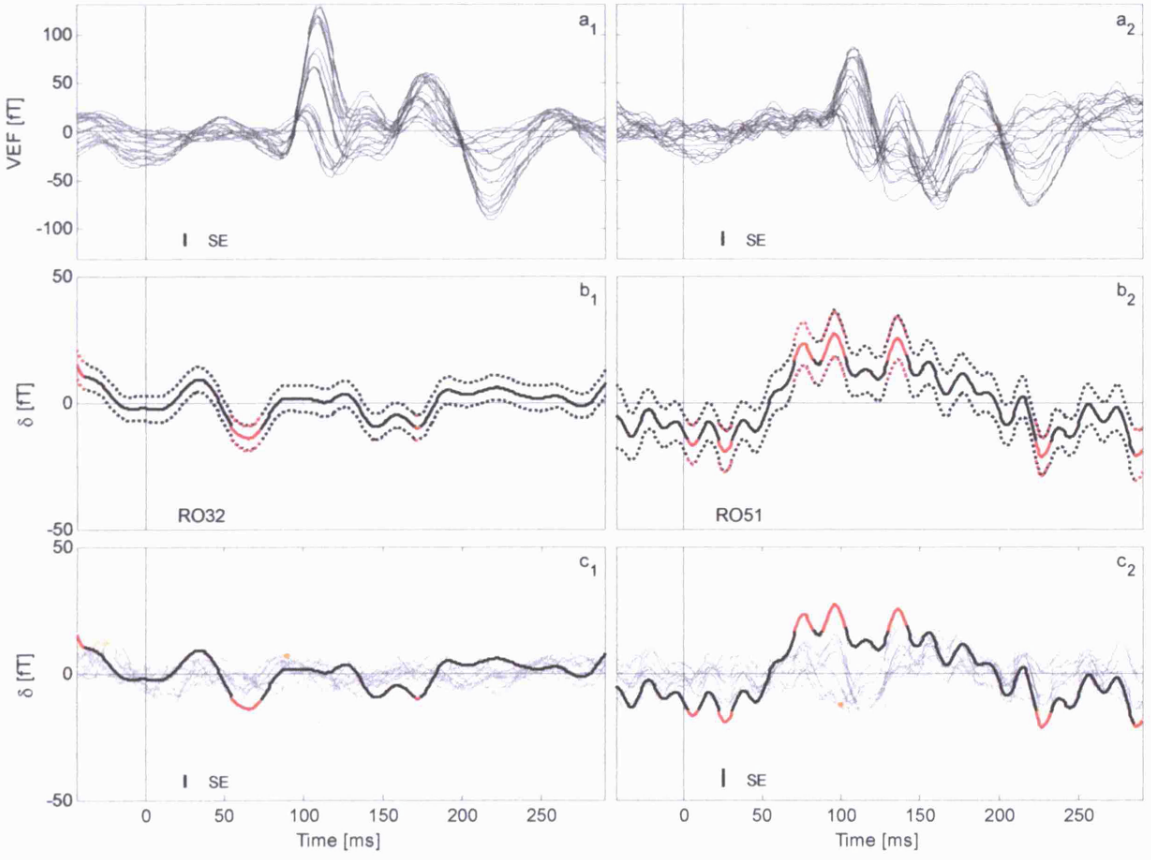

Figure 6-6: same as Figure 6-4 but for the group average of 3 control (left) and 4 active (right) MD-EIT recordings (right occipital channels). a) VEF for all channels. b) Average (solid) ±SE (dotted) magnetic field changes in the channel with uppermost and significant change between 50 and 200 ms. Significant decreases are marked in red (p < 0.05). c) Same as (b) for all channels but without SE (for brevity, median SE is marked at the bottom-left corner).Significant changes are marked in orange and the channel in black and red is the same as in (b).

6.5 Discussion

6.5.1 Summary of results

Significant magnetic field changes lasting more than 25 ms at the most expected delay between 50 and 250 ms were observed in 2/30 and 16/60 sensor groups in the 3 control and 6 active MD-EIT recordings respectively, mostly in the occipital and parietal regions (Table 6-2, Figure 6-4). For the maximal significant changes in the active recordings, the amplitude, noise (SE) and SNR were 60±30 fT, 20±9 fT and 3.2±0.7 (mean±SD) respectively. The largest change was 130±34 fT (mean±SE, SNR=3.7, p=0.003, $N_{1,2}$ = 340) in the left occipital sensor region of recording 5C. The mean background noise in the raw data was 160 and 310 fT in control and active recordings respectively, suggesting that the current source introduced additional noise to the endogenous physiological noise from the brain.

Visualization of the spatial distribution of the magnetic field changes in recording 5C revealed main negative components at 70 and 110 ms located in the left and right occipital sensor regions which coincide in time but not in space with the VEF components (Figure 6-5).

Group average was applied with 3 control and 4 active MD-EIT recordings but has attenuated the VEF signal and did not improve the SNR of the magnetic field changes. This is probably due to the variability between recordings with magnetic sensors which were not perfectly aligned and the resulting summation of bi-polar VEF or δ components from different recordings. Significant changes lasting more than 25 ms were observed only in the right occipital sensor group of the active recordings (Figure 6-6). The maximal change in this sensor group was 27 ± 9 fT (mean ± SE; p = 0.002; $N_{1,2}$ = 1870) with SNR of 3 and average current of 875 μA.

6.5.2 Technical issues

Bandwidth limiting: in this study, low pass filter of 40 Hz was applied to reduce the noise with the hope to increase the SNR. In the event, which limits the effective time resolution to about 25 ms. This could be reduced in future studies by increasing the bandwidth if improvements to the method would provide higher SNR.

Square wave non-idealities: ringing artefact due to switching of the current polarity limited the usable time to 300 ms out of each 500 ms half cycle. In addition, in each 1 minute recording, 30 seconds were recorded without visual stimuli for calibrating the distorted baseline which halved the total number of segments available for averaging. Further more, the current source doubled the magnitude of the background noise in the raw data comparing to the background noise originated from brain activity. Since the current source was located outside the MSR, this

was probably due to magnetic interference passing through the current electrode leads. This could be overcome by designing a battery driven and magnetically compatible current source to be placed within the MSR. Improving these hardware issues in future designs could potentially decrease the acquisition time by a factor of 2·2·4=16 for achieving similar SNR.

Limited group averaging: the group averaging in this study did not improve the SNR as it did in the LF-EIT study (Ch. 4). This was ascribed to 1) the additional noise introduced by the current source, 2) the 5 fold less segments used for the average as compared to the LF-EIT study and 3) the magnetic field changes are bi-polar and are not rectified as those for the electric case, resulting in attenuation during averaging when different head positions in the MEG helmet and different head and brain geometries are used. This was partly controlled in this analysis by excluding 2/6 active recordings with significantly different head position.

6.5.3 Comparison between modelling and measurements

Estimated changes: according to the modelling in Ch. 5, the magnitude of the maximal magnetic field changes due to 1% conductivity increase of 9 cm^3 volume of visual cortex was 27 ± 13 fT when using 1mA of EIT current. When assuming a physiological noise level of about 200 fT due to background brain activity in the occipital area when eyes are open (Cohen, 1968; Hamalainen, 1993) and averaging 1000 stimuli for 10 minutes, this noise reduces to 200 fT / $\sqrt{1000}$ = 6.3 fT. This predicts an SNR of 4.3 for the maximal values. The higher changes are estimated to occur over the back of the head when current is injected with semi-adjacent electrodes over the visual cortex.

Measured changes: in this study, the maximal measured change in individual MD-EIT recordings were 60±30 (range 30-130) fT and 27 ± 9 fT after the group average for average current of 875 μA. These results are in agreement with the modelling estimation. The physiological noise level measured in the control recordings was 160 fT similar to the literature (Cohen, 1968; Hamalainen, 1993). However, the current source introduced additional noise which doubled this value (310 fT measured in the active recordings). This could explain the slightly lower measured SNR of 3.2±0.7 as compared to that predicted (4.3). Furthermore, most of the significant changes were observed in proximity to the current injection electrodes, mainly over the occipital and parietal sensor regions as expected from the modelling.

6.5.4 Could these changes be due to an artefact?

Although the measured changes agreed with the modelling, the main possible source of artefact is still the potential alteration of the VEF waveform by the applied current as suggested in Ch. 4 (Section 4.5.5), which could translate into an artefactual impedance change during the

subtraction of the 1 Hz square wave polarities. The limited SNR did not allow any validation study for excluding such a possibility. However, for a higher SNR which might be available in future studies, several such methods have been suggested in the experimental LF-EIT chapter (Section 4.5.5) and could be applied for the MD-EIT case as well.

Furthermore, it was unclear why the largest changes appeared in recording 5C were not evident in recoding 5B taken from the same subject 10 minutes earlier (Figure 6-4). This lack of consistency requires further investigation in future studies.

6.5.5 Implications for designing future imaging systems

This study provided the first evidence for the feasibility of non-invasive measurement of fast resistivity changes related to neuronal activity in the human brain using MD-EIT.

With the existing method, the SNR when using single current injection pair and current of about 900 μA was 3.2±0.7 after averaging over about 10 minutes. The minimal SNR requirement for reliable image reconstruction was estimated to be 4 (Section 5.2.1). Hence, for slightly increasing the SNR, the recording time needs to be extended to $10 \cdot (4 / 3.2)^2 = 16$ minutes.

In addition, for image reconstruction, data is needed from multiple current injection pairs. For obtaining previous EIT images of haemodynamic changes in the brain, an electrode protocol consisting of 21 current pairs, each with 12 voltage measurement pairs was used (Tidswell, 2001; Tidswell, 2006). Due to reciprocity, similar results could be obtained with 12 current pairs, each with 21 voltage measurements. Since multiple voltage measurements could be done in parallel, the limiting factor is the number of current pairs. Assuming that the same number of sequential current pairs would be needed for MD-EIT, still with parallel acquisition with MEG, the overall recording time would be $12 \cdot 16 = 192$ minutes or about 3 hours which is impractical for human subjects to tolerate.

However, several improvements to the current source as suggested above (Section 6.5.2) could potentially reduce the recording time by a factor of 16 while achieving the same SNR. Another possible improvement is to record the impedance changes above the EEG (or MEG) band which could enhance the SNR by a factor of 5 (Section 1.4.6). This could potentially allow decreasing the recording time further by a factor of 25. Furthermore, recording at higher frequency would discard some of the problems related to the square wave and may provide a total reduction in recording time of up to 400 fold down to about 1 minutes if all are successfully implemented. These improvements could allow a tolerable recording time in the order of several minutes and are left to be evaluated in future work. The use of 275 sensors in MD-EIT as compared to 21 voltage measurement in EIT could allow using less than 12 current

pairs for achieving similar image quality. However, this quantification of this was left for future modelling study.

I therefore conclude that non-invasive imaging with MD-EIT method is not feasible with present technology. Future efforts should be focused on achieving a substantial improvement in SNR while decreasing the total recording time.

6.5.6 Future work

The following future work is suggested in descending importance:

1. Addressing the technical improvements to the current source and instrumentation as suggested above for reducing the noise and total recording time.
2. Measurements above the EEG (MEG) band for possible improved SNR. Measurement of changes in the complex admittivity rather than the real resistivity presented in this study could significantly reduce the main source of physiological noise. However, the magnitude of the changes above 100 Hz is expected to be lower (Section 1.4.6).
3. Applying other types of EPs from areas in the brain where background brain activity is lower such as the somatosensory and auditory evoked responses. However, the magnitude of these EPs is lower comparing to VEP and the overall SNR might be similar.

7. Discussion and future work

7.1 Answers to questions raised in the purpose and claims for novelty

1. *What is the highest current level, which could be used to maximize SNR in LF-EIT or MD-EIT experiments in terms of safety, skin sensation and minimizing the possibility altering the normal brain function with the applied current?*

In Ch. 2, a simulation and experimental study was undertaken to determine the maximal current which could be applied to the scalp without causing painful skin sensation or stimulation of underlying brain. A novel recessed electrode was designed, and the upper limit was established as 1 mA. FEM simulations indicated that the peak current density on underlying cortex was 0.3 A/m^2, which was below the threshold for stimulating cortical neurones, determined by a literature review.

In most clinical EIT studies, the applied current has been set at that permitted for auxiliary leakage current. The relevant British Standards (BS5724, 1979) require a current of less than 100 μA below 1 kHz. The findings here are that a greater current can be safely applied and tolerated but the position with respect to safety guidelines is unclear. Greater currents may certainly be applied for therapeutic purposes, but the position with respect to that specifically for diagnostic purpose appears not to be defined. I submit that the higher level could safely be used for EIT; perhaps this issue could be included in any future revisions of the safety standards.

To the author's knowledge, this is the first study addressing the limits related to current distribution in brain EIT using a 3D anatomically realistic model of the head which was also published in a peer review journal (Gilad, 2007b) . A later study by a research group at Manchester reproduced the modelling results with a larger mesh and slightly different conductivities and concluded that for a current of 1 mA applied on the scalp, the maximal current density n the brain was 0.5 A/m^2 (Davidson, 2007).

2. *What are the expected changes in scalp voltages and in magnetic field in the vicinity of the scalp during visual evoked responses and LF-EIT or MD-EIT?*

For LF-EIT (Ch. 3), numerical simulations using a 3D anatomically realistic model of the head predicted that resistivity changes of 1% in a 9 cm^3 primary visual cortex during evoked responses translate into average scalp voltage changes of 0.54 μV for 1 mA (0.0018%) while the maximal change could be double (1.03 μV). For MD-EIT (Ch. 5), the estimated mean external magnetic field changes were 4.7 fT for 1 mA (0.007%) and the maximum was 6 fold higher (27

fT). These studies included validation in tank and human boundary voltages for LF-EIT and in tank for MD-EIT.

Hitherto, these studies included the most detailed and realistic predictions for the application of imaging neuronal activity with EIT and were only preceded by recent studies performed in our group for LF-EIT (Ahadzi, 2004a; Gilad, 2005a; Gilad, 2005b) and MD-EIT (Ahadzi, 2004b; Gilad, 2006; Ahadzi, 2006).

3. *Where should the drive and measure electrodes as well as magnetic sensors be positioned to maximize sensitivity and SNR?*

For LF-EIT, the simulation study comparing a large set of possible electrodes placement (Ch. 3) predicted that the electrode combination which gave the largest peak changes was with current injection over the occipital region with an adjacent pair of electrodes (5 cm apart) and recording immediately lateral to these. Combinations which gave slightly lower changes were with injection over the occipital area from semi-adjacent electrodes (10 cm apart) and recording from a pair of electrode located near that injection pair (Table 3-4 and Figure 3-9). All these optimal combinations were intuitively justified as the close current injection pair was sensible for obtaining high current density in the occipital cortex just below the electrodes and the recording pair was located where high boundary voltage is expected near the two injection electrodes. The reciprocity principle allows each resulted optimal electrode placement to be interchangeably considered as reciprocal current injection and measurement pairs.

For MD-EIT, the simulation study (Ch. 5) predicted that the combinations which gave the largest peak changes were with current injection over the occipital region with an adjacent (5 cm apart) or semi-adjacent (10 cm apart) pair of electrodes and recording with magnetic sensors above the visual cortex (Figure 5-9).

These predictions were very useful for designing human experiments and to the author's knowledge were novel in the way that all realistic electrode and magnetic sensors combinations were evaluated, not incorporated in previous studies in our group for LF-EIT (Ahadzi, 2004a; Gilad, 2005a; Gilad, 2005b) and MD-EIT (Ahadzi, 2004b; Gilad, 2006; Ahadzi, 2006).

4. *Could the equivalent changes in surface potentials or magnetic field be measured with existing technologies and with what SNR?*

For LF-EIT (Ch. 4), measurements on healthy human subjects were made with a prototype system which was validated on a resistor network and crab peripheral nerve bundle. Significant changes were observed in 35% of scalp recordings. The magnitude of the changes after group average of all recordings was 0.25 ± 0.07 μV (0.0008 ± 0.0002 %) for an average current level

of 295 μA with SNR of 3.4. when normalized to current injection of 1 mA this became an anticipated change of 0.85 ± 0.07 μV (0.00080 ± 0.00006 %) with SNR of 12.1. The main source of noise was estimated to originate from background brain activity which was not synchronous to the visual stimuli and was recorded within the same band as the LF-EIT signal.

To the author's knowledge, these studies are the first successful attempt to measure the neuronal activity related impedance changes non-invasively with LF-EIT (Gilad, 2004; Gilad, 2005a; Gilad, 2005b; Gilad, 2007a). previous studies presented earlier (Section 1.4.5) suffered from major technical limitations (Holder, 1989; Murrieta-Lee, 2004; Murrieta-Lee, 2005; McCann, 2005; Enfield, 2005).

For MD-EIT (Ch. 6), the EIT apparatus was integrated into a MEG system and significant changes of 60 ± 30 (range 30-130) fT and SNR of 3.2±0.7 with an average current level of 875 μA were observed mostly from the occipital and parietal sensor regions in all subjects. Visualization of the spatial distribution of the magnetic field changes in the recording with the largest change, revealed main negative components at 70 and 110 ms located in the left and right occipital sensor regions which coincide in time but not in space with the VEF components. Group average did not improve the SNR due to uncontrolled alignment of the head position between recordings. The main source of noise was estimated to originate from background brain activity and instrumentation noise originated from the current source.

To the author's knowledge, this study, also presented in a conference (Gilad, 2006), is novel and was not preceded by any previous work.

5. Did the numerical and experimental estimations agree?

For both LF-EIT and MD-EIT, the size of the measured changes agreed with the numerical modelling when compared in physical units of μV or fT (Table 7-1). The normalized percentage values for LF-EIT were different due to the different way the normalization was implemented. For MD-EIT, they could not be derived experimentally since the strong static field from the electrodes and leads obscured the true static field. The main source for the variability in the modelling results was the deliberate range of conductivities chosen according to the uncertainty in the literature whereas for measurements, it was originated from the discrepancy between subjects and recordings as well as the background brain or instrumentation noise.

Table 7-1: summary of predicted and measured maximal changes for current of 1mA.

Ch.	Case	Changes [μV :fT]	Changes [%]	SNR[a] (n)
3	LF-EIT model	1.03 ± 0.75 μV	0.0039 ± 0.0034	-
4[c]	LF-EIT measure	0.85 ± 0.07 μV [b]	0.00080 ± 0.00006	12.1 [b] (n=16)
5	MD-EIT model	27 ± 13 fT	0.2 ± 0.5	-
6[d]	MD-EIT measure	60 ± 30 fT [a]	-	3.2±0.7 [a] (n=6)
		27 ± 9 fT [b]		3 [b] (n=4)

[a] Mean of individual recordings
[b] after group average across recordings
[c] for current of 1 mA, after normalizing from measurements with average current of 295 μA for which the original measurement was 0.25 ± 0.07 μV (0.0008 ± 0.0002 %) with SNR of 3.6
[d] For average current level of 875 μA.

6. What are the main limitations of the modelling and experimental measurements?

Modelling: an important factor limiting the accuracy of the model was the magnitude of the local impedance change during synchronized activity. This was taken in this study as 1% but could be in the range of 0.06-1.7% (Boone, 1995a; Liston, 2000; Liston, 2004a). However, for both LF-EIT and MD-EIT, the magnitude of the predicted changes agreed with the measured changes which were seemed to be genuine (Table 7-1), supporting the assumption that the local changes in the cortex are closer to 1%. Several additional factors affect the accuracy of the model but are only expected to result in an overall biasing factor of about 2-fold: 1) broader uncertainty in the conductivity values beyond that already taken into account in the model, 2) using a single standard head geometry not accounting for individual differences in anatomy, 3) inaccurate registration of experimental electrode positions on the standard mesh and 4) no allowance for tissue anisotropy.

LF-EIT measurements: the main limiting factor in technique is the low SNR resulting from the recording of impedance changes within the EEG band containing spontaneous brain activity. This could be overcome by recording just above this band (Section 1.4.6). During the study presented in this thesis (Ch. 4), several technical factor were gradually improved with the main factor of designing the recessed electrodes allowing the current level o be increased from 100 μA to 1 mA. Therefore, only 20% of the recordings were obtained with current of 1mA and the average level throughout the entire data set was 330 μA limiting the SNR which could be achieved with this method. Recordings at frequencies above 100 Hz with the maximal current level of 1 mA are left for future work. Additional technical limitations were the ringing artefact and settling time of the square wave due to the transient rise and fall times and the AC coupling at the acquisition system. Improving these issues could allow recording at faster stimulation rate of 4 Stimuli/sec and without a control calibration. This is also left for future work.

MD-EIT measurements: in addition to the limitations of the LF-EIT system, the current source located outside the MSR transmitted magnetic noise into the MSR through the current electrode leads which was double than the background physiological noise. This could be overcome in future designs by using a magnetically compatible battery driven current source located within the MSR.

7. Was the electric or magnetic method better and why?

Overall, the LF-EIT and MD-EIT methods had similar performance throughout the studies undertaken in this thesis. Impedance changes, which appeared to be genuine, were measured with a very low SNR and agreed with modelling (Table 7-1). Group averaging across subjects and recordings resulted in higher SNR for LF-EIT but not for MD-EIT, probably due to uncontrolled alignment of the head position within the MEG helmet between experiments and the bi-polar nature of the magnetic field changes as compared to the rectified nature in the electric case. An additional factor discussed previously was related to the additional noise introduced by the current source in the MEG which also reduced the performance of the MD-EIT method.

8. What are the implications of the present findings for designing non-invasive imaging system?

For LF-EIT (Ch. 3 and 4), these studies provided the first evidence for the feasibility of non-invasive measurement of fast resistivity changes related to neuronal activity in the human brain. However, calculations made in Section 4.5.6 have estimation that a total recording time of 7 hours would be needed for acquiring data from multiple current pairs with sufficient SNR for image reconstruction. This is impractical for human subjects to tolerate.

However, several improvements to the hardware and protocol were suggested which could potentially reduce the total recording time to several minutes and could make this methods practically tolerable to human subjects.

For MD-EIT (Ch. 5 and 6), similarly to LF-EIT, neuronal activity related impedance changes were measured for the first time but similar calculations (Section 6.5.5) have estimated the total recording time for imaging to be about 3 hours, similar order of magnitude as for LF-EIT. The same improvements were suggested for reducing the recording time to several minutes have been suggested and left for future evaluation.

9. What does the future hold for neural imaging with EIT and other modalities?

Since EIT was originally proposed for use in imaging neuronal activity (Holder, 1987), several modelling and animal studies have been conducted to estimate the magnitude of the changes and to develop the methodology of measuring it. Although few non-invasive human measurements has been attempted, this thesis presents, for the first time, statistically significant measurements with LF-EIT and MD-EIT, which were consistent with modelling and which appeared to be genuine. However, the SNR in these single current injection measurements was very low and was obtained with prolonged averaging which is not practical for implementing a system capable to reconstruct images of neuronal activity. I foresee two main directions for further development of LF-EIT or MD-EIT methods:

Invasive imaging: as the present technology did not provide sufficient SNR for non-invasive imaging, our group is now developing an invasive *in-vivo* alternative for use in animals and epilepsy patients with temporarily implanted intracranial electrodes. By placing electrode arrays directly on the cortical surface, we hope to achieve that goal as the absence of the skull and the possibility to control various technical and physiological factors could enhance SNR. If successful, this could become an additional tool for brain research as well as a clinical diagnostic tool for localizing epilepsy sources and investigating abnormal brain function. The theoretical advantages of the proposed EIT method are 1) that impedance changes are rectified and reflect the overall membrane depolarization comparing to EEG. These are reflecting the integral of the electric or magnetic fields which mostly vanish through the un-aligned orientation of neuron populations. In fact, these methods are mainly sensitive to the activity of the cortical pyramidal cells which happened to be aligned and are only a subset of the overall brain activity which EIT has the potential to measure. 2) Better posed inverse problem comparing to EEG and MEG since the sources are well defined as the current driving electrodes and the conductivities of the volume conductor are the unknowns. In EEG and MEG the neuronal sources are also unknowns.

For pursuing this goal, based on the continuing work in our group and the work presented in this thesis, we were recently awarded a major grant from the NIH under the call "new ways to image neuronal activity".

Non-invasive imaging: following the ongoing work on the invasive imaging and the conclusions drawn in this thesis, several improvements to the non-invasive technique could enhance the SNR to a level sufficient for imaging in a realistic recording time much shorter than the present several hours. The main direction which could be foreseen at present are reducing the noise level originated by the current source, particularly in a MEG environment, increasing the current level to 1 mA in LF-EIT measurements and further investigating the case when the frequency of the EIT current is just above the EEG band above 100 Hz.

Other modalities also have the potential to achieve non-invasive imaging of neuronal activity (Section 1.2.2). These are EEG (Baillet, 2001a; Baillet, 2001b; Michel, 2004), MEG (Hamalainen, 1992; Baillet, 2001a), Multi-modality fusion (Dale, 2001), Direct MRI mapping (Xiong, 2003; Lin, 2006) and DOI (Franceschini, 2004).

Multi-modality fusion, typically integrating EEG or MEG data with haemodynamic fMRI data, has already achieved partial success towards this goal but will be always limited by the EEG and MEG inverse problem, when both neuronal activity sources and volume conductor properties are unknown or only partially known. These methods are also limited to sources close to the surface of the cortex and may also suffer from erroneous results as the haemodynamic response is not always correlated in time and space with the neuronal activity.

Direct MRI mapping of the neuromagnetic signal has the potential to achieve a high spatial resolution without ambiguous localization as the magnetic field is probed at each voxel. Recent advances in developing ultra fast fMRI reconstruction methods allowed improved time resolution of 20 ms which might be implemented for this purpose (Lin, 2006). However, detecting the fast component with MRI is at the borders of detectability for current MRI techniques and both positive and negative findings have been reported in the literature, with no clear consensus as to the feasibility of direct detection (Parkes, 2007).

Applications of non-invasive *optical imaging* methods to image the fast neuronal signals are still preliminary and require further validations but are generally seem to be a promising way of obtaining information from the surface of the cortex. However, the lack of penetration of near infra-red light into the highly scattering white matter limit the fast optical imaging methods form detecting activity in deep structures, providing true 3D imaging.

7.2 Future work

7.2.1 Instrumentation

Current source noise in MD-EIT: reduce the noise level introduced by the current source, the MEG synthesizer and interference through the leads driving the current into the MSR. This could be achieved by developing a magnetically compatible battery driven current source to be located within the MSR. This could decrease the noise by a factor of 2 and hence allow a factor of 4 reduced recording time.

Square wave stability: minimizing the ringing artefact due to the rise and fall times of the polarity switching would increase the usable time window from 300 to 500 ms and could allow increasing the stimulation rate to 4 stimuli/sec and shorten the recording time by a factor of 2.

Square wave settling time: the AC coupling at the LF-EIT acquisition distorts the square wave and requires a double amount of time to record and additional control calibration data.

This could be overcome by applying a DC coupled acquisition, stabilizing the square wave amplitude further or by polynomial fitting algorithm correcting for the distortions without using a calibration recording. This has a potential to reduce the recording time by a factor of 2.

Recording above the EEG MEG band with a sine wave: this could reduce the noise by a factor of 10 but the impedance changes at frequencies above 100 Hz are expected to decrease by a factor of 2. A total improvement in the SNR of 5-fold is anticipated which could reduce the recording time by a factor of 25. This method could also overcome some of the previous problems with the square wave.

Electrode design: for minimizing skin sensation at current levels of up to 1 mA, a novel recessed electrode design was used to keep the current density uniform at the contact surface (Ch. 2). In future invasive studies involving direct placement of the electrodes on the cortical surface, this would also be beneficial to minimize possible stimulation of underlying neuronal tissue beneath the electrode. The recessed design is limited by the burden of filling the gap between the electrode and the tissue with conducting jelly and the height of the electrode which could become a limiting factor in animal experiments requiring placement of electrodes between the skull and the brain. This could be achieved by implementing the technique of interfacing with layers of varying and high resistivity as proposed by Papazov (Papazov, 2002)(Ch. 2).

7.2.2 Invasive measurements

Quantify the local impedance changes: hitherto, no satisfactory data is available for validating the local impedance changes with *in-vivo* cortical measurements apart from a pilot study in our group (Boone, 1995a). As part of our ongoing research, we intend to measure these impedance changes in animal models with surface electrodes on the exposed cortex or with depth electrodes in the brain. The purpose is to quantify the magnitude and frequency response of these changes under various conditions.

Invasive imaging: as previously described, ongoing NIH funded work in our laboratory is to develop an *in-vivo* invasive imaging system for use in animals and epilepsy patients with temporarily implanted intracranial electrodes.

7.2.3 Non-invasive human measurements

Repeated measurements: repeating the LF-EIT and MD-EIT measurements after applying some of the improvements suggested above. If such measurements will achieve a higher SNR, validation studied to exclude possible sources for artefact could be performed (Section 4.5.5).

Other EPs: Applying other types of EPs from areas in the brain where background brain activity is lower such as the somatosensory and auditory evoked responses. However, the magnitude of these EPs is lower comparing to VEP and the overall SNR might be similar.

7.2.4 Data analysis

Explore additional advanced data analysis methods not incorporated in this thesis. These could possibly be adopted from MEG, EEG and fMRI statistical and other data analysis methods. One example could be the application of Independent Component Analysis (ICA) methods for separating the different components in our recorded signal and enhance the SNR. These include the EIT signal, evoked potentials, α rhythm, other background brain signals, cardiac, respiratory and muscular electrical activity as well as physiological and instrumentation artefacts.

7.2.5 Forward model

Multiple current injections: for the application of imaging neuronal activity it might be beneficial to simultaneously apply current through multiple electrodes so that the total acquisition time would be reduced. However, the current level from each electrode will have to be lower than 1 mA as this will already reach the limit for changing neuronal activity when transmitted from one pair (Ch. 2). However; the highest current density in the brain is located just beneath each electrode so the contribution of other remote current carrying electrodes could be minor. A modelling study is suggested to characterize this problem and conclude about the maximal current level which could be used in such case and suggest the optimal electrode positions and transmission protocol.

Feasibility studies for other magnetic methods: apart from MD-EIT, other magnetic variants of EIT have been previously developed for other applications. These included IC-EIT, MIT, EMIT, MR-EIT, VS-MR-EIT and IC-MR-EIT (Section 1.3.7). It is therefore suggested that a thorough feasibility study will be conducted for some of these methods for the specific application of imaging neuronal activity to evaluate if they could outperform the LF-EIT or MD-EIT methods studied throughout this thesis.

7.2.6 Inverse problem

For LF-EIT, evaluate the different linear inverse problem techniques (Horesh, 2006a) under realistic conditions for the LF-EIT application for neuronal activity for determining the minimal SNR requirements for reliable image reconstruction. *For MD-EIT,* adopt the existing inverse problem algorithms, developed for other applications (Ahlfors, 1992; Tozer, 1999; Ireland, 2004), for the specific application of neuronal activity and perform a similar study for determining the SNR requirements and optimal current injection protocol.

Appendix A. Dielectric properties : definitions

In the following, I describe some basic concepts and definitions of material properties. The complex parallel admittance of a sample placed between two parallel electrodes of area A and separated by distance d (Figure A-1) is defined as:

$$Y^* = G + j\omega C = \frac{A}{d}\sigma^* = \frac{A}{d}[\sigma + j\omega\varepsilon_0\varepsilon] \qquad (A\text{-}1)$$

Where, $j = \sqrt{-1}$, $\omega = 2\pi f$ is the angular frequency in radians/sec, f is the frequency in Hz , $Y^*, G, C, \sigma^*, \sigma$ and ε are frequency dependant and are defined in Table A-1

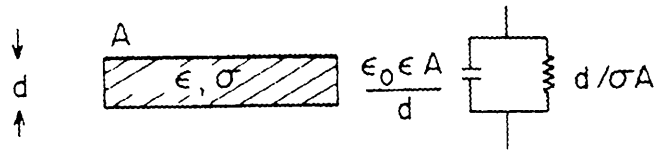

Figure A-1: Equivalent circuit of an idealized parallel-plate capacitor filled with material or relative permittivity ε and conductivity σ. The plate area is A, and the distance between plates is d. Reproduced from Foster and Schwan (Foster, 1989).

The series equivalent complex impedance Z^* is defined as:

$$Z^* = \frac{1}{Y^*} = R + jX = \frac{d}{A}z^* = \frac{d}{A}[\rho' + j\rho''] \qquad (A\text{-}2)$$

Where Z^*, R, X, z^*, ρ' and ρ'' are frequency dependent and are defined in Table A-1

And can be also written in the form:

$$Z^* = \frac{1}{Y^*} = R + jX = \frac{1}{G + j\omega C} = \frac{G - j\omega C}{G^2 + (\omega C)^2} \qquad (A\text{-}3)$$

Dividing by d/A gives the specific complex impedance z^*:

$$z^* = \frac{1}{\sigma^*} = \rho' + j\rho'' = \frac{\sigma - j\omega\varepsilon_0\varepsilon}{\sigma^2 + (\omega\varepsilon_0\varepsilon)^2} \qquad (A\text{-}4)$$

The resistivity is defined as $\rho = 1/\sigma$ which does not equal to the real specific resistance ρ', which according to equation 1.6-4 is defined as:

$$\rho' = \frac{\rho}{1 + (\omega\varepsilon_0\varepsilon\rho)^2} \qquad (A\text{-}5)$$

The complex capacitance C^* can be defined as

$$C^* = \frac{Y^*}{j\omega} \qquad (A\text{-}6)$$

Which leads to the definition of the complex relative permittivity ε^*

$$\varepsilon^* = \varepsilon' - j\varepsilon'' = \varepsilon' - j\sigma / \varepsilon_0 \omega \qquad (A\text{-}7)$$

Where $\varepsilon' = \varepsilon_r = \varepsilon$

The complex conductivity and complex permittivity are related by

$$\sigma^* = j\omega\varepsilon^*\varepsilon_0 \qquad (A\text{-}8)$$

Table A-1: Definition of physical properties of materials

Name	Symbol / definition	Units
Conductance ; Conductivity	G ; σ	S ; S/m
Capacitance ; specific capacitance	C ; $c = \varepsilon_0\varepsilon_r$	F ; F/m
Admittance	$Y^* = G + j\omega C$	S
complex conductivity / admittivity	$\sigma^* \equiv \gamma = \sigma + j\omega\varepsilon_0\varepsilon_r$	S/m
Permittivity of vacuum	$\varepsilon_0 = 8.85 \cdot 10^{-12}$	F/m
Relative permittivity	$\varepsilon \equiv \varepsilon_r \equiv \varepsilon'$	-
Out of phase loss factor	$\varepsilon'' = \sigma / \varepsilon_0 \omega$	-
Complex relative permittivity	$\varepsilon^* = \varepsilon' - j\varepsilon'' = -j\sigma^* / \varepsilon_0 \omega$	-
Resistivity	$\rho = 1/\sigma$	Ωcm
Resistance ; real specific resistance	R; $\rho' = \rho / \left[1 + (\omega\varepsilon_0\varepsilon\rho)^2\right]$	Ω ; Ωcm
Reactance ; imaginary specific resistance	X ; $\rho'' = (\omega\varepsilon_0\varepsilon\rho^2) / \left[1 + (\omega\varepsilon_0\varepsilon\rho)^2\right]$	Ω ; Ωcm
Impedance	$Z^* = R + jX$	Ω
Specific impedance / impedivitty	$z^* = \rho' + j\rho''$	Ωcm

S=1/Ω (Siemens=1/ohms) ;F=Farad

Appendix B. Accuracy of constant current sources

B.1 Introduction

When measuring impedance changes in EIT, a constant current source is used to apply current through a pair of electrodes while the voltage is measured with another pair of electrodes. Assuming the current is indeed constant, the changes in the measured voltages can be ascribed to impedance changes. Therefore, it is important to quantify how constant are the currents produced by the constant current sources. When the impedance of the measured object is changing, the load to the current source is changing and may slightly change the current level it produces. It is therefore important to show that this effect is negligible and that the changes in the measured voltage reflect changes in impedance and not changes in the response of the current source. The purpose of this study was to quantify the response of the custom made and DS-5 current sources to different loads and estimate the possible bias in impedance measurements. This was achieved by a series of resistor measurements with both current sources.

B.2 Methods

The isolated custom made constant current source was initially introduced in Appendix B of Boone's thesis (Boone, 1995a)(Figure B-1). A set of resistors was attached as a load to the output of the two current sources and the voltage was measured at the same terminals. The current was then calculated by dividing the voltage by the resistance for each measurement.

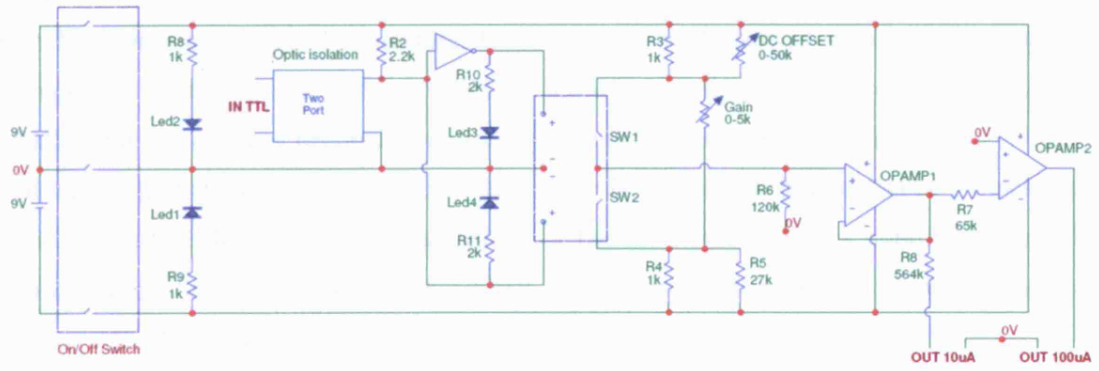

Figure B-1: Circuit diagram of the isolated constant current source.

B.3 Results

For the Custom made current source, the current level decreased linearly with load up to 70 kΩ with slope of -10^{-5} %/Ω. For the DS-5 unit, the change was linear up to 300 kΩ and the slope was 5 times larger, $-5 \cdot 10^{-5}$ %/Ω (Figure B-2).

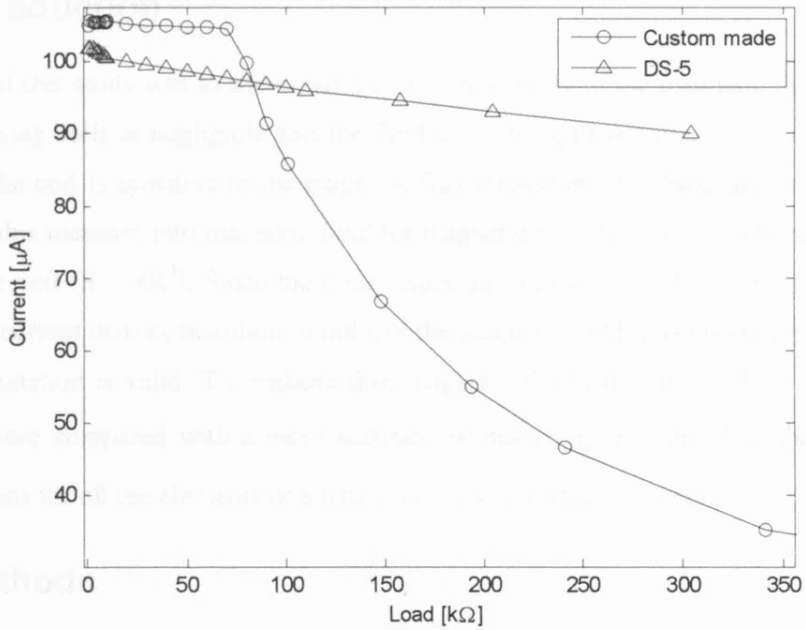

Figure B-2: Current versus load for the two current sources

B.4 Discussion

In the human experiments, a current of 100 μA produced a voltage of about 10 mV (Ch. 4) reflecting a transfer resistance of the head of approximately 100 Ω. According to the modelling work in Ch. 3, the expected changes in the boundary voltages during neuronal activity in the visual cortex were 0.0018 ± 0.0015% (Mean ± SD) which are 0.0018 ± 0.0015 Ω out of the transfer resistance of 100 Ω. Therefore, for the custom made current source, such a resistance change will change the current by $(0.0018 \pm 0.0015) \cdot 10^{-5}$ %, which is 5 orders of magnitude smaller than the changes resulted from the physiological resistivity change (0.0018 ± 0.0015 %) and has negligible bias effect on the results. For the DS-5 unit, the bias would be 5 times higher which is still negligible. The typical load in a human measurement is approximately 1 kΩ, mainly introduced by the electrodes contact impedance. This load is well within the linear domain of both current sources.

In conclusion, the current produced by the constant current sources is indeed constant for the load and resistivity changes measured throughout this thesis and no significant bias is introduced by the response of the current source to load changes.

Appendix C. Magnetic field homogeneity near the sensing coil

C.1 Introduction

This aim of this study was to show that the in-homogeneity of the magnetic field at the vicinity of the sensing coils is negligible and the field could be approximated at the centre of the coil (Ch. 5). The coil is sensitive to the magnetic flux throughout its plane, and the MEG machine translates this measure into magnetic field (or magnetic flux density) units by dividing it by the area of the coil ($S = \pi R^2$). Since the coils, especially in the lower layer, are close to the head where the current density distribution induces the magnetic field, it is questionable whether such an approximation is valid. To evaluate this, magnetic field calculations from the centre of the coil $\mathbf{B}_k$ were compared with a more accurate estimator $\tilde{\mathbf{B}}_k$ calculated as the average of the contributions for all the elements of a triangular mesh modelling the coil.

C.2 Methods

C.2.1 Sensing coil mesh

Two triangular meshes with NT = 8 or 32 elements of areas Δs_j (j = 1, 2,...NT), were calculated using a Delaunay triangulation algorithm as implemented in the *initmesh* Matlab function (The MathWorks, Inc, MA, US). The centre of each element was calculated as the mean of its three nodes (Figure C-1). The surface area of the outer elements was increased by 11 and 5% for the 8 and 32 element meshes respectively to adjust for the residual sections of the 9 mm radius circle not included in the triangles.

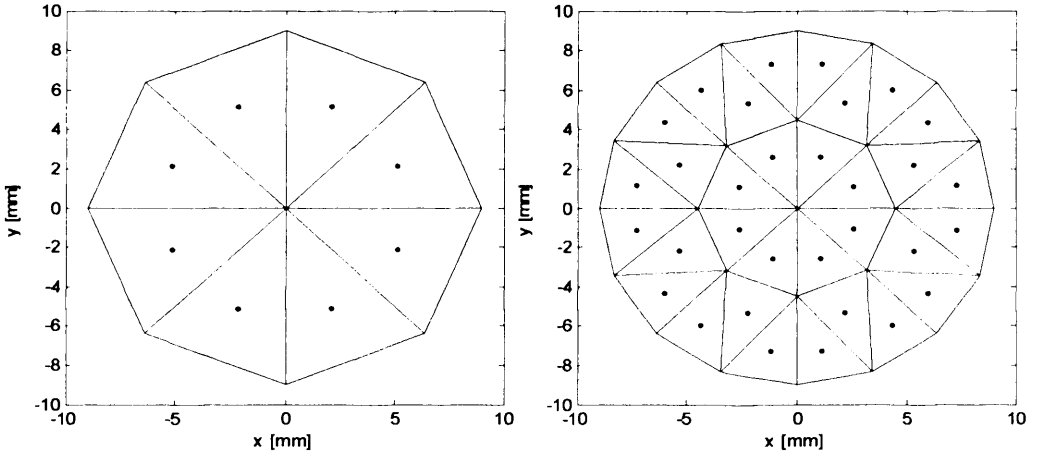

Figure C-1: 8 and 32 element triangular coil meshes. The points mark the centres of the elements where the magnetic field was calculated.

C.2.2 Magnetic field calculation

For the case where the magnetic field is approximated at the centre of the k^{th} coil, $\mathbf{r}$, the discrete form of the Biot–Savart law was:

$$\mathbf{B}_k(\mathbf{r}) = \frac{\mu_0}{4\pi}\sum_{i=1}^{NE}\mathbf{J}(\mathbf{r}_i)\times\frac{\mathbf{r}-\mathbf{r}_i}{|\mathbf{r}-\mathbf{r}_i|^3}\Delta v_i \qquad (C\text{-}1)$$

Where $\mathbf{J}(\mathbf{r}_i)$ is the current density at the i^{th} element (i = 1,2,... NE = 53,336) of the 3D head mesh and Δv_i is the volume of this element. When using a triangular mesh to model the coils, this calculation is repeated at each centre point $\mathbf{r}_j$ (j = 1,2,...NT = 8 or 32) of the triangular elements:

$$\mathbf{B}_k(\mathbf{r}_j) = \frac{\mu_0}{4\pi}\sum_{i=1}^{NE}\mathbf{J}(\mathbf{r}_i)\times\frac{\mathbf{r}_j-\mathbf{r}_i}{|\mathbf{r}_j-\mathbf{r}_i|^3}\Delta v_i \qquad (C\text{-}2)$$

The mean magnetic field over the NT triangular elements was calculated, weighted to the surface area of each element Δs_j:

$$\tilde{\mathbf{B}}_k = \frac{1}{S}\sum_{j=1}^{NT}\mathbf{B}_k(\mathbf{r}_j)\Delta s_j \qquad (C\text{-}3)$$

From here on, the calculations were similar to the case with the centre of coil approximation. This included calculating the radial and tangential components, the difference between the two coils and between the rest and perturbed states of the primary visual cortex:

$$\begin{aligned}\delta\tilde{\mathbf{B}}^{rad} &= \tilde{\mathbf{B}}^{rad}_{perturbed} - \tilde{\mathbf{B}}^{rad}_{non-perturbed}\\ \delta\tilde{\mathbf{B}}^{tan} &= \tilde{\mathbf{B}}^{tan}_{perturbed} - \tilde{\mathbf{B}}^{tan}_{non-perturbed}\end{aligned} \qquad (C\text{-}4)$$

C.2.3 Protocol

The changes between the perturbed and non-perturbed states were calculated using the centre of coil approximation and using triangular meshes of 8 and 32 elements. The calculations were made for the median conductivities σ_{median}, all 31·30/2 = 465 possible current injection pairs generated from the 31 electrodes, all 275 magnetic sensors and the lower and upper coils of each sensor. Therefore, the final dataset was made of 465·275 = 127,875 magnetic field changes for the both radial and tangential components. The maximal differences between the results form the three estimators for the magnetic field changes were used to evaluate the effect of inhomogeneous field.

C.3 Results

The maximal difference between the calculations with the centre of coil approximation $\delta \mathbf{B}^{rad}$ and the 8 elements triangular mesh, $\delta \tilde{\mathbf{B}}^{rad}$ was 1.2 and 0.3% for the lower and upper layers of coils respectively and was about 0.1 fT. When comparing the calculations between the 8 and 32 element triangular meshes, the differences were in the order of 0.4 and 0.1% for the lower and upper coils respectively. The results for the tangential component were similar.

C.4 Discussion

Inhomogeneous field at the sensing coils could cause about 1% deviation in the predicted changes due to neuronal activity if the centre of coil approximation is used. This deviation was negligible and the approximation was adopted for the simplicity of the numeric calculations, reducing the computation time linearly according to the size of the triangular mesh. The reduced difference for the upper coils was expected, as the coils are further away from the current density sources and therefore sense a more homogenous field.

References

Abascal JF, Arridge SR, Lionheart WR, Bayford RH, Holder DS (2007a) Validation of a finite-element solution for electrical impedance tomography in an anisotropic medium. Physiol Meas 28(7):S129-S140

Abascal JFPJ (2007b) Improvements in reconstruction algorithms for Electrical Impedance Tomography of brain function. PhD Thesis, University College London, London, UK

Adachi Y, Kawai J, Miyamoto M, Kawabata S, Okubo H, Fukuoka Y, Komori H, Uehara G (2005) A 30-channel SQUID vector biomagnetometer system optimized for reclining subjects. Applied Superconductivity, IEEE Transactions on 15(2):672-675

Adachi Y, Kawai J, Miyamoto M, Uehara G, Kawabata S, Okubo H, Fukuoka Y, Komori H (2003) Three dimensionally configured SQUID vector gradiometers for biomagnetic measurement. Superconductor Science and Technology 16(12):1442-1446

Adair RK, Astumian RD, Weaver JC (1998) Detection of weak electric fields by sharks, rays, and skates. Chaos 8(3):576-587 DOI 10.1063/1.166339

Ahadzi GM (2006) Models and Image Reconstruction in Electrical Impedance Tomography of Human Brain Function. PhD Thesis, Middlesex University, London, UK

Ahadzi GM, Gilad O, Horesh L, Bayford RH, Holder DS (2004a) An EIT electrode protocol for obtaining optimal current density in the primary visual cortex. XII International Conference on Electrical Bio-Impedance, 621-624.

Ahadzi GM, Liston AD, Bayford RH, Holder DS (2004b) Neuromagnetic field strength outside the human head due to impedance changes from neuronal depolarization. Physiol Meas 25(1):365-378

Ahlfors S, Ilmoniemi R (1992) Magnetic Imaging of Conductivity. Engineering in Medicine and Biology Society, 1992. Vol.14. Proceedings of the Annual International Conference of the IEEE, 5:1717-1718.

Akhtari M, Bryant HC, Mamelak AN, Flynn ER, Heller L, Shih JJ, Mandelkern M, Matlachov A, Ranken DM, Best ED, DiMauro MA, Lee RR, Sutherling WW (2002) Conductivities of three-layer live human skull. Brain Topogr 14(3):151-167 DOI 10.1023/A:1014590923185

Andrews TJ, Halpern SD, Purves D (1997) Correlated size variations in human visual cortex, lateral geniculate nucleus, and optic tract. J Neurosci 17(8):2859-2868

Attwell D (2003) Interaction of low frequency electric fields with the nervous system: the retina as a model system. Radiat Prot Dosimetry 106(4):341-348

Bagshaw AP, Liston AD, Bayford RH, Tizzard A, Gibson AP, Tidswell AT, Sparkes MK, Dehghani H, Binnie CD, Holder DS (2003) Electrical impedance tomography of human brain function using reconstruction algorithms based on the finite element method. Neuroimage 20(2):752-764

Baillet S, Mosher JC, Leahy RM (2001a) Electromagnetic brain mapping. IEEE Signal Processing Magazine 18(6):14-30

Baillet S, Riera JJ, Marin G, Mangin JF, Aubert J, Garnero L (2001b) Evaluation of inverse methods and head models for EEG source localization using a human skull phantom. Phys Med Biol 46(1):77-96

Barber DC (1989) A review of image reconstruction techniques for electrical impedance tomography. Med Phys 16(2):162-169

Barbour DJ (1998) Feasibilty Study to investigate whether current impedance measurements can be used to detect C-fibre activity. M.Res Thesis, University College London

Baumann SB, Wozny DR, Kelly SK, Meno FM (1997) The electrical conductivity of human cerebrospinal fluid at body temperature. IEEE Trans Biomed Eng 44(3):220-223 DOI 10.1109/10.554770

Bawin SM, Sheppard AR, Mahoney MD, Abu-Assal M, Adey WR (1986) Comparison between the effects of extracellular direct and sinusoidal currents on excitability in hippocampal slices. Brain Res 362(2):350-354

Bawin SM, Sheppard AR, Mahoney MD, Adey WR (1984) Influences of sinusoidal electric fields on excitability in the rat hippocampal slice. Brain Res 323(2):227-237

Belliveau JW, Kennedy DN, Jr., McKinstry RC, Buchbinder BR, Weisskoff RM, Cohen MS, Vevea JM, Brady TJ, Rosen BR (1991) Functional mapping of the human visual cortex by magnetic resonance imaging. Science 254(5032):716-719

Bernhardt J (1979) The direct influence of electromagnetic fields on nerve- and muscle cells of man within the frequency range of 1 Hz to 30 MHz. Radiat Environ Biophys 16(4):309-323 DOI 10.1007/BF01340569

Binnie CD, Cooper R, Fowler CJ, Mauguiere F, Prior PF (1995) Normal finding by modality. In: Clinical Neurophysiology. EMG, Nerve Conduction and Evoked Potentials (Osselton JW, ed), Butterworth-Heinemann Ltd., Cambridge, UK

Birgul O, Eyuboglu BM, Ider YZ (2003) Current constrained voltage scaled reconstruction (CCVSR) algorithm for MR-EIT and its performance with different probing current patterns. Phys Med Biol 48(5):653-671

Boas DA, Dale AM, Franceschini MA (2004) Diffuse optical imaging of brain activation: approaches to optimizing image sensitivity, resolution, and accuracy. Neuroimage 23 Suppl 1:S275-S288

Bodurka J, Bandettini PA (2002) Toward direct mapping of neuronal activity: MRI detection of ultraweak, transient magnetic field changes. Magn Reson Med 47(6):1052-1058

Bodurka J, Jesmanowicz A, Hyde JS, Xu H, Estkowski L, Li SJ (1999) Current-induced magnetic resonance phase imaging. J Magn Reson 137(1):265-271

Boone K, Lewis AM, Holder DS (1994) Imaging of cortical spreading depression by EIT: implications for localization of epileptic foci. Physiol Meas 15 Suppl 2a:A189-A198

Boone KG (1995a) The possible use of applied potential tomography for imaging action potentials in the brain. PhD Thesis, University College London, London, UK

Boone KG, Holder DS (1995b) Design considerations and performance of a prototype system for imaging neuronal depolarization in the brain using 'direct current' electrical resistance tomography. Physiol Meas 16(3 Suppl A):A87-A98

Boone KG, Holder DS (1996) Current approaches to analogue instrumentation design in electrical impedance tomography. Physiol Meas 17(4):229-247

Brazier MA (1964) Evoked responses recorded from the depths of the human brain. Ann N Y Acad Sci 112:33-59

Brown BH (2003) Electrical impedance tomography (EIT): a review. J Med Eng Technol 27(3):97-108

Brown BH, Barber DC, Morice AH, Leathard AD (1994) Cardiac and respiratory related electrical impedance changes in the human thorax. IEEE Trans Biomed Eng 41(8):729-734

Brown BH, Barber DC, Seagar AD (1985) Applied potential tomography: possible clinical applications. Clin Phys Physiol Meas 6(2):109-121

Brown BH, Seagar AD (1987) The Sheffield data collection system. Clin Phys Physiol Meas 8 Suppl A:91-97 DOI 10.1088/0143-0815/8/4A/012

Brown BH, Smallwood RH, Lawford PV, Hose DR (1999) Medical Physics and Biomedical Engineering.Institute of Physics, Bristol

Bryan K, Haugh J, McCune D (2006) Fast imaging of partially conductive linear cracks using impedance data. Inverse problems 22(4):1337-1358

BS5724 (1979) Specification for safety of medical electrical equipment, Part 1. General requirements. British Standards Institution, London ISBN 058010690X

Burger HC, Van Dongen R (1960) Specific Electrical Resistance of Body Tissue. Phys Med Biol 5:431-447 DOI 10.1088/0031-9155/5/4/304

Burger HC, Van Milaan JB (1943) Measurements of the specific resistnace of the human body to direct current. Act Med Scand 114:584-607

Burghoff M, Burghoff M, Schleyerbach H, Drung D, Trahms L, Koch H (1999) A vector magnetometer module for biomagnetic application. IEEE Transactions on Applied Superconductivity 9(2):4069-4072

Burlakova YeV, Veprintsev BN, Rass IT (1959) Lag of the impedance effect behind the action potential in frog nerve. Biofizikia 4:617-620

Cafiso DS, Hubbell WL (1978) Estimation of transmembrane potentials from phase equilibria of hydrophobic paramagnetic ions. Biochemistry 17(1):187-195

Calder'on AP (1980) On an inverse boundary value problem. Seminar on Numerical Analysisand its applications to Continuum Physics, Soc Brasileira de Mat'ematica, Rio deJaneiro p. 65-73.

Carstensen EL, Buettner A, Genberg VL, Miller MW (1985) Sensitivity of the human eye to power frequency electric fields. IEEE Trans Biomed Eng 32(8):561-565

Chailakhian LM, Iur'ev SA (1957) An investigation of the time relations of the action potential and impedance changes on excitation in the frog nerve. Biophysics 4:415-424

Cheney MD, Isaacson D, Newell JC (1999) Electrical Impedance Tomography. SIAM Review 41(1):85-101

Cheng KS, Isaacson D, Newell JC, Gisser DG (1989) Electrode models for electric current computed tomography. IEEE Trans Biomed Eng 36(9):918-924 DOI 10.1109/10.35300

Chow LS, Cook GG, Whitby E, Paley MN (2006) Investigating direct detection of axon firing in the adult human optic nerve using MRI. Neuroimage 30(3):835-846

Chu R, de Zwart JA, van Gelderen P, Fukunaga M, Kellman P, Holroyd T, Duyn JH (2004) Hunting for neuronal currents: absence of rapid MRI signal changes during visual-evoked response. Neuroimage 23(3):1059-1067

Cohen D (1968) Magnetoencephalography: evidence of magnetic fields produced by alpha-rhythm currents. Science 161(843):784-786

Cohen LB (1973) Changes in neuron structure during action potential propagation and synaptic transmission. Physiol Rev 53(2):373-418

Cole SK, Curtis HJ (1939) Electrical Impedance of the squid giant axon during activity. J Gen Physiol 22:649-670

Dale AM, Halgren E (2001) Spatiotemporal mapping of brain activity by integration of multiple imaging modalities. Curr Opin Neurobiol 11(2):202-208

Dalziel CF (1972) Electric Shock Hazard. IEEE Spectrum 9(2):41-50

Davidson JL, Pomfrett CJD, McCann H (2007) Predicted EIT current densities in the brain using a 3D anatomically realistic model of the head. Scharfetter, H. and Merwa, R. Proc. of XIII Int. Conf. on Electrical Bio-Impedance and VIII Conference on Electrical Impedance Tomography, 17(1):376-379. IFMBE, Graz, Austria

Demidenko E, Hartov A, Soni N, Paulsen KD (2005) On Optimal Current Patterns for Electrical Impedance Tomography. Biomedical Engineering, IEEE Transactions on 52(2):238-248

Di Rienzo L, Haueisen J, Arturi CM (2005) Three component magnetic field data: Impact on minimum norm solutions in a biomedical application. COMPEL: The International Journal for Computation and Mathematics in Electrical and Electronic Engineering 24(3):869-881 DOI 10.1108/03321640510598193

Di Russo F, Pitzalis S, Spitoni G, Aprile T, Patria F, Spinelli D, Hillyard SA (2005) Identification of the neural sources of the pattern-reversal VEP. Neuroimage 24(3):874-886

Durand DM (2003) Electric field effects in hyperexcitable neural tissue: a review. Radiat Prot Dosimetry 106(4):325-331

Edwards RN (1974) The magnetometeric resistivity (MMR) method and its application to the mapping of a fault. Can J Earth Sci 11:1136-1156

Enfield L (2005) Electrical Impedance Tomography of Human Brain Function. PhD Thesis, University College London, London, UK

Eyuboglu BM, Brown BH, Barber DC (1988) Problems of cardiac output determination from electrical impedance tomography scans. Clin Phys Physiol Meas 9 Suppl A:71-77

Fabrizi L, Horesh L, McEwan A, Holder DS (2006a) A feasibility study for imaging of epileptic seizures by EIT using a realistic FEM of the head. Proc. of VII Int. Conf. on Biomedical Applications of Electrical Impedance Tomography, Joint Conference of World Congress on Medical Physics and Biomedical Engineering (WC2006), 14(1):3733-3736. IFMBE, Seoul, Korea

Fabrizi L, McEwan A, Woo E, Holder DS (2007) Analysis of resting noise characteristics of three EIT systems in order to compare suitability for time difference imaging with scalp electrodes during epileptic seizures. Physiol Meas 28(7):S217-S236

Fabrizi L, Sparkes M, Horesh L, Perez-Juste Abascal JF, McEwan A, Bayford RH, Elwes R, Binnie CD, Holder DS (2006b) Factors limiting the application of electrical impedance tomography for identification of regional conductivity changes using scalp electrodes during epileptic seizures in humans. Physiol Meas 27(5):S163-S174 DOI 10.1088/0967-3334/27/5/S14

Foster KR (2003) Mechanisms of interaction of extremely low frequency electric fields and biological systems. Radiat Prot Dosimetry 106(4):301-310

Foster KR, Schwan HP (1989) Dielectric properties of tissues and biological materials: a critical review. Crit Rev Biomed Eng 17(1):25-104

Franceschini MA, Boas DA (2004) Noninvasive measurement of neuronal activity with near-infrared optical imaging. Neuroimage 21(1):372-386

Freeston IL, Tozer RC (1995) Impedance imaging using induced currents. Physiol Meas 16(3 Suppl A):A257-A266

Frerichs I (2000) Electrical impedance tomography (EIT) in applications related to lung and ventilation: a review of experimental and clinical activities. Physiol Meas 21(2):R1-21

Frerichs I, Hinz J, Herrmann P, Weisser G, Hahn G, Quintel M, Hellige G (2002) Regional lung perfusion as determined by electrical impedance tomography in comparison with electron beam CT imaging. IEEE Trans Med Imaging 21(6):646-652

Freygang WH, Landau WM (1955) Some relations between resistivity and electrical activity in the cerebral cortex of the cat. J Cell Compar Physl 45:377-392 DOI 10.1002/jcp.1030450305

Gabriel C, Gabriel S, Corthout E (1996) The dielectric properties of biological tissues: I. Literature survey. Phys Med Biol 41(11):2231-2249 DOI 10.1088/0031-9155/41/11/001

Galambos R, Velluti R (1968) Evoked resistance shifts in unanaesthetized cats. Exp Neurol 22:243-252

Garcia LA, Pagan-Carlo LA, Stone MS, Kerber RE (1998) High perimeter impedance defibrillation electrodes reduce skin burns in transthoracic cardioversion. Am J Cardiol 82(9):1125-7, A9 DOI 10.1016/S0002-9149(98)00571-2

Geddes LA, Baker LE (1967) The specific resistance of biological material--a compendium of data for the biomedical engineer and physiologist. Med Biol Eng 5(3):271-293

Gencer NG, Tek MN (1999) Electrical conductivity imaging via contactless measurements. IEEE Trans Med Imaging 18(7):617-627

Ghai RS, Bikson M, Durand DM (2000) Effects of applied electric fields on low-calcium epileptiform activity in the CA1 region of rat hippocampal slices. J Neurophysiol 84(1):274-280

Gibson AP, Bayford RH, Holder DS (2000) Two-dimensional finite element modelling of the neonatal head. Physiol Meas 21(1):45-52

Gilad O, Ahadzi GM, Bayford RH, Holder DS (2004) Near DC conductivity change measurement of fast neuronal activity during human VEP. XII International Conference on Electrical Bio-Impedance, Gdansk, Poland, 279-282.

Gilad O, Horesh L, Ahadzi GM, Bayford RH, Holder DS (2005a) Could synchronized neuronal activity be imaged using Low Frequency Electrical Impedance Tomography (LFEIT)? VI International Conference on Biomedical Applications of Electrical Impedance Tomography, London, UK,

Gilad O, Horesh L, Akselrod S, Holder DS (2007a) Statistical analysis of non-invasive Low Frequency EIT human measurements of neuronal activity. Scharfetter, H. and Merwa, R. Proc. of XIII Int. Conf. on Electrical Bio-Impedance and VIII Conference on Electrical Impedance Tomography, 17(1):548-551. IFMBE, Graz, Austria

Gilad O, Horesh L, Holder DS (2005b) Non invasive imaging of synchronized neuronal activity using low frequency electrical impedance tomography. Hozman, J. and Kneppo, P. Proc. of the 3rd European Medical & Biological Engineering Conference (EMBEC'05), 11(1):179-182. IFMBE, Prague, Czech Republic

Gilad O, Horesh L, Holder DS (2006) Could Synchronized Neuronal Activity be Imaged Using Magnetic Detection Electrical Impedance Tomography (MD-EIT)? Proc. of VII Int. Conf. on Biomedical Applications of Electrical Impedance Tomography, Joint Conference of World Congress on Medical Physics and Biomedical Engineering (WC2006), 14(1):5196. IFMBE, Seoul, Korea

Gilad O, Horesh L, Holder DS (2007b) Design of electrodes and current limits for low frequency electrical impedance tomography of the brain. Med Biol Eng Comput 45(7):621-633 DOI 10.1007/s11517-007-0209-7

Gilad O, Swenne CA, Davrath LR, Akselrod S (2005c) Phase-averaged characterization of respiratory sinus arrhythmia pattern. Am J Physiol Heart Circ Physiol 288(2):H504-H510

Gisser DG, Isaacson D, Newell JC (1987) Current topics in impedance imaging. Clin Phys Physiol Meas 8 Suppl A:39-46 DOI 10.1088/0143-0815/8/4A/005

Gratton G, Brumback CR, Gordon BA, Pearson MA, Low KA, Fabiani M (2006) Effects of measurement method, wavelength, and source-detector distance on the fast optical signal. Neuroimage 32(4):1576-1590

Gratton G, Fabiani M (2001) Shedding light on brain function: the event-related optical signal. Trends Cogn Sci 5(8):357-363

Grinvald A (1992) Optical imaging of architecture and function in the living brain sheds new light on cortical mechanisms underlying visual perception. Brain Topogr 5(2):71-75

Haas HL, Jefferys JG (1984) Low-calcium field burst discharges of CA1 pyramidal neurones in rat hippocampal slices. J Physiol 354:185-201

Hagberg GE, Bianciardi M, Maraviglia B (2006) Challenges for detection of neuronal currents by MRI. Magn Reson Imaging 24(4):483-493

Hamalainen MS (1992) Magnetoencephalography: a tool for functional brain imaging. Brain Topogr 5(2):95-102

Hamalainen MS, Hari R, Ilmoniemi RJ, Knuutila J, Lounasmaa OV (1993) Magnetoencephalography-theory, instrumentation, and applications to noninvasive studies of the working human brain. Rev Mod Phys 65(2):413-497

Hashimoto T, Kashii S, Kikuchi M, Honda Y, Nagamine T, Shibasaki H (1999) Temporal profile of visual evoked responses to pattern-reversal stimulation analyzed with a whole-head magnetometer. Exp Brain Res 125(3):375-382

Haueisen J, Tuch DS, Ramon C, Schimpf PH, Wedeen VJ, George JS, Belliveau JW (2002) The influence of brain tissue anisotropy on human EEG and MEG. Neuroimage 15(1):159-166

Henderson RP, Webster JG (1978) An impedance camera for spatially specific measurements of the thorax. IEEE Trans Biomed Eng 25(3):250-254

Hochwald B, Hochwald B, Nehorai A (1997) Magnetoencephalography with diversely oriented and multicomponent sensors. IEEE Transactions on Biomedical Engineering 44(1):40-50

Hoekema R, Wieneke GH, Leijten FS, van Veelen CW, van Rijen PC, Huiskamp GJ, Ansems J, van Huffelen AC (2003) Measurement of the conductivity of skull, temporarily removed during epilepsy surgery. Brain Topogr 16(1):29-38 DOI 10.1023/A:1025606415858

Holder DS (1987) Feasibility of developing a method of imaging neuronal activity in the human brain: a theoretical review. Med Biol Eng Comput 25(1):2-11

Holder DS (1989) Impedance changes during evoked nervous activity in human subjects: implications for the application of applied potential tomography (APT) to imaging neuronal discharge. Clin Phys Physiol Meas 10(3):267-274

Holder DS (1992a) Detection of cerebral ischaemia in the anaesthetised rat by impedance measurement with scalp electrodes: implications for non-invasive imaging of stroke by electrical impedance tomography. Clin Phys Physiol Meas 13(1):63-75

Holder DS (1992b) Electrical impedance tomography with cortical or scalp electrodes during global cerebral ischaemia in the anaesthetised rat. Clin Phys Physiol Meas 13(1):87-98

Holder DS (1992c) Impedance changes during the compound nerve action potential: implications for impedance imaging of neuronal depolarisation in the brain. Med Biol Eng Comput 30(2):140-146

Holder DS, Gardner-Medwin AR (1988) Some possible neurological applications of applied potential tomography. Clin Phys Physiol Meas 9 Suppl A:111-119

Holder DS, Rao A, Hanquan Y (1996) Imaging of physiologically evoked responses by electrical impedance tomography with cortical electrodes in the anaesthetized rabbit. Physiol Meas 17 Suppl 4A:A179-A186 DOI 10.1088/0967-3334/17/4A/022

Horesh L (2006a) Some Novel Approaches in Modelling and Image Reconstruction for Multi-Frequency Electrical Impedance Tomography of the Human Brain. PhD Thesis, University College London, London, UK

Horesh L, Gilad O, Romsauerova A, McEwan A, Arridge SR, Holder DS (2005) Stroke type differentiation by multi - frequency electrical impedance tomography - a feasibility study. Hozman, J. and Kneppo, P. Proc. of the 3rd European Medical & Biological Engineering Conference (EMBEC'05), 11(1):1252-1256. IFMBE, Prague, Czech Republic

Horesh L, Romsauerova A, Fabrizi L, McEwan A, Arridge SR, Holder DS (2007a) Review of the dielectric properties of human head pathophysiology for Multi-Frequency Electrical Impedance Tomography (MFEIT). Med Biol Eng Comput. In Press

Horesh L, Romsauerova A, Gilad O, McEwan A, Arridge SR, Holder DS (2007b) Review of dielectric properties of the human head for Multi-Frequency Electrical Impedance Tomography (MFEIT). Med Biol Eng Comput. In Press

Horesh L, Schweiger M, Arridge SR, Holder DS (2006b) Novel large-scale 3D Electrical Impedance Tomography modelling of the human head. Proc. of VII Int. Conf. on Biomedical Applications of Electrical Impedance Tomography, Joint Conference of World Congress on Medical Physics and Biomedical Engineering (WC2006), 14(1):3717-3720. IFMBE, Seoul, Korea

Horesh L, Schweiger M, Bollhofer M, Douiri A, Holder DS, Arridge SR (2006c) Multilevel preconditioning for 3D large-scale soft field medical applications modelling. Int J Inf Syst Sci 2(4):532-556

Hua P, Woo EJ, Webster JG, Tompkins WJ (1993) Finite element modeling of electrode-skin contact impedance in electrical impedance tomography. IEEE Trans Biomed Eng 40(4):335-343 DOI 10.1109/10.222326

Hurt WD (1985) Multiterm Debye dispersion relations for permittivity of muscle. IEEE Trans Biomed Eng 32(1):60-64

ICNIRP (1998) Guidelines for limiting exposure to time-varying electric, magnetic, and electromagnetic fields (up to 300 GHz). International Commission on Non-Ionizing Radiation Protection. Health Phys 74(4):494-522

Ider YZ, Onart S, Lionheart WR (2003) Uniqueness and reconstruction in magnetic resonance-electrical impedance tomography (MR-EIT). Physiol Meas 24(2):591-604

IEC60601-1{ed3.0} (2005) Medical electrical equipment - Part 1: General requirements for basic safety and essential performance. International Electrotechnical Commission, Geneva

IEEE Std C95.6-2002 (2002) IEEE Standard for safety levels with respect to human exposure to electromagnetic fields, 0-3 kHz. IEEE, New York ISBN 0-7381-3390-6

Ireland RH, Tozer JC, Barker AT, Barber DC (2004) Towards magnetic detection electrical impedance tomography: data acquisition and image reconstruction of current density in phantoms and in vivo. Physiol Meas 25(3):775-796

Isaacson D (1986) Distinguishability of conductivities by electric current computed tomography. IEEE Trans Med Imaging MI-5:91-95

Isaacson D, Mueller JL, Newell JC, Siltanen S (2006) Imaging cardiac activity by the D-bar method for electrical impedance tomography. Physiol Meas 27(5):S43-S50

Jasper HH (1958) Appendix to report to Committee on Clinical Examination in EEG: the ten-twenty electrode system of the International Federation. Electroencephalogr Clin Neurophysiol 10:371-375

Jefferys JG, Deans J, Bikson M, Fox J (2003) Effects of weak electric fields on the activity of neurons and neuronal networks. Radiat Prot Dosimetry 106(4):321-323

Joy M, Scott G, Henkelman M (1989) In vivo detection of applied electric currents by magnetic resonance imaging. Magn Reson Imaging 7(1):89-94

Joy ML, Lebedev VP, Gati JS (1999) Imaging of current density and current pathways in rabbit brain during transcranial electrostimulation. IEEE Trans Biomed Eng 46(9):1139-1149 DOI 10.1109/10.784146

Jurgens I, Rosell J, Riu PJ (1996) Electrical impedance tomography of the eye: in vitro measurements of the cornea and the lens. Physiol Meas 17 Suppl 4A:A187-A195

Kaipio JP, Kolehmainen V, Vauhkonen M, Somersalo E (1998) Inverse problems with structural prior information. Inverse problems 15 (1999)(Printed in the UK PII: S0266-5611(99)99228-6):713-729

Kamei H, Iramina K, Yoshikawa K, Ueno S (1999) Neuronal current distribution imaging using magnetic resonance. Magnetics, IEEE Transactions on 35(5):4109-4111

Karbeyaz BU, Gencer NG (2003) Electrical conductivity imaging via contactless measurements: an experimental study. IEEE Trans Med Imaging 22(5):627-635

Kaup PG, Santosa F, Vogelius M (1996) Method for imaging corrosion damage in thin plates from electrostatic data. Inverse problems 12(3):279-293

Kayyali H, Durand D (1991) Effects of applied currents on epileptiform bursts in vitro. Exp Neurol 113(2):249-254

Kilner JM, Stephan KE, Josephs O, Friston KJ (2004) Comparison of phase and magnitude of the MR signal in measuring neuronal activity. Proceedings of the 10th Annual Meeting of the Organization for Human Brain Mapping, Abstract TH299. Organization for Human Brain Mapping, Budapest, Hungary

Kim SG, Ogawa S (2002) Insights into new techniques for high resolution functional MRI. Curr Opin Neurobiol 12(5):607-615

Klivington KA, Galambos R (1967) Resistance shifts accompanying the evoked cortical response in the cat. Science 157(3785):211-213

Klivington KA, Galambos R (1968) Rapid resistance shifts in cat cortex during click-evoked responses. J Neurophysiol 31(4):565-573

Kobayashi K, Uchikawa Y, ` (6-1-1998) Estimation of multiple sources using a three-dimensional vector measurement of a magnetoencephalogram. 83(11):6462-6464. AIP, San Francisco, California (USA)

Kolehmainen V, Vauhkonen M, Karjalainen PA, Kaipio JP (1997) Assessment of errors in static electrical impedance tomography with adjacent and trigonometric current patterns. Physiol Meas 18(4):289-303

Konig M (2003) Brain perfusion CT in acute stroke: current status. Eur J Radiol 45 Suppl 1:S11-S22

Konn D, Gowland P, Bowtell R (2003) MRI detection of weak magnetic fields due to an extended current dipole in a conducting sphere: a model for direct detection of neuronal currents in the brain. Magn Reson Med 50(1):40-49

Konn D, Leach S, Gowland P, Bowtell R (2004) Initial attempts at directly detecting alpha wave activity in the brain using MRI. Magn Reson Imaging 22(10):1413-1427

Koretsky AP (2004) New Developments in Magnetic Resonance Imaging of the Brain. Neurorx 1(1):155-164

Kowalski T, Silny J, Buchner H (2002) Current density threshold for the stimulation of neurons in the motor cortex area. Bioelectromagnetics 23(6):421-428 DOI 10.1002/bem.10036

Krasteva VT, Papazov SP (2002a) Estimation of current density distribution under electrodes for external defibrillation. Biomed Eng Online 1(1):7 DOI 10.1186/1475-925X-1-7

Krasteva VT, Papazov SP, Daskalov IK (2002b) Magnetic stimulation for non-homogeneous biological structures. Biomed Eng Online 1(1):3 DOI 10.1186/1475-925X-1-3

Law SK (1993) Thickness and resistivity variations over the upper surface of the human skull. Brain Topogr 6(2):99-109 DOI 10.1007/BF01191074

Leach SA, Hamandi L, Lemieux L, Gowland P, Allen P, Bowtell R (2004) Using simultaneous EEG-MRI to test the feasibility of directly detecting neuronal currents associated with alpha wave activity by MRI. Proceedings of the 10th Annual Meeting of the Organization for Human Brain Mapping, Abstract TH304. Organization for Human Brain Mapping, Budapest, Hungary

Lee BI, Oh SH, Woo EJ, Lee SY, Cho MH, Kwon O, Seo JK, Lee JY, Baek WS (2003) Three-dimensional forward solver and its performance analysis for magnetic resonance electrical impedance tomography (MREIT) using recessed electrodes. Phys Med Biol 48(13):1971-1986

Levy S, Adam D, Bresler Y (2002) Electromagnetic impedance tomography (EMIT): a new method for impedance imaging. IEEE Trans Med Imaging 21(6):676-687

Lin FH, Wald LL, Ahlfors SP, Hamalainen MS, Kwong KK, Belliveau JW (2006) Dynamic magnetic resonance inverse imaging of human brain function. Magn Reson Med 56(4):787-802

Lindenblatt G, Silny J (2002) Electrical phosphenes: on the influence of conductivity inhomogeneities and small-scale structures of the orbita on the current density threshold of excitation. Med Biol Eng Comput 40(3):354-359 DOI 10.1007/BF02344219

Lionheart WR, Kaipio J, McLeod CN (2001) Generalized optimal current patterns and electrical safety in EIT. Physiol Meas 22(1):85-90 DOI 10.1088/0967-3334/22/1/311

Lionheart WRB (2004) EIT reconstruction algorithms: pitfalls, challenges and recent developments. Physiological Measurement 25(1):125-142

Liston AD (2004a) Models and Image Reconstruction in Electrical Impedance Tomography of Human Brain Function. PhD Thesis, Middlesex University, London, UK

Liston AD, Bayford RH, Boone KG, Holder DS (2000) Estimation of Impedance Changes Inside the Human Head During Neuronal Depolarisation; Implications for Electrical Impedance Imaging of the Brain. World Congress on Medical Physics and Biomedical Engineering, Chicago, Chicago

Liston AD, Bayford RH, Tidswell AT, Holder DS (2002) A multi-shell algorithm to reconstruct EIT images of brain function. Physiol Meas 23(1):105-119

Liston AD, Salek-Haddadi A, Kiebel SJ, Hamandi K, Turner R, Lemieux L (2004b) The MR detection of neuronal depolarization during 3-Hz spike-and-wave complexes in generalized epilepsy. Magn Reson Imaging 22(10):1441-1444

Low KA, Leaver E, Kramer AF, Fabiani M, Gratton G (2006) Fast optical imaging of frontal cortex during active and passive oddball tasks. Psychophysiology 43(2):127-136

Lux HD, Heinemann U, Dietzel I (1986) Ionic changes and alterations in the size of the extracellular space during epileptic activity. Adv Neurol 44:619-639

Malmivuo J, Plonsey R (1995) Electroencephalography. In: Bioelectromagnetism: Principles and Applications of Bioelectric and Biomagnetic Fields (Malmivuo J, Plonsey R, eds), Oxford University Press., New York, Oxford

Malonek D, Dirnagl U, Lindauer U, Yamada K, Kanno I, Grinvald A (1997) Vascular imprints of neuronal activity: relationships between the dynamics of cortical blood flow, oxygenation, and volume changes following sensory stimulation. Proc Natl Acad Sci U S A 94(26):14826-14831

McArdle,FJ, Brown,BH, Pearse,RG, and Barber,DC. The effect of the skull of low-birthweight neonates on applied potential tomography imaging of centralised resistivity changes. Clin.Phys.Physiol.Meas. 1988;9 Suppl A:55-60. 1988.
Ref Type: Magazine Article

McCann H, Polydorides N, Murrieta-Lee JC, Ge K, Beatty PCW, Pomfrett CJD (2005) Fast functional imaging of the brain by Electrical Impedance Tomography. 6th Conference on Biomedical Applications of Electrical Impedance Tomography, London, UK,

McCreery DB, Agnew WF, Yuen TG, Bullara L (1990) Charge density and charge per phase as cofactors in neural injury induced by electrical stimulation. IEEE Trans Biomed Eng 37(10):996-1001 DOI 10.1109/10.102812

McEwan A, Romsauerova A, Yerworth R, Horesh L, Bayford R, Holder D (2006) Design and calibration of a compact multi-frequency EIT system for acute stroke imaging. Physiol Meas 27(5):S199-S210

Mehta AD, Jung JC, Flusberg BA, Schnitzer MJ (2004) Fiber optic in vivo imaging in the mammalian nervous system. Curr Opin Neurobiol 14(5):617-628

Merwa R, Hollaus K, Oszkar B, Scharfetter H (2004) Detection of brain oedema using magnetic induction tomography: a feasibility study of the likely sensitivity and detectability. Physiol Meas 25(1):347-354

Metherall P, Barber DC, Smallwood RH, Brown BH (1996) Three-dimensional electrical impedance tomography. Nature 380(6574):509-512

Michel CM, Murray MM, Lantz G, Gonzalez S, Spinelli L, Grave dP (2004) EEG source imaging. Clin Neurophysiol 115(10):2195-2222

Miranda PC, Hallett M, Basser PJ (2003) The electric field induced in the brain by magnetic stimulation: a 3-D finite-element analysis of the effect of tissue heterogeneity and anisotropy. IEEE Trans Biomed Eng 50(9):1074-1085 DOI 10.1109/TBME.2003.816079

Mueller JL, Isaacson D, Newell JC (1999) A reconstruction algorithm for electrical impedance tomography data collected on rectangular electrode arrays. IEEE Trans Biomed Eng 46(11):1379-1386

Mueller JL, Isaacson D, Newell JC (2001) Reconstruction of conductivity changes due to ventilation and perfusion from EIT data collected on a rectangular electrode array. Physiol Meas 22(1):97-106

Murrieta-Lee JC, Pomfrett CJD, Beatty PCW, Mussel CB, Waterfall RC, Polydorides N, McCann H (2005) EIT Voltage Changes on the Human Scalp Due to Brain Stimulus. 15th International Conference on Electronics, Communications and Computers (CONIELECOMP 2005), 229-234.

Murrieta-Lee JC, Pomfrett CJD, Beatty PCW, Polydorides N, Mussel CB, Waterfall RC, McCann H (2004) Subsecond observations of EIT voltage changes on the human scalp due to brain stimulus. 26th Annual International Conference of the IEEE Engineering in Medicine and Biology Society, San Francisco, CA, USA (EMBS 2004) , 1:1317-1320 Vol.2.

Newell JC, Edic PM, Ren X, Larson-Wiseman JL, Danyleiko MD (1996) Assessment of acute pulmonary edema in dogs by electrical impedance imaging. IEEE Trans Biomed Eng 43(2):133-138

Nitsche MA, Liebetanz D, Antal A, Lang N, Tergau F, Paulus W (2003a) Modulation of cortical excitability by weak direct current stimulation--technical, safety and functional aspects. Suppl Clin Neurophysiol 56:255-276

Nitsche MA, Liebetanz D, Lang N, Antal A, Tergau F, Paulus W (2003b) Safety criteria for transcranial direct current stimulation (tDCS) in humans. Clin Neurophysiol 114(11):2220-2222 DOI 10.1016/S1388-2457(03)00235-9

Obrig H, Villringer A (2003) Beyond the visible--imaging the human brain with light. J Cereb Blood Flow Metab 23(1):1-18

Oh TI, Woo EJ, Holder D (2007) Multi-frequency EIT system with radially symmetric architecture: KHU Mark1. Physiol Meas 28(7):S183-S196

Oostendorp TF, Delbeke J, Stegeman DF (2000) The conductivity of the human skull: results of in vivo and in vitro measurements. IEEE Trans Biomed Eng 47(11):1487-1492 DOI 10.1109/TBME.2000.880100

Oppenheim AV, Schafer RW, Buck JR (1999) Discrete-Time Signal Processing.Prentice Hall. ISBN 0137549202

Ozparlak L, Ider YZ (2005) Induced current magnetic resonance-electrical impedance tomography. Physiol Meas 26(2):S289-S305

Papazov S, Kostov Z, Daskalov I (2002) Electrical current distribution under transthoracic defibrillation and pacing electrodes. J Med Eng Technol 26(1):22-27 DOI 10.1080/03091900110102454

Park TS, Lee SY, Park JH, Cho MH, Lee SY (2006) Observation of the fast response of a magnetic resonance signal to neuronal activity: a snail ganglia study. Physiol Meas 27(2):181-190

Park TS, Lee SY, Park JH, Lee SY (2004) Effect of nerve cell currents on MRI images in snail ganglia. Neuroreport 15(18):2783-2786

Parkes LM, de Lange FP, Fries P, Toni I, Norris DG (2007) Inability to directly detect magnetic field changes associated with neuronal activity. Magn Reson Med 57(2):411-416

Paulsen KS, Breckon WR, Pidcock MK (1992) Electrode modelling in Electrical Impedance Tomography. SIAM J Appl Math 52:1012-1022 DOI 10.1137/0152059

Petridou N, Plenz D, Silva AC, Loew M, Bodurka J, Bandettini PA (2006) Direct magnetic resonance detection of neuronal electrical activity. Proc Natl Acad Sci U S A 103(43):16015-16020

Polydorides N, Lionheart WR (2002) A Matlab toolkit for three-dimensional electrical impedance tomography: a contribution to the Electrical Impedance and Diffuse Optical Reconstruction Software project. Meas Sci Technol 13 (12) 1871-83

Priori A (2003) Brain polarization in humans: a reappraisal of an old tool for prolonged non-invasive modulation of brain excitability. Clin Neurophysiol 114(4):589-595 DOI 10.1016/S1388-2457(02)00437-6

Prudnikova IF (1959) The effects of eserine on the action potential and impedance spike in frog nerve. Biofizikia 4:666-676

Radiat Prot Dosimetry (2003) Proceedings of the International Workshop on Weak Electric Field Effects in the Body. United Kingdom, March 24-25, 2003. Radiat Prot Dosimetry 106(4):295-400

Ranck JB, Jr. (1963) Specific impedance of rabbit cerebral cortex. Exp Neurol 7(2):144-152 DOI 10.1016/S0014-4886(63)80005-9

Ranck JB, Jr., BeMent SL (1965) The specific impedance of the dorsal columns of cat: an inisotropic medium. Exp Neurol 11(4):451-463 DOI 10.1016/0014-4886(65)90059-2

Rattay F (1998) Analysis of the electrical excitation of CNS neurons. IEEE Trans Biomed Eng 45(6):766-772 DOI 10.1109/10.678611

Rattay F (1999) The basic mechanism for the electrical stimulation of the nervous system. Neuroscience 89(2):335-346 DOI 10.1016/S0306-4522(98)00330-3

Reilly JP (1998) Applied bioelectricity : from electrical stimulation to electropathology.Springer, London;New York. ISBN 0387984070

Reilly JP (2002a) Neuroelectric mechanisms applied to low frequency electric and magnetic field exposure guidelines--part I: sinusoidal waveforms. Health Phys 83(3):341-355

Reilly JP, Diamant AM (2002b) Neuroelectric mechanisms applied to low frequency electric and magnetic field exposure guidelines--part II: non sinusoidal waveforms. Health Phys 83(3):356-365

Reilly JP, Diamant AM (2003) Spatial relationships in electrostimulation: application to electromagnetic field standards. IEEE Trans Biomed Eng 50(6):783-785 DOI 10.1109/TBME.2003.812156

Riu PJ, Rosell J, Lozano A, Pallas-Areny R (1995) Multi-frequency static imaging in electrical impedance tomography: Part 1. Instrumentation requirements. Med Biol Eng Comput 33(6):784-792

Robinson RO, Ferrie CD, Capra M, Maisey MN (1999) Positron emission tomography and the central nervous system. Arch Dis Child 81(3):263-270

Romsauerova A, McEwan A, Fabrizi L, Holder DS (2007) Evaluation of the performance of the Multifrequency Electrical Impedance Tomography (MFEIT) intended for imaging acute stroke. Scharfetter, H. and Merwa, R. Proc. of XIII Int. Conf. on Electrical Bio-Impedance and VIII Conference on Electrical Impedance Tomography, 17(1):543-547. IFMBE, Graz, Austria

Romsauerova A, McEwan A, Holder DS (2006a) Identification of a suitable current waveform for acute stroke imaging. Physiol Meas 27(5):S211-S219 DOI 10.1088/0967-3334/27/5/S18

Romsauerova A, McEwan A, Horesh L, Yerworth R, Bayford RH, Holder DS (2006b) Multi-frequency electrical impedance tomography (EIT) of the adult human head: initial findings in brain tumours, arteriovenous malformations and chronic stroke, development of an analysis method and calibration. Physiol Meas 27(5):S147-S161

Rosell-Ferrer J, Merwa R, Brunner P, Scharfetter H (2006) A multifrequency magnetic induction tomography system using planar gradiometers: data collection and calibration. Physiol Meas 27(5):S271-S280

Rush S, Driscoll DA (1968) Current distribution in the brain from surface electrodes. Anesth Analg 47(6):717-723

Saunders RD (2003) Rapporteur report: weak field interactions in the central nervous system. Radiat Prot Dosimetry 106(4):357-361

Saunders RD, Jefferys JG (2002) Weak electric field interactions in the central nervous system. Health Phys 83(3):366-375

Schwan HP (1957) Electrical properties of tissue and cell suspensions. Adv Biol Med Phys 5:147-209

Schwan HP (1983) Electrical properties of blood and its constituents: alternating current spectroscopy. Blut 46(4):185-197

Seidemann E, Arieli A, Grinvald A, Slovin H (2002) Dynamics of depolarization and hyperpolarization in the frontal cortex and saccade goal. Science 295(5556):862-865

Shibata K, Osawa M, Iwata M (2000) Visual evoked potentials in cerebral white matter hyperintensity on MRI. Acta Neurol Scand 102(4):230-235

Shoham D, Glaser DE, Arieli A, Kenet T, Wijnbergen C, Toledo Y, Hildesheim R, Grinvald A (1999) Imaging cortical dynamics at high spatial and temporal resolution with novel blue voltage-sensitive dyes. Neuron 24(4):791-802

Smallwood RH, Mangnall YF, Leathard AD (1994) Transport of gastric contents. Physiol Meas 15 Suppl 2a:A175-A188

Soni NK, Hartov A, Kogel C, Poplack SP, Paulsen KD (2004) Multi-frequency electrical impedance tomography of the breast: new clinical results. Physiol Meas 25(1):301-314

Soulsby CT, Khela M, Yazaki E, Evans DF, Hennessy E, Powell-Tuck J (2006) Measurements of gastric emptying during continuous nasogastric infusion of liquid feed: electric impedance tomography versus gamma scintigraphy. Clin Nutr 25(4):671-680

Steinbrink J, Kempf FC, Villringer A, Obrig H (2005) The fast optical signal--robust or elusive when non-invasively measured in the human adult? Neuroimage 26(4):996-1008

Stepnoski RA, LaPorta A, Raccuia-Behling F, Blonder GE, Slusher RE, Kleinfeld D (1991) Noninvasive detection of changes in membrane potential in cultured neurons by light scattering. Proc Natl Acad Sci U S A 88(21):9382-9386

Stockard JJ, Hughes JF, Sharbrough FW (1979) Visually evoked potentials to electronic pattern reversal: latency variations with gender, age and technical factors. Am J EEG Technol 19:171-204

Suesserman MF, Spelman FA, Rubinstein JT (1991) In vitro measurement and characterization of current density profiles produced by non-recessed, simple recessed, and radially varying recessed stimulating electrodes. IEEE Trans Biomed Eng 38(5):401-408 DOI 10.1109/10.81558

Syre F, Obrig H, Steinbrink J, Kohl M, Wenzel R, Villringer A (2003) Are VEP correlated fast optical signals detectable in the human adult by non-invasive nearinfrared spectroscopy (NIRS)? Adv Exp Med Biol 530:421-431

Taki M, Suzuki Y, Wake K (2003) Dosimetry considerations in the head and retina for extremely low frequency electric fields. Radiat Prot Dosimetry 106(4):349-356

Tidswell AT (2006) Functional Electrical Impedance Tomography of adult and neonatal brain function. PhD Thesis, University College London, London, UK

Tidswell AT, Bagshaw AP, Holder DS, Yerworth RJ, Eadie L, Murray S, Morgan L, Bayford RH (2003) A comparison of headnet electrode arrays for electrical impedance tomography of the human head. Phsyiological Measurement 24(2):527-544

Tidswell AT, Gibson A, Bayford RH, Holder DS (2001) Three-dimensional electrical impedance tomography of human brain activity. Neuroimage 13(2):283-294 DOI 10.1006/nimg.2000.0698

Tizzard A, Horesh L, Yerworth RJ, Holder DS, Bayford RH (2005) Generating accurate finite element meshes for the forward model of the human head in EIT. Physiol Meas 26(2):S251-S261 DOI 10.1088/0967-3334/26/2/024

Towers CM, McCann H, Wang M, Beatty PC, Pomfrett CJ, Beck MS (2000) 3D simulation of EIT for monitoring impedance variations within the human head. Physiol Meas 21(1):119-124

Tozer JC, Ireland RH, Barber DC, Barker AT (1999) Magnetic impedance tomography. Ann N Y Acad Sci 873:353-359

Traynelis SF, Dingledine R (1988) Potassium-induced spontaneous electrographic seizures in the rat hippocampal slice. J Neurophysiol 59(1):259-276

Tuch DS, Wedeen VJ, Dale AM, George JS, Belliveau JW (2001) Conductivity tensor mapping of the human brain using diffusion tensor MRI. Proc Natl Acad Sci U S A 98(20):11697-11701

Van Harreveld A, Murphy T, Nobel KW (1963) Specific Impedance of rabbit's cortical tissue. Am J Physiol 205(1):203-207

Vauhkonen M (1997) Electrical impedance tomography and prior information. PhD Thesis, Kuopio University,Finland

Vauhkonen PJ, Vauhkonen M, Kaipio JP (2000) Errors due to the truncation of the computational domain in static three-dimensional electrical impedance tomography. Physiol Meas 21(1):125-135

Vauhkonen PJ, Vauhkonen M, Savolainen T, Kaipio JP (1999) Three-dimensional electrical impedance tomography based on the complete electrode model. IEEE Trans Biomed Eng 46(9):1150-1160

Vrba J, Robinson SE (2001) Signal processing in magnetoencephalography. Methods 25(2):249-271

Vrba J, Robinson SE (2002) SQUID sensor array configurations for magnetoencephalography applications. Superconductor Science and Technology 15(9):R51-R89

Weaver JC, Vaughan TE, Adair RK, Astumian RD (1998) Theoretical limits on the threshold for the response of long cells to weak extremely low frequency electric fields due to ionic and molecular flux rectification. Biophys J 75(5):2251-2254

Wikipedia contributors. Hilbert transform - Wikipedia, The Free Encyclopedia. 12-31-2006.
Ref Type: Internet Communication

Williams RA, Beck MS (1995) Process Tomography, principles, techniques and applications.Butterworth-Heinemann Ltd, Oxford

Williamson A, Hoggart B (2005) Pain: a review of three commonly used pain rating scales. J Clin Nurs 14(7):798-804 DOI 10.1111/j.1365-2702.2005.01121.x

Williamson SJ, Kaufman L (1981) Biomagnetism. Journal of Magnetism and Magnetic Materials 22(2):129-201

Wilson AJ, Milnes P, Waterworth AR, Smallwood RH, Brown BH (2001) Mk3.5: a modular, multi-frequency successor to the Mk3a EIS/EIT system. Physiol Meas 22(1):49-54

Wolf M, Wolf U, Choi JH, Gupta R, Safonova LP, Paunescu LA, Michalos A, Gratton E (2002) Functional frequency-domain near-infrared spectroscopy detects fast neuronal signal in the motor cortex. Neuroimage 17(4):1868-1875

Xiong J, Fox PT, Gao JH (2003) Directly mapping magnetic field effects of neuronal activity by magnetic resonance imaging. Hum Brain Mapp 20(1):41-49

Yerworth RJ, Bayford RH, Brown B, Milnes P, Conway M, Holder DS (2003) Electrical impedance tomography spectroscopy (EITS) for human head imaging. Physiol Meas 24(2):477-489 DOI 10.1088/0967-3334/24/2/358

Yerworth RJ, Bayford RH, Cusick G, Conway M, Holder DS (2002) Design and performance of the UCLH mark 1b 64 channel electrical impedance tomography (EIT) system, optimized for imaging brain function. Physiol Meas 23(1):149-158

Zlochiver S, Radai MM, Abboud S, Rosenfeld M, Dong XZ, Liu RG, You FS, Xiang HY, Shi XT (2004) Induced current electrical impedance tomography system: experimental results and numerical simulations. Physiol Meas 25(1):239-255